HYDRODYNAMICAL PROPERTIES OF NONLINEAR GAUGE-COUPLED QUANTUM FLUIDS

by

Yvan Buggy

Submitted for the degree of
Doctor of Philosophy

INSTITUTE OF PHOTONICS AND QUANTUM SCIENCES
SCHOOL OF ENGINEERING AND PHYSICAL SCIENCES
HERIOT-WATT UNIVERSITY

August 2019

Abstract

In this thesis, we investigate certain hydrodynamical properties of quantum fluids subject to a density-dependent gauge potential. Such potentials have been shown to emerge, for instance, in a weakly interacting Bose cloud of optically addressed two-level atoms. By constructing a hydrodynamic canonical formalism for the matter-field, we show that an arbitrary effective density-dependent gauge potential invariably leads to nonlinear flow terms in the wave equation for the phase. In turn, the implications for the mechanical momentum transport equation of the fluid, are two-fold, where a body-force of dilation emerges and a flow-dependent pressure term features in the stress tensor of the fluid.

In order to restore the immediate lack of Galilean invariance, we derive covariant transformation laws for the nonlinear potentials, which leave the canonical field equations form invariant. We also show how density-dependent gauge potentials are physical vector potentials which may *not* be "gauged-away". In a one-dimensional system, we find that attempting to do so generates the flow-dependent pressure in the Hamiltonian density of the field, which in turn leads to an additional flow term in the wave equation for the phase.

Further, we study elementary excitations and derive a generalised expression relating the velocity of sound to the fluid pressure. We find that the velocity of sound is anisotropic, where the nonlinear gauge potential acts as a moving medium for sound propagation. Sound is not merely carried along with the ground state flow imparted by the gauge potential, but with an increased flow due the flow-dependent fluid pressure. To consolidate these results, we simulate the dynamics of a gauge-coupled superfluid and evaluate the velocity of sound numerically.

Finally, we study the interaction of a gauge-coupled superfluid with a foreign impurity. We learn that the ground state of an inhomogenous superfluid adopts a non-trivial local phase profile due to spatial density variations. For an immobile Gaussian impurity, this leads to the formation of a canonical flow (or phase flow) dipole about the object and an asymmetrical pressure field which compresses the object along the direction of the gauge potential. Further, we drag the impurity through the superfluid and examine the mechanical flow and phase winding fields during vortex formation. By studying the phase-slip accumulation in the superfluid, we evaluate the critical velocity for vortex formation, which decreases as the orientation of the flow imparted by the

gauge potential increasingly opposes the impurity. We also derive an expression for the drag force acting on the impurity and evaluate the force numerically. We find that the instantaneous drag force decays to a positive value when the impurity velocity exceeds the flow of the medium carrying sound along the direction of motion of the impurity. This latter velocity is distinct from the critical velocity for vortex formation. As such, in the case of a nonlinear gauge potential, the drag force is *not* a suitable quantity for estimating the critical velocity.

Acknowledgements

First and foremost, I would like to express my gratitude and appreciation to my supervisor Prof. Patrik Öhberg for his excellent guidance, patience and kindness.
Thanks to the rest of the research group for the stimulating exchanges and enjoyable meetings.
I am very grateful to my sister, mother and step father, for their unwavering support, patience and love. Thanks to my other family members and friends for their support and good company.
Last, but not least, I am grateful for the financial support received from the CM-CDT and appreciate the hard work and dedication from everyone involved.

Contents

Chapter 1

Introduction

Bose-Einstein condensates with dilute atomic gases, which were first implemeted experimentally in 1995 [1–4], present a versatile experimental testing ground for elucidating the physics of quantum fluids. The robust character of these ultracold systems stems from their phase coherence, which allows for the observation of quantum mechanical effects at the macroscopic level. Interactions play a crucial role in this regard, allowing phase correlation over large distances [5, 6]. The ability to fine tune interactions [7] and manipulate atoms through optical and magnetic fields [8, 9], has enabled the emulation of a variety of effects predicted by our theoretical models. For instance, the superfluid to Mott insulator transition in optical lattices [10–12].

More recently, efforts have been made to implement artificial electromagnetic potentials for charge neutral systems [13, 14]. These are generally engineered through combined-interactions, such that a system exhibits spatially varying local eigenstates [15, 16]. In other words, the action of a gauge potential can be mimicked by imparting a geometric phase onto the condensate wavefunction [15–18]. Although initial implementations involved static synthetic fields, further proposals [19–24] have since been put forward for creating "dynamical" gauge fields, which are described by their own Hamiltonian and not merely imposed on the system. One possibility for realising a dynamical gauge potential, is to introduce a "back-action" where the dynamics of the gauge potential are tied to the motion of the condensate. Such a prospect has been proposed in [25–31], where the effective field depends on the spatial configuration of the atoms, in particular, the atomic density. Very recently, a density-dependent gauge potential has been experimentally demonstrated in a two-dimensional optical lattice, by modulating the interaction strength in synchrony with the lattice shaking [32], where

the tunelling rate depends on the occupation number.

Nonlinear gauge potentials have been shown to give rise to a number of interesting properties, such as anyonic structures and chiral solitons [25, 33–35]. From a hydrodynamical point of view, density-dependent vector potentials entail a fluid flow which depends explicitly on the density profile of the fluid, where the rate of flow of a volume element of fluid typically increases as the volume shrinks. As a result, the kinetic energy density of the fluid becomes nonlinear in the density. One important, direct consequence of this, is the occurrence of flow-dependent terms in the resulting wave equation of the fluid. Hence, a density-dependent gauge potential leads to an exotic type of nonlinearity. This is exemplified in particular by the fluid pressure, which now depends explicitly on both of the independent dynamical fluid variables, namely, the density and the canonical flow (or phase flow). The implications of the canonical flow pressure on the hydrodynamical properties of a fluid, will be explored at length in our study.

The basic outline of this thesis may be summarised as follows. Chapters 2-4 are review chapters, with some original work in between. To begin with, we review several topics of analytical mechanics which will be recalled throughtout the text. Our aim here is essentially to provide an overview of the Hamilton-Jacobi formalism, which is intimately linked with the hydrodynamical description of a quantum fluid. In doing so, we recall how the canonical equations of motion may be viewed as Euler-Lagrange equations for the canonical variables and review the basic structure of canonical transformations. Further, in chapter 3, we discuss the microscopic theory underpinning a weakly-interacting dilute Bose gas and the Gross-Pitaevskii equation describing the mean-field dynamics. Subsequently, we construct a hydrodynamic canonical formalism for the classical field, by using both the Dirac-Bergmann algorithm for constrained Hamiltonian systems and the Faddeev-Jackiw method for first order Lagrangians. In chapter 4, we outline the general framework for implementing artificial gauge potentials in charge neutral systems and consider a particular model yielding an effective gauge-coupled mean-field Hamiltonian for an ultracold Bose gas, where the effective gauge potential is proportional to the atomic density. In chapter 5, we derive the hydrodynamic momentum transport equation for a wide class of nonlinear gauge-coupled quantum fluids. In particular, we show how nonlinear gauge potentials lead to a flow-dependent fluid pressure and a body-force term which is related to the dilation rate of the fluid. We also report the occurrence of a non-trivial local phase profile adopted by the ground state of an

inhomogeneous superfluid, where a canonical flow-dipole forms in the vicinity of an immobile impurity. Further, in chapter 6, we investigate the symmetry properties of the fluid. Here, we examine how the canonical field equations transform under both external and nonlinear gauge transformations and derive the covariant transformation laws for the potentials under a Galilean transformation. In chapter 7, we study the elementary excitations of the fluid and derive a generalised expression for obtaining the velocity of sound from the fluid pressure. Here, we find that the nonlinear gauge potential leads to an anisotropic sound velocity, where the speed of sound along a given direction depends on the relative angle of the gauge potential. Finally, in chapter 8, we investigate the breakdown of superfluidity by dragging an impurity through the system.

Chapter 2

Elements of analytical mechanics

2.1 Introduction

The motivation for an analytical treatment of mechanics emerges naturally when attempting to solve for the motion in time of mechanical *systems*. When mutual interactions occur between the constituent particles, it becomes clear that the trajectory of any individual particle generally depends on the trajectories of all the other particles, implicitly leaving one with the inevitable task of having to solve for all trajectories simultaneously. In analytical mechancis (AM), the entire set of equations of motion follow from an underlying variational principle. The principle implicitly contains these equations. When carried out to its logical conclusion, AM reveals the role taken by the action as a generating function for a very special kind of coordinate transformation in phase space. This exceptional type of *canonical transformation* is at the heart of the Hamilton-Jacobi (HJ) formalism of AM. As we shall come to appreciate, the HJ method gives rise to a full set of *cyclic* dynamical variables[1], which in turn permits a straight forward integration of the equations of motion. As a starting point to unravelling some of the key ingredients which will hopefully elucidate subsequent ideas explored in this thesis, we briefly review the Lagrangian and Hamiltonian formalisms. We then consider a rather general form of Lagrangian function, discuss the significance of its physical constituent variables and investigate the form of the associated generalised force. Further, we introduce the basic framework of canonical transformations and the HJ formalism, before extending the equations of motion to the case of continuous systems, or fields.

[1] A cyclic variable q_i (sometimes also called an ignorable or kinosthenic variable), is a variable whose time derivative $\dot{q}_i$ appears in the Lagrangian function, but not the variable itself.

2.2 The Lagrangian Formalism

In Lagrangian mechanics, the equations of motion are covariant under arbitrary coordinate transformations, so long as both sets of coordinates are in one-to-one correspondence. The coordinates are positional variables, labelled in a generalised fashion $q_1(t), q_2(t), \cdots, q_n(t)$. The space formed by these coordinates is called the *configuration space*. A point in this space completely specifies the configuration of the system, which is to say the positions of all the particles in physical space. Hence, the motion of the entire system may be pictured as the motion of a single point in this n-dimensional space. The Lagrangian equations of motion follow from the condition that the action integral

$$S = \int_{t_1}^{t_2} dt L(q_\alpha, \dot{q}_\alpha, t), \tag{2.1}$$

be stationary under arbitrary variations[2]of the q_i, where $q_\alpha \equiv q_1, \cdots, q_n$ and L is the Lagrangian of the system[3]. Note that the times t_1 and t_2 are arbitrary so that the action is in fact extremised infinitesimally throughout the motion, where a set of n differential equations for the generalised coordinates emerges in the form

$$\frac{\partial L}{\partial q_i} - \frac{d}{dt}\left(\frac{\partial L}{\partial \dot{q}_i}\right) = 0, \tag{2.2}$$

known as the *Euler-Lagrange* (EL) equations of motion. Notice how the Lagrangian is not unique, in the sense that, $L'(q_\alpha, \dot{q}_\alpha, t) = L(q_\alpha, \dot{q}_\alpha, t) + \frac{d}{dt}F(q_\alpha, \dot{q}_\alpha, t)$, gives rise to identical equations of motion, since the end point configurations $q_\alpha(t_1)$ and $q_\alpha(t_2)$ are fixed when varying the time integral (2.1). In fact, when $L' = L + \frac{d}{dt}F(q_\alpha, t)$, the transformation is equivalent to a gauge transformation, where F is the gauge function. By transforming over to phase space and normalising the Lagrangian function to its canonical form, gauge transformations may be viewed as a subset of canonical transformations [36].

[2]Note that the variation δq_i also implies the variation $\delta \dot{q}_i$. Although q_i and $\dot{q}_i$ are independent dynamical variables, δq_i and $\delta \dot{q}_i$ are not independent.

[3]This functional dependence of the Lagrangian follows from the fact that Newton's equations are second order in time. Hence both the position coordinates and velocities need to be specified at any given time in order to specify the motion. These variables are prescribed independently of each other.

2.3 The Hamiltonian Formalism

The structure of Hamilton's principle of stationary action suggests that we do not consider the differential quantities $\dot{q}_i$ as independent variables, but another set of variables which are of algebraic type. These new positional-type variables are obtained by performing a Legendre transformation of the Lagrangian function. In particular, we would like to transform $L\left(q_\alpha, \dot{q}_\alpha, t\right)$ to a representation which treats the set of partial derivatives $\partial L/\partial \dot{q}_\alpha$ as independent variables, in substitution of the $\dot{q}_\alpha$. To achieve this, one introduces the Hamiltonian function

$$H\left(q_\alpha, \frac{\partial L}{\partial \dot{q}_\alpha}, t\right) = \sum_{i=1}^{n} \dot{q}_i \frac{\partial L}{\partial \dot{q}_i} - L(q_\alpha, \dot{q}_\alpha, t). \tag{2.3}$$

Note that a substitution of this kind is always possible if the Hessian matrix of elements, $\partial^2 L/\partial \dot{q}_i \partial \dot{q}_j$, is non-singular. It is customary to denote the new variables of the transformation, by

$$p_i = \frac{\partial L}{\partial \dot{q}_i}, \tag{2.4}$$

which are referred to as the canonical momenta, each one being conjugate to its respective i^{th} generalised coordinate.

The Legendre transform maps the set of n dynamical second order EL equations, onto a set of $2n$ first order equations. In doing so, the generalised velocities transform into a set of variables which are no longer first order in time, but new positional variables in their own right. To see this, we may consider Eq. (2.3) in reverse:

$$L = \sum_{i=1}^{n} p_i \dot{q}_i - H, \tag{2.5}$$

and normalise the action integral (2.1) to the canonical form

$$A = \int dt \left[\sum_{i=1}^{n} p_i \dot{q}_i - H(q_\alpha, p_\alpha) \right]. \tag{2.6}$$

Following Lanczos [37], let us examine the variation of the Lagrangian from Eq. (2.5) with respect to the p_i, which reads

$$\delta L = \sum_{i=1}^{n} \left(\dot{q}_i - \frac{\partial H}{\partial p_i} \right) \delta p_i. \tag{2.7}$$

Yet, from the duality of the Legendre transform (e.g. $\dot{q}_i = \partial H/\partial p_i$), we see that Eq. (2.7) vanishes. In other words, varying the p_i leaves L unchanged and with it the action integral (2.6). Hence, we are free to vary the p_i arbitrarily and treat these as a second set of independent variables subject to the EL equations. Doing so, we find[4]

$$\frac{\partial L}{\partial q_i} - \frac{d}{dt}\left(\frac{\partial L}{\partial \dot{q}_i}\right) = -\frac{\partial H}{\partial q_i} - \dot{p}_i = 0 \tag{2.8}$$

$$\frac{\partial L}{\partial p_i} - \frac{d}{dt}\left(\frac{\partial L}{\partial \dot{p}_i}\right) = \dot{q}_i - \frac{\partial H}{\partial p_i} = 0, \tag{2.9}$$

We may therefore conclude that the variation of action functionals normalised to the form (2.6), invariably imply the set of $2n$ first order differential equations

$$\begin{aligned} \dot{q}_i &= \frac{\partial H}{\partial p_i}, \\ \dot{p}_i &= -\frac{\partial H}{\partial q_i}, \end{aligned} \tag{2.10}$$

called Hamilton's *canonical equations* of motion. The first set of equations in (2.10) holds on account of the duality of the Legendre transform, while the second follows from the EL equations of motion (2.2). In contrast to the $\dot{q}_i$, which are differential quantities, the p_i are algebraic quantities which may be treated as positional variables subject to their own set of EL equations [37]. These join the coordinates q_i to form a new dynamical space (q_α, p_α), called *phase space*. The canonical equations then determine the velocity components of a point in phase space. Therefore, in analogy with the streamlines of a fluid as integral curves of the velocity field, notice that a given point in phase space is in fact part of a complete phase trajectory, since the motion is completely specified given a single point. This is in contrast to the situation in configuration space where the motion of the configuration point can have any direction. If we then consider an ensemble of initial conditions over some region of phase space at a given instant of time, the phase trajectories trace out an ordered set of curves which never cross or touch each other. Including the time t as an additional dimension of the $2n+1$-dimensional space, the motion can be viewed as that of a $2n$-dimensional fluid - the *phase fluid* [37]- where a given streamline represents the motion of the system for a specific choice of initial conditions.

As a final point, note that the change in time of a function $f(q_\alpha, p_\alpha)$ defined on phase

[4]We also have the relation $\frac{\partial L}{\partial t} = -\frac{\partial H}{\partial t}$ for non-autonomous systems.

space, may be written in terms of Poisson brackets. The Poisson bracket of two functions $f(q_\alpha, p_\alpha, t)$ and $g(q_\alpha, p_\alpha, t)$ on phase space, is defined as

$$\{f, g\}_{q,p} = \sum_{i=1}^{n} \left(\frac{\partial f}{\partial q_i} \frac{\partial g}{\partial p_i} - \frac{\partial f}{\partial p_i} \frac{\partial g}{\partial q_i} \right). \tag{2.11}$$

The change in time of a phase space function, then takes the compact form

$$\frac{df}{dt} = \frac{\partial f}{\partial t} + \sum_{i=1}^{n} \left(\frac{\partial f}{\partial q_i} \dot{q}_i + \frac{\partial f}{\partial p_i} \dot{p}_i \right) = \frac{\partial f}{\partial t} + \{f, H\}_{q,p}. \tag{2.12}$$

2.4 Generalised potential and potential energy

It is instructive to consider the Hamiltonian function associated with a Lagrangian

$$L(q_\alpha, \dot{q}_\alpha, t) = T(q_\alpha, \dot{q}_\alpha) - U(q_\alpha, \dot{q}_\alpha, t), \tag{2.13}$$

which is quadratic in the velocities, where

$$T = \frac{1}{2} \sum_{i,j=1}^{n} a_{ij}(q_\alpha) \dot{q}_i \dot{q}_j, \tag{2.14}$$

is the *kinetic energy function* and U is the *generalised potential* which includes any remaining first order and zero order velocity terms. Note that the generalised potential is the negative of the work function $W = -U$ (see Eq. (2.22)). To begin with, observe that when T takes the form (2.14), the canonical momenta in turn, read

$$p_k = \sum_{i=1}^{n} a_{ki} \dot{q}_i - \frac{\partial U}{\partial \dot{q}_k}, \tag{2.15}$$

where we have assumed that $a_{ij} = a_{ji}$. Inserting these into the Legendre transform (2.3), the Hamiltonian is

$$H = \sum_{i,j=1}^{n} a_{ij} \dot{q}_i \dot{q}_j - \sum_{i=1}^{n} \frac{\partial U}{\partial \dot{q}_i} \dot{q}_i - L \tag{2.16}$$

which for $L = T - U$, gives

$$H = T + U - \sum_{i=1}^{n} \frac{\partial U}{\partial \dot{q}_i} \dot{q}_i. \tag{2.17}$$

Therefore, when velocity-dependent terms enter U, the Hamiltonian may be expressed as the sum of kinetic and potential energies, insofar as the potential energy is defined, according to

$$V = U - \sum_{i=1}^{n} \frac{\partial U}{\partial \dot{q}_i} \dot{q}_i. \tag{2.18}$$

Although at first sight this may appear as a Legendre transform $U\left(q_\alpha, \dot{q}_\alpha\right) \to V\left(q_\alpha, \frac{\partial U}{\partial \dot{q}_\alpha}\right)$ with active variable transformation $\dot{q}_i \to \frac{\partial U}{\partial \dot{q}_i}$, this is not the case. Indeed, unlike the Lagrangian function which may be viewed as the following Legendre transform of the Hamiltonian:

$$L\left(q_\alpha, \dot{q}_\alpha\right) = \sum_{i=1}^{n} \frac{\partial H}{\partial p_i} p_i - H\left(q_\alpha, p_\alpha\right), \tag{2.19}$$

there is no associated dual transformation to Eq. (2.18). This is because U is a linear form in the velocities, so that the $\dot{q}_i$ completely drop out of V. Therefore, one should view expression (2.18) merely as a defining combination for the potential energy. In fact, we shall witness a similar situation for the Hamiltonian formalism of the Gross-Pitaevskii field developed further in section 3.2.3, where the duality of the usual Legendre transform (2.3) is destroyed on account of the Lagrangian being first order in the field velocities.

2.5 A general form of Lagrangian

For an extensive range of mechanical systems, it is typically the case that the Lagrangian is at most quadratic in the velocities. As such, let us consider the following rather general form for the Lagrangian:

$$L\left(q_\alpha, \dot{q}_\alpha, t\right) = \frac{1}{2} \sum_{i,j=1}^{n} a_{ij}\left(q_\alpha\right) \dot{q}_i \dot{q}_j + \sum_{i=1}^{n} a_i\left(q_\alpha, t\right) \dot{q}_i + a_0\left(q_\alpha, t\right). \tag{2.20}$$

Three polynomial forms appear here. One which is quadratic in the $\dot{q}_i$, another which is linear and a zero order term. These require, respectively, a matrix of coefficients a_{ij} defined over configuration space, a vector a_i and a scalar a_0 in order for L to be a scalar quantity. From Eqs. (2.13) and (2.18), we see that the function $-a_0 = V$ plays the role of a potential energy. In turn, $a_i = A_i$ has the character of a vector potential. This may be seen from the fact that the transformation $A_i \to A_i + \frac{\partial}{\partial q_i}\chi\left(q_\alpha, t\right)$ is equivalent to adding a total time derivative to the Lagrangian, which does not affect the dynamics of

the system. Thus, for the Lagrangian (2.20), the generalised potential may be presented as

$$U = -\sum_{i=1}^{n} A_i \dot{q}_i + V. \tag{2.21}$$

The remaining term in the Lagrangian (2.20) is the kinetic term from Eq. (2.14), which characterises the inertia of the system. Although we shall not pursue the following, we briefly point out that the a_{ij} are connected with the geometry of configuration space, which generally takes a Riemannian form when holonomic constraints exist between the $3N$ coordinates. We suggest the reader consult [37–40] for further details on this matter. As a particular case of Eq. (2.20), consider the Lagrangian of a nonrelativistic particle of mass m and charge e interacting with the electromagnetic field. In this situation, the generalised potential reads $U(\mathbf{r}, \mathbf{v}, t) = -e\mathbf{v} \cdot \mathbf{A}(\mathbf{r}, t) + e\phi(\mathbf{r}, t)$, where ϕ and $\mathbf{A}$ are the electromagnetic scalar and vector potentials, respectively. From Eq. (2.18), the potential energy of the charge is then $V = e\phi$ and the Hamiltonian is $H = \frac{(\mathbf{p}-e\mathbf{A})^2}{2m} + e\phi = T + V$. Notice that the vector potential is determined by the slopes of U with respect to the velocities, e.g. $A_i = -\partial U/\partial \dot{q}_i$, similar to $p_i = \partial L/\partial \dot{q}_i$.

2.6 Generalised force

The two fundamental scalar quantities of analytical mechanics are the kinetic energy function and the work function [37]. The first characterises the inertia of the system (the left hand side of Eq. (2.24)) while the second determines the *generalised force* (the right hand side of Eq. (2.24)). When the work function depends only on the coordinates q_i, the infinitesimal work due to the generalised force is given by the differential[5]

$$dW = \sum_{i=1}^{n} F_i dq_i, \tag{2.22}$$

in configuration space. Although the vector F_i encoding the dynamical action of all forces in the system generally changes under a point transformation in configuration space, the differential dW is invariant. The generalised force components are derived from the work function, as

$$F_i = \frac{\partial W}{\partial q_i}, \tag{2.23}$$

[5]Here we assume that the differential dW is exact.

and it is customary to write $-W(q_\alpha) = V(q_\alpha)$, which may be interpreted as the potential energy of the system.

When the work function depends also on the velocities $\dot{q}_i$, the Lagrangian of the system takes the form (2.13) and the EL equation (2.2), separates into two parts:

$$-\frac{\partial T}{\partial q_i} + \frac{d}{dt}\left(\frac{\partial T}{\partial \dot{q}_i}\right) = F_i, \tag{2.24}$$

where the generalised force, now reads

$$F_i = -\frac{\partial U}{\partial q_i} + \frac{d}{dt}\left(\frac{\partial U}{\partial \dot{q}_i}\right), \tag{2.25}$$

Comparing the right hand side of the above equation with Eq. (2.23), we see that the inclusion of velocity-dependent terms in the generalised potential gives rise to an additional force term. Substituting Eq. (2.21) for the generalised potential into (2.25), the generalised force associated with the Lagrangian (2.20) may be expressed in terms of the potentials V and A_i, according to

$$F_i = -\frac{\partial V}{\partial q_i} + \sum_j \dot{q}_j \frac{\partial A_i}{\partial q_j} - \frac{dA_i}{dt}. \tag{2.26}$$

Notice that the total time derivative appearing in this equation is the change in A_k as seen by a moving point in configuration space and not by a fixed point. Therefore

$$\frac{dA_i}{dt} = \frac{\partial A_i}{\partial t} + \sum_j \dot{q}_j \frac{\partial A_i}{\partial q_j}, \tag{2.27}$$

and the force takes a generalised Lorentz form

$$F_i = -\frac{\partial V}{\partial q_i} - \frac{\partial A_i}{\partial t} + \sum_j \dot{q}_j \left(\frac{\partial A_j}{\partial q_i} - \frac{\partial A_i}{\partial q_j}\right). \tag{2.28}$$

2.7 Action differential along solution curves

Although the equations of motion follow from the condition of stationary action, we may also consider the change in the action along the actual path of motion. As such, the action may be viewed as a function rather than a functional. Recalling that the action is insensitive to arbitrary variations of the p_i, the action differential is then a function of the coordinates q_i and the time t, i.e. $dA(q_\alpha, t)$. To obtain its spatial

dependence, we may proceed by varying the endpoint of integration $q_i(t_2)$ of the action integral associated with the actual path, as discussed in [37, 41]. This gives rise to a non-vanishing boundary term which characterises the spatial part of the differential. Similarly, the time dependence of dA may be obtained by considering deviations in the upper time limit of integration. Doing so, one finds that the action differential takes the form

$$dS(q_\alpha, t) = \sum_i p_i dq_i - H dt. \tag{2.29}$$

Hence, the canonical momenta

$$p_i = \frac{\partial S}{\partial q_i}, \tag{2.30}$$

and the Hamiltonian

$$H = -\frac{\partial S}{\partial t}, \tag{2.31}$$

are obtained from the action function through simple differentiation. It is interesting to note that if one treats the time t as a mechanical variable subject to the process of variation and writes the equations of motion in parametric form [37], the canonical momentum associated with the time variable may be shown to be the negative of the Hamiltonian: $p_t = -H$. Then, from Eqs. (2.30) and (2.31), we notice that the action function takes on the physical role of a "momentum-potential" in this extended configuration space.

2.8 Canonical transformations

When no direct integration methods exist for solving dynamical equations, perhaps the most powerful tool at our disposal is that of coordinate transformations. In the Lagrangian formalism, any point transformation in configuration space

$$q_i = q_i(Q_\alpha), \tag{2.32}$$

leaves the form of the Lagrangian equations of motion unchanged. The reason for this is essentially because the velocities are connected by a linear transformation

$$\dot{q}_i = \sum_j \frac{\partial q_i}{\partial Q_j} \dot{Q}_j, \tag{2.33}$$

which is identical to that connecting the coordinate variations

$$\delta q_i = \sum_j \frac{\partial q_i}{\partial Q_j} \delta Q_j. \tag{2.34}$$

Hence, the velocities are not changed in an arbitrary fashion, but transform in a well determined manner according to how the coordinates q_i themselves transform. Notice how the situation is different in the case of an arbitrary point transformation in phase space, since the new momenta are restricted by $P_i = \partial L / \partial \dot{Q}_i$. Although a more extensive group of point transformations exists for the $2n$ phase space coordinates q_α, p_α compared to the n configuration space coordinates q_α, an arbitrary point transformation in phase space generally destroys the structure of the canonical equations, given that the canonical action integral

$$A = \int \sum_i p_i dq_i - H dt, \tag{2.35}$$

is not left invariant for arbitrary transformations [37]. Only a restricted subset of point transformations preserve the form of the action integral and with it the canonical equations (2.10). Such transformations are called *canonical transformations*.

Before examining the general case, it is instructive to consider first the case of a single degree of freedom with independent dynamical variables q and p and Hamiltonian $H(q,p)$. Here we simply summarise several key points and refer the reader to [37, 38, 41–43] for further details. Let us perform a point transformation in phase space, by introducing a new set of independent variables

$$Q = Q(q,p), \qquad P = P(q,p). \tag{2.36}$$

Since these can be viewed as functions on phase space, their time derivatives are given, by

$$\dot{Q} = \{Q, H\}_{q,p}, \qquad \dot{P} = \{P, H\}_{q,p}. \tag{2.37}$$

However, we would like to express the above equations in terms of the Hamiltonian $\bar{H}(Q,P) = H(q(Q,P), p(Q,P))$ with respect to the new variables. Expanding the

Poisson brackets and using chain rules, it is easy to show [42] that

$$\dot{Q} = \frac{\partial \bar{H}}{\partial P} \{Q, P\}_{q,p}, \qquad \dot{P} = -\frac{\partial \bar{H}}{\partial Q} \{Q, P\}_{q,p}. \tag{2.38}$$

Therefore, the variables Q, P obey canonical equations of motion with Hamiltonian $\bar{H}$ if the Poisson bracket of the new variables with respect to the old variables, reads

$$\{Q, P\}_{q,p} = 1. \tag{2.39}$$

In other words, we are guaranteed that transformation (2.36) is canonical when Eq. (2.39) holds. Another way of viewing a canonical transformation is that the above condition ensures that the differential $pdq - PdQ$ is exact and we may write [42]

$$dF = pdq - PdQ. \tag{2.40}$$

The function $F(q, Q)$ here is called the *generating function* of the point transformation (2.36) and dF relates the action differentials between both sets of coordinates. Note that F is not a function on phase space but relates two sets of coordinates. The name generating function stems from the fact that the new variables Q, P are obtained from the old ones through differentiation of F. Indeed, supposing F is a function of q, Q as in Eq. (2.40), we then have

$$p = \frac{\partial F(q, Q)}{\partial q}, \qquad P = -\frac{\partial F(q, Q)}{\partial Q}. \tag{2.41}$$

The first of these two equations allows us to solve for Q in terms of q, p and substituting this $Q(q, p)$ into the second, gives $P(q, p)$.

Consider now the more general case of a time-dependent point transformation, replacing the $2n$ independent variables q_α, p_α governed by a Hamiltonian $H(q_\alpha, p_\alpha, t)$, by the set of new variables

$$Q_i = Q_i(q_\alpha, p_\alpha, t), \qquad P_i = P_i(q_\alpha, p_\alpha, t). \tag{2.42}$$

Hence, a point transformation is generated at each instant of time. If we denote the new Hamiltonian[6] by $K(Q_\alpha, P_\alpha, t)$ and the transformation is canonical, the new coordinates evolve under

$$\dot{Q}_i = \frac{\partial K(Q_\alpha, P_\alpha, t)}{\partial P_i}, \qquad \dot{P}_i = -\frac{\partial K(Q_\alpha, P_\alpha, t)}{\partial Q_i}, \tag{2.43}$$

and the action differential from Eq. (2.29) is preserved up to a total differential, such that

$$\sum_i p_i dq_i - H dt = \sum_i P dQ_i - K dt + dF, \tag{2.44}$$

where F is an arbitrary function of the $4n$ variables $q_\alpha, p_\alpha, Q_\alpha, P_\alpha$ and t. However, since the $4n$ variables are connected by the $2n$ equations (2.42), only $2n$ of these variables are independent. Consider the case where $F = F_1(q_\alpha, Q_\alpha, t)$ is a function of the mixed variables q_α, Q_α and the time t, such that

$$dF_1 = \sum_i \left(\frac{\partial F_1}{\partial q_i} dq_i + \frac{\partial F_1}{\partial Q_i} dQ_i \right) + \frac{\partial F_1}{\partial t} dt. \tag{2.45}$$

Generating functions of this kind are referred to as type 1. Comparing Eqs. (2.44) and (2.45), we see that

$$p_i = \frac{\partial F_1(q_\alpha, Q_\alpha, t)}{\partial q_i}, \qquad P_i = -\frac{\partial F_1(q_\alpha, Q_\alpha, t)}{\partial Q_i}, \qquad K = H + \frac{\partial F_1(q_\alpha, Q_\alpha, t)}{\partial t}. \tag{2.46}$$

Thus, for a given generating function, there are 3 characteristic equations which define the canonical transformation. Now, it may be the case that the transformation we want to implement cannot be generated by a type 1 generating function and that another kind of generating function which depends on some other mixture of old and new variables is required. Inspecting the form of Eq. (2.46), we see that this is in fact the case for the identity transformation ($Q_i = q_i$, $P_i = p_i$), which will be of interest below. Let us then consider another type of generating function with mixed variables q, P by writing $\sum_i P_i dQ_i = d\sum_i P_i Q_i - \sum_i Q_i dP_i$ in Eq. (2.44). Rearranging we find that

$$\sum_i p_i dq_i + Q_i dP_i + (K - H) dt = dF_2, \tag{2.47}$$

[6]Notice that we have not denoted the new Hamiltonian by $\bar{H}$, as previously. The reason for this is that in the case of time-dependent canonical transformations, the new Hamiltonian differs from the old Hamiltonian so that $K(Q_\alpha, P_\alpha, t) \neq H(q_\alpha(Q_\beta, P_\beta, t), p_\alpha(Q_\beta, P_\beta, t), t)$. See Eq. (2.46).

where

$$F_2 = F_1 + \sum_i Q_i P_i, \tag{2.48}$$

is a type 2 generating function with functional dependence $F_2 = F_2(q_\alpha, P_\alpha, t)$, which follows from the LHS of Eq. (2.47). Hence, we have

$$dF_2 = \sum_i \left(\frac{\partial F_2}{\partial q_i} dq_i + \frac{\partial F_2}{\partial P_i} dP_i \right) + \frac{\partial F_2}{\partial t} dt, \tag{2.49}$$

and comparing Eqs. (2.47) and (2.49), yields

$$p_i = \frac{\partial F_2(q_\alpha, P_\alpha, t)}{\partial q_i}, \qquad Q_i = \frac{\partial F_2(q_\alpha, P_\alpha, t)}{\partial P_i}, \qquad K = H + \frac{\partial F_2(q_\alpha, P_\alpha, t)}{\partial t}. \tag{2.50}$$

In turn, we see that the identity transformation $Q_i = q_i$, $P_i = p_i$, may be taken to be the result of the type 2 generating function

$$F_{iden} = \sum_i q_i P_i. \tag{2.51}$$

2.9 Hamilton-Jacobi formalism

Now that we have a suitable generating function for the identity transformation, let us consider the infinitesimal canonical transformation generated by

$$F_2(q_\alpha, P_\alpha, t) = \sum_i q_i P_i + \epsilon G(q_\alpha, P_\alpha, t), \tag{2.52}$$

where $\epsilon \ll 1$ is an infinitesimal quantity and G is an arbitrary function. This maps each point of phase space onto a neighbouring point, by generating the transformation

$$Q_i = q_i + \epsilon \frac{\partial G(q_\alpha, P_\alpha, t)}{\partial P_i}, \qquad p_i = P_i + \epsilon \frac{\partial G(q_\alpha, P_\alpha, t)}{\partial q_i}, \tag{2.53}$$

in accordance with the transformation equations (2.50). To first order in ϵ, G may be taken to be a function on phase space, where $G = G(q_\alpha, p_\alpha, t)$, leading to the infinitesimal canonical transformation

$$Q_i = q_i + \epsilon \frac{\partial G(q_\alpha, p_\alpha, t)}{\partial p_i}, \qquad P_i = p_i - \epsilon \frac{\partial G(q_\alpha, p_\alpha, t)}{\partial q_i}. \tag{2.54}$$

Accordingly, ϵG is called the generator of the infinitesimal transformation. Of particular interest, consider the case where $\epsilon = dt$, a small time interval and $G = H$, the Hamiltonian. Then, the new variables are

$$Q_i = q_i + dt\frac{\partial H}{\partial p_i} = q_i\left(t + dt\right) \tag{2.55}$$

$$P_i = p_i - dt\frac{\partial H}{\partial q_i} = p_i\left(t + dt\right). \tag{2.56}$$

In other words, we have the important result that the infinitesimal canonical transformation generated by the Hamiltonian is the actual physical change undergone by the phase space coordinates over time dt. Since canonical transformations have the "group" property [37], an arbitrary transformation can be constructed from a succession of infinitesimal transformations and the entire motion of the system may be viewed as a continuous unfolding of an infinitesimal canonical transformation, associated with a finite canonical transformation

$$q = q\left(q_\alpha^0, p_\alpha^0, t\right), \qquad p = p\left(q_\alpha^0, p_\alpha^0, t\right), \tag{2.57}$$

where q_α^0, p_α^0 are the initial canonical coordinates. Therefore, starting from this initial point, the Hamiltonian continuously generates a point transformation in phase space which traces out some trajectory in the space of old variables q_α, p_α. Although H is the infinitesimal generator of time translation, it would be useful to obtain a generating function for the finite transformation associated with the whole trajectory. To do so, consider this trajectory plotted in extended phase space (q_α, p_α, t), which takes the form of some curve. Notice that the problem would be greatly simplified if we could find a succession of transformations which map the curve onto a straight line, such that the transformed canonical coordinates are all constant in time: $\dot{Q}_i = 0$, $\dot{P}_i = 0$. In doing so, all coordinates would become cyclic and the integration problem trivial. From Eq. (2.43), this is clearly guaranteed when the new Hamiltonian K continually vanishes from one infinitesimal transformation to the next. Hence, recalling Eq. (2.50), we would like the generating function of the finite transformation to solve

$$H + \frac{\partial F_2}{\partial t} = 0. \tag{2.58}$$

In other words, we can guarantee that the canonical variables are cyclic by choosing F_2 such that $K = 0$. Furthermore, notice how this method permits the solution of problems involving time-dependent Hamiltonians. It is conventional to denote $F_2 = S$, referred to as Hamilton's principal function. Therefore, the partial differential equation which should be solved, is

$$H\left(q_\alpha, \frac{\partial S}{\partial q_\alpha}, t\right) + \frac{\partial S\left(q_\alpha, P_\alpha, t\right)}{\partial t} = 0. \tag{2.59}$$

This is the *Hamilton-Jacobi* (HJ) equation. Now, the type 2 generating function $S\left(q_\alpha, P_\alpha, t\right)$ depends on the old set of coordinates q_α, the new canonical momenta P_α and time t. However, the new canonical coordinates are cyclic and therefore constant:

$$Q_i = a_i, \qquad P_i = b_i. \tag{2.60}$$

Thus, $S = S\left(q_\alpha, b_\alpha, t\right)$ and Eq. (2.59) is a first order partial differential equation in the $n + 1$ variables q_α, t. Although we will not be concerned with obtaining explicit solutions to this equation, for completeness we briefly outline the methodology for doing so. In order to solve for the motion of the system and obtain $q_\alpha\left(t\right)$ and $p_\alpha\left(t\right)$, we turn to the following two relations defining the transformation:

$$p_i = \frac{\partial S\left(q_\alpha, b_\alpha, t\right)}{\partial q_i}, \qquad Q_i = \frac{\partial S\left(q_\alpha, b_\alpha, t\right)}{\partial b_i} = a_i. \tag{2.61}$$

Inverting the second of these two relations, we may express the generalised coordinates q_i in terms of the $2n$ constants of integration and time: $q_i = q_i\left(a_\alpha, b_\alpha, t\right)$. After solving for the q_i, direct substitution into the first of the above equations then allows us to solve for the momenta in terms of the constants and time: $p_i = p_i\left(a_\alpha, b_\alpha, t\right)$. Thus, the general methodology for solving by the HJ method may be summarised as follows. Given a certain Hamiltonian, we construct the HJ equation 2.59, then solve for $S\left(q_\alpha, b_\alpha, t\right)$, differentiate S to obtain Q_i and rearrange this expression in the form $q_i = q_i\left(a_\alpha, b_\alpha, t\right)$.

Recalling section 2.7 where we considered the action differential along a solution curve, it was noted in Eq. (2.31) that the Hamiltonian may be derived from the action through differentiation with respect to time. Yet, this is precisely the partial differential equation (2.59) which the generating function must solve in order for K to vanish in Eq. (2.50). In other words, the action function always solves the HJ equation and can

be taken as the generating function of the finite transformation (2.57). As such, we shall not distinguish between Hamilton's principal function and the action function.

2.10 Charged particle in an electromagnetic field

As an example, let us examine the HJ equation for a charged particle interacting with the electromagnetic field. The Lagrangian of the charge, takes the form

$$L(\mathbf{r},\mathbf{v},t)=\frac{1}{2}mv^2+e\mathbf{A}(\mathbf{r},t)\cdot\mathbf{v}-e\phi(\mathbf{r},t), \tag{2.62}$$

where $v=|\mathbf{v}|$. Since the charge couples to a vector potential, there is a field momentum contribution to the total mechanical momentum, $m\mathbf{v}$, of the charge, where the canonical momentum of the particle takes the form

$$\mathbf{p}=m\mathbf{v}+e\mathbf{A}. \tag{2.63}$$

The Hamiltonian is obtained from the Legendre transform (2.3) of the Lagrangian function (2.62), as

$$H=\frac{(\mathbf{p}-e\mathbf{A})^2}{2m}+e\phi. \tag{2.64}$$

In accordance with Eq. (2.30), the action function S and the vector potential $\mathbf{A}$, define the mechanical momentum

$$m\mathbf{v}(\mathbf{r},t)=\boldsymbol{\nabla}S(\mathbf{r},t)-e\mathbf{A}(\mathbf{r},t), \tag{2.65}$$

for the charged particle. Hence, the HJ equation in this instance, reads

$$\frac{\partial S}{\partial t}+\frac{(\boldsymbol{\nabla}S-e\mathbf{A})^2}{2m}+e\phi=0. \tag{2.66}$$

For the Lagrangian (2.62), the equation of motion (2.24) with generalised Lorentz force (2.28), is abridged to

$$m\frac{d\mathbf{v}}{dt}=e(\mathbf{E}+\mathbf{v}\times\mathbf{B}), \tag{2.67}$$

where $\mathbf{E}$ and $\mathbf{B}$ are the electric and magnetic force fields, related to the potentials according to

$$\mathbf{E}=-\boldsymbol{\nabla}\phi-\frac{\partial\mathbf{A}}{\partial t},\qquad \mathbf{B}=\boldsymbol{\nabla}\times\mathbf{A}. \tag{2.68}$$

The equation of motion (2.67) may be retrieved from the HJ equation (2.66) as follows. Comparing Eqs. (2.65) and (2.66), we see that the dynamics of the momentum field may be obtained by taking the gradient of the HJ equation. Doing so, we find that

$$m\left(\frac{\partial}{\partial t}+\mathbf{v}\cdot\boldsymbol{\nabla}\right)\mathbf{v}=e\left(-\frac{\partial\mathbf{A}}{\partial t}-\boldsymbol{\nabla}\phi+\mathbf{v}\times\boldsymbol{\nabla}\times\mathbf{A}\right), \tag{2.69}$$

where we have used the identities $\boldsymbol{\nabla}\left(\mathbf{v}\cdot\mathbf{v}\right)=1/2\left(\mathbf{v}\cdot\boldsymbol{\nabla}\mathbf{v}+\mathbf{v}\times\boldsymbol{\nabla}\times\mathbf{v}\right)$ and $\boldsymbol{\nabla}\times\boldsymbol{\nabla}S=0$. Substituting the force fields from Eq. (2.68) for the electromagnetic potentials and noting the appearance of a total time derivative as in Eq. (2.27), yields the Lorentz equation of motion (2.67).

2.11 Lagrangian and Hamiltonian equations for continuous systems

Thus far, we have been concerned with discrete dynamical systems which possess a finite number of degrees of freedom. Let us now extend the equations of AM to systems exhibiting a continuous set of dynamical variables. This extension is necessary for the dynamical description of a Bose-Einstein condensate, where the configuration of the system is determined by the value of the matter-field at *all* points of space. Hence, we have a degree of freedom at each point of space and the Lagrangian is now given by the integral $L=\int d^3\mathbf{r}\mathcal{L}$, where the function $\mathcal{L}$ is the *Lagrangian density* of the system. Notice that the Lagrangian is no longer a function, but a functional, a map from functions to $\mathbb{R}$. When the system is comprised of a collection of fields $\phi_\alpha\equiv\phi_1,\cdots,\phi_N$, the Lagrangian then appears as a functional of ϕ_α and $\dot{\phi}_\alpha$, in the form

$$L\left[\phi_\alpha,\dot{\phi}_\alpha\right]=\int d^3\mathbf{r}\mathcal{L}\left(\phi_\alpha,\dot{\phi}_\alpha,\boldsymbol{\nabla}\phi_\alpha\right), \tag{2.70}$$

where we have assumed that $\mathcal{L}$ depends explicitly on the gradient of the field components, but not on higher order spatial derivatives[7]. Note that the inclusion of such higher order terms does not affect the form of the EL field equations (2.73), insofar as the functional derivatives (2.72) are modified accordingly. The Lagrangian equations of

[7]The dependence of $\mathcal{L}$ on the spatial derivatives signifies that the motion of the field at a given point of space is coupled to that at neighbouring points of space. This endows the field with the characteristic of a medium in which disturbances are propagated.

motion of the field follow from Hamilton's principle of stationary action, which yields

$$\frac{\partial \mathcal{L}}{\partial \phi_k} - \boldsymbol{\nabla} \cdot \left(\frac{\partial \mathcal{L}}{\partial \left(\boldsymbol{\nabla} \phi_k \right)} \right) - \frac{\partial}{\partial t} \left(\frac{\partial \mathcal{L}}{\partial \dot{\phi}_k} \right) = 0. \tag{2.71}$$

These may be rendered into the form of the EL equations (2.2) for a discrete system, by introducing the *functional* or *variational derivatives* applied to a functional $F\left[\phi\right] = \int d^3 r \mathcal{F}\left(\phi, \boldsymbol{\nabla}\phi, \dot{\phi}\right)$ of a field ϕ, which read [38, 40, 44, 45]

$$\begin{aligned} \frac{\delta F}{\delta \phi} &= \frac{\partial \mathcal{F}}{\partial \phi} - \boldsymbol{\nabla} \cdot \left(\frac{\partial \mathcal{F}}{\partial \left(\boldsymbol{\nabla} \phi \right)} \right), \\ \frac{\delta F}{\delta \dot{\phi}} &= \frac{\partial \mathcal{F}}{\partial \dot{\phi}}. \end{aligned} \tag{2.72}$$

Hence, the EL field Eqs. (2.71) may be written in terms of the total Lagrangian (2.70), in the form

$$\frac{\delta L}{\delta \phi_k} - \frac{\partial}{\partial t} \left(\frac{\delta L}{\delta \dot{\phi}_k} \right) = 0. \tag{2.73}$$

The generalisation of the canonical equations of motion (2.10) to continuous systems is also straight-forward. To begin with, we define the momenta conjugate to the field components, as

$$\pi_i \left(\mathbf{r} \right) = \frac{\delta L}{\delta \dot{\phi}_i \left(\mathbf{r} \right)}. \tag{2.74}$$

The Hamiltonian of the system may be constructed from the Lagrangian in an identical fashion to the discrete case, through the Legendre transform

$$\begin{aligned} H\left[\phi_\alpha, \pi_\alpha\right] &= \int d^3 \mathbf{r} \sum_{i=1}^{N} \pi_i \dot{\phi}_i - L\left[\phi_\alpha, \dot{\phi}_\alpha\right] \\ &= \int d^3 \mathbf{r} \mathcal{H}\left(\phi_\alpha, \boldsymbol{\nabla}\phi_\alpha, \pi_\alpha\right), \end{aligned} \tag{2.75}$$

where

$$\mathcal{H} = \sum_i \pi_i \dot{\phi}_i - \mathcal{L}, \tag{2.76}$$

is the *Hamiltonian density*. The canonical field equations of motion may be obtained by normalising the action integral to the canonical form

$$S = \int dt \left[\int d^3 \mathbf{r} \sum_i \pi_i \dot{\phi}_i - H\left[\phi_\alpha, \pi_\alpha\right] \right]. \tag{2.77}$$

Requiring that Eq. (2.77) assume a stationary value for arbitrary variations of the ϕ_i and π_i, yields the system of canonical equations [40, 44, 45]

$$\begin{aligned} \dot{\phi}_i &= \frac{\delta H}{\delta \pi_i}, \\ \dot{\pi}_i &= -\frac{\delta H}{\delta \phi_i}. \end{aligned} \tag{2.78}$$

Note that these equations hold only for non-singular systems where the determinant of the Hessian matrix is non-vanishing. In the case of a singular system, the fields ϕ_i and momenta π_i become restricted by certain kinematic constraint equations and as a consequence, may not be varied independently of each other. In fact, both the Schrödinger and Dirac fields of a quantum mechanical particle exhibit this singular property. This stems from the Lagrangian of these systems being first order in the time derivatives of the field. We will consider this point in greater detail further in section 3.2.3 when we construct a hydrodynamic canonical formalism for the Gross-Pitaevskii field.

Chapter 3

Hydrodynamic formalisms for quantum fluids

3.1 Bose-Einstein condensates

3.1.1 Introduction

In this section, we give a brief overview of the microscopic theory underpinning a dilute gas of Bose particles. When the number N of particles in a quantum mechanical system becomes large, the system behaves asymptotically as a field. In order to describe the physics of the many-body system, it is convenient to adopt the formalism of second quantisation. In this framework, the field $\hat{\Psi}$ takes on the role of an operator which acts on the many-particle Hilbert space[1]. The Hamiltonian of the dilute bosonic gas may be represented in position space, as [5, 6, 46–48]

$$\hat{H} = \int d^3\mathbf{r} \left[\hat{\Psi}^\dagger (\mathbf{r}) \left(-\frac{\hbar^2}{2m} \boldsymbol{\nabla}^2 + V_{ext} (\mathbf{r}) \right) \hat{\Psi} (\mathbf{r}) \right] + \frac{1}{2} \int d^3\mathbf{r} d^3\mathbf{r}' \left[\hat{\Psi}^\dagger (\mathbf{r}) \hat{\Psi}^\dagger (\mathbf{r}') \mathcal{U} (\mathbf{r}' - \mathbf{r}) \hat{\Psi} (\mathbf{r}') \hat{\Psi} (\mathbf{r}) \right], \quad (3.1)$$

where the boson field operator $\hat{\Psi}^\dagger (\mathbf{r})$ ($\hat{\Psi} (\mathbf{r})$) adds (removes) a particle at point $\mathbf{r}$, m is the mass of one of the bosons, V_{ext} is an external potential and $\mathcal{U}$ is a two-body interaction potential. The field operators satisfy the well-known commutation relations

$$\left[\hat{\Psi} (\mathbf{r}) , \hat{\Psi}^\dagger (\mathbf{r}') \right] = \delta (\mathbf{r} - \mathbf{r}') , \qquad \left[\hat{\Psi} (\mathbf{r}) , \hat{\Psi} (\mathbf{r}') \right] = 0. \quad (3.2)$$

[1] Here we have assumed that no internal degrees of freedom (such as spin) play a role in the physical description of the system.

The first integral in Eq. (3.1) is the single particle Hamiltonian, while the second describes pairwise interactions between the particles. Let $\phi_0(\mathbf{r}), \phi_1(\mathbf{r}), \cdots$ denote a complete orthonormal set of single particle wavefunctions. It is sometimes useful to expand the field operators $\hat{\Psi}$ and $\hat{\Psi}^\dagger$ in terms of the operators $\hat{a}_i$ and $\hat{a}_i^\dagger$ which remove and add a particle with wavefunction ϕ_i:

$$\hat{\Psi}(\mathbf{r}) = \sum_i \phi_i(\mathbf{r})\,\hat{a}_i, \qquad \hat{\Psi}^\dagger(\mathbf{r}) = \sum_i \phi_i^*(\mathbf{r})\,\hat{a}_i^\dagger. \tag{3.3}$$

The linear vector space formed by the single particle states is the Fock space $|n_0, n_1, \cdots\rangle$ [49, 50] and the state of the system is represented by a vector in this space. Here, n_k indicates the occupancy of the single particle state ϕ_k, which is to say the eigenvalue of the number operator $\hat{n}_k = \hat{a}_k^\dagger \hat{a}_k$. As such, the action of the single particle operators on a state in Fock space, is defined according to

$$\hat{a}_k\,|n_0, \cdots, n_k, \cdots\rangle = \sqrt{n_k}\,|n_0, \cdots, n_k - 1, \cdots\rangle\,, \tag{3.4}$$

$$\hat{a}_k^\dagger\,|n_0, \cdots, n_k, \cdots\rangle = \sqrt{n_k + 1}\,|n_0, \cdots, n_k + 1, \cdots\rangle\,. \tag{3.5}$$

Note that the operators must satisfy

$$\left[\hat{a}_i, \hat{a}_j^\dagger\right] = \delta_{ij}, \qquad [\hat{a}_i, \hat{a}_j] = 0, \tag{3.6}$$

in order for the commutation relations (3.2) to hold.

It will also be useful to work in the Heisenberg representation. Here one describes the time-evolution of expectation values by evolving each operator, keeping the state of the system fixed in time. In the Hamiltonian formalism of analytical mechanics, we saw that a dynamical phase space variable $X(q, p)$ develops in time according to the Poisson bracket $\{X, H\}_{q,p}$. In the Heisenberg representation, the time-evolution of an operator $\hat{X}$, follows from the equation of motion

$$i\hbar \frac{\partial \hat{X}}{\partial t} = \left[\hat{X}(t), \hat{H}(t)\right]. \tag{3.7}$$

When the Hamiltonian does not explicitly depend on time, the time-evolved operator resulting from Eq. (3.7), is given by

$$\hat{X}(t) = e^{\frac{i}{\hbar}\hat{H}t}\hat{X}e^{-\frac{i}{\hbar}\hat{H}t}, \tag{3.8}$$

where $\hat{X} \equiv \hat{X}(0)$. As an example, let us consider a free system of bosons in a box of volume V with periodic boundary conditions. In this case, the particles occupy plane wave states and the field operator expansion (3.3), reads

$$\hat{\Psi}(\mathbf{r}) = \frac{1}{\sqrt{V}} \sum_{\mathbf{p}} e^{i\mathbf{p}\cdot\mathbf{r}} \hat{a}_{\mathbf{p}}, \qquad \hat{\Psi}^{\dagger}(\mathbf{r}) = \frac{1}{\sqrt{V}} \sum_{\mathbf{p}} e^{-i\mathbf{p}\cdot\mathbf{r}} \hat{a}^{\dagger}_{\mathbf{p}}. \tag{3.9}$$

Represented in terms of these momentum modes, the Hamiltonian is

$$\hat{H} = \sum_{\mathbf{p}} \epsilon_{\mathbf{p}} \hat{a}^{\dagger}_{\mathbf{p}} \hat{a}_{\mathbf{p}}, \tag{3.10}$$

where $\epsilon_{\mathbf{p}} = \mathbf{p}^2/2m$. The time-evolved mode operators may be obtained by substituting the above Hamiltonian into Eq. (3.7), which leads to the equation of motion

$$\frac{\partial \hat{a}_{\mathbf{p}}}{\partial t} = -\frac{i}{\hbar} \epsilon_{\mathbf{p}} \hat{a}_{\mathbf{p}}. \tag{3.11}$$

Hence, we find that

$$\hat{a}_{\mathbf{p}}(t) = e^{-\frac{i}{\hbar}\epsilon_{\mathbf{p}} t} \hat{a}_{\mathbf{p}}, \qquad \hat{a}^{\dagger}_{\mathbf{p}}(t) = e^{\frac{i}{\hbar}\epsilon_{\mathbf{p}} t} \hat{a}^{\dagger}_{\mathbf{p}}, \tag{3.12}$$

such that the field operators from Eq. (3.9) take the time-dependence

$$\hat{\Psi}(\mathbf{r}, t) = \frac{1}{\sqrt{V}} \sum_{\mathbf{p}} e^{i(\mathbf{p}\cdot\mathbf{r} - \epsilon_{\mathbf{p}} t)} \hat{a}_{\mathbf{p}}, \qquad \hat{\Psi}^{\dagger}(\mathbf{r}, t) = \frac{1}{\sqrt{V}} \sum_{\mathbf{p}} e^{-i(\mathbf{p}\cdot\mathbf{r} - \epsilon_{\mathbf{p}} t)} \hat{a}^{\dagger}_{\mathbf{p}}. \tag{3.13}$$

3.1.2 The condensate

The robust character of superfluid systems rests on the manifestation of a condensate at sufficiently low temperatures, which is to say, a macroscopic occupation of the single particle ground state of the system. If we denote the number of condensed particles by N_0 and $N_0 \gg 1$, states with N_0 and $N_0 + 1$ particles correspond essentially to the same state and the operators $\hat{a}_0$ and $\hat{a}^{\dagger}_0$ may be treated as complex numbers with value $\hat{a}_0 = \hat{a}^{\dagger}_0 = \sqrt{N_0}$. It is interesting to consider the behaviour of the single-particle density matrix, which can be expressed as a correlation function

$$\rho_1(\mathbf{r}, \mathbf{r}') = \left\langle \hat{\Psi}^{\dagger}(\mathbf{r}) \hat{\Psi}(\mathbf{r}') \right\rangle, \tag{3.14}$$

between the fields at points $\mathbf{r}$ and $\mathbf{r}'$, which is essentially the amplitude for removing a particle from equilibrium at $\mathbf{r}'$ and replacing it at $\mathbf{r}$. Note that the expectation value is taken in the grand canonical ensemble. The diagonal elements list the density $\rho_1(\mathbf{r}) = |\Psi(\mathbf{r})|^2$ of the condensate. For normal systems, the off-diagonal elements vanish as $|\mathbf{r} - \mathbf{r}'| \to \infty$ [51]. However, for a Bose gas of particles at sufficiently low temperatures, the correlation function takes on a finite value irrespective of the space separation. To see this, let us consider the free system of Bosons with Hamiltonian (3.10) and substitute the mode operators (3.9) into the density matrix (3.14), which gives

$$\rho_1(\mathbf{r}, \mathbf{r}') = \frac{1}{V} \sum_{\mathbf{p}} e^{i\mathbf{p}\cdot(\mathbf{r}'-\mathbf{r})} \left\langle \hat{a}_{\mathbf{p}}^{\dagger} \hat{a}_{\mathbf{p}} \right\rangle, \tag{3.15}$$

Now, $N_{\mathbf{p}} = \left\langle \hat{a}_{\mathbf{p}}^{\dagger} \hat{a}_{\mathbf{p}} \right\rangle$ is the expectation value of the number of particles occupying the $\mathbf{p}$ momentum state, which, for a system of Bosons in the grand canonical ensemble, is given by

$$N_{\mathbf{p}} = \frac{1}{e^{\beta(\epsilon_{\mathbf{p}} - \mu)} - 1}, \tag{3.16}$$

where $\beta = 1/(kT)$ and μ is the chemical potential. At zero temperature, all particles occupy the $p = 0$ state: $N_0 = N$ and $N_{\mathbf{p}} = 0$ for $p \neq 0$. Hence, the correlation function (3.15) remains constant:

$$\rho_1(\mathbf{r}, \mathbf{r}') = \frac{N}{V} = n. \tag{3.17}$$

As was shown by Onsager and Penrose [52], this same structure persists in the case of a weakly interacting Bose system, where the off-diagonal elements of the density matrix furnish the following criterion for Bose-Einstein condensation:

$$\left\langle \hat{\Psi}^{\dagger}(\mathbf{r}) \hat{\Psi}(\mathbf{r}') \right\rangle \xrightarrow{|\mathbf{r}-\mathbf{r}'|\to\infty} \Psi_0^*(\mathbf{r}) \Psi_0(\mathbf{r}'), \tag{3.18}$$

where $\Psi_0(\mathbf{r}) = \left\langle \hat{\Psi}(\mathbf{r}) \right\rangle$ is the condensate wavefunction, a complex valued function. The field operator may then be written as the sum of a macroscopic condensed component $\phi_0 \hat{a}_0$ and an operator representing the non-condensed fraction of Bosons:

$$\hat{\Psi}(\mathbf{r}) = \Psi_0(\mathbf{r}) + \delta\hat{\Psi}(\mathbf{r}), \tag{3.19}$$

where $\Psi_0(\mathbf{r}) = \sqrt{N_0}\phi_0(\mathbf{r})$ and $\delta\hat{\Psi}(\mathbf{r}) = \sum_{i\neq 0} \phi_i(\mathbf{r}) \hat{a}_i$ is the depletion of the condensate. Therefore, when the number of condensed particles becomes macroscopic at $T = 0K$, the condensate wavefunction takes on a physical meaning which extends into the classical

domain by virtue of the existence of a single phase function common to all particles in the system. This feature is central to the manifestation of Bose-Einstein condensation and the observation of quantum phenomena at the macroscopic level.

3.1.3 The Gross-Pitaevskii equation

At sufficiently low temperatures and weak interactions, we may discard the field fluctuations and retain only the condensate wavefunction. In effect, this is equivalent to treating the many-body wavefunction of the system as a classical complex scalar field with a well-defined phase [45, 53]. Further, we will consider a variety of formalisms for this classical field. In this low-temperature regime, interparticle collisions are dominated by s-wave scattering [5, 54] and we may model these interactions using a pseudopotential [54] $\mathcal{U}(\mathbf{r}-\mathbf{r}') = g\delta(\mathbf{r}-\mathbf{r}')$, with $g = 4\pi\hbar^2 a/m$, where a is the scattering length. Substituting this potential into Eq. (3.1), the Hamiltonian then reads

$$\hat{H} = \int d^3\mathbf{r} \left[\hat{\Psi}^\dagger(\mathbf{r}) \left(-\frac{\hbar^2}{2m}\boldsymbol{\nabla}^2 + V_{ext}(\mathbf{r}) \right) \hat{\Psi}(\mathbf{r}) + \frac{g}{2}\hat{\Psi}^\dagger(\mathbf{r})\,\hat{\Psi}^\dagger(\mathbf{r})\,\hat{\Psi}(\mathbf{r})\,\hat{\Psi}(\mathbf{r}) \right], \quad (3.20)$$

and taking the expectation value of the Heisenberg equation of motion (3.7) for the operator $\hat{\Psi}$, leads to the nonlinear Schrödinger equation [6, 55–58]

$$i\hbar\frac{\partial}{\partial t}\Psi_0(\mathbf{r},t) = \left(-\frac{\hbar^2}{2m}\boldsymbol{\nabla}^2 + V_{ext} + g\left|\Psi_0\right|^2 \right)\Psi_0(\mathbf{r},t), \quad (3.21)$$

known as the *Gross-Pitaevskii* (GP) equation. It differs from the usual Schrödinger equation through the occurrence of a nonlinear interaction term $g|\Psi_0|^2$ which is proportional to the density of atoms occupying the condensate. The effect of this density nonlinearity is to suppress spatial density variations of the condensate wavefunction.

Alternatively, the Gross-Pitaevskii equation may be retrieved as a mean field approximation to the true dynamics of the system, by treating the many-body wavefunction as a product of identical single particular states:

$$\Psi(\mathbf{r}_1, \mathbf{r}_2, \cdots, \mathbf{r}_N) = \prod_{i=1}^{N} \phi(\mathbf{r}_i), \quad (3.22)$$

where $\int d^3\mathbf{r}\left|\phi\left(\mathbf{r}\right)\right|^2 = 1$. To do so, it is convenient to introduce the Lagrangian of the many-body system [59–63]

$$L = \int \prod_{i=1}^{N} d^3\mathbf{r}_i \Psi^* \left(i\hbar\partial_t - \hat{H}\right)\Psi, \tag{3.23}$$

whose variation with respect to Ψ^* yields the many-body Schrödinger equation. This variational principle is originally due to Frenkel and Dirac [59, 60]. We refer the reader to [62] for a general review of quantum variational principles. In the case of a dilute cloud of Bose atoms with weak contact interactions, the Hamiltonian from Eq. (3.23), takes the form

$$\hat{H} = \sum_i \left(\frac{\hat{\mathbf{p}}_i^2}{2m} + V\left(\mathbf{r}_i\right)\right) + \sum_{i\neq j} g\delta\left(\mathbf{r}_i - \mathbf{r}_j\right) = \sum_i \hat{H}_i + \sum_{i\neq j} \hat{H}_{ij}, \tag{3.24}$$

where we have denoted the external potential by V. Inserting Eq. (3.22) for Ψ into Eq. (3.23), the mean field Lagrangian comprises three parts: $L_{MF} = L_t + \sum_i L_i + \sum_{i\neq j} L_{ij}$, where the first of these, is

$$L_t = \int \prod_{i=1}^{N} d^3\mathbf{r}_i \phi^*\left(\mathbf{r}_i\right) i\hbar\partial_t\phi\left(\mathbf{r}_i\right) = N\int d^3\mathbf{r}\phi^*\left(\mathbf{r}\right) i\hbar\partial_t\phi\left(\mathbf{r}\right). \tag{3.25}$$

The remaining terms associated with $\hat{H}_i$ and $\hat{H}_{ij}$, describe one and two particle expectation values respectively. Indeed, since $\hat{H}_i$ acts only on $\phi\left(\mathbf{r}_i\right)$, we have

$$L_i = -\int \prod_{k=1}^{N} d^3\mathbf{r}_k \phi^*\left(\mathbf{r}_k\right)\hat{H}_i\phi\left(\mathbf{r}_k\right) = -\int d^3\mathbf{r}_i \phi^*\left(\mathbf{r}_i\right)\hat{H}_i\phi\left(\mathbf{r}_i\right). \tag{3.26}$$

Therefore, the total contribution of the single particle Hamiltonian to the Lagrangian, is then

$$\begin{aligned}\sum_{i=1}^{N} L_i &= -\sum_{i=1}^{N}\int d^3\mathbf{r}\phi^*\left(\mathbf{r}\right)\left(-\frac{\hbar^2}{2m}\nabla^2 + V\left(\mathbf{r}\right)\right)\phi\left(\mathbf{r}\right) \\ &= -N\int d^3\mathbf{r}\left(\frac{\hbar^2}{2m}\left|\boldsymbol{\nabla}\phi\right|^2 + V\left|\phi\right|^2\right),\end{aligned} \tag{3.27}$$

where we have integrated by parts accordingly. Similarly, since $\hat{H}_{ij}$ acts only on $\phi(\mathbf{r}_i)$ and $\phi(\mathbf{r}_j)$, we find

$$L_{ij} = -\int \prod_{k=1}^{N} d^3\mathbf{r}_k \phi^*(\mathbf{r}_k)\, \hat{H}_{ij}\phi(\mathbf{r}_k) = -\int d^3\mathbf{r}_i d^3\mathbf{r}_j \phi^*(\mathbf{r}_i)\,\phi^*(\mathbf{r}_j)\,\hat{H}_{ij}\phi(\mathbf{r}_i)\,\phi(\mathbf{r}_j)\,, \tag{3.28}$$

so that

$$\begin{aligned}\sum_{i\neq j}^{N} L_{ij} &= -\sum_{i\neq j}^{N}\int d^3\mathbf{r} d^3\mathbf{r}' \phi^*(\mathbf{r})\,\phi^*(\mathbf{r}')\, g\delta(\mathbf{r}-\mathbf{r}')\,\phi(\mathbf{r})\,\phi(\mathbf{r}') \\ &= -\frac{g}{2}N(N-1)\int d^3\mathbf{r}\,|\phi|^4\,. \end{aligned} \tag{3.29}$$

Normalising the macroscopic condensate wavefunction to $\psi(\mathbf{r}) = \sqrt{N}\phi(\mathbf{r})$, the mean field Lagrangian of system, becomes

$$L_{MF} = \int d^3\mathbf{r}\psi^*\left(i\hbar\partial_t - \hat{H}_{MF}\right)\psi, \tag{3.30}$$

where $\hat{H}_{MF}$ acts on this macroscopic wavefunction, as

$$\hat{H}_{MF}\psi = \left(-\frac{\hbar^2}{2m}\nabla^2 + V + \frac{g}{2}|\psi|^2\right)\psi. \tag{3.31}$$

In accordance with Eqs. (3.30) and (3.31), the mean field Lagrangian density function presents itself, as

$$\mathcal{L}_{MF} = \psi^* i\hbar\dot{\psi} - \frac{\hbar^2}{2m}\boldsymbol{\nabla}\psi^*\cdot\boldsymbol{\nabla}\psi - V|\psi|^2 - \frac{g}{2}|\psi|^4\,, \tag{3.32}$$

where we have denoted partial differentiation with respect to time by a dot. Note that the Lagrangian density is a function, whereas the Lagrangian

$$L_{MF}\left[\psi,\psi^*,\dot{\psi},\dot{\psi}^*\right] = \int d^3\mathbf{r}\mathcal{L}_{MF}\left(\psi,\boldsymbol{\nabla}\psi,\psi^*,\boldsymbol{\nabla}\psi^*,\dot{\psi},\dot{\psi}^*\right), \tag{3.33}$$

is a functional. Observe further that $\mathcal{L}_{MF}$ from Eq. (3.32), is not real on account of the first term. In general, the action associated with a non-Hermitian Lagrangian, is a complex quantity, $S \equiv S_c = S_r + iS_i$, where $S_r, S_i \in \mathbb{R}$. Although hermiticity is not a requirement in deriving the Gross-Pitaevskii equation (see for instance [61, 64]), notice that a stationary action principle for S_c is equivalent to two stationary action principles

for S_r and S_i, leading to two sets of EL field equations. By performing a Madelung transformation (3.38), the reader may verify that, for $\mathcal{L}_{MF}$ from Eq. (3.32), the EL equations associated with L_i give rise to the equation $0 = 0$, both for ρ and θ. This superfluous set of field equations may be eliminated from the problem by performing the gauge transformation, $\mathcal{L}_{MF} \to \mathcal{L}_{MF} - \frac{i\hbar}{2}\partial_t(\psi^*\psi)$, which gives

$$\mathcal{L}_{MF} = \frac{i\hbar}{2}\left(\psi^*\dot{\psi} - \psi\dot{\psi}^*\right) - \frac{\hbar^2}{2m}\boldsymbol{\nabla}\psi\cdot\boldsymbol{\nabla}\psi^* - \frac{g}{2}|\psi|^4 - V|\psi|^2. \tag{3.34}$$

The Gross-Pitaevskii equation may now be derived by requiring that the action $S[\psi,\psi^*] = \int dt L_{MF}$, be stationary with respect to variations of the fields $\psi(\mathbf{r})$ and $\psi^*(\mathbf{r})$. Inserting the Lagrangian density (3.34) into the EL field equation (2.73) for ψ^*, yields the Gross-Pitaevskii equation (3.21), while carrying out the same procedure for ψ, yields the complex conjugate of the Gross-Pitaevskii equation.

3.1.4 The Gross-Pitaevskii field as a singular Lagrangian system

We have seen that at zero temperature, the state of a weakly interacting dilute Bose gas is well described by a complex wavefunction, whose time evolution is governed by the Gross-Pitaevskii equation (3.21). Notice how a complex field variable ψ automatically requires that $\mathcal{L}$ also depend on ψ^* in order for the action to be real [45]. Yet, the fact that the Gross-Pitaevskii equation is first order in time, signifies that ψ, ψ^*, $\dot{\psi}$ and $\dot{\psi}^*$ are not independent and that an excess of dynamical variables are contained in the Lagrangian [45, 61]. As we shall soon learn, this is invariably the situation when the Lagrangian density is linear in the time derivatives of the fields. However, at first sight this should not come as surprise, since the dynamical state of the field is completely specified by its configuration ψ, whereas the Lagrangian equations of motion are second order in time [45]. As a consequence, a mechanical field governed by a first order Lagrangian must comprise at least two real components in order for the configuration of the field to be specified at all times, some combination of these serving as field velocity. When the dynamical state of a field can be completely specified by a single complex variable ψ, the remaining 6 real variables contained in $\psi^*, \dot{\psi}$ and $\dot{\psi}^*$, are clearly not dynamically independent of the components of ψ, by definition. As a starting point to eliminating redundant variables, let us now examine more closely which characteristic

makes the Gross-Pitaevskii field a singular Lagrangian system.

Nonrelativistic Bose-condensed quantum fluids are generally described by multi-component Lagrangian densities $\mathcal{L}\left(\phi_\alpha, \boldsymbol{\nabla}\phi_\alpha, \dot{\phi}_\alpha\right)$ which are linear in the time derivatives of the fields, where $\phi_\alpha \equiv \phi_1, \cdots, \phi_n$. In this situation, the total Lagrangian of the system may be presented as

$$L\left[\phi_\alpha, \dot{\phi}_\alpha\right] = \int d^3\mathbf{r} \sum_i \mathcal{A}_i\left(\phi_\alpha, \boldsymbol{\nabla}\phi_\alpha\right)\dot{\phi}_i - V\left[\phi_\alpha\right], \tag{3.35}$$

where V is an interaction functional of the field components:

$$V\left[\phi_\alpha\right] = \int d^3\mathbf{r}\mathcal{V}\left(\phi_\alpha, \boldsymbol{\nabla}\phi_\alpha\right). \tag{3.36}$$

The key point to appreciate is that when L is of the form (3.35), the canonical momenta are given as functions of ϕ_α and $\boldsymbol{\nabla}\phi_\alpha$ and as such, can not be treated as independent dynamical variables. Indeed, notice that if the total Hamiltonian of the system is defined in the usual fashion, according to the Legendre transform (2.75), the field velocities $\dot{\phi}_i$ do not appear on the right hand side of (2.75) as they would typically, given that $\pi_i = \mathcal{A}_i\left(\phi_\alpha, \boldsymbol{\nabla}\phi_\alpha\right)$ when $\mathcal{L}$ is first order in the $\dot{\phi}_i$. Hence, the Hamiltonian reduces to $H = V$, namely, the interaction functional (3.36) and it is not possible to invert $\dot{\phi}_i$ as a function of ϕ_α and π_α, since

$$\frac{\partial^2\mathcal{L}}{\partial\dot{\phi}_j\partial\dot{\phi}_i} = \frac{\partial\mathcal{A}_i}{\partial\dot{\phi}_j} = 0, \tag{3.37}$$

at every point of space. Dynamical systems with this property are called *singular Lagrangian systems* or *constrained Hamiltonian systems* [65, 66]. Two equivalent [67] methods have been devised to eliminate redundant variables and construct a reduced phase space for such systems: the *Dirac-Bergmann* (DB) method [66, 68–76] and the *Faddeev-Jackiw* (FJ) method [72, 77–80]. In the particular case of the Schrödinger field, an alternative route is made available by performing a suitable canonical transformation [45,81], where one begins by decomposing the field into real and imaginary parts and then supplements the resulting Lagrangian by a total time derivative to obtain a single pair of real conjugate variables. Several other field transformations yielding Schrödinger's equation from a canonical field equation, can also be found in the literature [61, 82]. However, these depend either on one or two complex pairs of conjugate variables, meaning redundant variables have not entirely been eliminated. For a review of these

formalisms, and an application of the DB and the FJ methods to the Schrödinger field, see [64].

In our study, we take a different approach and derive a canonical formalism for the matter-field in terms of the single pair of real variables (ρ, θ), namely the modulus and the phase of the Gross-Pitaevskii field ψ. These constitute the natural pair of variables connecting the field and fluid descriptions of a condensate. Accordingly, we shall refer to this formalism as the "hydrodynamic canonical formalism". Note that it is absent from review [64], but well-known to classical and quantum hydrodynamics [83–89]. However, in the literature (see [5, 46, 88, 90, 91] for instance), the canonical equations of the hydrodynamic field are all too often postulated a priori, on account of the fact that they yield the correct wave equations for the field components. Here, we present an alternative, original derivation of the problem by treating the Gross-Pitaevskii field as a singular Lagrangian system and applying both the DB and FJ methods.

3.2 Hydrodynamic formalisms for the Gross-Pitaevskii field

3.2.1 The hydrodynamic variables

Following up on previous discussions, let us represent the Gross-Pitaevskii field ψ in terms of the two-component real field (ρ, θ), defined according to

$$\psi = \sqrt{\rho} e^{i\frac{\theta}{\hbar}}, \qquad \psi^* = \sqrt{\rho} e^{-i\frac{\theta}{\hbar}}, \tag{3.38}$$

and treat these components as the independent variables subject to the process of variation. Note that θ has the dimension of action, measured in units of $\hbar$. For a macroscopic occupation of the superfluid state, $\rho = \psi\psi^*$ represents the condensate particle density and θ determines the superfluid flow. This 'superflow' is of the potential type (3.41), depicting an irrotational velocity field which can be obtained in terms of θ, by substituting Eq. (3.38) into the following expression for the current density:

$$\mathbf{J} = \frac{i\hbar}{2m} \left(\psi \boldsymbol{\nabla} \psi^* - \psi^* \boldsymbol{\nabla} \psi \right). \tag{3.39}$$

This yields the more perspicuous form

$$\mathbf{J} = \frac{\rho}{m}\boldsymbol{\nabla}\theta. \tag{3.40}$$

Given that the fluid occupies a simply-connected region whilst in the superfluid state, Eq. (3.40) allows for the identification of θ/m as the potential of the velocity field

$$\mathbf{v} = \frac{\boldsymbol{\nabla}\theta}{m}. \tag{3.41}$$

Thus, regardless of the physical interpretation of the field ψ, there remains from a mathematical perspective, a clear role played by the fields ρ and θ in establishing matter-wave dynamics: the first of these defines the distribution or amplitude of the matter-field over physical space, while the second dictates the flow of this distribution. From a hydrodynamical perspective, given a density distribution $\rho(\mathbf{r}, t_0)$ and phase function $\theta(\mathbf{r}, t_0)$ at time t_0 over physical space, the density associated with every elementary volume element of fluid simply flows along a curve which is tangent at every point to the local directions of maximally increasing phase. If we imagined a situation where we had configured the phase function of the fluid over space, the gradient of the phase carries the density distribution along a continuous set of integral curves of the velocity field. Although the form of these streamlines depend on a velocity field which is also generally changing in time, their tangents remain well defined at any given instant of time. The ensemble of such curves then serves as a representation of the solution to the motion of the fluid. In an identical fashion to the classical domain where the flow of the phase fluid is directed along the normal to the surface of constant action, quantum mechanical flow is directed along the normal to the surface of constant phase. As such, we may already anticipate that the quantum phase plays a role analogous to the generating function of a finite canonical transformation dictating the dynamics of classical systems, where we would expect the wave equation for θ to take on the form of a HJ-type equation.

3.2.2 Lagrangian formalism

Let us now derive the wave equations for the field components. These may be obtained from the EL field equations by substituting the polar form (3.38) of the condensate wavefunction into the Lagrangian density (3.34). Doing so, we find the following form

for $\mathcal{L}$ in terms of the new variables:

$$\mathcal{L} = -\rho\left(\dot{\theta} + \frac{(\boldsymbol{\nabla}\theta)^2}{2m} + \frac{g}{2}\rho + V\right) - \frac{\hbar^2}{8m\rho}(\boldsymbol{\nabla}\rho)^2. \tag{3.42}$$

The EL field equations (2.73) for the field components ρ and θ, yield respectively, the wave equations

$$\partial_t\theta + \frac{1}{2}mv^2 + g\rho + V + Q = 0, \tag{3.43}$$

$$\partial_t\rho + \boldsymbol{\nabla}\cdot\mathbf{J} = 0, \tag{3.44}$$

where $v = |\mathbf{v}|$ is the modulus of the superfluid velocity field (3.41), $\mathbf{J}$ is given by Eq. (3.40) and

$$Q = -\frac{\hbar^2}{2m}\frac{\nabla^2\sqrt{\rho}}{\sqrt{\rho}}, \tag{3.45}$$

is the *quantum potential* or *Bohm potential* [92–95]. Although, some texts refer to Q as the "quantum pressure", we shall reserve this name for the diagonal components of the stress tensor associated with Q, which we introduce further in chapter 5. Equation (3.44) takes the form of an equation of continuity and expresses the conservation of superfluid mass, while Eq. (3.43) may be interpreted as a quantum Hamilton-Jacobi (QHJ) equation and expresses the conservation of mechanical momentum. This pair of equations are coupled to each other through the occurrence of θ in the current density in Eq. (3.44) and ρ in the quantum potential and nonlinear interaction term in Eq. (3.43). They are entirely equivalent to the Gross-Pitaevskii Eq. (3.21), where relation (3.38) provides a mapping between both sets of equations known as a *Madelung transformation* [96].

3.2.3 Canonical formalism

Furthering our investigation of the different available field formalisms for quantum fluids, we now turn our attention to the construction of a hydrodynamical canonical formalism for the field. In particular, we will show that the reduced phase space of the system comprises the single pair of conjugate variables (ρ, θ), which are dynamically

governed by the following canonical field equations:

$$\dot{\rho}\left(\mathbf{r}\right)=\frac{\delta H}{\delta\theta\left(\mathbf{r}\right)}, \tag{3.46}$$

$$\dot{\theta}\left(\mathbf{r}\right)=-\frac{\delta H}{\delta\rho\left(\mathbf{r}\right)}, \tag{3.47}$$

where H is the total canonical Hamiltonian of the field, introduced further through Eq. (3.89). Inspecting the form of this Hamiltonian density, we may observe that the pair of hydrodynamical wave equations (3.44) and (3.43), emerge as solutions of the set of canonical field equations (3.47). However, notice that this presupposes that ρ and θ are conjugate variables to be begin with. In our study, this property arises as a consequence of the phase space reduction to the physical dynamical variables of the theory. It is also worth mentioning that the canonical equations (3.47) appear in configuration space ensembles of the Schrödinger system [97–99]. Finally, note that the conjugate nature of the hydrodynamic variables of a nonlinear quantum fluid, implies that the Poisson bracket of two dynamical variables f and g on phase space, is of the form [100–102]

$$\left\{f\left(\mathbf{x}\right),g\left(\mathbf{y}\right)\right\}=\int d^{3}\mathbf{r}\left(\frac{\delta f\left(\mathbf{x}\right)}{\delta\rho\left(\mathbf{r}\right)}\frac{\delta g\left(\mathbf{y}\right)}{\delta\theta\left(\mathbf{r}\right)}-\frac{\delta f\left(\mathbf{x}\right)}{\delta\theta\left(\mathbf{r}\right)}\frac{\delta g\left(\mathbf{y}\right)}{\delta\rho\left(\mathbf{r}\right)}\right)\equiv\left\{f,g\right\}_{\rho,\theta}. \tag{3.48}$$

In the following section, we retrieve the above expression for the Poisson bracket, as the reduced Dirac bracket on the full phase.

3.2.3.1 The Dirac-Bergmann algorithm

As a starting point to applying the DB algorithm, we shall exploit the fact that the dynamics of the system are left unchanged by the addition of a total time-derivative to the Lagrangian density (3.42), which we transform according to

$$\mathcal{L}\rightarrow\mathcal{L}+\frac{d}{dt}\left(\frac{\rho\theta}{2}\right)=\frac{1}{2}\left(\theta\dot{\rho}-\rho\dot{\theta}\right)-\rho\left(\frac{\left(\boldsymbol{\nabla}\theta\right)^{2}}{2m}+\frac{g}{2}\rho+V\right)-\frac{\hbar^{2}}{8m\rho}\left(\boldsymbol{\nabla}\rho\right)^{2}. \tag{3.49}$$

The reason for performing this gauge transformation will become clear later. For now, we merely state that it allows for the possibility of readily identifying a canonical transformation (3.84), which separates out the relevant pair of physical conjugate variables from the redundant pair of conjugate variables, the latter representing the constraints of the theory. The first order nature of the Lagrangian density (3.49), means

that the canonical momenta

$$\pi_\rho = \frac{\partial \mathcal{L}}{\partial \dot{\rho}} = \frac{\theta}{2}, \qquad \pi_\theta = \frac{\partial \mathcal{L}}{\partial \dot{\theta}} = -\frac{\rho}{2}, \tag{3.50}$$

can not be treated as independent dynamical variables. In other words, the phase space variables are restricted by the following equations:

$$\begin{aligned} C_1 &= \pi_\theta + \frac{\rho}{2} = 0, \\ C_2 &= \pi_\rho - \frac{\theta}{2} = 0. \end{aligned} \tag{3.51}$$

and may not be varied independently of each other. Notice how transformation (3.49) ensures that the momentum π_ρ is not singled out as a vanishing quantity over the other momentum π_θ. In the Dirac treatment [68,69] of singular Lagrangian systems, equations (3.51) take the form of constraint equations on the full phase space $(\rho, \theta, \pi_\rho, \pi_\theta)$, in the sense that the motion of the system evolves within the confines of the hypersurface Γ_c defined by the constraints. Constraints which can be rendered into the form (3.51) are known as *primary constraints*. The dimensionality of phase space becomes reduced as a result of such constraints and the resulting space formed by the physically relevant conjugate variables is referred to as the *reduced phase space*. Hence, from the four original phase space variables, only two canonical variables play a physical role in the dynamical description of the system. Before proceeding with this reduction, it is instructive to examine the form of the dynamical equations on Γ_c, as embedded in the full phase space of the system. To this end, Dirac [69] introduced the symbol '$\approx$' to denote weak equalities which hold only on Γ_c. For instance, two dynamical variables f and g are said to be "weakly equal" ($f \approx g$) if they are equal on Γ_c and strongly equal ($f = g$) if equality holds throughout phase space. In practice, this means that all Poisson brackets must be worked out before implementing constraint equations in the relevant dynamical variables [69]. Although the duality of the Legendre transform is destroyed by the singular nature of the system, we may nonetheless define a canonical Hamiltonian density $\mathcal{H}$ according to the usual prescription

$$\mathcal{H} = \pi_\rho \dot{\rho} + \pi_\theta \dot{\theta} - \mathcal{L}, \tag{3.52}$$

which on Γ_c, is given by

$$\mathcal{H} \approx \rho \left[\frac{(\boldsymbol{\nabla}\theta)^2}{2m} + \frac{g}{2}\rho + V \right] + \frac{\hbar^2}{8m\rho} \left(\boldsymbol{\nabla}\rho\right)^2 . \tag{3.53}$$

However, notice that the Hamiltonian is not unique since we can add to it any linear combination of the C's from Eq. (3.51), which vanish. We may then define the primary Hamiltonian [66] which incorporates the primary constraints, as

$$H_p = \int d^3\mathbf{r} \left(\mathcal{H} + \dot{\theta} C_1 + \dot{\rho} C_2 \right), \tag{3.54}$$

where the Lagrange multipliers are identified [70] with the field velocities $\dot{\theta}$ and $\dot{\rho}$, which are unknown functions on phase space. Note also that $\mathcal{H}_p \approx \mathcal{H}$. On the full phase space, the time evolution of an arbitrary dynamical variable f is generated by the primary Hamiltonian rather than the canonical Hamiltonian [69–72], through the Poisson bracket

$$\dot{f} \approx \{f, H_p\}, \tag{3.55}$$

where the Poisson bracket of two variables may be written explicitly, as

$$\begin{aligned} &\{f, g\} \equiv \{f(\mathbf{x}), g(\mathbf{y})\} \\ &= \int d^3\mathbf{r} \left(\frac{\delta f(\mathbf{x})}{\delta\rho(\mathbf{r})} \frac{\delta g(\mathbf{y})}{\delta\pi_\rho(\mathbf{r})} - \frac{\delta f(\mathbf{x})}{\delta\pi_\rho(\mathbf{r})} \frac{\delta g(\mathbf{y})}{\delta\rho(\mathbf{r})} + \frac{\delta f(\mathbf{x})}{\delta\theta(\mathbf{r})} \frac{\delta g(\mathbf{y})}{\delta\pi_\theta(\mathbf{r})} - \frac{\delta f(\mathbf{x})}{\delta\pi_\theta(\mathbf{r})} \frac{\delta g(\mathbf{y})}{\delta\theta(\mathbf{r})} \right). \end{aligned} \tag{3.56}$$

Note that we will frequently adopt the shorthand form $\{f, g\} = \{f, g\}_{\rho,\pi_\rho} + \{f, g\}_{\theta,\pi_\theta}$. The unknown functions $\dot{\rho}$ and $\dot{\theta}$ may be obtained on Γ_c, from the consistency requirement that the constraint equations must be preserved in time: $\dot{C}_i \approx 0$. To see this, let us replace f in Eq. (3.55) by C_i and expand out the Poisson bracket, which gives

$$\dot{C}_i(\mathbf{r}) \approx \int d^3\mathbf{r}' \left(\frac{\delta C_i(\mathbf{r})}{\delta\rho(\mathbf{r}')} \frac{\delta H_p}{\delta\pi_\rho(\mathbf{r}')} - \frac{\delta C_i(\mathbf{r})}{\delta\pi_\rho(\mathbf{r}')} \frac{\delta H_p}{\delta\rho(\mathbf{r}')} + \frac{\delta C_i(\mathbf{r})}{\delta\theta(\mathbf{r}')} \frac{\delta H_p}{\delta\pi_\theta(\mathbf{r}')} - \frac{\delta C_i(\mathbf{r})}{\delta\pi_\theta(\mathbf{r}')} \frac{\delta H_p}{\delta\theta(\mathbf{r}')} \right). \tag{3.57}$$

For the constraint $C_1 = \pi_\theta + \rho/2$, the first and last of the four terms under the integral survive:

$$\dot{C}_1(\mathbf{r}) \approx \int d^3\mathbf{r}' \left(\frac{1}{2}\delta(\mathbf{r}' - \mathbf{r}) \frac{\delta H_p}{\delta\pi_\rho(\mathbf{r}')} - \delta(\mathbf{r}' - \mathbf{r}) \frac{\delta H_p}{\delta\theta(\mathbf{r}')} \right) \approx \frac{1}{2}\frac{\delta H_p}{\delta\pi_\rho(\mathbf{r})} - \frac{\delta H_p}{\delta\theta(\mathbf{r})}, \tag{3.58}$$

while for $C_2 = \pi_\rho - \theta/2$, the other two terms survive:

$$\dot{C}_2(\mathbf{r}) \approx \int d^3\mathbf{r}' \left(-\delta(\mathbf{r}' - \mathbf{r}) \frac{\delta H_p}{\delta \rho(\mathbf{r}')} - \frac{1}{2}\delta(\mathbf{r}' - \mathbf{r}) \frac{\delta H_p}{\delta \pi_\theta(\mathbf{r}')} \right) \approx -\frac{\delta H_p}{\delta \rho(\mathbf{r})} - \frac{1}{2}\frac{\delta H_p}{\delta \pi_\theta(\mathbf{r})}. \tag{3.59}$$

Using Eq. (3.54) for H_p, with C_i given by (3.51), we then find

$$\dot{C}_1 \approx \frac{\dot{\rho}}{2} - \frac{\delta H}{\delta \theta} + \frac{\dot{\rho}}{2} \approx 0, \tag{3.60}$$

$$\dot{C}_2 \approx -\frac{\delta H}{\delta \rho} - \frac{\dot{\theta}}{2} - \frac{\dot{\theta}}{2} \approx 0, \tag{3.61}$$

which shows that the consistency equations for the constraints are equivalent to the canonical system of equations (3.47). However, these have emerged as weak equalities on Γ_c, where substitution of the canonical Hamiltonian density (3.53) into Eqs (3.60) and (3.61), yields respectively

$$\dot{\rho} + \boldsymbol{\nabla} \cdot \mathbf{J} \approx 0, \tag{3.62}$$

$$\dot{\theta} + \frac{1}{2}mv^2 + g\rho + V + Q \approx 0, \tag{3.63}$$

namely, the equation of continuity (3.44) and the quantum Hamilton-Jacobi Eq. (3.43) for the phase of the complex field.

Let us now proceed with the phase space reduction. To this end, notice that although the constraints are weakly vanishing ($C_i \approx 0$), the Poisson bracket of an arbitrary dynamical variable f with the constraints, does not vanish in general, with $\{f, C_i\} \not\approx 0$. This incompatibility of the constraints with the Poisson bracket is a general feature of constrained Hamiltonian systems which may be addressed through appropriate implementation of Dirac brackets instead of Poisson brackets, constructed as follows. In the case of a discrete system with a finite number of degrees of freedom, one defines a matrix with elements given by the Poisson brackets of the constraints: $Q_{ij} = \{C_i, C_j\}$. It was shown by Dirac [69, 70] that this matrix is nonsingular and therefore possesses an associated inverse matrix Q^{-1}_{ij}, such that $\sum_j Q_{ij} Q^{-1}_{jk} = \delta_{ik}$. The Dirac bracket of two phase space variables, is then defined [66, 68–74] as

$$\{f, g\}_D = \{f, g\} - \sum_{i,j} \{f, C_i\} Q^{-1}_{ij} \{C_j, g\}. \tag{3.64}$$

The reason for defining such a bracket can be seen by replacing g with C_k, which gives

$$\begin{aligned}\{f, C_k\}_D &= \{f, C_k\} - \sum_{i,j} \{f, C_i\} Q^{-1}_{ij} \{C_j, C_k\} \\ &= \{f, C_k\} - \sum_{i,j} \{f, C_i\} Q^{-1}_{ij} Q_{jk} = \{f, C_k\} - \{f, C_k\} = 0. \end{aligned} \tag{3.65}$$

In other words, the Dirac bracket of an arbitrary phase space variable with the primary constraints vanishes. In practice, this means that one can implement the constraints directly in the definitions of the physical variables (e.g the Hamiltonian) when using Dirac brackets [69, 70]. Furthermore, in contrast to Eq. (3.55), time-evolution is now generated by the canonical Hamiltonian, through the Dirac bracket

$$\dot{f} = \{f, H\}_D . \tag{3.66}$$

Note that it is the Dirac brackets which should be quantised rather than the Poisson brackets, when quantising a classical theory. This is because under a suitable canonical transformation, all redundant field variables drop out of the Dirac bracket, meaning that the phase space reduces to the physical degrees of freedom of the system. Let us examine how this manifests for the hydrodynamical formalism of the Gross-Pitaevskii field.

For continuous systems, the constraint Poisson bracket matrix takes on the positional dependence $Q_{ij}(\mathbf{r}, \mathbf{r}') = \{C_i(\mathbf{r}), C_j(\mathbf{r}')\}$. In turn, the previous product defining the inverse Poisson bracket matrix, now involves integration over the intermediate space coordinate:

$$\sum_j \int d^3\mathbf{r}'' Q_{ij}(\mathbf{r}, \mathbf{r}'') Q^{-1}_{jk}(\mathbf{r}'', \mathbf{r}') = \delta_{ik} \delta(\mathbf{r} - \mathbf{r}'), \tag{3.67}$$

while the Dirac bracket of two phase space variables, is given by [70]

$$\{f(\mathbf{x}), g(\mathbf{y})\}_D = \{f(\mathbf{x}), g(\mathbf{y})\} - \sum_{i,j} R_{ij}, \tag{3.68}$$

where

$$R_{ij} = \iint d^3\mathbf{r} d^3\mathbf{r}' \{f(\mathbf{x}), C_i(\mathbf{r})\} Q^{-1}_{ij}(\mathbf{r}, \mathbf{r}') \{C_j(\mathbf{r}'), g(\mathbf{y})\}. \tag{3.69}$$

Recalling Eq. (3.51) for the constraints, let us now explicitly construct $Q_{ij}(\mathbf{r}, \mathbf{r}')$ for our system, by evaluating (3.56), replacing f and g by C_i and C_j respectively. In

view of the anti-symmetric property of the Poisson bracket, the diagonal elements are $Q_{11} = \{C_1(\mathbf{r}), C_1(\mathbf{r}')\} = Q_{22} = \{C_2(\mathbf{r}), C_2(\mathbf{r}')\} = 0$, while for the off-diagonal elements, we find

$$\begin{aligned} Q_{12} &= \{C_1(\mathbf{r}), C_2(\mathbf{r}')\}_{\rho,\pi_\rho} + \{C_1(\mathbf{r}), C_2(\mathbf{r}')\}_{\theta,\pi_\theta} \\ &= \frac{1}{2}\delta(\mathbf{r}-\mathbf{r}') + \frac{1}{2}\delta(\mathbf{r}-\mathbf{r}') = \delta(\mathbf{r}-\mathbf{r}') = -Q_{21}, \end{aligned} \tag{3.70}$$

Thus, the constraint Poisson bracket matrix, takes the form

$$Q(\mathbf{r},\mathbf{r}') = \begin{pmatrix} 0 & 1 \\ -1 & 0 \end{pmatrix} \delta(\mathbf{r}-\mathbf{r}'), \tag{3.71}$$

whose inverse is given by

$$Q^{-1}(\mathbf{r},\mathbf{r}') = \begin{pmatrix} 0 & -1 \\ 1 & 0 \end{pmatrix} \delta(\mathbf{r}-\mathbf{r}'), \tag{3.72}$$

in accordance with Eq. (3.67). For the present problem, evaluation of the Dirac bracket (3.68) involves the two terms R_{12} and R_{21} associated with the off-diagonal elements of Q^{-1}. Since both constraints (3.51) depend on two phase space variables, only two out of four terms are retained in any Poisson bracket comprised in R_{12} and R_{21} from Eq. (3.69). For instance, for R_{12}, we have

$$\begin{aligned} R_{12} = \iiiint d^3\mathbf{r} d^3\mathbf{r}' d^3\mathbf{x}' d^3\mathbf{y}' \left(-\frac{\delta f(\mathbf{x})}{\delta\pi_\rho(\mathbf{x}')}\frac{\delta C_1(\mathbf{r})}{\delta\rho(\mathbf{x}')} + \frac{\delta f(\mathbf{x})}{\delta\theta(\mathbf{x}')}\frac{\delta C_1(\mathbf{r})}{\delta\pi_\theta(\mathbf{x}')} \right) \\ \times Q_{12}^{-1}(\mathbf{r},\mathbf{r}') \left(-\frac{\delta C_2(\mathbf{r}')}{\delta\pi_\rho(\mathbf{y}')}\frac{\delta g(\mathbf{y})}{\delta\rho(\mathbf{y}')} + \frac{\delta C_2(\mathbf{r}')}{\delta\theta(\mathbf{y}')}\frac{\delta g(\mathbf{y})}{\delta\pi_\theta(\mathbf{y}')} \right). \end{aligned} \tag{3.73}$$

Substituting Eqs. (3.51) and (3.72) into the above equation and making use of standard delta function relations, gives

$$R_{12} = \int d^3\mathbf{r} \left(-\frac{1}{2}\frac{\delta f(\mathbf{x})}{\delta\pi_\rho(\mathbf{r})} + \frac{\delta f(\mathbf{x})}{\delta\theta(\mathbf{r})} \right) \left(\frac{\delta g(\mathbf{y})}{\delta\rho(\mathbf{r})} + \frac{1}{2}\frac{\delta g(\mathbf{y})}{\delta\pi_\theta(\mathbf{r})} \right), \tag{3.74}$$

while pursuing a similar procedure for R_{21}, leads to the following equation:

$$R_{21} = \int d^3\mathbf{r} \left(\frac{\delta f(\mathbf{x})}{\delta\rho(\mathbf{r})} + \frac{1}{2}\frac{\delta f(\mathbf{x})}{\delta\pi_\theta(\mathbf{r})} \right) \left(\frac{1}{2}\frac{\delta g(\mathbf{y})}{\delta\pi_\rho(\mathbf{r})} - \frac{\delta g(\mathbf{y})}{\delta\theta(\mathbf{r})} \right). \tag{3.75}$$

Therefore, the total reduction contribution to the Dirac bracket, amounts to

$$R_{12}+R_{21}=\{f,g\}_{\theta,\rho}+\frac{1}{2}\left[\{f,g\}_{\theta,\pi_\theta}+\{f,g\}_{\rho,\pi_\rho}\right]+\frac{1}{4}\{f,g\}_{\pi_\theta,\pi_\rho}. \tag{3.76}$$

Hence, from Eqs. (3.68) (3.69) and (3.76), we find that the Dirac bracket takes the form

$$\{f,g\}_D=\{f,g\}_{\rho,\theta}+\frac{1}{2}\left[\{f,g\}_{\rho,\pi_\rho}+\{f,g\}_{\theta,\pi_\theta}\right]+\frac{1}{4}\{f,g\}_{\pi_\rho,\pi_\theta}, \tag{3.77}$$

where we have used $\{f,g\}=\{f,g\}_{\rho,\pi_\rho}+\{f,g\}_{\theta,\pi_\theta}$ and the antisymmetric property of brackets under exchange of field variables, e.g. $\{f,g\}_{\rho,\theta}=-\{f,g\}_{\theta,\rho}$. From here, the Dirac brackets of the canonical field variables may be read off, as

$$\{\rho(\mathbf{r}),\rho(\mathbf{r}')\}_D=\{\theta(\mathbf{r}),\theta(\mathbf{r}')\}_D=\{\pi_\rho(\mathbf{r}),\pi_\rho(\mathbf{r}')\}_D=\{\pi_\theta(\mathbf{r}),\pi_\theta(\mathbf{r}')\}_D=0, \tag{3.78}$$

$$\{\rho(\mathbf{r}),\pi_\theta(\mathbf{r}')\}_D=\{\theta(\mathbf{r}),\pi_\rho(\mathbf{r}')\}_D=0, \tag{3.79}$$

$$\{\rho(\mathbf{r}),\pi_\rho(\mathbf{r}')\}_D=\{\theta(\mathbf{r}),\pi_\theta(\mathbf{r}')\}_D=\frac{1}{2}\delta(\mathbf{r}-\mathbf{r}'), \tag{3.80}$$

$$\{\pi_\rho(\mathbf{r}),\pi_\theta(\mathbf{r}')\}_D=\frac{1}{4}\delta(\mathbf{r}-\mathbf{r}'),\qquad\{\rho(\mathbf{r}),\theta(\mathbf{r}')\}_D=\delta(\mathbf{r}-\mathbf{r}'). \tag{3.81}$$

The reduction of phase space to the physical degrees of freedom of the system may be achieved by a suitable canonical transformation. In particular, we would like to find a transformation

$$\begin{pmatrix}\rho & \theta\\ \pi_\rho & \pi_\theta\end{pmatrix}\quad\rightarrow\quad\begin{pmatrix}Q_1 & Q_2\\ P_1 & P_2\end{pmatrix}, \tag{3.82}$$

which transforms one of the set of conjugate variables, (θ,π_θ) say, into the pair of constraints (3.51), such that $Q_2=\pi_\theta+\rho/2$ and $P_2=\pi_\rho-\theta/2$ [2]. As such, we seek to split phase space into two submanifolds: a constraint subspace whose constituent variables all vanish and a complement subspace (the reduced phase space) constructed from the remaining relevant (generally non-vanishing) dynamical variables. In fact, the existence of such a canonical transformation is guaranteed by a theorem due to Maskawa and Nakajima [75]. Under this canonical transformation, the Dirac bracket on the full phase space should reduce to the Poisson bracket on the reduced phase space [76], so that $\{f,g\}_D=\{f,g\}_{Q_1,P_1}$. To obtain the transformation, recall that in order for the transformation to be canonical, the Poisson brackets of the new variables

[2]Note that this is in harmony with the requirement that (Q_2,P_2) form a conjugate pair, since $\{Q_2(\mathbf{r}),P_2(\mathbf{r}')\}=\delta(\mathbf{r}-\mathbf{r}')$ in accordance with (3.83).

with respect to the old variables, should satisfy

$$\begin{aligned}\{Q_i(\mathbf{r}), Q_j(\mathbf{r}')\} &= \{P_i(\mathbf{r}), P_j(\mathbf{r}')\} = 0,\\ \{Q_i(\mathbf{r}), P_j(\mathbf{r}')\} &= \delta_{ij}\delta(\mathbf{r}-\mathbf{r}').\end{aligned} \tag{3.83}$$

Given these observations, it is not difficult to see that the transformation

$$\begin{pmatrix}\rho & \theta\\ \pi_\rho & \pi_\theta\end{pmatrix} \quad\rightarrow\quad \begin{pmatrix}Q_1=\rho/2-\pi_\theta & Q_2=\pi_\theta+\rho/2\\ P_1=\theta/2+\pi_\rho & P_2=\pi_\rho-\theta/2\end{pmatrix}, \tag{3.84}$$

transforms the second pair of conjugate variables into the constraints and is canonical. Let us examine the from of the Dirac bracket (3.77) written in terms of the new canonical variables. For this purpose, it is useful to express the functional derivatives with respect to the old variables, in terms of the new ones. Using simple chain rules, we find

$$\begin{aligned}\frac{\delta}{\delta\rho} &= \frac{1}{2}\left(\frac{\delta}{\delta Q_1}+\frac{\delta}{\delta Q_2}\right), & \frac{\delta}{\delta\theta} &= \frac{1}{2}\left(\frac{\delta}{\delta P_1}-\frac{\delta}{\delta P_2}\right),\\ \frac{\delta}{\delta\pi_\rho} &= \frac{\delta}{\delta P_1}+\frac{\delta}{\delta P_2}, & \frac{\delta}{\delta\pi_\theta} &= -\frac{\delta}{\delta Q_1}+\frac{\delta}{\delta Q_2}.\end{aligned} \tag{3.85}$$

From the sign of each of these terms and the ordering of the fields in the brackets appearing in the Dirac bracket (3.77), each bracket contribution may be read off, as

$$\begin{aligned}\{f,g\}_{\rho,\theta} &= \frac{1}{4}\left[\{f,g\}_{Q_1,P_1}-\{f,g\}_{Q_1,P_2}+\{f,g\}_{Q_2,P_1}-\{f,g\}_{Q_2,P_2}\right],\\ \frac{1}{2}\{f,g\}_{\rho,\pi_\rho} &= \frac{1}{4}\left[\{f,g\}_{Q_1,P_1}+\{f,g\}_{Q_1,P_2}+\{f,g\}_{Q_2,P_1}+\{f,g\}_{Q_2,P_2}\right],\\ \frac{1}{2}\{f,g\}_{\theta,\pi_\theta} &= \frac{1}{4}\left[\{f,g\}_{Q_1,P_1}-\{f,g\}_{Q_1,P_2}-\{f,g\}_{Q_2,P_1}+\{f,g\}_{Q_2,P_2}\right],\\ \frac{1}{4}\{f,g\}_{\pi_\rho,\pi_\theta} &= \frac{1}{4}\left[\{f,g\}_{Q_1,P_1}+\{f,g\}_{Q_1,P_2}-\{f,g\}_{Q_2,P_1}-\{f,g\}_{Q_2,P_2}\right].\end{aligned} \tag{3.86}$$

Therefore, the Dirac bracket (3.77), reduces to

$$\{f,g\}_D = \{f,g\}_{Q_1,P_1}, \tag{3.87}$$

namely, the Poisson bracket on the reduced phase space. Implementing the constraints (3.51) directly in transformation (3.84), gives $Q_1=\rho$ and $P_1=\theta$, so that the Dirac bracket reduces to the Poisson bracket from Eq. (3.48), where the reduced phase space of the system comprises the single pair of conjugate variables ρ and θ. Hence from Eq.

(3.66), it follows that the time-evolution of the conjugate pair of variables, is governed by the following canonical field equations:

$$\begin{aligned}\dot{\rho}(\mathbf{r}) &= \{\rho(\mathbf{r}), H\}_D = \frac{\delta H}{\delta\theta(\mathbf{r})},\\ \dot{\theta}(\mathbf{r}) &= \{\theta(\mathbf{r}), H\}_D = -\frac{\delta H}{\delta\rho(\mathbf{r})}.\end{aligned} \tag{3.88}$$

The canonical Hamiltonian density (3.53) becomes a strong equality on the reduced phase space:

$$\mathcal{H} = \rho\left[\frac{(\boldsymbol{\nabla}\theta)^2}{2m} + \frac{g}{2}\rho + V\right] + \frac{\hbar^2}{8m\rho}(\boldsymbol{\nabla}\rho)^2, \tag{3.89}$$

and the wave equations generated by the canonical field equations (3.88) are respectively, the equation of continuity (3.44) and the quantum Hamilton-Jacobi Eq. (3.43).

3.2.3.2 The Faddeev-Jackiw method

When the Lagrangian is at most first order in the time derivatives of the fields, the FJ method provides a more direct approach to the DB algorithm. In fact, the method was designed specifically for such Lagrangians. Here we follow closely Jackiw's paper "Quantization without tears" [78], which we tailor to the specific system of interest. In the Dirac approach, one viewed the canonical momenta associated with the linear velocity terms of the Lagrangian density (3.49), as constraint equations (3.51) in phase space. As we shall see, from the FJ perspective, such constraints are never introduced. The essence of the FJ approach, follows from an observation already carried out in section 2.3. In particular, it was noted that the momenta could be viewed as additional positional variables subject to their own EL equations of motion. Therefore, for a given Hamiltonian description governed by $H(q,p)$, it is always possible to construct a first order Lagrangian

$$L(q,p) = \sum_i p_i\dot{q}_i - H(q,p), \tag{3.90}$$

whose configuration space is identical to the Hamiltonian phase space [78], where the EL equations for the Lagrangian $L(q,p)$ coincide with the canonical equations associated with $H(q,p)$, as indicated by Eqs. (2.8) and (2.9). This is the key point to appreciate in the FJ method, the reason being that we can reverse the formulation of the problem. Hence, if the Lagrangian presents itself in a first order form, we can readily identify the conjugate pairs of variables from the linear velocity form of the Lagrangian.

Let us examine how this works in practice for a nonrelativistic Bose-condensed quantum fluid, whose first order Lagrangian density may be written generically in the form

$$\mathcal{L} = \sum_i \mathcal{A}_i \left(\phi_\alpha\right) \dot{\phi}_i - \mathcal{V}\left(\phi_\alpha, \boldsymbol{\nabla}\phi_\alpha\right), \tag{3.91}$$

where $V\left[\phi_\alpha\right] = \int d^3\mathbf{r}\mathcal{V}$ is an interaction functional of the field components. Since $\mathcal{L}$ is linear in the field velocities, the interaction functional may be identified with the canonical Hamiltonian $H = V$, such that

$$\mathcal{L} = \sum_i \mathcal{A}_i \dot{\phi}_i - \mathcal{H}. \tag{3.92}$$

As a special case, which is of interest in the present discussion, consider the situation where the functions $\mathcal{A}_i$ are linear in the fields:

$$\mathcal{A}_i = \frac{1}{2}\sum_j \phi_j \omega_{ji}, \tag{3.93}$$

where ω is a matrix of constant coefficients. Notice that the Lagrangian density (3.42) of the Gross-Pitaevskii field appears in this form. In such instances, Eq. (3.92) may be presented, as

$$\mathcal{L} = \sum_{i,j} \frac{1}{2}\phi_j \omega_{ji} \dot{\phi}_i - \mathcal{H}. \tag{3.94}$$

As a further observation, notice that the symmetric part of ω is equivalent to a total time derivative in $\mathcal{L}$ and, therefore, may be discarded [78]. Indeed, a little manipulation reveals that $\sum_{i,j} \phi_j \omega_{ij} \dot{\phi}_i = d\left(\sum_{i,j} \phi_j \omega_{ij} \phi_i\right) / (2dt)$ when $\omega_{ij} = \omega_{ji}$. As a consequence, only the antisymmetric part of ω will be retained in our treatment. Taking this into account, the EL field equations (2.73) for a field described by a Lagrangian density of the form (3.94), are equivalent to the following system of equations:

$$\dot{\phi}_j = \sum_k \omega^{-1}_{jk} \frac{\delta H}{\delta \phi_k}. \tag{3.95}$$

Thus, given the canonical Hamiltonian of a particular first order Lagrangian with linear functions $\mathcal{A}_i$, the associated canonical field equations may be obtained simply by evaluating the inverse of the antisymmetric part of the constant matrix ω characterising the system. For the particular case of the Gross-Pitaevskii field described by the hydrodynamical Lagrangian density (3.42), let us denote the field components by $\phi_1 = \rho$

and $\phi_2 = \theta$. Then, in accordance with Eq. (3.93), it is clear that ω should solve the following system of equations:

$$\begin{aligned} \mathcal{A}_1 &= \frac{1}{2}\left(\rho\omega_{11} + \theta\omega_{21}\right) = 0 \\ \mathcal{A}_2 &= \frac{1}{2}\left(\rho\omega_{12} + \theta\omega_{22}\right) = -\rho, \end{aligned} \tag{3.96}$$

so that

$$\omega = \begin{pmatrix} 0 & -2 \\ 0 & 0 \end{pmatrix}. \tag{3.97}$$

The antisymmetric part of this matrix, is

$$\omega^A = \begin{pmatrix} 0 & -1 \\ 1 & 0 \end{pmatrix}, \tag{3.98}$$

and should be identified with ω appearing in Eq. (3.95). Notice that dropping the symmetric part of ω is equivalent to performing transformation (3.49) on the Lagrangian density. From the inverse of Eq. (3.98), we find that the canonical equations (3.95) are equivalent to those of Eq. (3.47). For completeness, note that Poisson brackets are defined so as to reproduce the canonical equations through Poisson commutation with the Hamiltonian, so that [78]

$$\{f, g\} = \sum_{i,j} \int d^3\mathbf{r} \frac{\delta f}{\delta\phi_i} \omega_{ij}^{-1} \frac{\delta g}{\delta\phi_j}, \tag{3.99}$$

which again yields expression (3.48) as the Poisson bracket for the hydrodynamical system.

Chapter 4

Artificial gauge potentials

4.1 Introduction

In classical mechanics, the interaction of charged particles with the electromagnetic field can be completely described in terms of the force fields **E** and **B**. The electromagnetic potentials ϕ and **A** on the other hand, enter merely as auxiliary mathematical quantities bearing no physical significance. The situation is drastically different in quantum physics: quantisation of a classical theory proceeds from knowledge of the canonical momenta, and it is the energies and momenta which are the central quantities determining the phases of quantum wavefunctions. As a result, charged particles couple directly to the electromagnetic potentials in the quantum theory, where the form of this coupling notably leads to the so-called *Aharonov-Bohm* effect [18, 103–106] and the local gauge invariance of quantum mechanics. The implications of the fundamental role played by the potentials [103], have since led to a diverse range of intriguing physical effects. These arise through the interplay between particle-particle interactions and applied fields. Although the weak field behaviour of gauge-coupled systems is well described by linear response theory, large perturbing field values do not generally allow for a meaningful first order expansion [107]. As the field is gradually increased, the ordering of the system changes abruptly at certain critical values and a variety of physical phenomena become associated with each intensity range [108]: from paramagnetic effects [109], to the quantum Hall [110–112] and spin quantum Hall [113–116] effects observed in two-dimensional electron systems. This notably led to the classification of symmetry protected topological phases of matter [117, 118] and paved the way for the implementation of topological insulators [119, 120], illustrating the range of intriguing

phenomena which emerge in gauge-coupled many-body systems.

The charge neutrality of Bose-condensed atomic systems seemingly restricts the discovery of exotic states of matter of the kind discussed above. However, the versatility, controllability and robust character of ultracold quantum gases, have since allowed for the possibility of simulating artificial gauge potentials for charge-neutral systems[1]. As we shall see, these are generally engineered through combined-interactions, such that a system exhibits spatially varying local eigenstates [15, 16]. When the motion of the atoms is slow enough, this positional dependence of the eigenstates leads to a Berry connection in physical space, which acts as a vector potential on the material components of the system. In other words, the action of a gauge potential can be mimicked by imparting a geometric phase onto the wavefunction [15–18]. In this regard, the elucidation of the geometrical nature of the Aharonov-Bohm phase [17] was a landmark in understanding magnetism in quantum mechanics. Local eigenstates can be induced in a variety of different ways. Initial attempts exploited the equivalence of the Lorentz and Coriolis forces, by stirring the condensate with a focused laser beam in a magnetic trap [122], a technique that quickly led to the observation of vortex lattices [123]. More recent implementations have relied almost exclusively on dressing the bare atomic states using light-matter interactions. For instance, a two-photon Raman scheme [124] was employed in a series of experiments to engineer both electric [13] and magnetic [14] synthetic force fields, as well as synthetic spin-orbit coupling [125], spin Hall effect [126] and partial waves [127]. Atomic light-dressing has also opened up the possibility for generating non-Abelian vector potentials with non-commuting components. These can be implemented for atoms with degenerate eigenstates, and generally emerge when coupling to a laser field produces a degenerate subspace of dressed states [15]. In addition, efforts have been made to extend the first generation of synthetic potentials - whose space and time dependence are prescribed externally and unaffected by particle motion - and endow these with dynamical properties [124]. For instance, we shall examine how the introduction of weak collisional interactions in an ultracold dilute Bose gas of optically addressed two-level atoms, gives rise to a nonlinear effective vector potential $\mathbf{A}(\rho)$ acting on the condensate [25], where $|\mathbf{A}|$ is modulated by the density of the atomic cloud. Density-dependent gauge potentials have also been proposed [28] in

[1]Here we have a concrete example of Feynman's vision of quantum simulation, proposed in 1982 [121].

spin-dependent optical lattices, by combining periodically modulated interactions and Raman-assisted hopping.

4.2 Potentials and quantum phases

In this section, we examine the connection which exists between the potentials and the space-time dependence of quantum phases. This will help elucidate how a scalar potential acts dynamically on the phase through an active local rotation of the phase between neighbouring points of time, while a vector potential acts geometrically on the phase through a passive rotation of the local basis for the phase between neighbouring points of space.

4.2.1 Dynamic Phase

To begin with, let us consider a particle occupying the stationary state $\psi_0(\mathbf{r}, 0)$ of some Hamiltonian $\hat{H}_0$, with definite energy E_0. What influence would the introduction of a time-dependent constant scalar potential $\phi(t)$, have on the state of the system? Since there is no variation of the potential over space, the amplitude of the wavefunction will remain unchanged in time i.e. $|\psi_0(\mathbf{r}, t)| = |\psi_0(\mathbf{r}, 0)|$. The constant potential then simply alters the total energy of the stationary state, so that the wavefunction acquires an additional phase factor $S_d = \int dt\phi(t)$. In other words, if $\psi_0(\mathbf{r}, t)$ is a solution of $\hat{H}_0$, then the solution $\psi(\mathbf{r}, t)$ of the time-dependent Hamiltonian $\hat{H} = \hat{H}_0 + \phi(t)$, reads

$$\psi(\mathbf{r}, t) = \psi_0(\mathbf{r}, t)\, e^{-\frac{i}{\hbar}\int dt\phi(t)}. \tag{4.1}$$

In order to observe an effect of this feature, an interference experiment may be devised in which a single coherent particle beam is passed through a coherent beam splitter, where the wavefunction along either path experiences different time-varying constant potentials $\phi_1(t)$ and $\phi_2(t)$. When the two beams overlap, the resulting interference will depend on the relative phase

$$\Delta S_d = \frac{1}{\hbar}\int dt\,[\phi_1 - \phi_2] = \frac{1}{\hbar}\oint dt\phi(t) \tag{4.2}$$

where $\phi(t)$ is evaluated at the centres of the wave packets. The total phase shift ΔS_d gained by the wavefunction is purely dynamical, in the sense that it is acquired over a path in time.

4.2.2 The Aharonov-Bohm phase

In 1959, Aharonov and Bohm discovered an interesting feature of the electromagnetic potentials within the quantum theory, where a wavefunction defined over a multiply-connected region acquires a phase shift which - in the special case where time is held constant - is proportional to the circulation of the vector potential $\mathbf{A}$ within the region [103–106]. For a comprehensive review of this effect, we refer the reader to [18, 128]. Here, we follow the original line taken by the authors in their seminal paper [103]. By formulating a covariant expression for Eq. (4.2), they discovered that ΔS_d can be viewed as a special case of the more general result

$$\Delta S = \frac{e}{\hbar} \oint \left[dt\phi(t) - d\mathbf{r} \cdot \mathbf{A} \right]. \tag{4.3}$$

The total phase shift arises from the particular configuration of the 4-potential A_μ along a given circuit $\mathcal{C}$ in spacetime. We may consider two limiting cases. The first is the previous setup discussed in section 4.2.1, involving a contour in time. Conversely, the second corresponds to a path in space only, in which time is held constant. Here, a wavefunction defined over a region with circulating vector potential acquires a purely geometric phase, given by

$$\Delta S_g = -\frac{e}{\hbar} \oint d\mathbf{r} \cdot A = -\frac{e}{\hbar} \iint d\mathbf{S} \cdot (\boldsymbol{\nabla} \times \mathbf{A}), \tag{4.4}$$

where $d\mathbf{S}$ is a surface element. In their letter, Aharonov and Bohm proposed an experimental setup for detecting the effect of the circulation of $\mathbf{A}$ on a wavefunction. As illustrated in FIG. 4.1, a coherent electron beam is split into two parts, each of which remains in a simply connected region. A magnetic flux is produced in an enclosure by providing a steady current to long cylindrical solenoid. However, the magnetic field is assumed to be confined within the enclosure. The vector potential on the other hand, is not, since the circulation of $\mathbf{A}$ is constant for any closed circuit about the enclosure. The observed phase shift of the interference pattern produced at the screen may be expressed in terms of the magnetic flux $\Phi_B = \iint d\mathbf{S} \cdot (\boldsymbol{\nabla} \times \mathbf{A})$. However, if we are

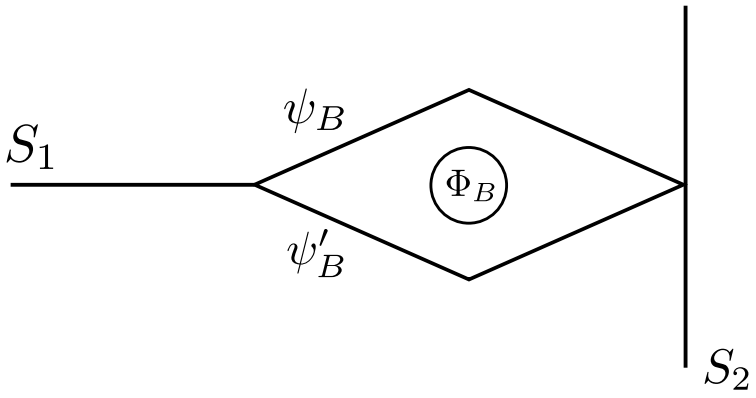

Figure 4.1: Split coherent electron beam passing on either side of a confined magnetic flux Φ_B produced by a long cylindrical solenoid, before recombining to yield a phase shifted interference pattern on the screen S_2.

to consider those effects arising from fields which only interact locally, it is clear that one should interpret ΔS_g as resulting from $\mathbf{A}$ rather than $\mathbf{B}$, since $\mathbf{B}$ vanishes at all points where the wavefunction is defined. The effect was first observed in 1982 [129] by electron holography, where the confined magnetic flux was achieved using small toroidal ferromagnets. Several other observations [130–132] were carried out over the course of the 1980s which seemed to confirm these initial results, yet still featured large error values. Multiple high-precision experiments have since been reported in various physical setups [133–139].

4.2.3 Berry phase

In the last section we considered a special case in which the wavefunction acquired a purely geometric phase, in the sense that it was acquired over a path in space. We shall now attempt to give a clearer meaning to the term "geometric phase", by introducing a more general concept devised by Berry in 1984 [17]. To do so, it useful to consider the simple case of a single particle in dimension $d = 1$ which occupies the n^{th} eigenstate ψ_n of some time-independent Hamiltonian H. By definition, the particle remains in this stationary state, simply acquiring a dynamic phase over time. Now, if the Hamiltonian becomes time-dependent, the stationary states themselves will also change in time, so that $\psi_n = \psi_n(x,t)$. This could be achieved for instance by varying any of the parameters of the system which determine H, for instance, the width of a well, the natural frequency of an oscillator and so on. Notice that in varying only the parameters we are not altering the essential form of the Hamiltonian. Let us construct a space

formed by the independent parameters $R_1, R_2 \ldots, R_N$ determining our Hamiltonian and denote a point in this space by $\mathbf{R}$. Then, the eigenstates of the system vary from point to point in this space and we may consider a particular path (parameterised by time), where each point along the path specifies a given parameterised Hamiltonian. If the path evolves over a long enough time within the adiabatic limit [140, 141], a particle which starts in the n^{th} eigenstate of the system remains in the n^{th} eigenstate of the system, even if the state is changing in time. Observe however that the form of each eigenstate typically remains the same. For instance, upon adiabatically varying the natural frequency of a quantum harmonic oscillator, the n^{th} eigenstate remains a similar product of a Gaussian and Hermite polynomial functions with the same number $n-1$ of nodes. Thus, insofar as we slowly vary the parameters of the system, the state of the particle will at most gain a phase factor, so that

$$\Psi_n(x,t) = \psi_n(x,t)\, e^{i\epsilon_n(t)} e^{i\gamma_n(t)} \tag{4.5}$$

where $\epsilon_n(t) = -1/\hbar \int dt E_n(t)$ is our usual dynamic phase factor and $\gamma_n(t)$ is a possible phase factor which could appear as a result of the path taken by the system in parameter space. In other words, the adiabatic theorem does not exclude this possibility. Now, observe that if Ψ_n from Eq. (4.5) is to be a solution of Schrödinger's equation, it must be the case that

$$i\hbar\partial_t \Psi_n = H(t)\,\Psi_n = i\hbar\left[\partial_t \psi_n - \frac{i}{\hbar} E_n(t)\,\psi_n + i\psi_n \frac{d\gamma_n(t)}{dt}\right] e^{i\epsilon_n} e^{i\gamma_n}. \tag{4.6}$$

Hence, in order for $i\hbar\partial_t\Psi_n = E_n\Psi_n$ to be satisfied, we find that the following relation must hold for the phase factor:

$$\partial_t \psi_n + i\psi_n \frac{d\gamma_n}{dt} = 0. \tag{4.7}$$

Taking the inner product of Eq. (4.7) with ψ_n, then yields

$$\frac{d\gamma_n}{dt} = i\left\langle \psi_n | \partial_t \psi_n \right\rangle. \tag{4.8}$$

If the Hamiltonian depends on a single parameter, we find that

$$\gamma_n(t) = i\int_0^t dt' \frac{dR}{dt'} \left\langle \psi_n | \partial_R \psi_n \right\rangle = i\int_{R_i}^{R_f} dR \left\langle \psi_n | \partial_R \psi_n \right\rangle, \tag{4.9}$$

so that a closed excursion after some time T does not produce any phase factor, with $\gamma_n(T) = 0$. However in the more general context in which H depends on a set of parameters, then $\partial_t \psi_n = (\nabla_R \psi_n) \cdot \frac{d\mathbf{R}}{dt}$, and Eq. (4.9) becomes

$$\gamma_n(t) = i \int_{R_i}^{R_f} d\mathbf{R} \cdot \langle \psi_n | \boldsymbol{\nabla}_R \psi_n \rangle . \tag{4.10}$$

Thus, in the case where the Hamiltonian returns to its original form after time T, we have

$$\gamma_n(T) = i \oint d\mathbf{R} \cdot \langle \psi_n | \boldsymbol{\nabla}_R \psi_n \rangle , \tag{4.11}$$

known as the *Berry phase* [17, 142–144].

4.3 Artificial magnetism for neutral atoms

4.3.1 General framework

In the previous section, we saw that a geometric phase is acquired by a wavefunction during the adiabatic following of an eigenstate along a closed contour in the parameter space of the Hamiltonian. Therefore, if we can design an environment exhibiting local eigenstates which vary from point to point and prepare a charge neutral atom in one of the local eigenstates of the Hamiltonian, a slow excursion through physical space would entail a geometric phase acquired by the wavefunction, thereby giving rise to the possibility of artificially inducing magnetism for the charge neutral atom. In order to illustrate the basic framework for such physics, let us consider a single particle of mass m with some internal non-degenerate level structure and denote the basis of the Hilbert space of the internal degrees of freedom by $\{|0\rangle, |1\rangle, \cdots, |N\rangle\}$, where $|0\rangle$ represents the ground state, $|1\rangle$ the first excited state and so on. In the next section, we will consider the particular case of a two-level atom interacting with a monochromatic laser field, as discussed in [15]. This should exemplify the more general formalism presented here. We assume that the particle interacts with space-dependent external fields, which couple the internal levels of the particle. This will produce local eigenstates which vary from point to point. Although we do not specify the particular form of these fields, we presume these to be of an electromagnetic origin. The Hamiltonian describing the

system, may then be presented, as

$$\hat{H} = \left[\frac{\hat{p}^2}{2m} + V(\mathbf{r})\right] \otimes \mathbb{1} + \hat{H}_{int}(\mathbf{r}), \tag{4.12}$$

where $\hat{p} = -i\hbar\boldsymbol{\nabla}$ is the canonical momentum operator of the particle, $\mathbb{1}$ is the identity operator in the internal Hilbert space and $\hat{H}_{int}$ is a time-independent coupling operator describing the interaction of the particle with the electromagnetic field. Since $\hat{H}_{int}(\mathbf{r})$ has space-dependent parameters, its eigenvectors and associated eigenvalues are also generally space-dependent: $\hat{H}_{int}(\mathbf{r})|\chi_i(\mathbf{r})\rangle = E_i(\mathbf{r})|\chi_i(\mathbf{r})\rangle$. These eigenstates are referred to as *dressed states*, where we have the picture of an atom which is "dressed" by the interaction field. They are superpositions of the uncoupled bare states. The full state of the particle may then be written in terms of this basis, as

$$|\Psi(\mathbf{r},t)\rangle = \sum_n \psi_n(\mathbf{r},t)|\chi_n(\mathbf{r})\rangle, \tag{4.13}$$

where $|\psi_n(\mathbf{r})|^2$ gives the probability of finding the particle at point $\mathbf{r}$ in the n^{th} dressed state. It is instructive to examine the action of the momentum operator on this state: $\hat{\mathbf{p}}|\Psi\rangle = -i\hbar\sum_n(\boldsymbol{\nabla}\psi_n|\chi_n\rangle + \psi_n|\boldsymbol{\nabla}\chi_n\rangle)$. We can resolve the second vector onto the basis of the first, by invoking the completeness relation $\mathbb{1} = \sum_m |\chi_m\rangle\langle\chi_m|$, which gives

$$\hat{\mathbf{p}}|\Psi\rangle = \sum_{n,m}\left[\left(\delta_{n,m}\hat{\mathbf{p}} - i\hbar\langle\chi_m|\boldsymbol{\nabla}\chi_n\rangle\right)\psi_n\right]|\chi_m\rangle. \tag{4.14}$$

Hence, there is an additional contribution term

$$\mathbf{A}_{m,n}(\mathbf{r}) = i\hbar\langle\chi_m(\mathbf{r})|\boldsymbol{\nabla}\chi_n(\mathbf{r})\rangle \tag{4.15}$$

which emerges under the action of $\hat{\mathbf{p}}$ as a result of the space-dependence of the dressed states. In particular, notice how the diagonal elements of $\mathbf{A}_{m,n}$ each have the character of a Berry connection from Eq. (4.11). To consolidate this observation, let us imagine that the particle is prepared in one of the dressed states, $|\chi_k\rangle$ say, such that $|\psi_l| = 0$ for $l \neq k$. Assuming that the particle moves slowly enough within the adiabatic limit, the particle remains in this particular dressed state and we may project the Schrödinger equation $i\hbar\partial_t|\Psi\rangle = \hat{H}|\Psi\rangle$ onto $|\chi_k\rangle$. This will lead to a closed equation

for the probability amplitude ψ_k. For the projected kinetic term, one finds [15, 16, 144]

$$\left\langle \chi_k(\mathbf{r}) \left| \frac{\hat{\mathbf{p}}^2}{2m} \right| \Psi(\mathbf{r},t) \right\rangle = \left[\frac{\left(\hat{\mathbf{p}} - \mathbf{A}_k(\mathbf{r})\right)^2}{2m} + W_k(\mathbf{r}) \right] \psi_k(\mathbf{r},t), \tag{4.16}$$

where

$$\mathbf{A}_k(\mathbf{r}) = i\hbar \langle \chi_k | \boldsymbol{\nabla} \chi_k \rangle, \tag{4.17}$$

$$W_k(\mathbf{r}) = \sum_{j \neq k} \frac{\hbar^2}{2m} \left| \langle \chi_j | \boldsymbol{\nabla} \chi_k \rangle \right|^2. \tag{4.18}$$

Using these definitions, the projected equation for ψ_k, then takes the form

$$i\hbar \partial_t \psi_k(\mathbf{r},t) = \left[\frac{\left(\hat{\mathbf{p}} - \mathbf{A}_k(\mathbf{r})\right)^2}{2m} + W_k(\mathbf{r}) + E_k(\mathbf{r}) \right] \psi_k(\mathbf{r},t), \tag{4.19}$$

where E_k is the energy of the dressed state. Hence, an effective gauge potential $\mathbf{A}_k$ enters the closed equation for ψ_k, which has the structure of a Berry connection. In addition, an effective scalar potential W also acts on the particle. Equation (4.19) then takes the form of a Schrödinger equation for a particle of unit charge subject to a vector potential $\mathbf{A}_k$ and scalar potential $\phi_k = W_k + E_k$.

4.3.2 The two-level system

As an example of the general framework presented in the previous section, let us examine how artificial gauge potentials may be implemented for a charge neutral atom with two relevant internal states $|g\rangle$ and $|e\rangle$, coupled by an electric dipole transition of frequency ω_0. The energy difference between these two states is $E_e - E_g = \hbar\omega_0$. We then consider a quasi-resonant excitation of the atom by means of a monochromatic radiation field of frequency ω, which we treat classically, whose electric field takes the plane wave form $\mathbf{E} = \mathbf{E_0} \cos(\mathbf{k}\cdot\mathbf{r} - \omega t)$. This leads to a detuning $\Delta = \omega - \omega_0$ from atomic resonance. Invoking both the dipole and rotating wave approximations [45, 145, 146], the interaction Hamiltonian $\hat{H}_{int}$ from Eq. (4.12), describing the atom-laser coupling, may be written as [15, 45, 144, 146]

$$\hat{H}_{int} = \frac{\hbar}{2} \begin{pmatrix} \Delta & \kappa^* \\ \kappa & -\Delta \end{pmatrix}, \tag{4.20}$$

where $\kappa = \langle e| \hat{\mathbf{d}} \cdot \mathbf{E_0} |g\rangle / \hbar$ is the Rabi-frequency characterising the strength of coupling between the atom and the light field and $\hat{\mathbf{d}}$ is the dipole operator of the atom. It is convenient to introduce the generalised Rabi-frequency Ω, the mixing angle θ and the phase angle ϕ of the electric field, defined through the following relations:

$$\Omega = \sqrt{\Delta^2 + |\kappa|^2}, \qquad \cos\theta = \frac{\Delta}{\Omega}, \qquad \sin\theta = \frac{|\kappa|}{\Omega}, \qquad \kappa = |\kappa| \, e^{i\phi}, \tag{4.21}$$

after which $\hat{H}_{int}$ presents itself, as

$$\hat{H}_{int} = \frac{\hbar\Omega}{2} \begin{pmatrix} \cos\theta & e^{-i\phi}\sin\theta \\ e^{i\phi}\sin\theta & -\cos\theta \end{pmatrix}. \tag{4.22}$$

Notice that the mixing angle and the phase angle are space-dependent parameters of $\hat{H}$. The dressed states of the atom, obtained as the eigenstates of Eq. (4.22), are given by

$$|\chi_+\rangle = \begin{pmatrix} \cos(\theta/2) \\ e^{i\phi}\sin(\theta/2) \end{pmatrix}, \qquad |\chi_-\rangle = \begin{pmatrix} -e^{-i\phi}\sin(\theta/2) \\ \cos(\theta/2) \end{pmatrix}, \tag{4.23}$$

with eigenvalues $\hbar\Omega/2$ and $-\hbar\Omega/2$ respectively. Then, if we suppose that the atom is prepared in the dressed state $|\chi_\pm\rangle$, the Berry connection (4.17) which emerges from the adiabatic following of this local eigenstate, reads [15, 16, 144]

$$\mathbf{A}_\pm = \pm\frac{\hbar}{2}(\cos\theta - 1)\,\boldsymbol{\nabla}\phi, \tag{4.24}$$

while the geometric scalar potential (4.18), is

$$W_\pm = \frac{\hbar^2}{8m}\left[(\boldsymbol{\nabla}\theta)^2 + (\sin\theta\boldsymbol{\nabla}\phi)^2\right]. \tag{4.25}$$

In turn, the artificial magnetic field acting on the atom, takes the functional form

$$\mathbf{B}_\pm = \pm\frac{\hbar}{2}\boldsymbol{\nabla}(\cos\theta) \times \boldsymbol{\nabla}\phi. \tag{4.26}$$

4.3.3 Nonlinear gauge potentials

We now turn our attention to the study of nonlinear (density-dependent) gauge potentials. These have been shown to emerge in ultracold atom systems, by introducing weak collisional interactions in a dilute cloud of optically adressed two-level atoms [25].

Modelling these weak interactions by a delta function pseudopotential, the microscopic Hamiltonian of the atomic gas, may be written as [25, 147]

$$\hat{H} = \sum_{i=1}^{N} \left[\left(\frac{\hat{\mathbf{p}}_i^2}{2m} + V(\mathbf{r}_i) \right) \otimes \mathbb{1}_i + \hat{H}_{int}(\mathbf{r}_i) \right] \otimes \mathbb{1}_{\mathcal{H}\backslash i} + \sum_{i<j}^{N} G_{i,j} \delta(\mathbf{r}_i - \mathbf{r}_j) \otimes \mathbb{1}_{\mathcal{H}\backslash\{i,j\}}, \quad (4.27)$$

where i and j label the atoms, $\mathbb{1}_i$ is the identity on the Hilbert space for particle i, while $\mathbb{1}_{\mathcal{H}\backslash\{i,j\}}$ is the identity on the compliment of the Hilbert space for particles i and j. The first term represents the single-particle Hamiltonian, where for simplicity, we set the detuning from atomic resonance to zero, so that the light-matter interaction $\hat{H}_{int}$ from Eq. (4.22), takes on the pure coupling form

$$\hat{H}_{int}(\mathbf{r}) = \frac{\hbar\Omega}{2} \begin{pmatrix} 0 & e^{-i\phi(\mathbf{r})} \\ e^{i\phi(\mathbf{r})} & 0 \end{pmatrix}. \quad (4.28)$$

The second term in Eq. (4.27) describes pairwise interactions between the atoms, where $G_{i,j}$ takes the diagonal form $G_{i,j} = \mathrm{diag}[g_{11}, g_{12}, g_{12}, g_{22}]$ in the internal Hilbert space of the interacting particles. The coupling constants are related to the associated scattering lengths, in the customary form $g_{ij} = 4\pi\hbar^2 a_{ij}/m$.

In order to obtain the dynamics of the field within the meanfield approximation, it is useful to introduce the Lagrangian of the system, in the form (3.23). A Gross-Pitaevskii-like equation for the system may be obtained in the usual way, by assuming that the N-body wavefunction is a product of N identical single-particle wavefunctions: $\Psi(\mathbf{r}_1, \mathbf{r}_2, \cdots, \mathbf{r}_N) = \prod_{i=1}^{N} \phi(\mathbf{r}_i)$, where the single-particle wavefunctions satisfy the normalisation condition $\int d^3\mathbf{r}\phi^\dagger\phi = 1$. This leads to the following meanfield Lagrangian for the macroscopic wavefunction $\psi(\mathbf{r}) = \sqrt{N}\phi(\mathbf{r})$:

$$L_{MF} = \int d^3\mathbf{r} \left[\psi^* \left(i\hbar\partial_t - \hat{H}_{MF} \right) \psi \right], \quad (4.29)$$

where the meanfield Hamiltonian $\hat{H}_{MF}$ acts on this macroscopic wavefunction, as

$$\hat{H}_{MF}\psi(\mathbf{r}) = \left(\frac{\hat{\mathbf{p}}^2}{2m} + \hat{H}_{int} + \hat{U}_{MF} \right) \psi(\mathbf{r}), \quad (4.30)$$

where $\hat{U}_{MF}$ describes the meanfield collisional effects, and is given by [25, 147]

$$\hat{U}_{MF} = \frac{1}{2}\begin{pmatrix} \Delta_1 & 0 \\ 0 & \Delta_2 \end{pmatrix}, \tag{4.31}$$

with

$$\Delta_1 = g_{11}\rho_1 + g_{12}\rho_2, \tag{4.32}$$

$$\Delta_2 = g_{12}\rho_1 + g_{22}\rho_2, \tag{4.33}$$

where $\rho_i = |\psi_i|^2$ is the density of atoms occupying the i^{th} internal state: $|i\rangle$, $i = 1, 2$. The full wavefunction may be written $\sum_{i=\pm} \psi_i(\mathbf{r})|\chi_i\rangle$, where $|\chi_\pm\rangle$ denote the eigenstates of $\hat{H}_{int} + \hat{U}_{MF}$. When the light-matter coupling is much stronger than the inter-particle potential, which we will assume to the case in what follows, these can be approximated by treating the meanfield interaction $\hat{U}_{MF}$ as a perturbation to the atom-laser coupling $\hat{H}_{int}$. To first order, we have

$$|\chi_\pm\rangle = \left|\chi_\pm^{(0)}\right\rangle \pm \frac{\Delta_1 - \Delta_2}{\hbar\Omega}\left|\chi_\mp^{(0)}\right\rangle, \tag{4.34}$$

where $\left|\chi_\pm^{(0)}\right\rangle = \left(|1\rangle \pm e^{i\phi}|2\rangle\right)/\sqrt{2}$ are the dressed states, namely, the eigenstates of Eq. (4.28). Furthermore, in accordance with the adiabatic assumption, if most of the population remains in a particular dressed state $|\chi_\pm\rangle$ for the duration of motion, we obtain a projected meanfield Lagrangian (4.29), where the meanfield Hamiltonian governing the dynamics of $\psi_\pm$, is obtained as

$$\hat{H}_\pm = \frac{(\hat{\mathbf{p}} - \mathbf{A}_\pm)^2}{2m} + W \pm \frac{\hbar\Omega}{2} + \frac{g}{2}\rho_\pm, \tag{4.35}$$

where $g = (g_{11} + g_{22} + 2g_{12})/4$, and synthetic potentials enter the Hamiltonian in the form of a scalar function W and Berry connection $\mathbf{A}$, as in Eqs. (4.17) and (4.18). Notice that the $|\chi_\pm\rangle$ from Eq. (4.34) depend on ρ, and $\mathbf{A}$ inherits this dependence: thus we have a density-dependent synthetic gauge potential. To first order, the synthetic potentials read

$$W = \frac{\left|\mathbf{A}^{(0)}\right|^2}{2m}, \tag{4.36}$$

$$\mathbf{A}_\pm = \mathbf{A}^{(0)} + \mathbf{a}\rho_\pm, \tag{4.37}$$

where $\mathbf{A}^0 = -\frac{\hbar}{2}\boldsymbol{\nabla}\phi$ is the single particle contribution to the vector potential, ϕ is the phase of the laser field and

$$\mathbf{a} = \frac{g_{11} - g_{22}}{8\Omega}\boldsymbol{\nabla}\phi, \tag{4.38}$$

controls the effective strength and orientation of the nonlinear vector potential. Let us consider, without loss of generality, the + branch of $\hat{H}_{\pm}$. Then, inserting the meanfield Lagrangian (4.29) (with $\hat{H}_{MF}$ given by $\hat{H}_{+}$) into the EL field equation (2.73) for ψ^*, yields the following Gross-Pitaevskii-like equation for the condensate:

$$i\hbar\partial_t\psi = \left[\frac{\left(\hat{\mathbf{p}} - \mathbf{A}\right)^2}{2m} - \mathbf{a}\cdot\mathbf{J} + W + g\rho\right]\psi, \tag{4.39}$$

where an additional nonlinear current term $-\mathbf{a}\cdot\mathbf{J}$ joins the usual nonlinear meanfield interaction term $g\rho$, in which $\mathbf{J}$ takes the gauge-covariant form

$$\mathbf{J} = \frac{i\hbar}{2m}\left[\psi\left(\boldsymbol{\nabla} + \frac{i}{\hbar}\mathbf{A}\right)\psi^* - \psi^*\left(\boldsymbol{\nabla} - \frac{i}{\hbar}\mathbf{A}\right)\psi\right]. \tag{4.40}$$

Equation (4.39) is the central result of this section. It should be emphasised that while the nonlinear potential enters the effective gauge-coupled Hamiltonian in the form of a Berry connection, its origin is clearly different from the gauge fields encountered in field theory. Indeed, the degrees of freedom of a gauge field are tied to the points of space and the field evolves under its own equations of motion, in accordance with some prescribed Lagrangian density. In contrast, the "degrees of freedom" of a nonlinear synthetic gauge potential are tied to those material elements of a system which are subject to the synthetic potential. There is no interaction between matter-field and gauge "field" since the situation is not that of a dynamical coupling between fields. Rather, there are not two, but one single field - the matter-field - whose condensed fraction is dynamically governed by a nonlinear wave equation featuring a density-dependent vector potential as a result of the form taken by the Berry connection entering the effective Hamiltonian.

In the following chapter, we shall consider a more extended class of density-dependent vector potentials and cast the meanfield formalism presented in this section, into its hydrodynamical canonical form. In doing so, we will observe such nonlinear current terms emerging in the wave equation for the phase of the quantum fluid, whenever the kinetic energy density is nonlinear in the fluid density.

Chapter 5

Hydrodynamics of nonlinear gauge-coupled quantum fluids

In this chapter, we investigate the types of fluid stress and body-forces which emerge when a quantum fluid couples to a nonlinear gauge potential. We shall refer to such fluids as *nonlinear gauge-coupled quantum fluids*. From a hydrodynamical point of view, density-dependent vector potentials entail a fluid flow which depends explicitly on the density profile, where the magnitude of flow of a volume element of fluid typically increases as the volume shrinks. This is an interesting situation because the kinetic energy density becomes nonlinear in the fluid density. As a result, additional flow-dependent scalar terms enter the wave equation for the phase and we would expect such terms to play a crucial role in determining the stress of the fluid.

When a fluid couples to *external* scalar and vector potentials, the potentials enter the momentum transport equation as body-type forces, whereas the stress tensor stems from internal-type forces associated with effective potentials. For an external vector potential, the associated body-force appears through the (gauge-covariant) kinetic term of the quantum Hamilton-Jacobi equation, due to the non-vanishing vorticity $\boldsymbol{\omega} = \boldsymbol{\nabla} \times \mathbf{v}$ in the system. However, in the case of a nonlinear vector potential, $\mathbf{A}$ appears in two places in the wave equation, both in the kinetic term and in the flow-dependent nonlinearity. For normal systems, one would expect the kinetic term to produce a transverse body-force and the nonlinearity to produce forces of stress, but for a nonlinear vector potential it is unclear whether such a separation is tenable, since $\mathbf{A}$ has both internal and external features. For instance, while the magnitude of $\mathbf{A}$ in the Gross-Pitaevskii-like equation (4.39) is modulated by the density, its orientation is externally prescribed through Eq.

(4.38). In section 5.3.2, we shall address these points and separate out the body forces from the forces of stress accordingly. To begin with, we consider a certain class of density-dependent "single-component" gauge potentials, and later extend this class to encompass more general "multi-component" potentials.

5.1 Introducing the nonlinear gauge potential

In section 4.3.3, we saw how an effective nonlinear vector potential could be implemented in a Bose-condensed cloud of optically-addressed two-level atoms, by subjecting the atoms to weak contact interactions. On the other hand, the aim of this thesis is to investigate general hydrodynamical properties associated with density-dependent gauge potentials, without being held to a particular microscopic model. As such, we shall take a step back from the underlying microscopic model and suppose that an effective density-dependent vector potential $\mathbf{A}(\rho)$ emerges in the meanfield Hamiltonian. Since an effective gauge potential enters in a manner consistent with the minimal substitution $\hat{\mathbf{p}} \to \hat{\mathbf{p}} - \mathbf{A}$, the meanfield Hamiltonian with effective density-dependent scalar and vector potentials, $\eta(\rho)$ and $\mathbf{A}(\rho)$, assumes the form

$$\hat{H}_{MF} = \frac{\left(\hat{\mathbf{p}} - \mathbf{A}(\rho)\right)^2}{2m} + \eta(\rho) + V(\mathbf{r}, t). \tag{5.1}$$

In accordance with Eq. (4.29), the Lagrangian density of the nonlinear field, may be presented as

$$\mathcal{L} = \frac{i\hbar}{2}\left(\psi^*\dot{\psi} - \dot{\psi}^*\psi\right) - \frac{1}{2m}\left[\left(\hat{\mathbf{p}} - \mathbf{A}\right)\psi\right]^*\left[\left(\hat{\mathbf{p}} - \mathbf{A}\right)\psi\right] - \rho\eta - \rho V, \tag{5.2}$$

where we have performed the transformation $\mathcal{L} \to \mathcal{L} - i\hbar\partial_t\left(\psi^*\psi\right)/2$, in order for $\mathcal{L}$ to be real, as discussed at the end of section 3.1.3.

5.2 Hydrodynamic canonical formalism for the nonlinear field

Perhaps the most conspicuous feature of a density-dependent gauge potential, is the occurrence of a current nonlinearity in the wave equation. One may gain insight into the appearance of such a term, by casting the meanfield description into a hydrodynamical

form. To do so, we write the wavefunction in the polar form (3.38) and consider ρ and θ as the independent variables. Carrying out this substitution, the Lagrangian density (5.2), assumes the form

$$\mathcal{L} = -\rho\left(\dot{\theta} + \frac{1}{2}mv^2 + \eta + V\right) - \mathcal{Q}, \tag{5.3}$$

where $v = |\mathbf{v}|$, and $\mathbf{v}$ is the velocity field, or mechanical flow field, given by

$$\mathbf{v} = \frac{1}{m}\left(\boldsymbol{\nabla}\theta - \mathbf{A}\right), \tag{5.4}$$

and we have denoted the energy density contribution from the quantum potential Q from Eq. (3.45), by

$$\mathcal{Q} = \frac{\hbar^2}{8m\rho}\left(\boldsymbol{\nabla}\rho\right)^2. \tag{5.5}$$

Although the adopted notation for Q and $\mathcal{Q}$ is similar, note that these are two different quantities. In accordance with Eq. (5.4), the gauge-covariant current density (4.40), reads

$$\mathbf{J} = \frac{\rho}{m}\left(\boldsymbol{\nabla}\theta - \mathbf{A}\right). \tag{5.6}$$

Note that we shall distinguish the *canonical flow* from the *gauge flow*. In the canonical flow, $\mathbf{u}$, we include the total flow which can be accounted for locally by a phase twist in a suitable gauge, whereas the gauge flow denotes any additional flow contribution from $\mathbf{A}$ which can not be accounted for in the phase without destroying the form of the dynamical equation of the fluid. For example, if in our choice of gauge, the wave equation of a fluid reads

$$\partial_t\theta + \frac{\left(\boldsymbol{\nabla}\theta - \mathbf{A}\right)^2}{2m} + \phi\left(\mathbf{r}, t\right) = 0, \tag{5.7}$$

where $\mathbf{A} = \mathbf{c}$ is a constant vector potential, the flow conveyed to the fluid by $\mathbf{A}$ is purely canonical, since performing the transformations

$$\theta \to \theta - \int_{\mathcal{C}} d\mathbf{r}\cdot\mathbf{c}$$
$$\mathbf{A} \to \mathbf{A} - \mathbf{c},$$

leaves the wave equation unchanged, but the velocity now takes the purely potential form $\mathbf{v} = \boldsymbol{\nabla}\theta/m$. Further, in chapter 6, we shall learn that it is not possible to gauge

away density-dependent vector potentials without destroying the form of the wave equation. As such, the flow imparted by a nonlinear gauge potential is always of gauge flow type. From Eq. (5.4), we see that the transverse component of $\mathbf{A}$ leads to fluid circulation whereas the longitudinal component leads to fluid dilation. The former tends to bias or curve the streamlines of a fluid, while the latter tends to stretch or shrink streamlines. This is in contrast to the gauge field of standard electrodynamic theory, where only the transverse components enter as dynamical degrees of freedom, the longitudinal component being redundant. In the absence of a physical gauge field, the rate at which a fluid flows between neighbouring points of space is dictated by the phase twist: $\mathbf{v} = \mathbf{u} = \boldsymbol{\nabla}\theta/m$. The inclusion of a geometric vector potential $\mathbf{A}$ in Eq. (5.4) then alters this twist, and does so by rotating or twisting the local basis for the phase along the direction of $\mathbf{A}$ (see FIG.5.1). This is an example of a geometric phase being imparted onto the fluid [15, 16].

Since $\mathcal{L}$ from Eq. (5.3) is linear in the field velocities and the linear form appears as $-\rho\dot{\theta}$, the field components ρ and θ play the role of conjugate variables (see section 3.2.3.2), governed by the canonical field equations

$$\dot{\rho}\left(\mathbf{r}\right) = \frac{\delta H}{\delta\theta\left(\mathbf{r}\right)} \tag{5.8}$$

$$\dot{\theta}\left(\mathbf{r}\right) = -\frac{\delta H}{\delta\rho\left(\mathbf{r}\right)}, \tag{5.9}$$

where $H = \int d^3\mathbf{r}\mathcal{H}$, and the Hamiltonian and Lagrangian densities are related by $\mathcal{L} = -\rho\dot{\theta} - \mathcal{H}$, such that

$$\mathcal{H} = \rho\left(\frac{1}{2}mv^2 + \eta + V\right) + \mathcal{Q}. \tag{5.10}$$

Inserting the above Hamiltonian density into the canonical field equations (5.8) and (5.9), yields, respectively, the wave equations

$$\partial_t\rho + \boldsymbol{\nabla}\cdot\left(\rho\mathbf{v}\right) = 0, \tag{5.11}$$

$$\partial_t\theta + \frac{1}{2}mv^2 - \rho\mathbf{v}\cdot\frac{\partial\mathbf{A}}{\partial\rho} + \eta + \rho\frac{\partial\eta}{\partial\rho} + V + Q = 0, \tag{5.12}$$

where the density-dependence of the kinetic term within the brackets of Eq. (5.10) has produced an additional nonlinear flow-dependent term in the quantum Hamilton-Jacobi

equation (QHJE) for the phase and Q is the quantum potential (3.45). Note that we have assumed that the effective gauge potential does not depend explicitly on spatial derivatives of the density.

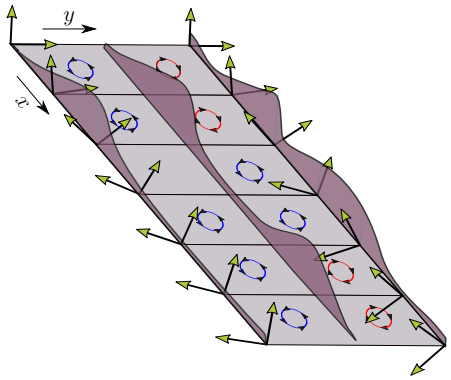

Figure 5.1: A pictorial representation of the twist undergone by the local basis for the phase along two constant-time paths due to a unidirectional density-modulated gauge potential $\mathbf{A} = \rho\,|\mathbf{a}|\,\hat{\mathbf{x}}$. The waveforms represent three slices of the density $\rho\,(x, y)$ in the direction of $\mathbf{A}$. The density-dependent gauge potential sets up a gauge flow along $-\mathbf{x}$. Fluid circulation occurs through the spatial dependence of ρ along y (clockwise circulation loops in red and anticlockwise in blue). The basis twist becomes path-dependent in fluid regions with non-vanishing circulation.

In summary, the following key findings may be highlighted. When a fluid is subject to a nonlinear vector potential, the flow $\mathbf{v}$ in Eq. (5.15) depends explicitly on the density of the fluid and the kinetic energy density $\kappa = \rho m v^2/2$ becomes nonlinear in ρ. Thus, the change $\delta\kappa$ in an infinitesimal volume due to $\delta\rho$, is not determined simply by the kinetic energy $mv^2/2$ of the volume as it is typically, since $\delta\kappa = (mv^2/2 + \rho m\mathbf{v}\cdot\partial\mathbf{v}/\partial\rho)\,\delta\rho$. As a result, a nonlinear flow-dependent term enters the wave equation or the phase. This is a general feature which is intrinsic to systems whose effective Hamiltonian (5.1) features a density-dependent vector potential $\mathbf{A}\,(\rho)$. We may also note that the procedure followed in this section outlines a simple method for exploring the implications of introducing effective nonlinear ρ-dependent or θ-dependent interaction terms. One could envisage other forms of coupling between the fields ρ and θ, or introduce additional atomic species, and check whether these give rise to interesting dynamical terms in the resulting wave equation.

5.3 The single-component nonlinear gauge potential

5.3.1 Quantum Hamilton-Jacobi equation of the fluid

The formalism outlined in the previous section was general, in the sense that the nonlinear gauge potential was viewed as an arbitrary function of the density. In our study, we shall assume that the basis for $\mathbf{A}$ is externally prescribed and unaffected

by the motion of the fluid. To begin with, we consider the case of a nonlinear gauge potential

$$\mathbf{A} = \alpha(\rho)\,\mathbf{a}, \tag{5.13}$$

whose amplitude is modulated by a density-dependent function α and whose orientation is prescribed by some external vector field $\mathbf{a}(\mathbf{r})$, which we take to be static. This ensures that the dynamics of the gauge potential depend only on the dynamics of the fluid, but one could easily consider the situation of a time-dependent vector field $\mathbf{a}(\mathbf{r}, t)$. The function α, may be represented as a power series in $|\psi|$. The configuration of $\mathbf{a}(\mathbf{r})$ would depend on the details of the underlying microscopic model which has produced spatially varying local eigenstates across the system. In the case of a dilute Bose gas of optically addressed two-level atoms from section 4.3.3, where $\mathbf{a}$ is given by Eq. (4.38), a geometric phase is acquired by the condensate along constant-time excursion curves, when the phase of the laser field changes along the curve. For convenience, we assume that all the relevant effective strengths have been absorbed into the function α, such that $|\mathbf{a}| = 1$. Lastly, although $\mathbf{A}$ is tied to the dynamics of the fluid through $|\mathbf{A}|$, its orientation along $\mathbf{a}$ is fixed in time and as such, possesses only a single dynamical component. Later, we widen the dynamical scope of $\mathbf{A}$ by considering multiple basis vectors $\mathbf{a}_i$, each with their own $\alpha_i(\rho)$. Proceeding in this order, we hope to gain a clear picture of the essential physical features of the elementary case, at which point a mathematical extension of the problem becomes straight forward.

To begin with, observe that when $\mathbf{A}$ takes the form of Eq. (5.13), the wave equation (5.12), may be written in the form

$$\partial_t\theta + \frac{1}{2}mv^2 - \gamma\mathbf{v}\cdot\mathbf{A} + \lambda\eta + V + Q = 0, \tag{5.14}$$

where

$$\mathbf{v} = \frac{1}{m}\left[\mathbf{u} - \mathbf{a}\alpha(\rho)\right], \tag{5.15}$$

with $\mathbf{u} = \boldsymbol{\nabla}\theta/m$, and γ and λ are dimensionless functions, defined as

$$\gamma(\rho) = \frac{\rho}{\alpha}\frac{\partial\alpha}{\partial\rho} \tag{5.16}$$

$$\lambda(\rho) = \frac{\rho}{\eta}\frac{\partial\eta}{\partial\rho} + 1. \tag{5.17}$$

These essentially characterise the form taken by the wave Eq. (5.14), for given functions $\alpha(\rho)$ and $\eta(\rho)$. For instance, in the simple case where $\alpha \propto \rho^n$ and $\eta \propto \rho^m$, then $\gamma = n$ and $\lambda = m + 1$ are just numbers regulating the strengths of the flow and density nonlinear terms $-\mathbf{v} \cdot \mathbf{A}$ and η. More generally however, these will depend on position through ρ. In the particular case where $\eta = g\rho/2$ and $\alpha = |\mathbf{a}|\,\rho$ are both proportional to ρ (as in Eq. (4.35)), the quantum Hamilton-Jacobi Eq. (5.14) together with the equation of mass conservation (5.11), map to the Gross-Pitaevskii-like equation

$$i\hbar\partial_t\psi = \left[\frac{(\mathbf{P} - \mathbf{A})^2}{2m} - \mathbf{a} \cdot \mathbf{J} + g\,|\psi|^2 + V\right]\psi, \tag{5.18}$$

under the field transformations (3.38), where $\mathbf{A} = \mathbf{a}\,|\psi|^2$ and $\mathbf{J}$ is given by Eq. (5.6). The above equation is equivalent to Eq. (4.39), where the zero order term $\mathbf{A}^{(0)}$ may be gauged away with the transformation $\psi \to e^{i\phi/2}\psi$.

5.3.2 Cauchy's equation

The remainder of section 5.3 will be devoted to deriving a hydrodynamic Cauchy equation describing the transport of mechanical momentum in the fluid. To this end, we begin by stating the general form of this equation and highlight the central quantities relevant to the problem. Denoting the time derivative operator in the reference frame of the fluid or *convective derivative* operator, by a total time derivative

$$\frac{d}{dt} \equiv \frac{\partial}{\partial t} + \mathbf{v} \cdot \boldsymbol{\nabla}, \tag{5.19}$$

and adopting the usual summation convention over indices appearing twice, Cauchy's equation [148] then takes the form

$$\rho m \frac{dv_k}{dt} = \rho f_k + \nabla_j \Pi_{jk}, \tag{5.20}$$

where f_k denote the *body forces* and Π_{jk} are the components of the *stress tensor* of the fluid. Equation (5.20) holds true for any fluid medium, irrespective of the manner in which stress is connected to the rate of strain. The distinction between body and stress forces is established according to the manner in which each type act on an infinitesimal volume element of fluid. The former act throughout the volume thereby changing the overall rate of flow of the volume element, whereas the latter deform the volume element

by acting on its bounding surface and lead to propagation of fluid disturbances. In other words, the Π_{jk} define a linear map between the surface normal vectors and the forces acting on these. Thus, the stress tensor of a fluid may be written in the form

$$\Pi_{jk} = -P\delta_{jk} + \sigma_{jk}, \tag{5.21}$$

where P is the fluid pressure associated with normal forces and the σ_{jk} account for shearing forces. It should be emphasised that in accordance with Eqs. (5.20) and (5.19), P does not represent the pressure at a fixed point of space, but the pressure of an infinitesimal volume element which flows with the fluid. As a final point, notice how body-forces will typically be the result of the fluid interacting with external fields. In contrast, fluid stress emerges due to internal-type interactions between the fluid particles, these generally giving rise to nonlinear effective potentials in the wave equation for the fluid. However, if the nonlinear potential is not simply a scalar but a tensor of higher rank whose orientation or basis is prescribed externally ($\mathbf{a}$ in this instance), this separation no longer applies. Thus, $\mathbf{A}(\rho)$ will be seen to play a double role in Eq. (5.20), bearing implications for both Π_{jk} and f_k.

5.3.3 Momentum-transport equation

Inspecting the form of Eq. (5.4), reveals that the dynamics of the velocity field can be obtained by taking the gradient of the quantum Hamilton-Jacobi Eq. (5.14). Doing so, we find that

$$m\left(\frac{\partial}{\partial t} + \mathbf{v}\cdot\boldsymbol{\nabla}\right)\mathbf{v} + \frac{\partial \mathbf{A}}{\partial t} + m\mathbf{v}\times\boldsymbol{\omega} = -\boldsymbol{\nabla}\left(V + Q + \lambda\eta - \gamma\mathbf{A}\cdot\mathbf{v}\right), \tag{5.22}$$

where the kinetic energy term in Eq. (5.14) combines to give rise to a convective derivative operator (5.19) and also leads to a vortical force due to the non-vanishing fluid vorticity

$$\omega_k = \epsilon_{ijk}\nabla_i v_j, \tag{5.23}$$

stemming from the rotational component of the vector potential, where ϵ_{ijk} is the Levi-Civita pseudotensor. Alternatively, if we define a synthetic magnetic field

$$B_k = \epsilon_{ijk}\nabla_i A_j, \tag{5.24}$$

the vortical force can be given a familiar magnetic form through a trivial substitution of the vorticity for $B_k = -m\omega_k$. Similarly, the time dependence of the vector potential together with the spatial dependence of the scalar field

$$\phi = \lambda\eta - \gamma \mathbf{v} \cdot \mathbf{A}, \tag{5.25}$$

define a synthetic electric field

$$E_k = -\nabla_k \phi - \partial_t A_k. \tag{5.26}$$

Accordingly, the forces appearing in Eq. (5.22) as a result of the nonlinear potentials, now take the Lorentz form

$$\Lambda_k = E_k + \epsilon_{ijk} v_i B_j. \tag{5.27}$$

In turn, this leads to the following equation for the force acting on a infinitesimal volume element which flows with the fluid:

$$m\rho \frac{dv_k}{dt} = \rho\Lambda_k - \rho\nabla_k \left(V + Q\right). \tag{5.28}$$

It should be emphasised that E_k and B_k have been defined only to make contact with the Lorentz force of electromagnetism, the form of which generally emerges whenever a system is subject to scalar and vector potentials. On this note, although Λ_k may appear to take the form of a body-force as seen in Eq. (5.28), the nonlinear character of the potentials leading to Eq. (5.27) suggests that this is not the case. In fact, Λ_k will soon be given a different form when it becomes apparent that the density dependence of $\mathbf{A}$ signifies that both B_k and E_k are connected to the flow profile of the fluid, at which point a separation of Λ_k into body and stress terms will be made. This connection is already clearly apparent for magnetic forces, since $\mathbf{B}$ is proportional to the vorticity by definition. For a superfluid confined to a two-dimensional surface which is left to evolve freely from some initial configuration, this implies that the total synthetic magnetic flux is proportional to the fluid circulation on the boundary and therefore conserved during the motion of the fluid. Thus, a superfluid subject to $\mathbf{A}\left(\rho\right)$ is constrained to evolve within a subspace of density configurations having identical circulation on the boundary. In the case of a uniform field $\mathbf{a}$, infinitesimal circulation loops arise when ρ is asymmetrically distributed about $\mathbf{a}$ (see FIG.5.1). In the more general case of

non-vanishing

$$b_k = \epsilon_{ijk}\nabla_i a_j, \tag{5.29}$$

B_k is comprised of two parts:

$$B_k = \alpha b_k + \frac{\gamma}{\rho}\epsilon_{ijk}A_j\nabla_i\rho, \tag{5.30}$$

namely, an α-modulated body-type magnetic field stemming from the spatial dependence of $\mathbf{a}$, and a stress-like magnetic field associated with density variations transverse to $\mathbf{a}$.

While a transverse flow component can always be attributed to a synthetic magnetic field, the density-dependence of $\mathbf{A}$ connects the synthetic electric field to the longitudinal component of flow. Indeed, an equation of conservation (e.g. Eqs. (5.11, 5.72, 5.73)) relates the time dependence of a physical quantity to the longitudinal component of its current. For $\mathbf{A}$ in Eq. (5.13), this signifies that

$$\frac{\partial A_k}{\partial t} = -\frac{\gamma A_k}{\rho}\nabla_i J_i. \tag{5.31}$$

This simple yet significant equation, encapsulates the underlying connection between the dynamics of the gauge potential and the dynamical state of the condensate. As a result, the synthetic electric field defined in Eq. (5.26) can be spatially resolved, as

$$E_k = -\nabla_k\phi + \frac{\gamma A_k}{\rho}\nabla_i J_i, \tag{5.32}$$

indicating that a non-trivial type of force should be expected for the onset of current in the system.

Equations (5.23), (5.24) and (5.32) suggest that we dispose of the synthetic fields and express the Lorentz force in terms of the symmetric and antisymmetric parts of the velocity gradient tensor or *displacement field* tensor

$$\nabla_i v_j \equiv d_{ij} = e_{ij} + \Omega_{ij}, \tag{5.33}$$

where e_{ij} is the *deformation* or *rate of strain* tensor, given by

$$e_{ij} = \frac{1}{2}\left(\nabla_i v_j + \nabla_j v_i\right), \tag{5.34}$$

and Ω_{ij} is the *vorticity* tensor

$$\Omega_{ij} = \frac{1}{2}\left(\nabla_i v_j - \nabla_j v_i\right). \tag{5.35}$$

The diagonal components of e_{ij} dictate the rates of longitudinal strain connected with pure stretching whereas the off-diagonal components determine the rates of shear strain connected with pure shearing [148]. In terms of these objects, the longitudinal component of the velocity field or *dilation rate*, takes the form

$$\nabla_i v_i = \delta_{ij} d_{ij} = \delta_{ij} e_{ij}, \tag{5.36}$$

while the transverse component or vorticity from Eq. (5.23), reads

$$\omega_k = \epsilon_{ijk} d_{ij} = \epsilon_{ijk} \Omega_{ij}. \tag{5.37}$$

After inserting Eq. (5.32) into Eq. (5.27) and noting that $B_k = -m\epsilon_{ijk}\Omega_{ij}$, we find that the Lorentz force is related to e_{ij} and Ω_{ij}, in the form

$$\Lambda_k = -\nabla_k \phi + \gamma A_k \delta_{ij} e_{ij} + m v_i \left(2\Omega_{ik} + \frac{\gamma A_k}{m\rho}\nabla_i \rho\right). \tag{5.38}$$

The separation of $\mathbf{B}$ in Eq. (5.30), into body-type and stress-type fields, also applies to the vorticity, leading to the following relation for the vorticity tensor:

$$\Omega_{ik} = \frac{\alpha}{2m}\epsilon_{ijk} b_j + \frac{\gamma}{2m\rho}\left(A_i \nabla_k \rho - A_k \nabla_i \rho\right). \tag{5.39}$$

Substituting Eqs. (5.39) and (5.25) into Eq. (5.38), we notice the double role played by the stress-like vortical field depicted by the two last terms in Eq. (5.39). The second of these cancels the "convective" force contribution from the last term in Eq. (5.32), while the first combines with $-\nabla_k \phi$ to produce a force which is the divergence of the rank-two tensor

$$\Gamma_{jk} = \delta_{jk}\left[(1-\lambda)\rho\eta + \gamma J_i A_i\right], \tag{5.40}$$

such that

$$\Lambda_k = \gamma A_k \delta_{ij} e_{ij} + \alpha \epsilon_{ijk} v_i b_j + \frac{1}{\rho}\nabla_j \Gamma_{jk}. \tag{5.41}$$

In other words, Γ_{jk} characterises the fluid stress brought about by the nonlinear potentials. However, Γ_{jk} is not the full stress tensor of the fluid. The quantum potential defined in Eq. (3.45), gives rise to two additional stress terms, since a little manipulation reveals that $f_k^Q = -\nabla_k Q$ can be derived from a rank-2 tensor Q_{jk}:

$$\rho f_k^Q = \nabla_j Q_{jk}, \tag{5.42}$$

where, recalling Eq. (5.21), we decompose Q_{jk} into the form

$$Q_{jk} = -P_Q \delta_{jk} + \sigma_{jk}. \tag{5.43}$$

The first contribution on the right hand side of this equation, represents the quantum pressure

$$P_Q = -\frac{\hbar^2}{4m}\nabla^2\rho, \tag{5.44}$$

while the second, is the quantum stress tensor

$$\sigma_{jk} = -\frac{\hbar^2}{4m\rho}\nabla_j\rho\nabla_k\rho. \tag{5.45}$$

It is σ_{jk} which is responsible for the osmotic pressure driving quantum diffusion [149–151]. By introducing the osmotic velocity field [150]

$$w_k = -\frac{D}{\rho}\nabla_k\rho, \tag{5.46}$$

with diffusion coefficient $D = \hbar/(2m)$, Eq. (5.45) takes the form

$$\sigma_{jk} = -m\rho w_j w_k. \tag{5.47}$$

After substituting Eqs. (5.41) and (5.42) into Eq. (5.28), a Cauchy equation

$$m\rho\frac{dv_k}{dt} = \rho f_k + \nabla_j \Pi_{jk}, \tag{5.48}$$

is obtained for the fluid, where the body-forces read

$$f_k = -\nabla_k V + \gamma A_k e_{ij}\delta_{ij} + \alpha\epsilon_{ijk}v_i b_j, \tag{5.49}$$

and the stress tensor of the fluid, is given by

$$\Pi_{jk} = -\left[-\frac{\hbar^2}{4m}\nabla^2\rho + (\lambda - 1)\,\rho\eta - \gamma A_i J_i\right]\delta_{jk} + \sigma_{jk}. \tag{5.50}$$

5.3.4 Flow-dependent fluid pressure and body-force of dilation

Since the fluid pressure can be read from the diagonal components of the stress tensor (see Eq. 5.21), we see that

$$P = P_Q + (\lambda - 1)\,\rho\eta - \gamma A_i J_i, \tag{5.51}$$

depends on the overlap of the current density and the vector potential, and as such, depends explicitly on the canonical flow $\mathbf{u}$ of the fluid. In other words, the fluid pressure becomes a function of both independent dynamical variables ρ and $\mathbf{u}$. As we shall come to appreciate, this endows the fluid with a number of novel features. One such feature, which is readily apparent, is that the fluid pressure transforms from one Galilean frame of reference to another. In order to obtain Galilean covariant transformation laws where the pressure remains an invariant quantity, clearly, the nonlinear potentials will have to be transformed in some fashion. This is the subject of chapter 6. Expanding the current in expression (5.51), the fluid pressure may be presented in the form

$$P = P_Q + (\lambda - 1)\,\rho\eta + \frac{\gamma}{m}\rho A^2 - \gamma\rho A_i u_i. \tag{5.52}$$

We shall call the pressure term which depends explicitly on the canonical flow, the canonical flow pressure:

$$P_{\mathbf{u}} = -\gamma\rho A_i u_i. \tag{5.53}$$

Complementing the canonical flow pressure, two additional nonlinear body-forces enter Eq. (5.49) as a result of $\mathbf{A}\,(\rho)$. The last term in this expression, represents an α-modulated magnetic-like force due to the spatial dependence of $\mathbf{a}$. The second term

$$f_k^d = \gamma A_k e_{ij}\delta_{ij}, \tag{5.54}$$

results from the time-dependence of $\mathbf{A}$ in Eq. (5.31) and, interestingly, may be interpreted as a body-force of dilation. This follows from the continuity of fluid mass

from Eq. (5.11), which can be given the form

$$e_{ij}\delta_{ij} = -\frac{1}{\rho}\frac{d\rho}{dt}. \tag{5.55}$$

The right hand side of the above equation represents the dilation rate of the fluid [148]. Therefore, if we track an infinitesimal volume element of fluid as it flows, an additional body-force is exerted throughout the element of the fluid whenever the size of the volume changes.

5.4 The multi-component gauge potential

5.4.1 Quantum Hamilton-Jacobi equation of the fluid

So far, we have considered nonlinear vector potentials having a single dynamical component, the orientation of $\mathbf{A}$ at each point of space being fixed in time. From a mathematical perspective, this restriction can be circumvented by simply allowing for the possibility of additional dynamical components and a multi-component gauge potential to emerge in the form

$$\mathbf{A} = \sum_{n=1}^{N} \alpha'_n(\rho)\,\mathbf{a}'_n, \tag{5.56}$$

where the sum is carried over the total number of static vector fields $\mathbf{a}'_n$ determining the directions of gauge-flow imposed on the system. Although the $\mathbf{a}'_n$ are fixed and externally prescribed, the orientation of $\mathbf{A}$ will generally change in time through the ρ-dependence of the α'_n, so long as it is possible to find at least two independent linear combinations from the set $\mathbf{a}'_n$ which have different associated ρ-dependent component functions. When the $\mathbf{a}'_n$ take on values in physical space, the rank r of the matrix of coefficients $a_{ij}(\mathbf{x})$ is $r(\mathbf{x}) \leq 3$. An orthonormal local basis $a_{ij}(\mathbf{x}) = \hat{\mathbf{x}}_i \cdot \hat{\mathbf{a}}_j$ may be constructed for $\mathbf{A}$, such that

$$A_i = a_{ij}\alpha_j(\rho), \tag{5.57}$$

where $\alpha_i = \alpha_i(\alpha'_1, \cdots, \alpha'_N)$, and the $|\mathbf{a}_i|$ have been absorbed into the α_i so as to ensure $\mathbf{a}_i = \hat{\mathbf{a}}_i$. Since $a_{ij}a_{jk} = \delta_{ik}$, the α_i may be inverted as a function of the A_i, according to

$$\alpha_i = a_{ij}A_j. \tag{5.58}$$

Notice how each independent vector $\mathbf{A}_i$ comprising the multi-component gauge potential $\mathbf{A} = \hat{\mathbf{x}}_i A_i = \hat{\mathbf{a}}_i \alpha_i$, gives rise to an associated γ from Eq. (5.16). As a consequence, it will be useful to define the functions

$$\gamma_i = \frac{\rho}{\alpha_i} \frac{\partial \alpha_i}{\partial \rho}, \tag{5.59}$$

not summed over i. In the case where the α_i are identical functions of ρ, the multi-component gauge potential is abridged to the single component potential $A_i = a_i \alpha(\rho)$. In turn, when the orientation of the local basis is independent of position, a_{ij} can always be reduced to the identity matrix by performing a suitable orthogonal transformation. This is the multi-component equivalent of a uniform field $\mathbf{a}$ in the single-component system. In the more general case where a_{ij} depends on position, each basis vector $\mathbf{a}_i$ gives rise to an Eq. (5.29), calling for the extension

$$b_{kp} = \epsilon_{ijk} \nabla_i a_{jp}. \tag{5.60}$$

The dynamics of the field θ are governed by the canonical field Eq. (5.9). The Hamiltonian density of the field again takes the form of Eq. (5.10), but the components of the velocity field, now read

$$v_i = u_i - \frac{1}{m} a_{ij} \alpha_j(\rho), \tag{5.61}$$

where $u_i = \nabla_i \theta / m$ is the canonical flow. In this instance, Eq. (5.9) yields the quantum Hamilton-Jacobi equation

$$\partial_t \theta + \frac{1}{2} m v^2 - v_i \gamma_{ij} A_j + \lambda \eta + V + Q = 0, \tag{5.62}$$

where λ is again given by Eq. (5.17), but the dimensionless overlap modulation function γ regulating the strength of the nonlinear flow term, generalises to (see appendix A.2)

$$\gamma_{ij} = \sum_k a_{ik} \gamma_k a_{kj}, \tag{5.63}$$

where the γ_k are given by Eq. (5.59). The γ_{ij} define the couplings which take place in the wave equation between the components of flow v_i and the components of the gauge potential A_j from Eq. (5.57). Since the basis for $\mathbf{v}$ and the basis for $\mathbf{A}$ are different, the latter generally depending on position, the matrix of coefficients γ_{ij} at a given point of space will not be diagonal in general. If at point $\mathbf{x}_0$ both bases do coincide, $\gamma_{ij}(\mathbf{x}_0)$ is a diagonal matrix with diagonal elements γ_k.

5.4.2 Momentum-transport equation

In section 5.3.3, a Cauchy equation was derived by observing that the gradient of the Hamilton-Jacobi equation leads to an expression for the convective derivative of the velocity field. However, a more concise route to Cauchy's equation is furnished by the field description of the condensate. In this treatment, the dynamical state of the matter-field is completely specified by the stress-energy-momentum tensor

$$T_{\mu\nu} = -\sum_{\phi=\rho,\theta} \frac{\partial \mathcal{L}}{\partial(\partial_\mu \phi)} \partial_\nu \phi + \delta_{\mu\nu} \mathcal{L}, \tag{5.64}$$

while the transport equations governing the dynamics of energy-flow and momentum-flow, follow from the conservation law

$$\partial_\mu T_{\mu\nu} = \partial_\nu \mathcal{L}, \tag{5.65}$$

where we have adopted a relativistic-like notation with $\mu = 0, 1, 2, 3$. Recalling that the Lagrangian and Hamiltonian densities of a nonrelativistic Bose-condensed quantum fluid are related in the form $\mathcal{L} = -\rho\dot{\theta} - \mathcal{H}$, the field Lagrangian density associated with $\mathcal{H}$ from Eq. (5.10), assumes the form

$$\mathcal{L} = -\rho\left(\dot{\theta} + \frac{1}{2}mv^2 + \eta + V\right) - \mathcal{Q}. \tag{5.66}$$

Alternatively, $\mathcal{L}$ can be cast in terms of the fields and their spatial derivatives, by inserting the wave equation for θ into the above expression. Rendering $\mathcal{L}$ into this form is essential for evaluating the components of the stress tensor T_{ij}. For the particular case (5.61) considered here, substituting the wave equation (5.62) for θ into Eq. (5.66), yields

$$\mathcal{L} = -\frac{\hbar^2}{4m}\nabla^2\rho + (\lambda - 1)\,\rho\eta - J_i\gamma_{ij}A_j. \tag{5.67}$$

The stress-energy-momentum tensor in Eq. (5.64) characterises the dynamical state of the field by specifying the energy density, the momentum density, and the currents associated with both of these quantities. The energy density of the field is

$$-T_{00} \equiv \mathcal{H}. \tag{5.68}$$

The energy current density $-T_{k0} \equiv \mathcal{S}_k$, takes the form

$$\mathcal{S}_k = D\dot{\rho}w_k - \rho\dot{\theta}v_k, \tag{5.69}$$

where w_k is the osmotic velocity from Eq. (5.46) and D is the quantum diffusion coefficient. The canonical momentum density $T_{0k} \equiv \mathcal{P}_k$, reads

$$\mathcal{P}_k = \rho\nabla_k\theta = \rho m u_k. \tag{5.70}$$

Using both expressions (5.66) and (5.67) for $\mathcal{L}$, the canonical momentum current density or stress tensor T_{jk} of the field, is found to be

$$T_{jk} = \rho m\left(w_j w_k + v_j u_k\right) + \delta_{jk}\mathcal{L}. \tag{5.71}$$

The interpretation of Eqs. (5.69) and (5.71) as the respective current densities of the quantities defined in Eqs. (5.68) and (5.70), follows from the conservation law in Eq. (5.65), which separates out into an equation of continuity of energy

$$\partial_t\mathcal{H} + \boldsymbol{\nabla}\cdot\mathbf{S} = -\frac{\partial\mathcal{L}}{\partial t}, \tag{5.72}$$

and an equation of continuity of momentum

$$\partial_t\mathcal{P}_k + \nabla_j T_{jk} = \frac{\partial\mathcal{L}}{\partial x_k}. \tag{5.73}$$

Equation (5.73) is simply the field equivalent of Cauchy's equation (5.20). Note that the right hand sides of Eqs. (5.72) and (5.73) should be evaluated holding the fields and their derivatives constant. Notice also the difference in sign convention used for the fluid stress Π_{jk} in Eq. (5.20) and the field stress T_{jk} in Eq. (5.73). In addition to this sign difference, Π_{jk} and T_{jk} differ by a flow-stress term $m\rho v_j u_k$ as a result of the

relative motion between the fluid and field reference frames, such that

$$T_{jk} = -\Pi_{jk} + m\rho v_j u_k. \tag{5.74}$$

Substituting Eqs. (5.70) and (5.71) into (5.73) and making use of the continuity of fluid mass, leads to the following canonical momentum-transport equation for the fluid:

$$m\rho \left(\frac{\partial}{\partial t} + \mathbf{v} \cdot \boldsymbol{\nabla} \right) u_k = \frac{\partial \mathcal{L}}{\partial x_k} + \nabla_j \Pi_{jk}, \tag{5.75}$$

where the fluid stress takes the form

$$\Pi_{jk} = -P\delta_{jk} + \sigma_{jk}, \tag{5.76}$$

with σ_{jk} denoting the quantum stress tensor from Eq. (5.45), and P the fluid pressure, given by

$$P = P_Q + (\lambda - 1)\,\rho\eta - J_i \gamma_{ij} A_j. \tag{5.77}$$

This highlights the equivalence of the fluid pressure and the field Lagrangian density from Eq. (5.67). Supplementing the fluid stress, Eq. (5.73) indicates that a current

$$\frac{\partial \mathcal{L}}{\partial x_k} = \rho\,(-\nabla_k V + \alpha_j v_i \nabla_k a_{ij}) \tag{5.78}$$

is injected into the field as a result of the generally position-dependent local basis a_{ij}. The transport of canonical momentum in the fluid frame of reference is completely determined by the fluid stress and the body force density from Eqs. (5.76) and (5.78) respectively. A mechanical momentum-transport equation may then be obtained, simply by substituting the canonical flow u_k in Eq. (5.75) for the mechanical flow v_k from Eq. (5.61). In other words, the difference between canonical and mechanical momentum-transport stems from the additional body forces generated by the time dependence and the spatial dependence along fluid streamlines of the gauge potential, these taking the form

$$-\frac{dA_k}{dt} = \gamma_{kn} A_n \delta_{ij} e_{ij} - \alpha_j v_i \nabla_i a_{kj}. \tag{5.79}$$

Equations (5.61), (5.78) and (5.79), combine in expression (5.75) to yield a Cauchy equation (5.20) for the fluid, where the stress tensor of the fluid is given by Eq. (5.76)

and the body force of the single component case, generalises to

$$f_k = -\nabla_k V + \gamma_{kn} A_n \delta_{ij} e_{ij} + \alpha_n \epsilon_{ijk} v_i b_{jn}, \tag{5.80}$$

where b_{jn} is given by Eq. (5.60).

5.5 Ground state canonical flow-dipole in an inhomogeneous superfluid

In this final section, we illustrate an interesting effect of the flow nonlinearity on the ground state wavefunction of an inhomogeneous superfluid, described by the Gross-Pitaevskii-like Eq. (5.18). Here we assume that $\mathbf{a}(\mathbf{r})$ is constant. In the homogeneous case, the ground state exhibits a uniform flow equal to the gauge flow $-\mathbf{a}\rho_0/m$. For the inhomogeneous superfluid on the other hand, the ground state gauge flow varies generally from point to point. As we shall see, this leads to a non-trivial phase profile adopted by the ground state.

In order to numerically solve the ground state, it is convenient to scale our units for space and time: $\mathbf{r} \to \mathbf{r}/L$, $t \to t/T$, as outlined in appendix A.1. Under appropriate scaling, Eq. (5.18) reads as a dimensionless equation. Here, we present results for a condensate populated by $N = 1600$ particles in a box of dimension $d = 2$ with side length $L = 47$, containing 416×416 points. We let the origin of the system coincide with the center of the box and adopt Cartesian coordinates, denoting the horizontal and vertical axes by x and y, respectively. The effective strength and orientation of the gauge potential are prescribed by $\mathbf{a} = a\hat{\mathbf{a}}$. For our simulation, we have chosen, in units $\hbar L^2$, $a = 0.73$. We set the orientation of the gauge potential at angle $\pi/4$ relative to the x-axis, e.g. $\hat{\mathbf{a}} = (\hat{\mathbf{x}} + \hat{\mathbf{y}})/\sqrt{2}$. To establish an inhomogeneous ground state profile, we introduce an immobile impurity into the system, which we model as a Gaussian potential $V(\mathbf{r}) = V_0 e^{-\sigma r^2}$, where $r = |\mathbf{r}|$. Gaussian parameter values $\sigma = 0.5$ and $V_0 = 20$ were chosen.

In the case of a standard superfluid, the ground state of the system is that of a homogeneous density distribution, with the exception of the immediate region enclosing the impurity potential, where a density well is formed. The phase of the ground state

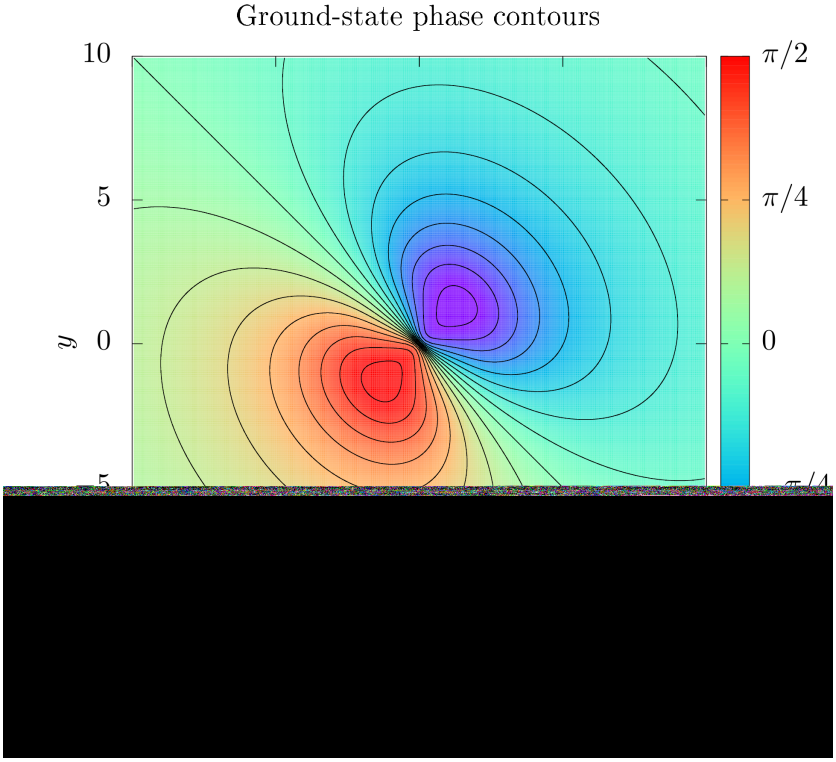

Figure 5.2: Plot showing the non-trivial phase profile adopted by the ground-state wavefunction in the vicinity of an immobile Gaussian impurity. 18 contours are included, equally spaced between $-\pi/2$ and $+\pi/2$.

wavefunction is constant over space and oscillates periodically in time. Let us consider the same situation in the case where a density-modulated gauge potential acts on the superfluid. When there is no impurity, the ground state is that of a homogeneous superfluid, where ρ and θ are constant over space. However, notice that the superfluid is not at rest, but exhibits a steady current as a result of the gauge-flow imparted by the potential. In other words, the ground state is in a steady state of flow even though no spatial phase twists occur in the system. Next, let us introduce the localised potential into the system. This leads to a density-depleted region in the vicinity of the impurity. As a consequence, the gauge-flow is no longer uniform as in the homogeneous case, but drops in magnitude upon approaching the center of the impurity. This introduces both non-vanishing transverse and longitudinal components for the gauge-flow $-\mathbf{a}\rho/m$. The longitudinal component is a significant energy expense for the system, due to the introduction of real-time dependence into the wave-amplitude of the state. One may verify numerically that an initial state (with non-vanishing ground state overlap), evolves in imaginary time in such a way that the divergence of the current assymptocially approaches zero throughout space. Notice that in order to achieve this and for the

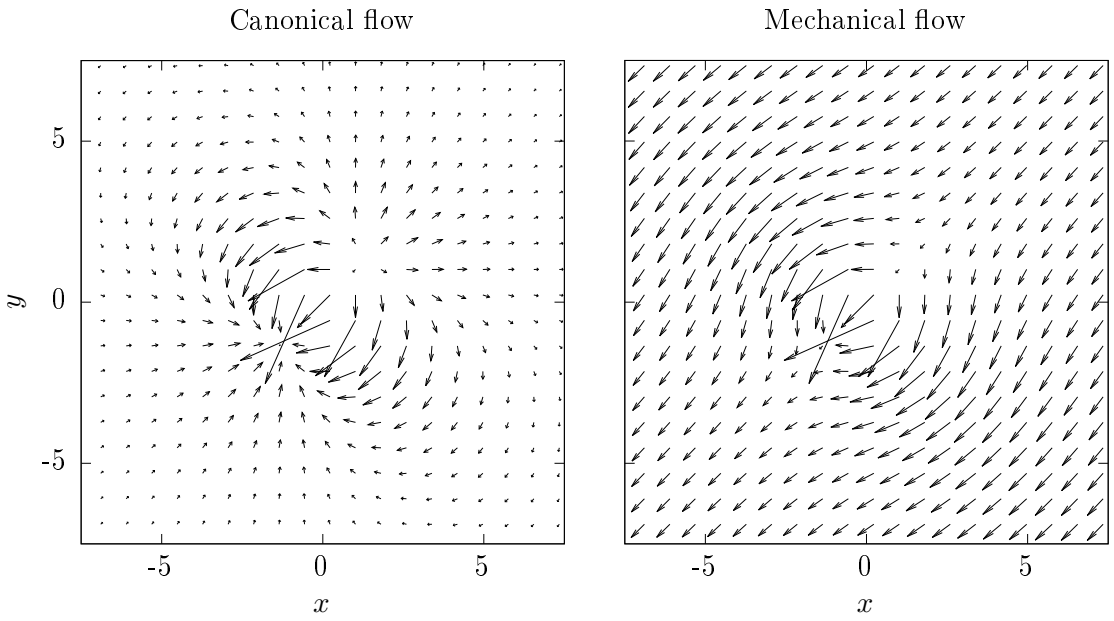

Figure 5.3: Plots showing the ground state canonical flow, $\mathbf{u}$, and mechanical flow, $\mathbf{v} = \mathbf{u} - \mathbf{A}/m$, in the vicinity of the impurity. The magnitude of the flow, in units $\hbar/(2mL)$, is given by the arrow length$\times 0.068$.

ground state density distribution to be preserved in time, a non-trivial local phase profile must be adopted by the wavefunction in order to compensate for the non-steady gauge-current. In other words, the ground state of the system exhibits a non-vanishing canonical flow. This is illustrated in FIG. 5.2, where we have plotted a series of ground state phase contours in the vicinity of the object, evenly spaced from $-\pi/2$ to $\pi/2$. Note that the ground state was obtained from an initial uniform state $\psi(\mathbf{r}) = 1$ by the method of imaginary time propagation, over a duration $\tau = 300$, with $\Delta\tau = 0.0017$. Although this may seem somewhat excessive, it is important to appreciate that both the amplitude and the phase are non-trivially configured in the ground state. This requires a significantly longer imaginary time compared to systems exhibiting a uniform ground state phase. From FIG. 5.2, we notice that the phase is antisymmetric under a parity transformation ($x \to -x, y \to -y$). In the bottom left half of the plot, the phase increases from 0 to $\pi/2$ as we approach $(-1.25, -1.25)$, whereas in the upper right half the phase decreases from 0 to $-\pi/2$ as we approach $(1.25, 1.25)$. In FIG. 5.3 we show a quiver plot of the associated ground-state canonical flow $\mathbf{u} = \left(\psi^* \boldsymbol{\nabla}\psi - \psi \boldsymbol{\nabla}\psi^*\right) / \left(i\left|\psi\right|^2\right)$ and mechanical flow $\mathbf{v} = \mathbf{u} - \mathbf{A}/m$, given in units $\hbar/(2mL)$. Here, we notice that $\mathbf{u}$ takes the form of a flow-dipole, leading to a mechanical flow field which skirts around the object. In turn, the canonical flow-dipole has interesting implications for the fluid

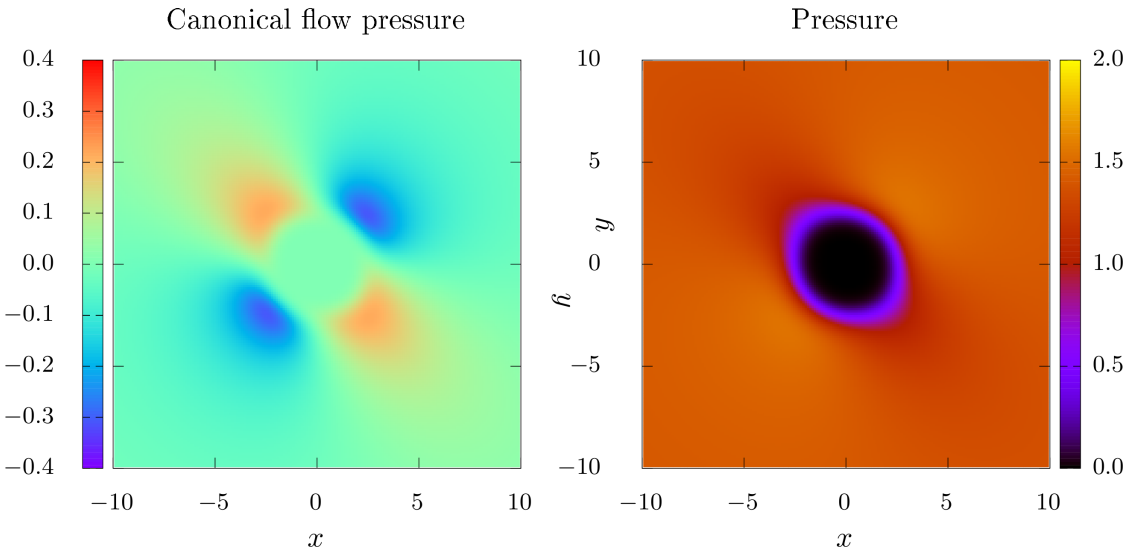

Figure 5.4: Plots showing the canonical flow pressure, $P_{\mathbf{u}}$, and the fluid pressure, P, of the ground state in the presence of an immobile impurity. The pressure is given in units $\hbar^2/(2mL^5)$ and asymmetric about the origin. The impurity is compressed along the axis of the nonlinear gauge ($y = x$) and stretched along the normal axis ($y = -x$).

pressure. For the superfluid studied here, the fluid pressure from Eq. (5.51), takes the form

$$P = -\frac{\hbar^2}{4m}\nabla^2\rho + \frac{g}{2}\rho^2 + \frac{a^2}{m}\rho^3 - \rho\mathbf{A}\cdot\mathbf{u}. \tag{5.81}$$

In figure 5.4, we show the ground state canonical flow pressure and total pressure, computed using the above expression. The flow nonlinearity favours occupation (inoccupation) of the blue (red) regions in the left image of FIG. 5.4, leading to an aspherical pressure about the impurity (right image). This leads to a strain, or deformation of the impurity, as seen in FIG. 5.5.

5.6 Conclusion

The hydrodynamic canonical formalism is an ideal framework for investigating the dynamical equations of a matter-field whose effective Hamiltonian features nonlinear interaction terms which take the simplest form when expressed as functionals of the amplitude and the phase of the complex field. For instance, when the effective kinetic energy of the field becomes nonlinear in the density, through a density-dependent gauge potential, it is easy to see that nonlinear flow-dependent terms invariably enter the wave equation of the condensate. In turn, two non-trivial terms emerge in the mechanical momentum-transport equation of the fluid: a flow-dependent fluid pressure and a body force of dilation. These should have important consequences for the Galilean covariance

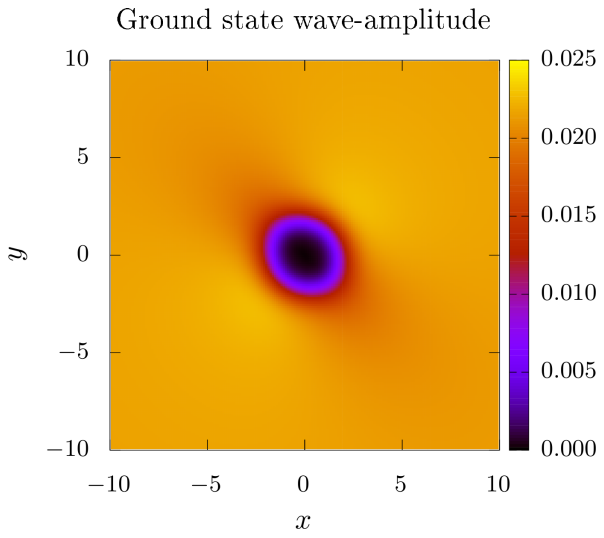

Figure 5.5: Ground state wave-amplitude, $\sqrt{\rho/N}$, in the vicinity of an immobile Gaussian impurity.

of the fluid, where new transformations laws may be required in order to restore the invariance of the fluid under the transformation group. The immediate lack of Galilean invariance should also carry significant implications for the elementary excitations of the fluid. For instance, it should no longer be the case that the velocity of sound be determined simply by $\partial P/\partial\rho$, since P depends explicitly on the canonical flow. This calls for a generalisation of the expression used to derive the velocity of sound from the fluid pressure. Finally, the nonlinear body force of dilation will appear in the expectation value of the time derivative of the mechanical momentum and could therefore be investigated numerically in the drag force acting on an impurity moving through the fluid. For typical quantum fluids, the drag force is determined by the configuration of the fluid density in the vicinity of the localised object potential. In contrast, the reaction to the body force of dilation exerted on a fluid subject to $\mathbf{A}(\rho)$, should occur throughout the whole fluid, taking place wherever the mechanical flow displays non-vanishing divergence.

Chapter 6

Gauge transformations and Galilean covariance

6.1 Introduction

In this chapter, we investigate the invariance properties of a nonlinear gauge-coupled quantum fluid. In particular, we derive the covariant transformation laws for the nonlinear potentials under a space-time Galilean boost and consider $U(1)$ gauge transformations. Generally speaking, a symmetry transformation constitutes any set of transformations of the physical system which leaves the form of the dynamical equations unchanged. The dynamical state of an ideal fluid is completely specified by the fluid distribution ρ and the flow field $\mathbf{v}$. These are the independent dynamical variables. In the context of field transformations (no space-time transformations), it is clear that the density ρ at any given time t_0 can not be changed in general. However, the situation is not so restricted for the flow field $\mathbf{v}$ of a quantum fluid. Since the absolute value of the phase bears no influence on $\mathbf{v}$ but only local spatial differences of θ, we can carry out local transformations of θ and introduce a (gauge) field which counter-balances the resulting flow accordingly. This is the premise of local $U(1)$ gauge transformations. Notice that if we had demanded something similar for ρ, a local transformation of ρ would require a counter-balancing mass injection field. Alternatively, instead of performing active field transformations, we can consider space-time coordinate transformations and investigate how fields must transform in order to ensure the form invariance of the dynamical equations.

To begin with, we give an overview of the Galilean and gauge symmetries of the

Schrödinger field coupled to *external* scalar and vector potentials $\phi(\mathbf{r},t)$ and $\mathbf{A}(\mathbf{r},t)$. In doing so, we introduce the basic framework used for the more general nonlinear problem and establish a ground for comparison with known results. Furthermore, the treatment of the Galilean covariance of the Schrödinger equation under coupling to a vector potential is surprisingly absent from standard quantum mechanics textbooks. For these reasons, the Schrödinger field was deemed suitable as a preliminary case study. It should be emphasised that our concern lies not with the physical origin of the coupling to the potentials, but rather, the formal structure of the dynamical equations which result from the coupling. Thus, although ϕ and $\mathbf{A}$ may enter as a result of coupling to the electromagnetic field, this need not strictly be the case. The only requirement that we make of the potentials is that these act "externally" on the Schrödinger field, thereby taking the form of space-time dependent external functions which couple linearly to the density and the flow of the matter-field.

6.2 Symmetries of the Schrödinger field

6.2.1 Hydrodynamics of the Schrödinger field

The Schrödinger equation for a particle subject to external scalar and vector potentials $\phi(\mathbf{r},t)$ and $\mathbf{A}(\mathbf{r},t)$, is given by

$$i\hbar\partial_t\psi = \left[\frac{\left(\hat{\mathbf{p}} - \mathbf{A}(\mathbf{r},t)\right)^2}{2m} + \phi(\mathbf{r},t)\right]\psi. \tag{6.1}$$

This wave equation may be derived from a hydrodynamic canonical field formalism, where the amplitude ρ and the phase θ of the Schrödinger wavefunction $\psi = \sqrt{\rho}e^{i\frac{\theta}{\hbar}}$, form a canonical pair of conjugate variables, governed by the field equations

$$\dot{\rho}(\mathbf{r}) - \frac{\delta H}{\delta\theta(\mathbf{r})} = 0, \tag{6.2}$$

$$\dot{\theta}(\mathbf{r}) + \frac{\delta H}{\delta\rho(\mathbf{r})} = 0, \tag{6.3}$$

where the Hamiltonian functional of the field, is given by

$$H[\rho,\theta] = \int d^3\mathbf{r}\left\{\rho\left[\frac{(\boldsymbol{\nabla}\theta - \mathbf{A})^2}{2m} + \phi\right] + \mathcal{Q}\right\}, \tag{6.4}$$

with $\mathcal{Q}$ denoting the quantum energy density from Eq. (5.5). Inserting Eq. (6.4) into the field Eqs. (6.2) and (6.3), yields, respectively, the wave equations

$$\partial_t \rho + \boldsymbol{\nabla} \cdot (\rho \mathbf{v}) = 0, \tag{6.5}$$

$$\partial_t \theta + \frac{1}{2} m v^2 + \phi + Q = 0, \tag{6.6}$$

where $v = \mathbf{v}$, is the modulus of the mechanical flow

$$\mathbf{v} = \frac{1}{m} \left(\boldsymbol{\nabla} \theta - \mathbf{A} \right), \tag{6.7}$$

and Q is the quantum potential from Eq. (3.45). Under a Madelung transformation (3.38), the pair of real coupled equations (6.5) and (6.6) map onto the Schrödinger equation (6.1).

The quantum Hamilton-Jacobi equation of the Schrödinger field, from Eq. (6.6), may be cast into a hydrodynamic Cauchy form

$$m\rho \left(\frac{\partial}{\partial t} + \mathbf{v} \cdot \boldsymbol{\nabla} \right) v_k = \rho f_k + \nabla_j \Pi_{jk}. \tag{6.8}$$

As such, we follow the language of Madelung [96] and Rosen [152] and refer to the Schrödinger field as a pseudofluid. The stress tensor of the pseudofluid, is given by

$$\Pi_{jk} = -P_Q \delta_{jk} + \sigma_{jk}, \tag{6.9}$$

where P_Q is the quantum pressure from Eq. (5.44) and σ_{jk} is the quantum stress tensor from Eq. (5.45). In turn, the body-force takes the 'Lorentz' form

$$f_k = -\nabla_k \phi - \partial_t A_k + v_i \left(\nabla_k A_i - \nabla_i A_k \right). \tag{6.10}$$

6.2.2 Gauge invariance of the Schrödinger pseudofluid

It is well-known that the wave Eqs. (6.5) and (6.6) (or equivalently Eq. (6.1)), are form invariant under local phase transformations (unitary transformations of ψ)

$$\theta \to \theta' = \theta + \chi \left(\mathbf{r}, t \right), \tag{6.11}$$

if one demands that the potentials simultaneously undergo the transformations

$$\mathbf{A} \to \mathbf{A}' = \mathbf{A} + \boldsymbol{\nabla}\chi\left(\mathbf{r}, t\right), \tag{6.12}$$

$$\phi \to \phi' = \phi - \partial_t \chi\left(\mathbf{r}, t\right), \tag{6.13}$$

where χ is an arbitrary single-valued scalar function of $\mathbf{r}$ and t. The combination of transformations (6.11)-(6.13) is referred to as a *gauge transformation*.. The form invariance of the wave equations under a gauge transformation may be seen from the canonical field Eqs. (6.2) and (6.3), which transform to

$$\dot{\rho}\left(\mathbf{r}\right) - \frac{\delta H'}{\delta \theta'\left(\mathbf{r}\right)} = 0, \tag{6.14}$$

$$\dot{\theta}'\left(\mathbf{r}\right) + \frac{\delta H'}{\delta \rho\left(\mathbf{r}\right)} = 0, \tag{6.15}$$

under Eqs. (6.11)-(6.13), where

$$H' = \int d^3\mathbf{r} \left\{ \rho \left[\frac{\left(\boldsymbol{\nabla}\theta' - \mathbf{A}'\right)^2}{2m} + \phi' \right] + \mathcal{Q} \right\}. \tag{6.16}$$

In the Madelung representation, it becomes evidently clear from Eqs. (6.11), (6.12) and (6.7), that an arbitrary gauge transformation leaves the mechanical flow field unchanged. In other words, $\mathbf{v}$ is a gauge invariant quantity. Hence, according to Eq. (6.16), the new and old Hamiltonians are related in the form

$$H'\left[\rho, \theta'\right] = H\left[\rho, \theta\right] - \int d^3\mathbf{r} \rho \frac{\partial \chi\left(\mathbf{r}, t\right)}{\partial t}. \tag{6.17}$$

Note here that χ is not a field variable, but an externally prescribed function, e.g. $\delta\chi = 0$. Hence, taking the first variation of both sides, we find

$$\frac{\delta H'}{\delta \theta'\left(\mathbf{r}\right)} = \frac{\delta H}{\delta \theta\left(\mathbf{r}\right)}, \tag{6.18}$$

$$\frac{\delta H'}{\delta \rho\left(\mathbf{r}\right)} = \frac{\delta H}{\delta \rho\left(\mathbf{r}\right)} - \frac{\partial \chi\left(\mathbf{r}, t\right)}{\partial t}, \tag{6.19}$$

Inserting the first and second of these equations into, respectively, Eqs. (6.14) and (6.15), we immediately recover the original field Eqs. (6.2) and (6.3). Hence, the canonical equations of the Schrödinger field are form invariant under a gauge transformation (6.11)-(6.13).

6.2.3 Galilean invariance of the Schrödinger pseudofluid

Having investigated a symmetry group associated with active transformations of the fields, we now trun our attention to a space-time symmetry group associated with coordinate transformations, namely, Galilean transformations. To this end, observe that the coordinate transformations from some inertial frame of reference Σ, to another frame Σ' moving with a uniform, nonrelativistic relative velocity $\mathbf{w}$, may be written in the general form [153–155]

$$\begin{aligned} x_i \to x_i' &= R_{ij}x_j - w_i t + a_i, \\ t \to t' &= t + t_0, \end{aligned} \tag{6.20}$$

where a_i and t_0 are constants representing offsets in position and time respectively, and R_{ij} is a unitary rotational matrix satisfying $R_{ij}R_{jk} = \delta_{ik}$. Transformations (6.20) define the *Galilean group*. Notice that differential operators will also generally transform between frames under (6.20), according to

$$\nabla_i \to \nabla_i' = R_{ij}\nabla_j, \tag{6.21}$$

$$\frac{\partial}{\partial t} \to \frac{\partial}{\partial t'} = \frac{\partial}{\partial t} + w_i R_{ij}\nabla_j. \tag{6.22}$$

In turn, the velocity transformation, is restricted by

$$v_i \to v_i'\left(\mathbf{r}', t'\right) = R_{ij}v_j\left(\mathbf{r}, t\right) - w_i. \tag{6.23}$$

Since the energy and momentum of a particle transforms under a Galilean boost, and these quantities are encoded in the phase, the phase also transforms between reference frames. Let us denote this transformation, by

$$\theta \to \theta'\left(\mathbf{r}', t'\right) = \theta\left(\mathbf{r}, t\right) + \chi\left(\mathbf{r}, t\right). \tag{6.24}$$

Furthermore, we should not exclude the possibility that the potentials may be subject to transformations in order to ensure the form invariance of the field equations. Accordingly,

let us write

$$\phi \to \phi'(\mathbf{r}', t') = \phi(\mathbf{r}, t) + \mu(\mathbf{r}, t), \tag{6.25}$$

$$A_i \to A_i'(\mathbf{r}', t') = R_{ij} A_j(\mathbf{r}, t) + G_i(\mathbf{r}, t). \tag{6.26}$$

In the frame Σ', the canonical field equations, read

$$\frac{\partial \rho'(\mathbf{r}', t')}{\partial t'} - \frac{\delta H'}{\delta \theta'(\mathbf{r}', t')} = 0, \tag{6.27}$$

$$\frac{\partial \theta'(\mathbf{r}', t')}{\partial t'} + \frac{\delta H'}{\delta \rho'(\mathbf{r}', t')} = 0, \tag{6.28}$$

where the Hamiltonian transforms to

$$H' = \int d^3\mathbf{r}' \left[\rho' \left(\frac{1}{2} m \mathbf{v}' \cdot \mathbf{v}' + \phi' \right) + \mathcal{Q}' \right], \tag{6.29}$$

where, for convenience, we now denote $\rho' \equiv \rho'(\mathbf{r}', t')$, $\phi' \equiv \phi'(\mathbf{r}', t')$ and so on, and $\mathbf{v}' = (\boldsymbol{\nabla}'\theta' - \mathbf{A}')/m$. However, recall that $\mathbf{v}'$ is restricted by Eq. (6.23). Hence, the Hamiltonians in the two frames are related, by

$$H'[\rho', \theta'] = H[\rho, \theta] + \int d^3\mathbf{r} \rho \left(\frac{1}{2} m w^2 - m w_i R_{ij} v_j + \mu \right), \tag{6.30}$$

where $\rho \equiv \rho(\mathbf{r}, t)$, $\theta \equiv \theta(\mathbf{r}, t)$ and so on. Since $\rho' = \rho$ and $\delta\chi = 0$, the first variation of both sides, gives

$$\frac{\delta H'}{\delta \rho'} = \frac{\delta H}{\delta \rho} + \frac{1}{2} m w^2 - m w_i R_{ij} v_j + \mu, \tag{6.31}$$

$$\frac{\delta H'}{\delta \theta'} = \frac{\delta H}{\delta \theta} + w_i R_{ij} \nabla_j \rho. \tag{6.32}$$

To obtain Eq. (6.32), we have substituted Eq. (6.7) for $\mathbf{v}$ into Eq. (6.30) and integrated by parts accordingly. Inserting Eqs. (6.22) and (6.32) into Eq. (6.27), reveals that the field equation for ρ is form invariant under transformations (6.20) and (6.24). Notice here that no demands are being made of μ, $\mathbf{G}$ or χ, other than the restriction that χ be independent of θ, since the violation of the latter introduces additional terms in Eq. (6.32). Turning our attention to the field equation for θ, let us substitute Eqs. (6.22),

(6.24) and (6.30) into Eq. (6.28), which gives

$$\dot{\theta} + \frac{\delta H}{\delta \rho} + \xi = 0, \tag{6.33}$$

where we have grouped the additional terms generated by the Galilean transformation, in the function

$$\xi = \left(\frac{\partial}{\partial t} + w_i R_{ij} \nabla_j \right) \chi + w_i R_{ij} \left(\nabla_j \theta - m v_j \right) + \frac{1}{2} m w^2 + \mu. \tag{6.34}$$

In other words, a suitably chosen set of transformations (6.24), (6.25) and (6.26) which solve $\xi = 0$, signals the form invariance of the field equation under a Galilean transformation. Observe in particular how the functional form of ξ in Eq. (6.34) holds true irrespective of whether the pseudofluid couples to a vector potential.

Coupling to an external scalar potential When the matter-field couples exclusively to an external scalar potential ϕ, the flow $\mathbf{v} = \boldsymbol{\nabla}\theta/m = \mathbf{u}$ is entirely potential and the momentum and energy transformations generated by a Galilean boost can be compensated fully by a suitable phase factor χ, with no additional transformations of the potentials being required. This follows immediately from the fact that the second bracket term in Eq. (6.34) vanishes for potential flows. Hence, we may set $\mu = 0$ and the form invariance of the field equation is ensured for a local phase factor $\chi(\mathbf{r}, t)$, satisfying

$$\left(\frac{\partial}{\partial t} + w_i R_{ij} \nabla_j \right) \chi + \frac{1}{2} m w^2 = 0. \tag{6.35}$$

Clearly, $\chi = m w^2 t/2 - m w_i R_{ij} x_j$ solves the above equation. Hence, the phase transformation

$$\theta \to \theta + \frac{1}{2} m w^2 t - m w_i R_{ij} x_j, \tag{6.36}$$

guarantees the form invariance of the field equation for θ under the Galilean group (6.20). This should not come as a surprise, since an overall momentum is imparted onto the pseudofluid through the spatial dependence of χ, by imprinting a uniform phase twist $\nabla_i \chi = -m R_{ij} w_j$. Similarly, the kinetic energy generated by the boost is accounted for through the time-dependent phase factor $m w^2 t/2$.

Additional coupling to an external vector potential When the Schrödinger field couples to an external "physical" vector potential $\mathbf{A}$, the flow $\mathbf{v}$ takes the covariant

form of Eq. (6.7). By physical, we mean a vector potential which cannot be eliminated through a suitable choice of gauge without destroying the form of the wave equation. In the case of interest here, namely when $\mathbf{A}$ is externally prescribed, this is equivalent to the condition that $\mathbf{A}$ possesses a non-vanishing rotational (transverse) component, since any residual irrotational (longitudinal) component can be absorbed into the phase. However, we emphasise that this equivalence holds because $\mathbf{A}$ is external. For instance, in the case of a density-dependent vector potential, we shall learn that it is not possible to absorb the longitudinal component of flow into the phase while simultaneously retaining the form of the wave equation.

Under coupling to $\mathbf{A}$, notice that the second bracket term in Eq. (6.34) no longer vanishes. As a result, the potentials now transform between frames, where the form invariance of the field equation is restored by demanding that

$$\begin{aligned} \phi &\to \phi - w_i R_{ij} A_j \\ A_i &\to R_{ij} A_j. \end{aligned} \tag{6.37}$$

Hence, the Schrödinger field is invariant under the symmetry group of transformations (6.20), (6.36) and (6.37). There are surprisingly few instances where transformations (6.37) have appeared in the quantum mechanics literature. This point was brought to attention in a paper by Brown and Holland [156] in 1998. After retrieving transformations (6.37) using a different formalism to that adopted here, they refer to the work of DeWitt [157] in 1957 and Takagi [158] in 1991 as the only 2 appearances of these transformations in quantum mechanics.

An equivalent way of establishing Galilean symmetry is to see whether the body-force acting on the pseudofluid, f_k from Eq. (6.10), is invariant under (6.20) and (6.37). If the origin of the coupling is electromagnetic, the electric field $E_k = -\nabla_k \phi - \partial_t A_k$ and magnetic field $B_k = \epsilon_{ijk} \nabla_i A_j$ acting on a charged pseudofluid of unit charge, transform as

$$E_k \to E_k + \epsilon_{ijk} w_i B_j \tag{6.38}$$

$$B_k \to B_k, \tag{6.39}$$

under (6.37). For simplicity we have assumed that $R_{ij} = \delta_{ij}$. Therefore, although the associated force fields $f_k^E = E_k$ and $f_k^B = \epsilon_{ijk} v_i B_j$, in turn, transform according to

$$f_k^E \to f_k^E + \epsilon_{ijk} w_i B_j, \tag{6.40}$$

$$f_k^B \to f_k^B - \epsilon_{ijk} w_i B_j, \tag{6.41}$$

the additional terms generated by the respective transformations of $\mathbf{E}$ and $\mathbf{B}$, cancel, thereby leaving the total Lorenz force $f_k = E_k + \epsilon_{ijk} v_i B_j$ invariant.

As a final note, we point out that transformations (6.37) emerge as the "magnetic limit" of Galilean electromagnetism, first discovered in 1973 by Lévy-Leblond and Le Bellac [159]. Here Galilean electromagnetism refers to the low-velocity limit of special relativity. In other words, the Galilean transformation of the electromagnetic potentials emerge as a limiting case of a Lorentz transformation. Two distinct Galilean limits exist in the Lorentz transformation of the 4-potential $(\phi/c, \mathbf{A})$: the timelike 4-vector limit where $|\mathbf{w}|/c \ll 1$ and $|\mathbf{A}| \ll \phi/c$, and the spacelike 4-vector limit where $|\mathbf{w}|/c \ll 1$ and $|\mathbf{A}| \gg \phi/c$. In the first limit, it is the electric field which remains unchanged by the transformation, whereas in the second limit it is the magnetic field, as seen in Eq. (6.39). Hence, these are refered to respectively, as "electric limit" and "magnetic limit". See [160–162] for recent reviews on this topic. Note that the Galilean covariance of nonrelativistic quantum mechanics was shown to be compatible only with the magnetic limit [156].

6.3 The nonlinear gauge-coupled field

Having concluded our review of the gauge invariance and Galilean covariant transformation laws of the Schrödinger field, we now turn our attention to the symmetry properties of the nonlinear gauge-coupled field. Our study pertains to the class of nonlinear fields characterised by a Hamiltonian of the form

$$H = \int d^3\mathbf{r} \left\{ \rho \left[\frac{\left(\boldsymbol{\nabla}\theta - \mathbf{A}\left(\rho\right)\right)^2}{2m} + \eta\left(\rho\right) \right] + \mathcal{Q} \right\}, \tag{6.42}$$

whose dynamics are governed by the canonical field Eqs. (6.2) and (6.3). Recall that the characteristic dynamical feature of a fluid subject to a density-dependent gauge potential, is that of a flow-dependent nonlinear term in the resulting wave equation. The latter emerging in the form

$$\partial_t \theta + \frac{1}{2} m v^2 + \Phi\left(\rho, \mathbf{u}\right) + Q = 0, \tag{6.43}$$

where, $\Phi = \eta + \rho \partial \eta / \partial \rho - \rho \mathbf{v} \cdot \partial \mathbf{A} / \partial \rho$, is a nonlinear scalar potential which depends on the density and is linear in the canonical flow $\mathbf{u} = \boldsymbol{\nabla} \theta / m$.

6.3.1 Gauge transformations

Under a gauge transformation

$$\theta \rightarrow \theta' = \theta + \chi, \tag{6.44}$$

$$\mathbf{A} \rightarrow \mathbf{A}' = \mathbf{A} + \boldsymbol{\nabla} \chi, \tag{6.45}$$

$$\eta \rightarrow \eta' = \eta - \partial_t \chi, \tag{6.46}$$

the canonical field equations, transform to Eqs. (6.14) and (6.15), where H' is given by Eq. (6.16), replacing ϕ' with η'. Hence, the relation between H and H' again takes the form of Eq. (6.17). We may therefore conclude that the canonical equations and associated wave equations of the nonlinear gauge-coupled field, are form invariant under gauge transformations associated with *external* gauge functions $\chi \equiv \chi\left(\mathbf{r}, t\right)$. In other words, we may perform arbitrary external gauge transformations without destroying the form of the dynamical equations.

6.3.2 Nonlinear gauge functions

Thus far in this thesis, we have treated the nonlinear gauge potential as a physical vector potential which could not be gauged away without destroying the form of the wave equation. In this section, we demonstrate why this is the case. To begin with, notice that any attempt to absorb $\mathbf{A}\left(\rho\right)$ into the phase, involves a gauge function χ which is related to the contour integral of some function of the density. Hence, one should examine how the field equations transform under a nonlinear gauge transformation of the form (6.44)-(6.46), where $\chi \equiv \chi\left[\rho\right]$ becomes a functional of the density. Notice that,

in doing so, the field variables, transform to

$$\begin{pmatrix} \rho \\ \theta \end{pmatrix} \rightarrow \begin{pmatrix} \rho' = \rho \\ \theta' = \theta + \chi\left[\rho\right] \end{pmatrix}. \tag{6.47}$$

Let us check whether the new variables form a canonical pair of conjugate variables. To this end, recall that the Poisson bracket of two dynamical variables, is given by Eq. (3.48). The Poisson bracket of the new variables with respect to the old variables, then gives

$$\left\{\rho'\left(\mathbf{x}\right), \theta'\left(\mathbf{y}\right)\right\}_{\rho,\theta} = \int d^3\mathbf{r} \left(\frac{\delta\rho'\left(\mathbf{x}\right)}{\delta\rho\left(\mathbf{r}\right)} \frac{\delta\theta'\left(\mathbf{y}\right)}{\delta\theta\left(\mathbf{r}\right)} - \frac{\delta\rho'\left(\mathbf{x}\right)}{\delta\theta\left(\mathbf{r}\right)} \frac{\delta\theta'\left(\mathbf{y}\right)}{\delta\rho\left(\mathbf{r}\right)} \right) = \delta\left(\mathbf{x}-\mathbf{y}\right), \tag{6.48}$$

on account of ρ' being independent of θ. Hence θ' and ρ may be treated as independent variables.

Since χ is independent of θ, Eq. (6.18) remains valid and the canonical equation for ρ is form invariant under the nonlinear transformation, However, the canonical equation for θ is no longer form invariant, but transforms according to

$$\dot{\theta}' + \frac{\delta H}{\delta\rho} - \frac{\delta}{\delta\rho} \int d^3\mathbf{r}\rho\partial_t\chi\left[\rho\right] = 0, \tag{6.49}$$

where an additional term appears due to $\chi\left[\rho\right]$. Although the form taken by the additional term depends on $\chi\left[\rho\right]$, one may see that current terms will generally be involved, through $\partial_t\chi\left[\rho\right]$. In the following section, we examine one such gauge functional.

6.3.3 The one-dimensional gauge-coupled superfluid

Typically, one may be interested in gauge functions which eliminate the gauge potential from the kinetic energy density. Here, we consider the superfluid described by the Gross-Pitaevskii-like equation (5.18), in dimension $d = 1$, since the last term in Eq. (6.49) becomes integrable. The system is described the wave equation

$$\partial_t\theta + \frac{1}{2}mv^2 - aJ + g\rho + Q = 0, \tag{6.50}$$

where $v = \left(\partial_x\theta - a\rho\right)/m$ and $J = \rho v$. The gauge functional which eliminates $\mathbf{A}$, is

$$\chi = -\int_{-\infty}^{x} dy a\rho\left(y,t\right). \tag{6.51}$$

In terms of the new field variable, θ', the Hamiltonian (6.16) is found to be

$$H' = \int dx \left\{ \rho \left[\frac{(\partial_x \theta')^2}{2m} + \frac{g}{2}\rho \right] + \mathcal{Q} \right\} - \int dx \rho^2 a v', \tag{6.52}$$

where $v' = \partial_x \theta'/m$. The first integral in Eq. (6.52) is simply the old Hamiltonian in the new variables. Hence, an additional term $-\int dx J' A$, appears in the Hamiltonian under the nonlinear gauge transformation. Recall that $-JA$ represents the gauge-pressure, namely, the contribution of the gauge potential to the fluid pressure. In other words, the gauge-pressure is generated in the Hamiltonian density when one attempts to eliminate the nonlinear vector potential. Inserting expression (6.52) for H' into the field Eq. (6.15), yields the wave equation

$$\partial_t \theta' + \frac{1}{2} m v' v' - 2aJ' + g\rho + Q = 0, \tag{6.53}$$

where $J' = \rho v'$ and we have used $\delta v'/\delta \rho = 0$, which holds on account of ρ and θ' being independent. Comparing Eqs. (6.50) and (6.53), we see that the wave equation has transformed under the nonlinear gauge transformation. In particular, the attempt to absorb the nonlinear gauge potential into the phase has produced an additional current term in the wave equation.

6.4 Galilean covariance

The extension of the Galilean covariant transformation laws of the Schrödinger field to the case of a nonlinear gauge-coupled field, is straight forward. Here, relations (6.20)-(6.24) still apply in the Σ' frame. However, in view of the ρ-dependence of the potentials, we anticipate that the previous transformation law (6.37) for external potentials, now takes the nonlinear form

$$\eta(\rho) \to \eta'(\rho') = \eta(\rho) + \mu(\rho), \tag{6.54}$$

$$A_i(\rho) \to A'_i(\rho') = R_{ij} A_j(\rho) + G_i(\rho), \tag{6.55}$$

where, as previously, primed and unprimed quantities are observed from, respectively, frames Σ' and Σ, e.g. $A'_i(\rho') \equiv A'_i(\rho'(\mathbf{r}', t'))$ and so on. The canonical field equations in the Σ' frame, read as Eqs. (6.27) and (6.28), where H' again takes the form of Eq.

(6.29), replacing ϕ' by η'. Similarly, the Hamiltonians in the two frames are related by Eq. (6.30). Since $\rho' = \rho$, $\delta\chi = 0$ and the transformed potentials are independent of θ, Eq. (6.32) is recovered and the field equation for ρ is form invariant under the transformation, as previously. However, due to the ρ-dependence of μ and $\mathbf{v}$, Eq. (6.31) becomes

$$\frac{\delta H'}{\delta \rho'} = \frac{\delta H}{\delta \rho} + \frac{1}{2} m w^2 - m w_i R_{ij} v_j + \mu + \rho \left(\frac{\partial \mu}{\partial \rho} + w_i R_{ij} \frac{\partial A_j}{\partial \rho} \right). \tag{6.56}$$

Inserting the above expression into the transformed field equation (6.28) and recalling Eq. (6.36) for the space-time dependent phase factor, leads to

$$\dot{\theta} + \frac{\delta H}{\delta \rho} + \xi = 0, \tag{6.57}$$

where, following our usual convention, we have denoted the additional terms generated under the transformation by ξ, which in this instance reads

$$\xi = \mu + w_i R_{ij} A_j + \rho \left(\frac{\partial \mu}{\partial \rho} + w_i R_{ij} \frac{\partial A_j}{\partial \rho} \right). \tag{6.58}$$

Clearly, $\xi = 0$ is ensured if $\mu(\rho) = -w_i R_{ij} A_j(\rho)$, demanding that the nonlinear potentials undergo the transformations

$$\eta \to \eta - w_i R_{ij} A_j, \tag{6.59}$$

$$A_i \to R_{ij} A_j. \tag{6.60}$$

Hence, we have obtained the covariant transformations of the nonlinear potentials between Galilean frames. These are identical in form to those of the Schrödinger field subject to external potentials, but represent a nonlinear transformation. In turn, we find that Φ from Eq. (6.43) undergoes the usual Galilean covariant transformation for scalar potentials, since performing (6.23) and (6.59) yields

$$\Phi \to \Phi - w_i R_{ij} A_j. \tag{6.61}$$

Similarly, although the fluid pressure

$$P = P_Q + \rho^2 \left(\frac{\partial \eta}{\partial \rho} - \mathbf{v} \cdot \frac{\partial \mathbf{A}}{\partial \rho} \right), \tag{6.62}$$

depends explicitly on $\mathbf{v}$ and $\mathbf{v}$ clearly changes under a Galilean transformation, the covariant transformations of the potentials between frames leave the pressure (6.62) invariant.

6.5 Conclusion

In summary, we have found that the dynamical equations of a nonlinear gauge-coupled field are invariant under local gauge transformations, insofar as the gauge function χ takes the form of an external scalar function of $\mathbf{r}$ and t. However, when χ becomes a functional of the density, the form invariance of the dynamical equation for θ is lost. In other words, the field equation changes under a nonlinear gauge transformation. Therefore, all density-dependent gauge potentials are physical, non-trivial gauge potentials which cannot be absorbed into the quantum phase (gauged away), since attempting to do so inevitably destroys the form of the wave equation. This should not come as too much of a surprise, since the form of the nonlinear flow term entering in the wave equation is the result of a particular ρ-dependence of the gauge potential. If the ρ-dependence of $\mathbf{A}$ is unchanged by the transformation, the nonlinear flow term remains intact. On the other hand, altering the ρ-dependence invariably changes the form of the nonlinear flow term. In the case of a gauge-coupled superfluid in dimension $d = 1$, the additional term generated in the field equation under a nonlinear gauge transformation, becomes integrable. In particular, the attempt to absorb the gauge potential into the phase, generates a gauge-pressure term in the Hamiltonian density. Finally, we investigated how the field equations transform under an arbitrary Galilean transformation. Here we found that the Galilean covariance of the nonlinear fluid may be restored by subjecting the potentials to a nonlinear transformation, which is identical in form to that of the Schrödinger field subject to external scalar and vector potentials.

Chapter 7

Elementary excitations and sound propagation

7.1 Introduction

Furthering our investigations of the hydrodynamical properties of nonlinear gauge-coupled quantum fluids, we now turn our attention to the study of low-lying elementary excitations and sound propagation. The ability of a fluid to propagate sound stems from its compressibility, since the propagation of a disturbance across the fluid is achieved through alternating compression and rarefaction. In fact, when no heat is exchanged across the fluid (ideal fluid) such that the motion is adiabatic, the speed of sound in a classical fluid is determined exclusively by its adiabatic compressibility [163], in the form

$$c = \sqrt{\frac{\partial P}{\partial \rho_m}}, \tag{7.1}$$

where c is the speed of sound, P is the fluid pressure and $\rho_m = m\rho$ is the fluid mass density. This relation is also recovered [5] for a standard superfluid in the Thomas-Fermi (long wavelength) limit, where the quantum pressure becomes insignificant and the meanfield interaction dominates. In this limit, one finds that $P = g\rho^2/2$, while the low-lying elementary excitations are sound waves which propagate at a local speed $c(\mathbf{r}) = \sqrt{g\rho(\mathbf{r})/m}$. This equation was first derived by Bogoliubov [164] and Lee, Huang, and Yang [165]. Clearly, relation (7.1) is satisfied for a standard superfluid.

The attractive feature of Eq. (7.1) is its generality, in the sense that the speed of sound may be derived immediately given the functional form of the fluid pressure on the density. This saves us the effort of having to repeat the procedure of linearising the

wave equations from one fluid to another, the procedure being implicit in Eq. (7.1). Notice that aside from the condition of adiabatic motion, the validity of Eq. (7.1) rests on the requirement that there should be a one-to-one correspondence between P and ρ. However, in the case of a density-dependent gauge potential, this correspondence breaks down due to the fluid pressure depending linearly on the canonical flow (see chapter 5). The dependence of the fluid pressure $P = P(\rho, \mathbf{u})$ on both dynamical fluid variables is a defining feature of a nonlinear gauge-coupled quantum fluid. Therefore, it would be somewhat surprising if the velocity of sound in such a fluid be accurately described by Eq. (7.1).

Before formulating the problem explicitly, there are two points we would like to bring to attention, which we will be investigating in particular. Recall that a nonlinear gauge potential gives rise to a density-dependent mechanical flow, where the mere occurrence of fluid substance generates an associated flow, so to speak. This means that a homogeneously distributed fluid is no longer at rest as it would be typically, but exhibits a flow which persists in the absence of local phase differences. Furthermore, in the last chapter we learned that this gauge-flow contribution could not be absorbed into the phase without destroying the form of the wave equation. Hence, we would expect the gauge-coupled fluid to behave like a moving medium for the elementary excitations, serving as a carrier for sound waves. However, this should be expected for any kind of physical gauge potential. A natural question which comes to mind is, whether this background carrier flow is simply the gauge-flow of the homogeneous fluid distribution. In addition, will the nonlinear gauge potential affect sound propagation along directions orthogonal to the gauge potential? In the following section, we will address these questions from a theoretical standpoint, by deriving a generalised equation for the velocity of sound, where Eq. (7.1) is recovered as a limiting case. Further, we test these results for the nonlinear gauge-coupled superfluid governed by the Gross-Pitaevskii-like Eq. (5.18). To do so, we evaluate the velocity of sound by numerical integration of this wave equation after a suitably chosen Gaussian phase imprinting of the ground state condensate wavefunction.

7.2 Generalisation of the velocity of sound to nonlinear gauge-coupled quantum fluids

7.2.1 Hydrodynamical equations of the fluid

From a hydrodynamical viewpoint, we would like to solve for a wide class of nonlinear fluids, assuming as little as possible about the particular functional form of the effective potentials, yet without loosing sight of the main physical features characterising the fluid. As such, we consider the case of a fluid subject to a single-component potential $\mathbf{A} = \mathbf{a}\alpha(\rho)$, governed by the quantum Hamilton-Jacobi Eq. (5.14). There is another advantage to taking this step back from the underlying microscopic model, namely, that it allows for the possibility of easily tracking how the strength of the flow nonlinearity enters the resulting sound wave equation. For instance, the factor of 2 which appears further in Eq. (7.24) for the particular case $\mathbf{A} = \mathbf{a}\rho$, emerges as the result of a term $(1 + \gamma_0)$, where the factor of 1 arises automatically due to the action of a gauge potential, whereas γ_0, which is equal to 1 in this case, stems from its nonlinear character.

The hydrodynamical equations of the fluid, may then be presented in the form (see Eq. (5.75))

$$\left(\frac{\partial}{\partial t} + \mathbf{v}\cdot\boldsymbol{\nabla}\right) u_k = \frac{1}{m\rho}\nabla_j\left[-\delta_{jk}P + \sigma_{jk}\right] \tag{7.2}$$

$$\left(\frac{\partial}{\partial t} + \mathbf{v}\cdot\boldsymbol{\nabla}\right)\rho + \rho\boldsymbol{\nabla}\cdot\mathbf{v} = 0, \tag{7.3}$$

where $\mathbf{u} = \boldsymbol{\nabla}\theta/m$ is the canonical flow, $\mathbf{v} = \mathbf{u} - \mathbf{a}\alpha/m$ is the mechanical flow, σ_{jk} is the quantum stress tensor from Eq. (5.45) and P is the fluid pressure from Eq. (5.51), which may be written as

$$P = -\frac{\hbar^2}{4m}\nabla^2\rho + (\lambda - 1)\rho\eta + \rho\gamma\frac{a^2\alpha^2}{m} - \gamma\mathbf{A}\cdot\mathbf{J}_{\mathbf{u}}, \tag{7.4}$$

with $a = |\mathbf{a}|$ and $\mathbf{J}_{\mathbf{u}} = \rho\mathbf{u}$. For simplicity, we have assumed $\mathbf{a}$ is uniform over space. This avoids extraneous body-force terms entering Eq. (7.2), which would unnecessarily cloud the final results. It should be emphasised that Eq. (7.2) describes the transport of canonical flow $\mathbf{u}$, not $\mathbf{v}$. Casting Cauchy's equation into this form lays out the problem appropriately, since we will be interested in phase deviations θ' away from

equilibrium. Inspecting Eq. (7.4), notice that the nonlinear gauge potential gives rise to two additional fluid pressure contributions, namely, the third and fourth terms. From a hydrodynamical point of view, the former acts in a similar manner to the usual nonlinear interaction term $g\rho$, by inducing a current flow from high density to low density regions, thereby suppressing density variations. The second term is the canonical flow Pressure, which favours the onset of a current between regions of low to high overlap of the gauge potential and the canonical flow.

7.2.2 The ground state

Let us adopt the convention of attaching a zero subscript to denote the ground state or equilibrium value of a physical quantity, e.g. $\gamma_0 = \gamma(\rho_0, \mathbf{u}_0)$ and so on. Just as with a standard superfluid, the lowest energy configuration of the system is that of a homogeneous fluid, distributed over space with a uniform density ρ_0. One significant distinctive feature exists however. Generally speaking, if, at a given instant of time, the canonical flow of a fluid is $\mathbf{u}(\mathbf{r}, t_0) = \mathbf{0}$ and there are no pressure gradients throughout the system, the fluid remains homogeneously distributed in time. For a typical superfluid, this is the situation of a fluid which remains at rest. However, for the nonlinear gauge-coupled fluid this is no longer the case, given the inherent gauge-flow associated with regions of non-vanishing ρ. In other words, the free homogeneous fluid is in a state of flow even when the background canonical flow $\mathbf{u}_0$ vanishes, where the ground state flow is given by

$$\mathbf{v}_0 = -\frac{\alpha(\rho_0)}{m}\mathbf{a}. \tag{7.5}$$

7.2.3 Wave equation for sound

The low-lying elementary excitations of the fluid may be investigated by considering small perturbations in the equilibrium values of the dynamical fluid variables and linearising the wave equations with respect to these. In this spirit, let us write the fluid variables, as

$$\rho = \rho_0 + \rho', \quad \mathbf{u} = \mathbf{u}_0 + \mathbf{u}' = \mathbf{u}', \tag{7.6}$$

where $\rho' \ll \rho_0$ and $\mathbf{u}' \ll \mathbf{1}$. Linearising the Cauchy equation (7.2) with respect to ρ' and $\mathbf{u}'$ is straight forward, yielding

$$\left(\frac{\partial}{\partial t} + \mathbf{v}_0 \cdot \boldsymbol{\nabla}\right) u_k' = -\frac{1}{m\rho_0}\nabla_k P', \tag{7.7}$$

where $\mathbf{v}_0$ is given by Eq (7.5) and P' is the change in fluid pressure due to the small perturbations. At a given point $\mathbf{x}$, P' may be related to the small phase deviation θ' through the line integral $P' = -m\rho_0 \int_{\mathcal{C}} d\mathbf{r} \cdot (\partial_t + \mathbf{v}_0 \cdot \boldsymbol{\nabla})\, \mathbf{u}'$, evaluated along any simply-connected curve joining the boundary to $\mathbf{x}$, yielding[1]

$$P' = -\rho_0 \left(\frac{\partial}{\partial t} + \mathbf{v}_0 \cdot \boldsymbol{\nabla}\right) \theta'. \tag{7.8}$$

Proceeding with the linearisation of the equation of continuity, it is convenient to rearrange Eq. (7.3) explicitly in terms of the independent variables ρ and $\mathbf{u}$, in the form

$$\left[\frac{\partial}{\partial t} + \left(\mathbf{u} - (1+\gamma)\,\frac{\mathbf{A}}{m}\right) \cdot \boldsymbol{\nabla}\right] \rho + \rho \boldsymbol{\nabla} \cdot \mathbf{u} = 0. \tag{7.9}$$

Notice how the term associated with the number 1 in the above equation, arises generally when a gauge potential acts on the system, while the term containing γ stems from the ρ-dependent character of $\mathbf{A}$. Linearising Eq. (7.9) with respect to ρ' and $\mathbf{u}'$, gives

$$\left[\frac{\partial}{\partial t} + (1+\gamma_0)\, \mathbf{v}_0 \cdot \boldsymbol{\nabla}\right] \rho' + \frac{\rho_0}{m} \nabla^2 \theta' = 0, \tag{7.10}$$

where we have written $\mathbf{u}'$ in terms of θ'. The linearised equations (7.8) and (7.10), feature three small deviation variables ρ',θ' and P'. However, only two of these are independent on account of the fluid pressure taking the functional dependence $P = P(\rho, \mathbf{u})$. Hence we can eliminate ρ' in favour of P' and θ', by means of the first order expansion

$$P' = \frac{\partial P}{\partial \rho_0}\rho' + \frac{\partial P}{\partial \mathbf{u}_0} \cdot \mathbf{u}', \tag{7.11}$$

evaluated about the ground state ρ_0, $\mathbf{u}_0 = \mathbf{0}$. Substituting Eqs. (7.8) and (7.11) into Eq. (7.10) and noting that

$$\frac{\partial P}{\partial \mathbf{u}_0} = m\gamma_0 \rho_0 \mathbf{v}_0 \tag{7.12}$$

[1]We have assumed P' vanishes on the boundary.

in accordance with Eq. (7.4), we find, after some manipulation, that the phase deviations obey the wave equation

$$\left\{\left[\frac{\partial}{\partial t}+\left(\mathbf{v}_0+\frac{1}{m\rho_0}\frac{\partial P}{\partial \mathbf{u}_0}\right)\cdot\boldsymbol{\nabla}\right]^2-\frac{1}{m}\frac{\partial P}{\partial \rho_0}\nabla^2\right\}\theta'=0. \tag{7.13}$$

The last differential operator appearing here is identical to that which appears in the sound wave equation of a classical adiabatic fluid, or a standard superfluid. At small wavelengths, where the quantum pressure contribution $-\hbar^2/4m\nabla^2\rho$ plays an important role, note that $\partial P/\partial\rho_0$ should be treated as a differential operator, leading to a quartic term $\propto\nabla^4\theta'$ in the above equation. The square bracket term on the other hand, takes the form of a convective derivative operator. This is typical of a sound wave equation for a moving medium. Observe in particular how the flow of the medium is not simply the ground state flow $\mathbf{v}_0$, but includes an additional contribution stemming from the canonical flow pressure. We now proceed to solving the wave equation and obtain the dispersion relation of the medium.

7.2.4 Dispersion relation and velocity of sound

Given the translational invariance of Eq. (7.13), we consider plane wave solutions

$$\theta'=\exp\left[i\left(\mathbf{k}\cdot\mathbf{r}-\omega t\right)\right]\equiv\theta, \tag{7.14}$$

which we henceforth simply write as θ. Substituting Eq. (7.14) into (7.13), yields the following dispersion relation in the long wavelength limit:

$$\omega\left(\mathbf{k}\right)=\left(\mathbf{v}_0+\frac{1}{m\rho_0}\frac{\partial P}{\partial \mathbf{u}_0}\right)\cdot\mathbf{k}+k\sqrt{\frac{1}{m}\frac{\partial P}{\partial\rho_0}}, \tag{7.15}$$

where $k=|\mathbf{k}|$. Hence, the velocity of sound $\mathbf{c}=\lim_{k\to0}\partial\omega/\partial\mathbf{k}$, is given by

$$\mathbf{c}=\mathbf{v}_0+\frac{1}{m\rho_0}\frac{\partial P}{\partial \mathbf{u}_0}+\hat{\mathbf{k}}\sqrt{\frac{1}{m}\frac{\partial P}{\partial\rho_0}}. \tag{7.16}$$

Equivalently, using Eq. (7.12), the velocity of sound may be stated in the form

$$\mathbf{c}=\left(1+\gamma_0\right)\mathbf{v}_0+\hat{\mathbf{k}}\sqrt{\frac{1}{m}\frac{\partial P}{\partial\rho_0}}. \tag{7.17}$$

The second term is the isotropic contribution to the velocity of sound, whereas the first is an anisotropic term. The anisotropy of the speed of sound is characterised by the orientation of the gauge potential along $\mathbf{a}$, which selects a particular direction in space. The speed of sound takes on a minimum value along $\mathbf{a}$ and a maximum value along $-\mathbf{a}$. In the limit where $\mathbf{a} \to 0$, Eqs. (7.16) and (7.17) reduce to Eq. (7.1). Hence, we have obtained a generalised version of Eq. (7.1) for deriving the velocity of sound from the fluid pressure, which extends to cases where a fluid is subject to a density-dependent vector potential $\mathbf{A} = \mathbf{a}\alpha(\rho)$. Of particular interest, the above equations highlight the fact that sound waves are not simply carried along with the ground state flow $\mathbf{v}_0$, but with an increased background flow $(1 + \gamma_0)\mathbf{v}_0$. This is a direct consequence of the explicit dependence of the fluid pressure on the canonical flow. In addition to this, the nonlinear potential introduces an isotropic background pressure contribution stemming from the third term appearing in Eq. (7.4). As a result, sound propagation will also be affected along directions orthogonal to $\mathbf{A}$.

7.3 The nonlinear gauge-coupled superfluid

7.3.1 Elementary excitation spectrum

As an example, let us investigate the propagation of sound in a particular type of nonlinear fluid, namely, the superfluid fraction of particles of an optically-addressed weakly interacting dilute Bose gas of two-level atoms. Further, we shall solve the dynamics of this superfluid numerically and design a method for evaluating the velocity of sound. This will provide a testing ground for our theoretical results. Recall that the superfluid is governed by the nonlinear wave equation

$$i\hbar\partial_t\psi = \left[\frac{(\mathbf{p} - \mathbf{A})^2}{2m} - \mathbf{a}\cdot\mathbf{J} + g\rho\right]\psi, \tag{7.18}$$

where the nonlinear gauge potential takes the density-modulated form $\mathbf{A} = \mathbf{a}\rho$, $\mathbf{a}$ is given by Eq. (4.38) and determines the effective strength and orientation of the gauge potential and $\mathbf{J}$ is the gauge-covariant current density. We shall assume that the laser field in the light-matter coupling is monochromatic, so that $\mathbf{a}$ is constant over space. In this situation, the fluid pressure may be evaluated from Eq. (7.4) with $\gamma = 1$ and

$\lambda = 2$, which gives

$$P = -\frac{\hbar^2}{4m}\nabla^2\rho + \frac{g}{2}\rho^2 + \frac{a^2}{m}\rho^3 - \rho^2\mathbf{a}\cdot\mathbf{u}. \tag{7.19}$$

Defining the quantities

$$\mathbf{p} = \hbar\mathbf{k} \tag{7.20}$$

$$\epsilon_p = \hbar\omega_p \tag{7.21}$$

$$\epsilon_p^0 = \frac{p^2}{2m}, \tag{7.22}$$

the excitation spectrum of the superfluid may be obtained from the dispersion relation (7.15) and the above expression for P, in the form

$$\epsilon_{\mathbf{p}} = 2\mathbf{v}_0\cdot\mathbf{p} \pm \sqrt{\epsilon_p^0\left(\epsilon_p^0 + 2g\rho_0 + 6\frac{(a\rho_0)^2}{m}\right)}, \tag{7.23}$$

where $\mathbf{v}_0 = -\mathbf{a}\rho_0/m$ is the ground state flow. Note that we have included the (small-wavelength) quantum pressure term $\propto k^4$ under the square root in the above expression, as discussed towards the end of section 7.2.3. In the limit $\mathbf{a} \to \mathbf{0}$, we recover the Bogoliubov excitation spectrum of a standard superfluid.

7.3.2 Anisotropic speed of sound

Discarding the lower energy band, the corresponding low lying excitations are anisotropic sound waves which propagate across the fluid with a velocity

$$\mathbf{c} = -\mathbf{a}\frac{2\rho_0}{m} + \hat{\mathbf{k}}\sqrt{\frac{g\rho_0}{m} + 3\left(\frac{a\rho_0}{m}\right)^2}. \tag{7.24}$$

Notice that the isotropic contribution $c_\perp$ to the velocity of sound, may be obtained from the combination

$$c_\perp = \frac{c_{+\mathbf{a}} + c_{-\mathbf{a}}}{2} = \sqrt{\frac{g\rho_0}{m} + 3\left(\frac{a\rho_0}{m}\right)^2}, \tag{7.25}$$

where

$$c_{\pm\mathbf{a}} = \mp 2\frac{a\rho_0}{m} + \sqrt{\frac{g\rho_0}{m} + 3\left(\frac{a\rho_0}{m}\right)^2}, \tag{7.26}$$

is the speed of sound along $\pm\mathbf{a}$. Similarly, the carrier flow of the medium for sound, c_M, follows from the combination

$$c_M = \frac{c_{+\mathbf{a}} - c_{-\mathbf{a}}}{2} = -\frac{2a\rho_0}{m}. \tag{7.27}$$

Hence, the medium carrying sound flows with speed $2a\rho_0/m$ in the opposite direction of the gauge potential.

7.3.3 Suppressed sound propagation

An interesting observation follows from equation (7.26), namely, that sound propagation along $+\mathbf{a}$ becomes suppressed at sufficiently high densities. Solving for $\partial c_{+\mathbf{a}}/\partial\rho_0 = 0$, leads to the quadratic equation

$$\rho_0^2 + \kappa\rho_0 - \frac{3}{4}\kappa^2 = 0, \tag{7.28}$$

where we have defined $\kappa = mg/(3a^2)$. Hence, the speed of sound along $+\mathbf{a}$ takes on a maximum value when

$$\rho_0 = \frac{\kappa}{2} = \frac{mg}{6a^2}. \tag{7.29}$$

Multiplying Eq. (7.29) by $\rho_0/2m$ and rearranging, we see that the stationary point occurs when the diamagnetic interaction term and the standard nonlinear interaction term, are related in the form $A_0^2/(2m) = g\rho_0/12$. Therefore, $c_{+\mathbf{a}}$ should begin to decrease when the number of particles reaches $N = g/(12\rho_0 a^2)$, which, for our simulation parameter values, corresponds to $N \simeq 1266$. Furthermore, setting Eq. (7.26) for $c_{+\mathbf{a}}$ to zero, we find that sound propagation along $\mathbf{a}$ becomes completely suppressed when $A_0^2/(2m) \geq g\rho_0/2$, which is to say for $N \geq 7595$.

7.3.4 Numerical results

7.3.4.1 Introducing a disturbance

In order to evaluate the velocity of sound in the anisotropic superfluid, some form of disturbance must be introduced in the condensate.

Density disturbance In the first experimental report on sound propagation in Bose-Einstein condensates [166], localised density perturbations were induced in a

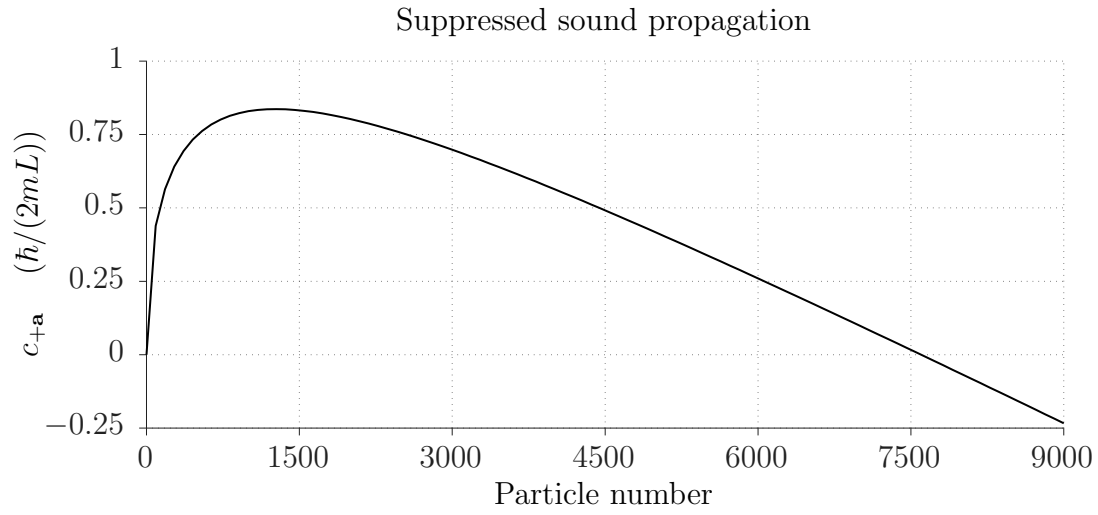

Figure 7.1: Speed of sound in the direction of the gauge potential, as predicted by Eq. (7.26). The effective interaction strengths g and a, are, in units $2m/(L\hbar^2)$ and $\hbar L^2$, respectively, $g = 3.66$ and $a = 0.73$. The speed of sound along $+\mathbf{a}$ takes on a maximum value when $A_0^2/(2m) = g\rho_0/12$ (or $N \simeq 1266$) and becomes suppressed when $A_0^2 \geq g\rho_0/2$ (or $N \geq 7595$).

magnetically trapped cigar-shaped condensate of sodium atoms, by using the repulsive optical dipole force of a focused blue-detuned off-resonant laser beam. For our purposes, a perturbation in the homogeneous ground state density distribution ρ_0 may be established by subjecting the condensate to a localised external potential, centered about $\mathbf{r} = \mathbf{0}$:

$$V(\mathbf{r}) = V_0 e^{-\sigma|\mathbf{r}|^2}, \tag{7.30}$$

and conducting a ground state search. Setting the potential to zero for subsequent times $t > 0$, the disturbance then propagates through the condensate as a result of the quantum pressure and nonlinear interaction terms. In FIG. 7.2, we plot the time-evolution of the nonlinear gauge-coupled superfluid due to such a disturbance. Depicted in this example, is a slice of the condensate wave amplitude (scaled) taken along $y = 0$, at 4 successive times. The gauge potential $\mathbf{A} = a\rho\hat{\mathbf{x}}$ imparts a gauge-flow along $-\hat{\mathbf{x}}$, which is revealed by the density perturbation. As the density minimum at $t = 0$ rises, two outwardly propagating density wells are produced, as seen in the second image. The gauge potential tends to impede rightward propagating modes and assist leftward modes, thereby creating an asymmetry in the system. This may be seen from the relative distance traversed by peaks on either side of $x = 0$ at a given time. Also, notice the significant disparity between the amplitude of the disturbance on the left and right.

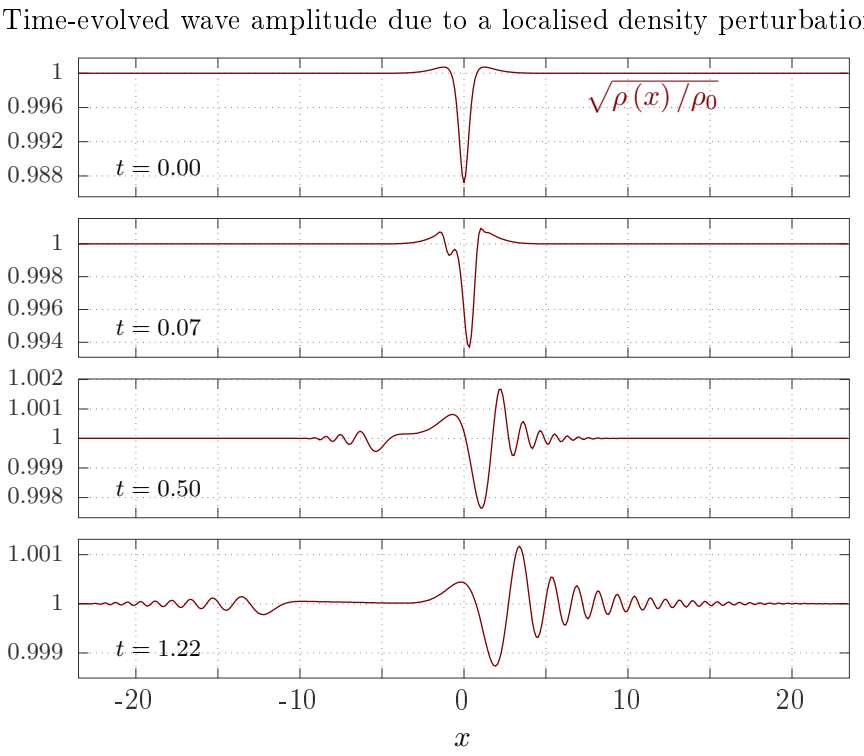

Figure 7.2: Plots showing the wave amplitude of a nonlinear gauge-coupled superfluid along the x axis, due to a density disturbance induced at $t = 0$ by a localised Gaussian potential 7.30 with parameters $V_0 = 0.5$ and $\sigma = 12$. The condensate is populated by $N = 3200$ particles and subject to a density-modulated vector potential directed along $\hat{\mathbf{x}}$. Note the change in scale between successive time plots.

Phase disturbance A "cleaner" approach is furnished by introducing a disturbance not in the density, but in the canonical flow field of the condensate. This may be achieved by a local phase imprinting of the wavefunction. From an experimental point of view, the phase imprinting method was originally developed as a means of exciting vortex structures in condensates [167–169]. The phase is engineered by passing a short off-resonant laser pulse through a suitably designed absorption plate and imprinting it on the condensate. This method was also adopted extensively in multiple experiments around the turn of the 20^{th} century, for generating solitons [170–173] and studying their interaction [174–176]. As such, we again consider the homogeneous condensate as our initial state, but now impart a Gaussian phase

$$\Omega(\mathbf{r}) = -\Omega_0 e^{-\sigma|\mathbf{r}|^2}, \tag{7.31}$$

onto the ground state wavefunction ψ_0, such that

$$\psi(\mathbf{r}, t = 0) = e^{i\Omega(\mathbf{r})}\psi_0. \tag{7.32}$$

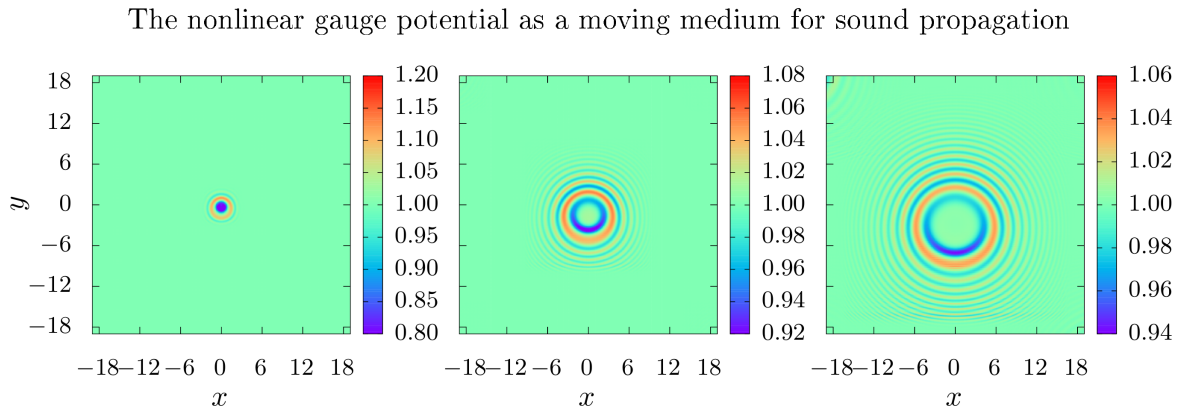

Figure 7.3: Plots showing the wave amplitude $\sqrt{\rho\left(\mathbf{r}\right)/\rho_0}$ of a nonlinear gauge-coupled superfluid at three successive instants of time $t_1 = 0.13$, $t_2 = 0.50$ and $t_3 = 0.92$, due to a Gaussian phase imprint at $t_0 = 0$. The condensate is populated by $N = 2800$ particles and the Gaussian phase imprint parameters are $\sigma = 5.5$ and $\Omega_0 = 1.5$. The orientation of the gauge potential $\mathbf{A} = \hat{\mathbf{y}} a\rho$ along $+\hat{\mathbf{y}}$, sets up a background flow along $-\hat{\mathbf{y}}$ with which sound is "carried".

This generates a spherically symmetric impulse-like velocity field for the condensate. Since the direction of flow follows that of increasing phase, the minus sign in Eq. (7.31) ensures that the flow is directed radially outward from $\mathbf{r} = \mathbf{0}$. The spatial extension of the velocity field is dictated by σ. The modulus of the velocity field on the other hand, depends both on Ω_0 and σ. In the language of collective excitations, the representation of a disturbance is achieved by means of a coherent mode expansion [177]. To ensure the excitations belong primarily to the linear phonon regime, it is important that the amplitude of the resulting oscillations be small compared to the equilibrium value ρ_0. Hence, the modulus of the velocity field should not be too large. In addition, the spatial extension of the phase imprint should be made relatively large in order to avoid population of high-momentum modes. Although density disturbances were initially considered in our investigations, the phase imprinting method produced more orderly contour plots, presented below.

7.3.4.2 The nonlinear gauge-coupled superfluid as a moving medium for sound propagation.

Our study of the elementary excitation spectrum of the anisotropic superfluid, led us to the assertion that the density-dependent gauge potential endows the nonlinear fluid with characteristics typical of that of a moving medium. This feature of the nonlinear gauge potential is illustrated in FIG. 7.3. Here, we clearly notice a downward motion of the medium as a result of the gauge potential along $+\hat{\mathbf{y}}$, which carries the surface

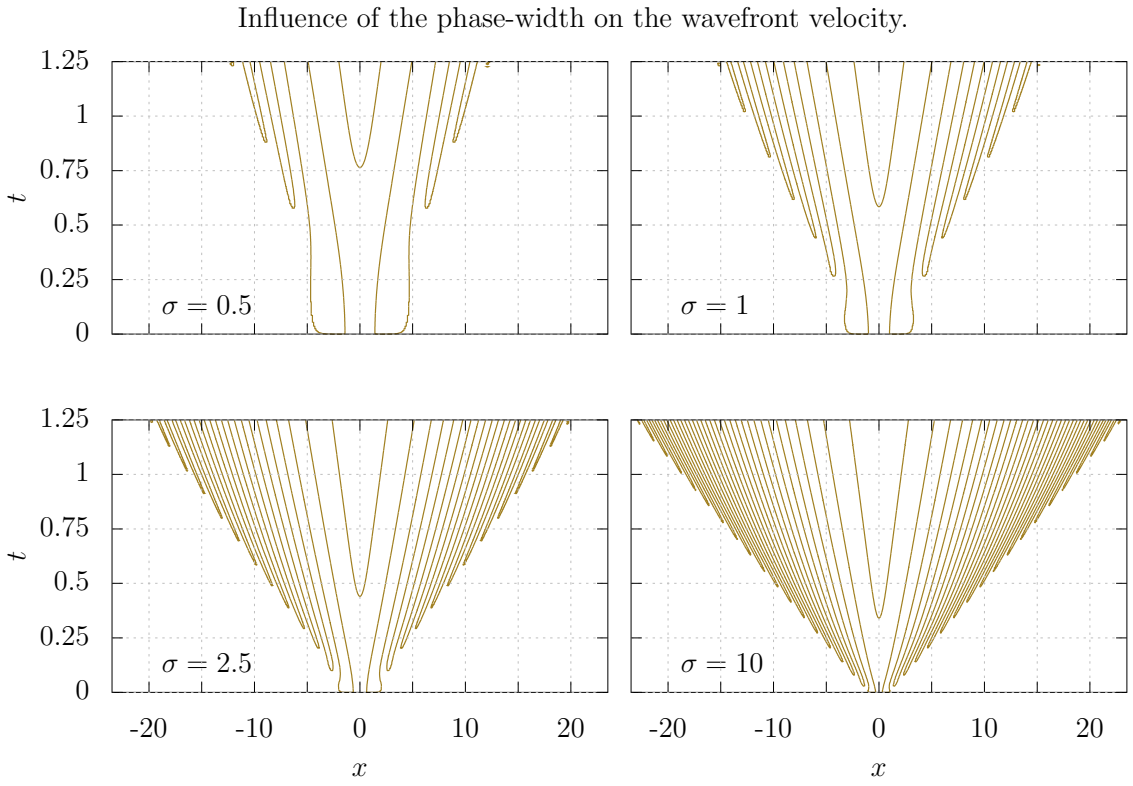

Figure 7.4: Time-evolved contour of the wave amplitude along $y = 0$ of a standard superfluid populated by $N = 2800$ particles. The contour level was set at $(1 + 10^{-5})\sqrt{\rho_0}$, the amplitude of the Gaussian phase imprint fixed at $\Omega_0 = 0.2$ and the time t is given in units $2mL^2/\hbar$. The phase width was varied, as indicated by the value of σ in each plot. For large phase-widths (low σ), low-lying energy modes are primarily excited. As σ is increased, high-momentum modes become increasingly populated and node formation occurs more frequently at the edges, leading to a higher wavefront velocity.

ripples. However, recall that this is to be expected of any type of vector potential, irrespective of its possibly nonlinear character. What we would like to investigate, is whether the flow carrying these ripples is $2\mathbf{v}_0$ and not simply $\mathbf{v}_0$, as predicted by Eq. (7.24). Note that the orientation of the gauge potential shall henceforth be fixed along $+\hat{\mathbf{x}}$ in our simulations.

7.3.4.3 Signal velocity and sound velocity

The spatial extension of the imprinted velocity field, or "phase-width", strongly influences which modes are excited in the system. Large phase-widths (low σ) excite predominantly low-momentum modes, while shorter phase-widths (high σ) excite increasingly high momentum modes. We illustrate this dependence for a standard superfluid, through the time-evolved wave amplitude contours appearing in FIG. (7.4). To obtain these images, we extract the wave amplitude along $y = 0$ at each instant

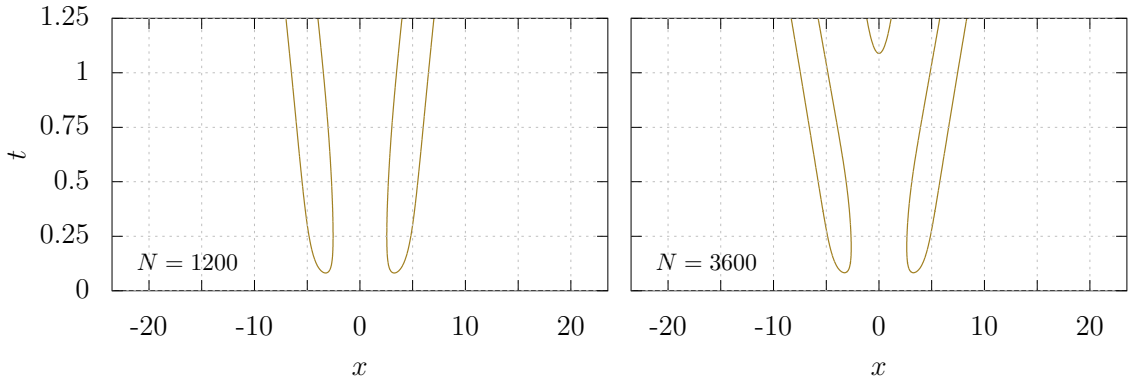

Figure 7.5: Time-evolved wave amplitude contours for a standard superfluid, due to a Gaussian phase imprint with $\sigma = 0.19$ and $\Omega_0 = 0.2$. The contour level was set at $(1 + 10^{-5})\sqrt{\rho_0}$ and the time t is given in units $2mL^2/\hbar$. Two counter-propagating bumps are induced by the Gaussian phase, as seen in the first image. An additional peak formed in the density well between the two bumps, crosses the contour level at $t \approx 1.1$ in the second image.

of time, define a contour level for this density slice equal to $(1 + 10^{-5})\sqrt{\rho_0}$ and then plot the time-evolution of the contour. Since a standard superfluid is isotropic, the time-evolved contours in FIG. 7.4 are symmetrically distributed about $x = 0$. The fan-like structure depicted in these images is due to the dispersive nature of the medium. For instance, in a dispersionless medium, a leftward travelling waveform would retain its shape and lead to a set of *parallel* left-inclined lines, rather than a fan. Each fan in FIG. (7.4) is characterised by *two* slopes: an inner slope about $x = 0$ and an outer slope defined by the tips of the level curves at the edge. The inner slope is associated primarily with the propagation of low-momentum modes through the fluid. It is this region which is of interest in evaluating the speed of sound. For the outer slope, notice how the formation of a node (as seen in FIG. 7.2 for instance), is indicated by the appearance of an additional level curve at the edge. The outer slope is then related to the speed of propagation of node formation. This is equivalent to the *wavefront* or *signal velocity* [178]. Notice in particular how the signal velocity increases with σ, as high-momentum modes are increasingly populated.

7.3.4.4 Calibration of the phase imprinting parameters

In order to ensure we are working in a phonon-like regime, let us calibrate the phase imprinting parameters Ω_0 and σ from Eq. (7.31), so that predominantly low-momentum modes are excited and the amplitude of the resulting density disturbance is small. As our calibration system, we consider a standard superfluid and retrieve the well-known

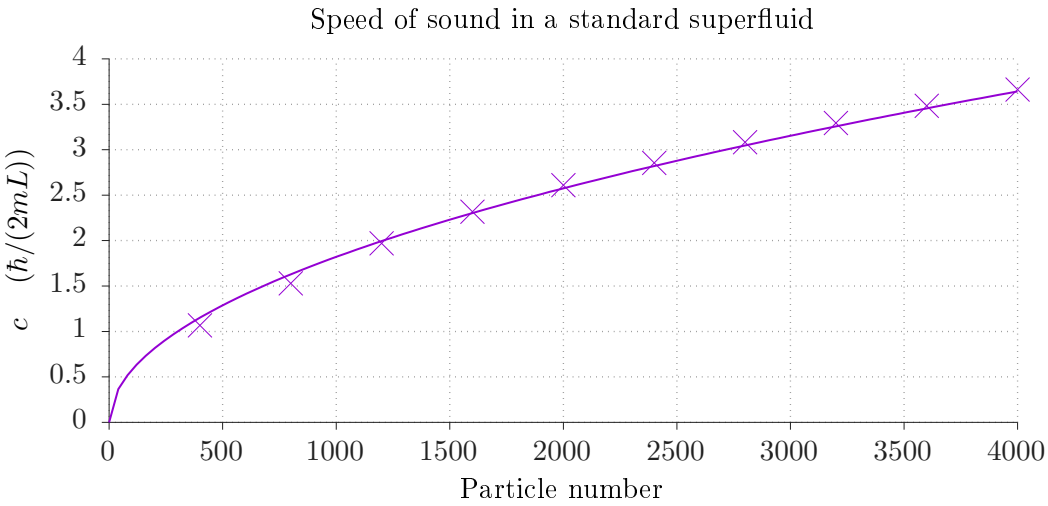

Figure 7.6: Speed of sound in a standard superfluid as a function of the condensate particle number, for phase imprint parameters $\sigma = 0.19$ and $\Omega_0 = 0.2$. The data points were obtained through linear fits of suitably chosen portions of the time-evolved wave amplitude contours. The solid curve represents the theoretical curve $c = \sqrt{2g\rho_0}$.

square root dependence of the speed of sound on the particle number. To this end, let us gradually decrease Ω_0 and σ, until the amplitude of the resulting density disturbance is within 1% of the equilibrium value and the inner slope of the time-evolved wave-amplitude contour along $y = 0$ (see FIG. 7.4) remains unchanged by this decrease. Parameter values $\Omega_0 = 0.2$ and $\sigma = 0.19$ were found to be satisfactory for our purposes. For the length and time spans of our simulations, these essentially produce two counter-propagating "bumps". However, a local maximum is eventually formed at the center of the density-depleted region left by the travelling bumps, signalling the introduction of two additional nodes in the system. This occurs as a result of the nonlinear interaction term $g\rho$, where the time taken for the local maximum to form decreases with the particle number. As an example, we have plotted the time-evolved wave amplitude contour for two different particle numbers in FIG. 7.5. In the left image, we notice two contours, symmetrically distributed about $x = 0$. Each curve represents the motion of the leading edge and the trailing edge of a bump. In the image on the right, we notice that a local maximum forms at $x = 0$, rises, and intercepts the contour level at $t \approx 1.1$, at which point it becomes visible in the plot. We shall evaluate the velocity of sound from the trajectory of the trailing edge of a bump, i.e. from the inner-half of a contour curve. To do so, it is important to choose a suitable lower bound for the time interval $[t_0, 1.25]$, over which the curve becomes well approximated by a line. This is particularly significant at low N. Having identified an appropriate portion of

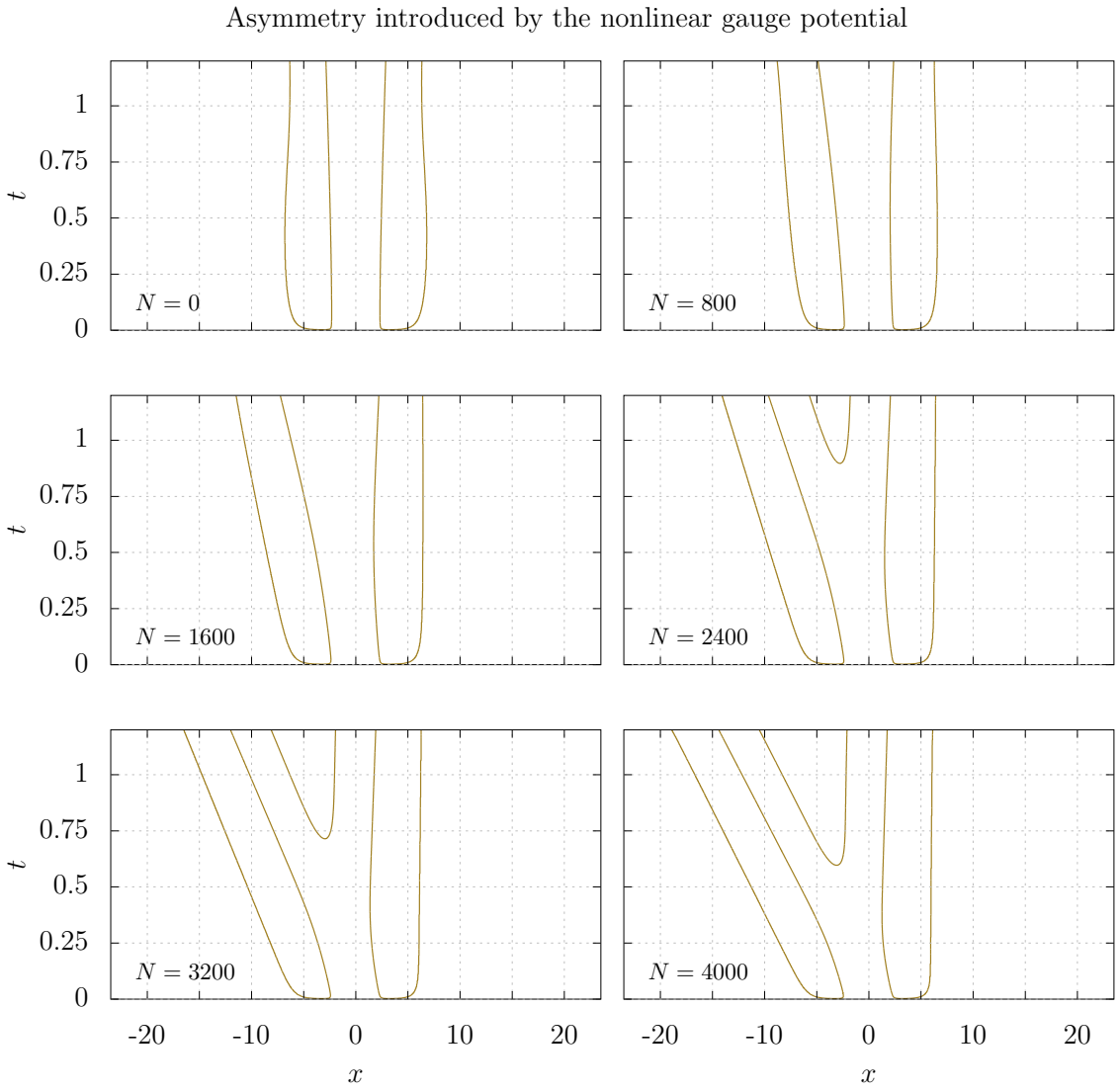

Figure 7.7: Time-evolved wave amplitude contours, along $y = 0$, of a superfluid subject to a density-modulated gauge potential $\mathbf{A} = \hat{\mathbf{x}} a\rho$. The Gaussian phase imprint parameters are $\sigma = 0.19$ and $\Omega_0 = 0.2$ and the contour level is $(1 + 10^{-5})\sqrt{\rho_0}$. The time t is given in units $2mL^2/\hbar$.

the contour, we carry out a linear fit to the curve. Then, the speed of sound may be estimated from the inverse slope of the linear approximation. Using this method, we retrieved the well-established square-root law for the speed of sound dependence on the particle number, shown in FIG. (7.6). Now that we have designed a satisfactory method for determining the velocity of sound and calibrated our Gaussian phase parameters accordingly, let us implement this procedure on the nonlinear gauge-coupled superfluid.

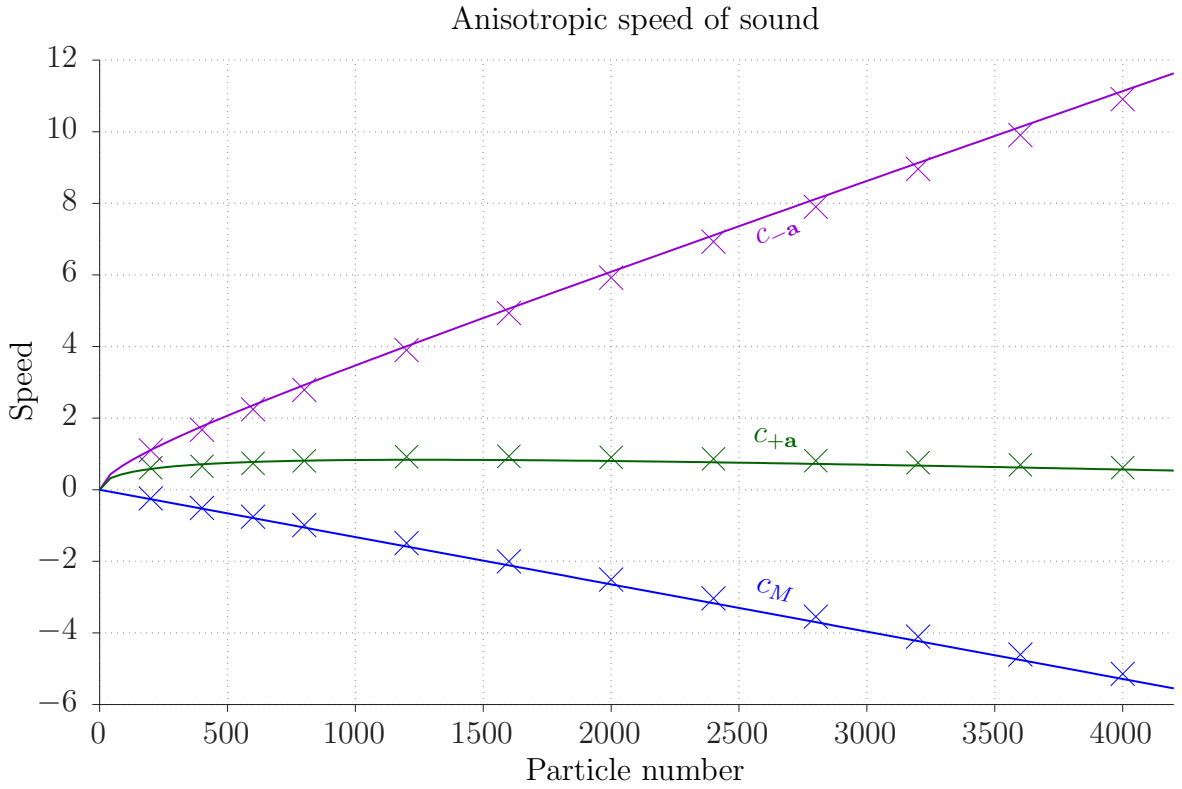

Figure 7.8: Numerical estimates for the speeds of sound $c_{-\mathbf{a}}$ and $c_{+\mathbf{a}}$ and the flow of the medium carrying sound c_M, at different particle numbers, all given in units $\hbar/(2mL)$. The theoretical (solid) curves follow from Eqs. (7.26) and (7.27). The speeds of sound along $-\mathbf{a}$ and $\mathbf{a}$, are depicted in purple (top) and green (middle), respectively, while C_M is given in blue (bottom).

7.3.4.5 Velocity of sound in the anisotropic superfluid

In the previous section, we discovered that phase parameter values $\Omega_0 = 0.2$ and $\sigma = 0.19$, essentially produced two counter-propagating bumps in the wave-amplitude of a standard superfluid along $y = 0$. Since the standard superfluid is isotropic, the time-evolved contours of the bumps were symmetrically distributed about $x = 0$ (see FIG. 7.5). Let us now examine the influence that a nonlinear gauge potential has on these wave amplitude contours. From the images in FIG. (7.7), we notice how the gauge potential introduces anisotropy in the system. Observe how the contours have become skewed towards the left as a result of the gauge potential directed towards the right. Hence, the leftward and rightward moving bumps, which previously travelled at the same speed, now travel with an increased and decreased speed, respectively. Notice how the contours on the left hand side of these images become increasingly skewed with the condensate particle number N, as the magnitude of $\mathbf{A}$ is increased. In contrast, the contours on the right hand side seem to be only slightly affected by N. This should

be expected from our theoretical curve for the rightward speed of sound $c_{+\mathbf{a}}$ appearing in FIG. 7.1, which changes only slightly over the particle number interval $[800, 4000]$. Comparing the image corresponding to $N = 3600$ in FIG. 7.5 with that of $N = 2400$ in FIG. 7.7, we notice that it takes significantly less time for a crest to form in the density-depleted region when a nonlinear gauge potential acts on the system. This is due to the additional density-dependent pressure term $a^2\rho^3/m$ from Eq. (8.31), which increases the suppression of density variations. We also see that the two characteristic slopes are ill-defined in the non-interacting case ($N = 0$), becoming increasingly regular for large N. Observe further that for sufficiently large N, the condensate particle number primarily affects the inner slope and does not influence the signal velocity in any significant manner.

Carrying out linear fits on curves similar to those of FIG. 7.7, over a suitable time-truncated portion, leads to the data depicted in FIG. 7.8, which is in very good agreement with the theoretical solid curves.

7.3.4.6 Group velocity exceeding signal velocity at large N

Recalling figure 7.7 for the particle number dependence of the contour plots of the wave amplitude in the presence of a density-dependent gauge potential, two slopes were apparent at sufficiently large N: the central slope representing the velocity of sound and the outer slope indicating the signal velocity. The signal velocity is fixed

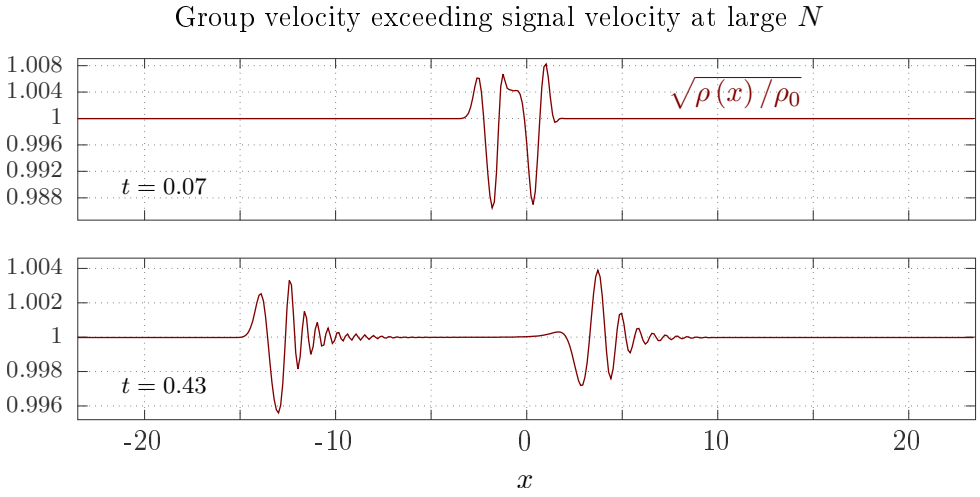

Figure 7.9: Free evolution of the wave amplitude of a nonlinear gauge-coupled superfluid due to a Gaussian phase imprint at $t = 0$, with parameters $\Omega_0 = 0.4$ and $\sigma = 10$. The condensate is populated by $N = 15000$ particles and subject to a density-modulated gauge potential along $\hat{\mathbf{x}}$. The time t is given in units $2mL^2/\hbar$. Note the change in scale between the two plots.

primarily by the Gaussian phase imprint parameter σ and remains unchanged at large N, with only a slight disparity between leftward and rightward signal speeds. The speed of sound on the other hand is greatly affected by N. It is then natural to ask whether the central slope may exceed the outer slope for sufficiently large N, thereby leading to node formation which occurs in the wake of the propagating disturbance. This phenomenon is illustrated in FIG. 7.9 for $N = 15000$, where we notice the leftward propagating waveform is flipped compared to that of FIG. 7.2 as a result of ripples forming in the wake of the disturbance. Note that the numercial time increment δt was reduced in order to compensate for the increase in energy of the system, thereby allowing a resolution of the dynamics.

Chapter 8

Vortex nucleation and the breakdown of superfluidity

8.1 Introduction

The discovery of superfluidity was marked by an epochal series of experiments carried out over the course of the 1930s [179–183]. These phases of matter display the remarkable property of a fluid which flows without friction, i.e. whose viscosity vanishes. In a viscous fluid, shear stress is produced by velocity gradients between streamlines, which lead to off-diagonal stress components $\sigma_{ij} = \eta\left(\nabla_i v_j + \nabla_j v_i\right)$, where η is the coefficient of viscosity [163]. For instance, in the laminar flow of a viscous fluid through a cylindrical pipeline, the friction between the fluid and the pipe leads to set of a straight parallel streamlines, where the velocity field of a given stream line decreases away from the center of the pipeline. In a weakly interacting dilute Bose-Einstein condensate, which presents a versatile testing ground for elucidating the physics of superfluid systems, there is no frictional viscosity associated with velocity gradients. Nevertheless, shear stress may arise due to non-vanishing off-diagonal stress tensor components, which allow for the possibility of fluid vorticity. These dilute systems are compressible nonlinear quantum fluids, whose time-evolution is well described by a nonlinear Schrödinger equation. This equation is equivalent to two hydrodynamical equations for mass transport and momentum transport, which are identical in form to those of a classical fluid, the essential difference resting on the form of the stress tensor in either case.

In turn, nonlinear media present a number of novel features, both in classical and

quantum mechanics. From a classical point of view, perhaps the most conspicuous example is the occurrence of shock waves. These arise, for instance, when a foreign object travels through a medium with a velocity exceeding the local velocity of sound. In doing so, the object displaces the fluid at a rate exceeding the rate with which information about the displacement is passed through the fluid, and a discontinuity forms as a shock front [184]. In a quantum nonlinear fluid, an additional phenomenon manifests under similar circumstances, in the form of an accumulated phase slip in the wake of the moving object, which, upon reaching π, suddenly jumps to $-\pi$ [185, 186]. This sudden reversal in the flow field signals the introduction of vorticity in the system. Recall that the circulation imparted to a quantum fluid occurs in quantised packets (of action), such that the net circulation of the fluid is given by

$$\Gamma = \oint d\mathbf{r} \cdot \mathbf{v} = \frac{2\pi\hbar}{m} n, \qquad (n = 0, 1, 2, \cdots) \,. \tag{8.1}$$

Since the angular momentum of the system is conserved under Kelvin's theorem and vanished to begin with, vorticity enters in the form of quantised vortices which emerge from a point in pairs, having opposite vorticity [185, 187, 188]. In a standard superfluid, this nucleation process occurs approximately periodically over time, each time the phase slip accumulates by 2π. Note that the possibility for vortex creation stems from the quantum stress tensor σ_{ij} from Eq. (5.45) [188]. Although there is no frictional viscosity, shear stress arises through the osmotic velocity field (5.46) connected with density gradients.

In this chapter, we investigate the influence that a nonlinear gauge potential has on the formation of quantised vortex pairs. As a system model, we consider the superfluid fraction of optically-addressed two-level Bose atoms described by the Gross-Pitaevskii-like Eq. (3.21) and introduce a travelling impurity in the form of a suitably chosen external localised potential. The impurity imparts mechanical momentum to the gauge-coupled superfluid, which results in a force acting between the impurity and the condensate. We would also like to evaluate this force. In the case of a standard superfluid, the force is simply the expectation value of the gradient of the impurity potential [189]:

$$F_k(t) = -\int d^3\mathbf{r} \rho \nabla_k V \equiv F_k^{imp}(t) \,. \tag{8.2}$$

Thus, if the object potential is spherically symmetric, an instantaneous force occurs when the superfluid density is asymmetrically distributed about the potential. We shall refer to the component of $\mathbf{F}$ along the direction of motion of the impurity, as the *drag force*. In the case of a nonlinear gauge-coupled superfluid, it is unclear whether relation (8.2) applies for evaluating drag. In fact, in chapter 5, we learned that a non-trivial body-force of dilation enters the mechanical momentum transport equation of such a fluid. Since the expectation value of a body-force is generally non-vanishing, we would expect this non-trivial force term to play a role in the drag force acting on the impurity. As a starting point to our study, we derive an expression for this force, by studying the time derivative of the expectation value of the superfluid mechanical momentum. Further, we derive the same force by integrating the hydrodynamical equation of momentum transport, before presenting our numerical results.

8.2 Drag force on a travelling impurity

8.2.1 Introduction

We shall consider the motion of an impurity through a superfluid subject to a uni-directional density-modulated gauge potential. The time-evolution of this superfluid state, is then governed by

$$i\hbar\partial_t \left|\psi\right\rangle = \hat{H} \left|\psi\right\rangle , \tag{8.3}$$

where $\hat{H}$ is a nonlinear operator, which, in the position representation, takes the form

$$\hat{H} = \frac{\left(\hat{\mathbf{p}} - \mathbf{A}\right)^2}{2m} + \Phi. \tag{8.4}$$

Here, $\hat{\mathbf{p}} = -i\hbar\boldsymbol{\nabla}$ is the canonical momentum operator, $\mathbf{A} = \mathbf{a}\rho$ is the density-dependent gauge potential and we have denoted the non-kinetic part of $\hat{H}$, by the scalar operator

$$\Phi = -\mathbf{a}\cdot\mathbf{J} + g\rho + V\left(\mathbf{r}, t\right), \tag{8.5}$$

where V is the impurity potential and $\mathbf{J}$ is the gauge-covariant current

$$\mathbf{J} = \frac{i\hbar}{2m}\left[\psi\left(\boldsymbol{\nabla} + \frac{i}{\hbar}\mathbf{A}\right)\psi^* - \psi^*\left(\boldsymbol{\nabla} - \frac{i}{\hbar}\mathbf{A}\right)\psi\right], \tag{8.6}$$

with $\psi(\mathbf{r}) = \langle \mathbf{r}| \psi\rangle$. Notice that although the current appears in Φ, the latter operates on the condensate wavefunction as a scalar. Finally, it will be useful to define a synthetic magnetic field for the nonlinear gauge potential. Since $\mathbf{a}$ is constant over space, we have

$$\mathbf{B} = \boldsymbol{\nabla} \times \mathbf{A} = \boldsymbol{\nabla}\rho \times \mathbf{a}. \tag{8.7}$$

Hence, a non-vanishing magnetic field occurs over regions where the superfluid density varies transversely to $\mathbf{a}$.

8.2.2 The superfluid mechanical momentum

Due to the coupling of the superfluid to a gauge potential, the superfluid mechanical momentum features a "gauge" contribution in addition to the bare canonical momentum. This is connected with the functional form of the kinetic energy operator in Eq. (8.4). One way to see this, which will be useful in what follows, is to observe that the expectation value of mechanical momentum $\mathbf{g} = \langle \hat{\mathbf{g}} \rangle$ is related to the total time derivative of the expectation value of position:

$$\mathbf{g} = m\frac{d}{dt}\langle \hat{\mathbf{x}} \rangle = i\frac{m}{\hbar}\left\langle \left[\hat{H}, \hat{\mathbf{x}}\right] \right\rangle, \tag{8.8}$$

where $\hat{H}$ is given by Eq. (8.4). Recall that Φ operates as a scalar function of position and may be treated as such in any commutator. Hence, Φ commutes with the position operator, giving

$$\left[\hat{H}, \hat{x}_i\right] = \frac{1}{2m}\sum_j \left[(\hat{p}_j - A_j)^2, \hat{x}_i\right] = \frac{-i}{m}(\hat{p}_i - A_i). \tag{8.9}$$

Invoking the above commutation relations in Eq. (8.8), we find that the expectation value of the mechanical momentum operator, takes the gauge-covariant form

$$\mathbf{g} = \langle \hat{\mathbf{p}} - \mathbf{A} \rangle, \tag{8.10}$$

which may be written in terms of the definite integral

$$\mathbf{g} = \int d^3\mathbf{r}\psi^* \left(-i\hbar\boldsymbol{\nabla} - \mathbf{A}\right)\psi. \tag{8.11}$$

The above expression for the forward momentum can be cast into a more symmetrical form, as half of the difference between forward and backward momenta. This may be achieved by integrating the first term by parts and reaarranging accordingly, yielding

$$\mathbf{g} = \frac{i\hbar}{2}\int d^3\mathbf{r}\left[\psi\left(\boldsymbol{\nabla} + \frac{i}{\hbar}\mathbf{A}\right)\psi^* - \psi^*\left(\boldsymbol{\nabla} - \frac{i}{\hbar}\mathbf{A}\right)\psi\right]. \tag{8.12}$$

Recalling expression (8.6) for the gauge-covariant current density, we see that the total mechanical momentum of the superfluid may be obtained from the following spatial integral of the current:

$$\mathbf{g} = m\int d^3\mathbf{r}\mathbf{J}. \tag{8.13}$$

Hence the mechanical momentum density and current density are proportional to each other by a factor equal to the superfluid mass, as one would expect.

8.2.3 Derivation of the drag force

Retracing the line of reasoning from the previous section, the net force acting on the condensate may be obtained from the total time-derivative of the expectation value of the mechanical momentum operator:

$$\mathbf{F}(t) = \frac{d}{dt}\langle\hat{\mathbf{g}}\rangle = \frac{i}{\hbar}\left\langle\left[\hat{H}, \hat{\mathbf{p}} - \mathbf{A}\right]\right\rangle - \left\langle\frac{\partial\mathbf{A}}{\partial t}\right\rangle. \tag{8.14}$$

We shall evaluate the drag force from the reaction of the impurity to this force. Hence, our investigation rests on determining the quantities

$$F_k(t) = \frac{i}{\hbar}\left\langle\left[\sum_j \frac{(\hat{p}_j - A_j)^2}{2m} + \Phi, \hat{p}_k - A_k\right]\right\rangle - \left\langle\frac{\partial A_k}{\partial t}\right\rangle. \tag{8.15}$$

Rearranging the above expression for F_k and using standard commutation relations, e.g. $[\hat{p}_k, f(\hat{\mathbf{r}})] = -i\hbar\nabla_k f$, we soon find that

$$F_k(t) = F_k^L(t) - \langle\nabla_k\Phi(\mathbf{r})\rangle - \left\langle\frac{\partial A_k}{\partial t}\right\rangle, \tag{8.16}$$

where we have denoted the force stemming from the kinetic operator, by

$$F_k^L(t) = \frac{1}{2m}\left\langle\sum_j \{(\hat{p}_j - A_j)(\nabla_k A_j - \nabla_j A_k) + (\nabla_k A_j - \nabla_j A_k)(\hat{p}_j - A_j)\}\right\rangle. \tag{8.17}$$

Notice how a purely conservative contribution to the force features in the second term in Eq. (8.16), as a result of the impurity potential and the density nonlinearity, which produce an irrotational field $-\langle\nabla_k\left(V+g\rho\right)\rangle$. Conversely, F_k^L vanishes in Eq. (8.17) when $j=k$. In fact, we shall soon find that $\mathbf{F}^L$ takes the form of a transverse Lorentz force, albeit of synthetic origin. Indeed, the terms in Eq. (8.17) are very similar to the usual components of a Lorentz force density, but involve operators for current flow which do not commute with the magnetic field components. If we define a synthetic magnetic field $B_k=\sum_{i,j}\epsilon_{ijk}\nabla_i A_j$, notice that $-B_i$ appears in the above expression for F_k^L. Permuting indices i and j, and writing the mechanical momentum operator as $\hat{g}_i=\hat{p}_i-A_i$, leads to the following more compact form for F_k^L:

$$F_k^L=\frac{1}{2m}\sum_{i,j}\epsilon_{ijk}\left\langle\hat{g}_iB_j+B_j\hat{g}_i\right\rangle \tag{8.18}$$

$$=\frac{1}{2m}\sum_{i,j}\epsilon_{ijk}\left\langle[\hat{g}_i,B_j]+2B_j\hat{g}_i\right\rangle. \tag{8.19}$$

Invoking $[\hat{g}_i,B_j]=-i\hbar\nabla_iB_j$ and carrying out a simple integration by parts, we soon find that

$$F_k^L\left(t\right)=\frac{i\hbar}{2m}\sum_{i,j}\epsilon_{ijk}\int d^3\mathbf{r}B_j\left[\psi\left(\nabla_i-\frac{i}{\hbar}A_i\right)\psi^*-\psi^*\left(\nabla_i+\frac{i}{\hbar}A_i\right)\psi\right]. \tag{8.20}$$

Notice here the appearance of the components of the gauge-covariant current, so that the Lorentz-type force takes on the customary form

$$F_k^L(t)=\sum_{i,j}\epsilon_{ijk}\int d^3\mathbf{r}J_iB_j=\left\langle\sum_{i,j}\epsilon_{ijk}v_iB_j\right\rangle, \tag{8.21}$$

where $\mathbf{v}$ is the gauge-covariant superfluid flow. Although this is the simplest form for F_k^L, it will be convenient to cast the above expression explicitly in terms of the superfluid density ρ, which appears in the synthetic magnetic field from Eq. (8.7). Doing so, the synthetic Lorentz force in turn, becomes

$$F_k^L(t)=\sum_i\int d^3\mathbf{r}\rho v_i\left(a_i\nabla_k\rho-a_k\nabla_i\rho\right). \tag{8.22}$$

Let us turn our attention to the remaining contribution terms to the total force

$$F_k(t) = F_k^L(t) - \langle \nabla_k \left(g\rho - \mathbf{a}\cdot\mathbf{J} + V \right) \rangle - \left\langle \frac{\partial A_k}{\partial t} \right\rangle . \tag{8.23}$$

An integration by parts reveals that the force resulting from the nonlinear interaction term $g\rho$, vanishes. Thus, impurity potential aside, the problem reduces to understanding how the following two terms combine:

$$\left\langle \nabla_k \left(\mathbf{a}\cdot\mathbf{J} \right) - \frac{\partial A_k}{\partial t} \right\rangle \equiv F_k^J(t). \tag{8.24}$$

To this end, notice that the dependence of $\mathbf{A}$ on ρ, signifies that the gauge potential and the current, are related in the form

$$\partial_t A_k + a_k \boldsymbol{\nabla}\cdot(\rho\mathbf{v}) = 0. \tag{8.25}$$

Making use of this connection translates the time derivative of the gauge potential into a spatial derivative of the current, thereby permitting a straight-forward collection of terms in Eq. (8.24). Performing this substitution and integrating by parts accordingly, we soon find that

$$F_k^J(t) = \sum_i \int d^3\mathbf{r}\rho v_i \left(-a_i\nabla_k\rho - a_k\nabla_i\rho \right). \tag{8.26}$$

Comparing Eqs. (8.26) and (8.22), we see that F_k^L and F_k^J differ through the sign of the first term appearing under each integral. This difference stems from the minus sign as prefactor to the current nonlinearity $-\mathbf{a}\cdot\mathbf{J}$ in the Hamiltonian and yields a total force

$$F_k^d(t) \equiv F_k^L + F_k^J = -2a_k \sum_i \int d^3\mathbf{r} J_i \nabla_i \rho. \tag{8.27}$$

By carrying out an integration by parts, expanding the resulting $\boldsymbol{\nabla}\cdot(\rho\mathbf{v})$ term and performing a subsequent integration by parts on the $\mathbf{v}\cdot\boldsymbol{\nabla}\rho$ term, we find, after rearranging, the following form for F_k^d:

$$F_k^d\left(t\right) = \int d^3\mathbf{r}\rho A_k \boldsymbol{\nabla}\cdot\mathbf{v}. \tag{8.28}$$

Hence, the net total force acting on the condensate, is given by

$$F_k\left(t\right) = F_k^{imp}\left(t\right) + F_k^d\left(t\right), \tag{8.29}$$

where F_k^{imp} is given by Eq. (8.2). This reveals that the force exerted between the impurity and the condensate is not simply the expectation value of the gradient of the impurity potential as it would be typically, but includes an additional term associated with the divergence of the superfluid flow.

8.2.4 Hydrodynamical derivation of the force

In our study of the hydrodynamics of a nonlinear gauge-coupled quantum fluid from section 5.3, we learned that the mechanical momentum transport equation features a canonical flow pressure term and a body-force of dilation. For the particular case of interest here, where the condensate is subject to a unidirectional density-modulated gauge potential, then $\gamma = 1$ and $\mathbf{b}$ from Eq. (5.29) vanishes. The stress tensor of the condensate may be obtained from Eq. (5.50), in the form

$$\Pi_{jk} = -P\delta_{ij} + \sigma_{jk}, \tag{8.30}$$

where σ_{jk} is the quantum stress tensor from Eq. (5.45) and P is the fluid pressure, given by

$$P = -\frac{\hbar^2}{4m}\nabla^2\rho + \frac{g}{2}\rho^2 + \frac{a^2}{m}\rho^3 - \rho^2\mathbf{a}\cdot\mathbf{u}. \tag{8.31}$$

The canonical momentum transport equation, may be written as

$$m\partial_t\left(\rho u_k\right) = -\nabla_j T_{jk} - \rho\nabla_k V, \tag{8.32}$$

where

$$T_{jk} = m\rho v_j u_k - \Pi_{jk}. \tag{8.33}$$

Substituting the canonical flow for the mechanical flow and making use of the continuity equation (8.25), we find

$$m\partial_t J_k = -\nabla_j T_{jk} - \rho\nabla_k V + 2a_k\rho\boldsymbol{\nabla}\cdot\mathbf{J}, \tag{8.34}$$

where $J_k = \rho v_k$. The force on an impurity moving through the condensate may be evaluated by integrating the above equation [186, 188], which gives

$$F_k = \partial_t\int_\Omega d\Omega m J_k = -\int_S dS n_j T_{jk} + \int_\Omega d\Omega\left[-\rho\nabla_k V + 2a_k\rho\boldsymbol{\nabla}\cdot\mathbf{J}\right], \tag{8.35}$$

where S is a control surface within the fluid, $\mathbf{n}$ is a unit vector along the outward normal to S and Ω is the volume enclosed by S. Expanding the last term, integrating by parts and rearranging, the above equation may be cast into the form

$$F_k = -\int_S dS n_j T_{jk} + \int_\Omega d\Omega \rho \left[-\nabla_k V + A_k \rho \boldsymbol{\nabla} \cdot \mathbf{v}\right]. \tag{8.36}$$

For a penetrable object potential moving through the fluid, the control surface may be taken to encompass the entire fluid. In our numerical simulations, we impose periodic boundary conditions on the system. When the impurity size is much smaller than the system, which we will assume to be the case in what follows, then, on the boundary, the density ρ is constant and the canonical flow $\mathbf{u}$ and density gradients $\nabla_i \rho$ tend to zero. Under these circumstances, the first integral on the right hand side of Eq. (8.36) is negligible and the force reads as

$$F_k(t) = \int d^3\mathbf{r} \rho \left[-\nabla_k V + A_k \boldsymbol{\nabla} \cdot \mathbf{v}\right]. \tag{8.37}$$

This is precisely the expectation value of the force obtained in the previous section, highlighting the equivalence between both methods. Now that we have obtained an expression for the force acting between the impurity and the condensate, let us simulate the dynamics of an object potential travelling through a nonlinear gauge-coupled superfluid, examine the structure of the vortex shedding and evaluate the drag force numerically.

8.3 Numerical results

The dimensionless Gross-Pitaevskii-like Eq. (A.1) was solved numerically for a condensate populated by $N = 1600$ particles in dimension $d = 2$ with periodic boundary conditions, as described in appendix A.1. The side length of the box is $L = 47$ and we use Cartesian coordinates, where x and y denote the horizontal and vertical axes, respectively. We simulate the interaction between the condensate and a moving impurity object, by the Gaussian potential barrier

$$V(\mathbf{r}, t) = V_0 e^{-\sigma[\mathbf{r} - (\mathbf{r}_0 + \mathbf{v}_{imp} t)]^2}, \tag{8.38}$$

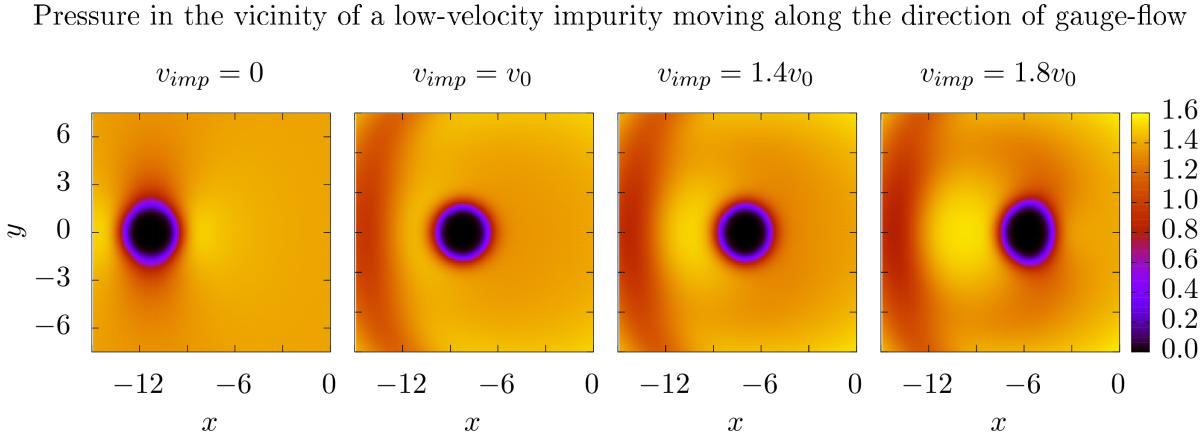

Figure 8.1: Plots showing the fluid pressure at time $t = 3$ in the vicinity of a travelling Gaussian impurity along the x-axis. The density-modulated gauge potential is oriented along $\alpha = \pi$ so that the impurity flows along the direction of the gauge-flow imparted to the superfluid. The pressure was calculated using Eq. (8.31) and is given in units $\hbar^2/(2mL^5)$. The time t is given in units $2mL^2/\hbar$. In the first image, the impurity is immobile and the pressure is aspherical about the impurity. As the impurity starts to move with the gauge-flow, the strain decreases, vanishing when the impurity speed is approximately equal to the ground state flow, $v_0 = |\mathbf{a}|\,\rho_0/m$ (second image). When the impurity speed exceeds v_0, a pressure gradient develops across the object.

produced by a far-off resonant blue-detuned laser, where $\sigma = 1.5$ and $V_0 = 40$. In our simulations, the direction of the travelling impurity is fixed along $+\mathbf{x}$ and we denote by α, the angle of the gauge potential relative to $+\hat{\mathbf{x}}$, e.g. $\alpha = 0$ denotes a density-modulated potential $\mathbf{A} = a\rho\hat{\mathbf{x}}$, while $\alpha = \pi/2$ corresponds to the situation $\mathbf{A} = a\rho\hat{\mathbf{y}}$. We shall refer to α as the gauge-angle. Choosing the origin of our system as the center of the box, we let the initial position of the impurity coincide with the point $\mathbf{r}_0 = -11.43\hat{\mathbf{x}} + 0\hat{\mathbf{y}}$. In the ground state, which was obtained by the method of imaginary time propagation, the fluid is homogeneously distributed over space with $\rho_0 \simeq N/L^2$, except for the enclosed region surrounding the immediate vicinity of the penetrable object potential, where a density-well is formed. In this region, a local phase profile is adopted by the ground state wavefunction which is antisymmetric under a parity transformation about the impurity, leading to a dipole-like canonical flow structure (see section 5.5).

8.3.1 Low velocity impurity flow along the direction of gauge-flow

In chapter 5, we learned that an immobile impurity placed in a nonlinear gauge-coupled superfluid, becomes compressed along the direction of the gauge potential. This is due

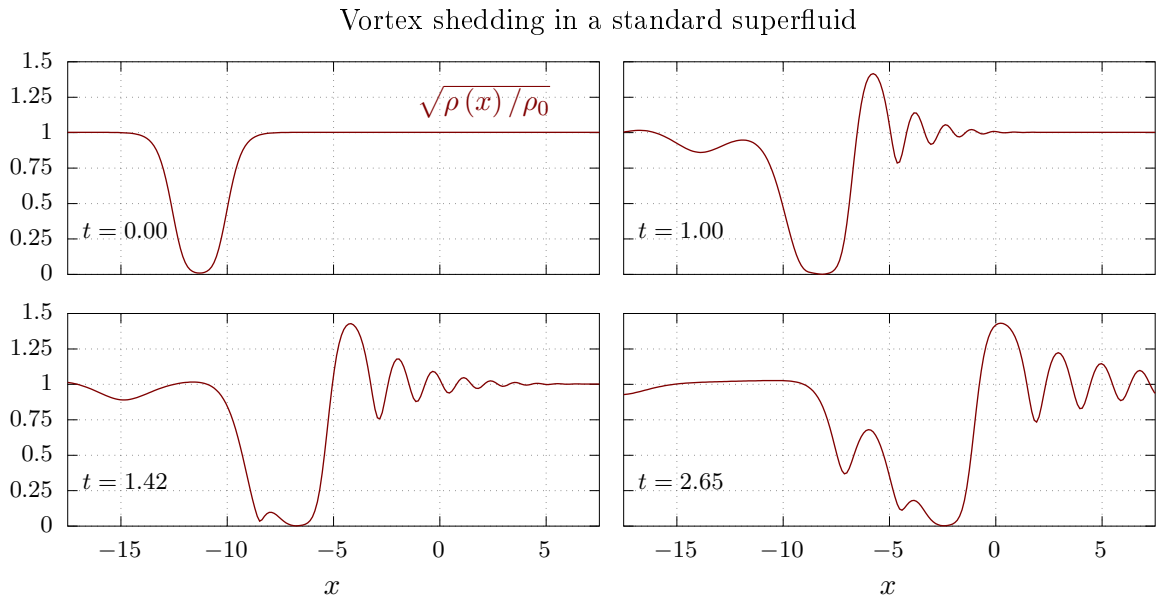

Figure 8.2: Plots showing the wave amplitude (scaled) along $y = 0$, in a standard superfluid with an impurity travelling at $v_{imp} = 3.46$ along the x-axis. Two vortex pairs are nucleated in succession, by, respectively, $t = 1.42$ and $t = 2.65$, as indicated by the density wells shed in the wake of the impurity. Here, v_{imp} and t are given in units $\hbar/(2mL)$ and $2mL^2/\hbar$, respectively.

to the canonical flow pressure connected with the non-trivial phase profile adopted by the ground state wavefunction, the latter accounting for the decrease in gauge-flow in the vicinity of the impurity. A natural question to ask is, what happens to the pressure when the impurity starts to move with the gauge-flow? To investigate this, we let the gauge-angle be $\alpha = \pi$, since for this orientation of $\mathbf{A}$, the impurity flows along the direction of gauge-flow. In FIG. 8.1, we show the fluid pressure at a given instant of time, for a variety of impurity speeds. In the first image, the impurity is immobile and the pressure is aspherically symmetric. Here, the impurity is compressed along the direction of gauge-flow and stretched in the orthogonal direction. In the second image, the pressure is spherically symmetric about the object. This occurs when the impurity flow matches the ground state flow, $v_0 = |\mathbf{a}|\,\rho_0/m$. Hence, the strain is relieved when the relative flow between the impurity and the superfluid, vanishes. When $v_{imp} > v_0$ (third and fourth images), but still below the critical velocity for vortex formation, a pressure gradient develops across the object. Finally, notice that the pressure in the vicinity of a spherically symmetric immobile impurity, is symmetric under $\mathbf{a} \to -\mathbf{a}$. However, in order to relieve the strain, the impurity should travel in the opposite direction, since the ground state phase is anti-symmetric under the transformation.

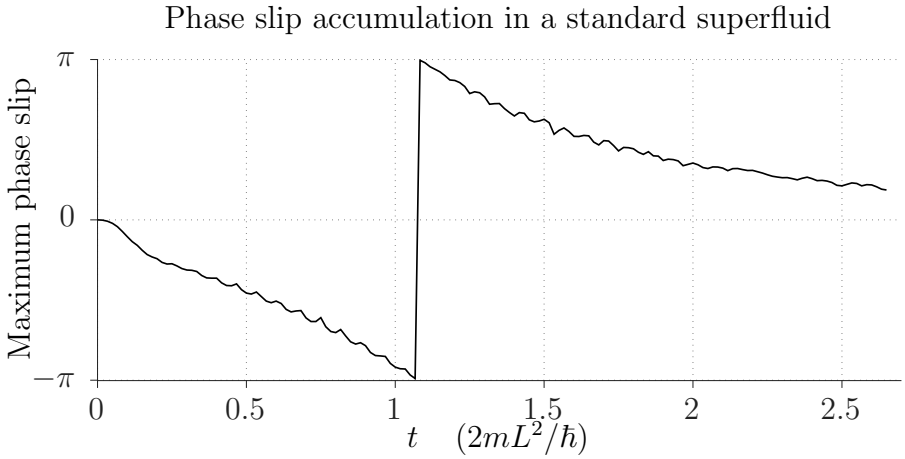

Figure 8.3: Evolution of the maximum phase slip along the x-axis, $\Delta\theta_{max}$, due to an impurity travelling just above the critical velocity. Upon reaching $-\pi$, $\Delta\theta_{max}$ changes sign. This coincides with the reversal of the on-axis flow close to the center of the impurity and marks the instant of vortex formation.

8.3.2 Vortex Shedding

Let us now drag the impurity through the superfluid at a velocity exceeding the critical velocity and investigate how the relative angle of the gauge potential affects the formation of vortices. For a standard superfluid, the travelling impurity excites density fluctuations in the fluid, where the density close to the center of the impurity becomes depleted a little further, as indicated by the top two images in FIG. 8.2. At the same time, the nonlinear interaction term $g\rho$ tends to suppress these density variations, by providing a current flow from high density to low density neighbouring regions. However, the motion induces a phase slip in the condensate [185]. At a given point (i, j) on the grid, the phase slip along x, is defined as $\Delta\theta_{i,j}(t) = \arg[\psi_{i+1,j} - \psi_{i,j}]$, with $-\pi < \Delta\theta_{i,j} \leq \pi$. The maximum phase slip, $\Delta\theta_{max}$, occurs on the x-axis, close to the center of the object potential. In FIG. 8.3, we see that $\Delta\theta_{max}$ accumulates over time and suddenly changes sign upon reaching the value $-\pi$, at which point quantised vortex pairs emerge in the wake of the impurity. The sign change coincides with the reversal of the on-axis flow near the object. In the density profile of the fluid, vortex nucleation is signalled by a well shed in the wake of the moving impurity, as seen in the bottom two images in FIG. 8.2. Vortex-pairs are nucleated approximately periodically in time, for each 2π phase slip accumulation. This is the signature for the breakdown of superfluidity and represents the quantum counterpart of turbulence in classical fluids. Note that the impurity velocities in the simulations from FIGs. 8.2 and 8.3, are different.

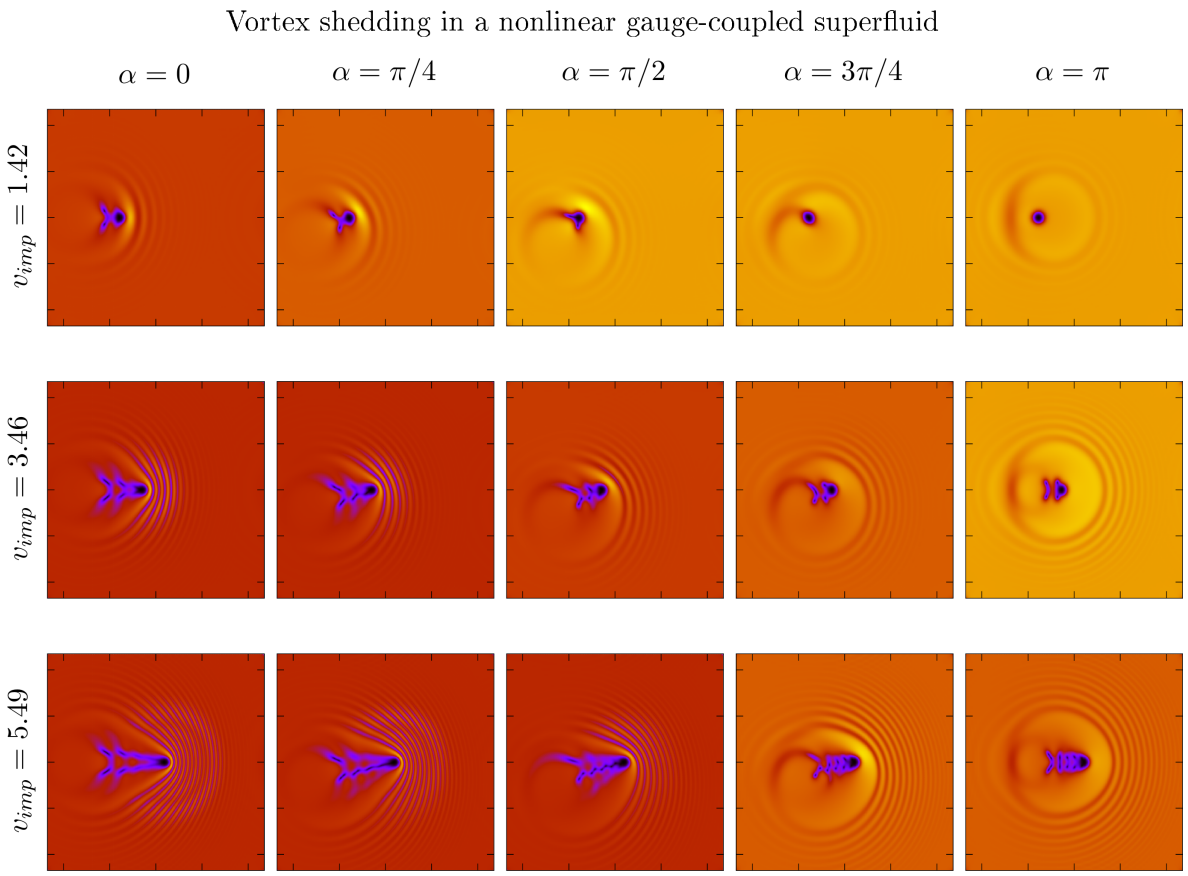

Figure 8.4: Plots showing the wave amplitude, $\sqrt{\rho/N}$, of a nonlinear gauge-coupled superfluid at time $t = 2.5$, for different angles α (columns) and impurity speeds v_{imp} (rows). The colour palette is identical to that of FIG. 8.1. Numbering images from left to right, top to bottom, the range of the colour box is $[0 - 0.025]$ for images $3 - 5, 10$, $[0 - 0.030]$ for images $2, 9, 14, 15$, $[0 - 0.035]$ for images $1, 8$ and $[0 - 0.040]$ for images $6, 7, 11 - 13$. The impurity velocity is given in units $\hbar/(2mL)$.

In the case of a nonlinear gauge-coupled superfluid, a density-modulated gauge-flow is imparted to the fluid, directed opposite to $\mathbf{A}$. In turn, the fluid pressure includes a canonical flow term, $-\rho\mathbf{u}\cdot\mathbf{A}$, which depends explicitly on the overlap between the gauge potential and the canonical current. Notice how the nonlinear gauge potential influences the form of the ripples and vortex nucleation which appear in the series of wave amplitude surface plots in FIG. 8.4. In particular, observe how the direction of gauge-flow influences the formation of bow-like or circular wave crests, the normal direction to these fronts and the position of the impurity relative to these (from left to right). Furthermore, the top row of images gives a qualitative indication that the critical velocity for vortex formation depends strongly on the orientation of the gauge potential relative to the travelling impurity. Here, we clearly notice that $v_{imp} = 1.42$, is above the critical velocity when $\alpha = 0$ and below the critical velocity when $\alpha = \pi$. This is not surprising insofar as we would expect the critical velocity to decrease when the

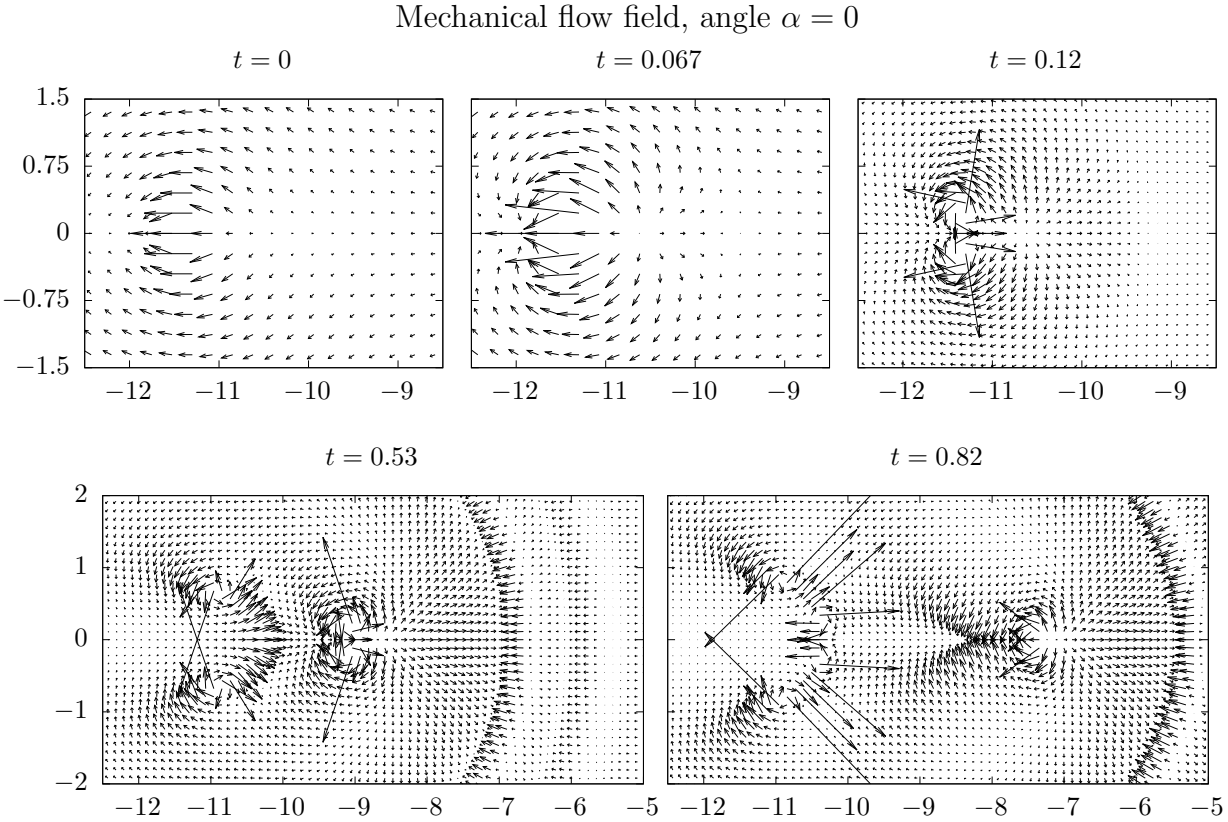

Figure 8.5: Quiver plots showing the mechanical flow field, $\mathbf{v}$, in the vicinity of the impurity during vortex formation. The gauge potential is oriented along $\alpha = 0$ and the impurity speed, in units $\hbar/(2mL)$, is $v_{imp} = 5.49$. The time t is given in units $2mL^2/\hbar$. The horizontal and vertical axes label the x and y coordinates, respectively. The magnitude of the field, in units $\hbar/(2mL)$, is given by the arrow length $\times 0.068$ in the $t = 0$ and $t = 0.067$ images, and the arrow length $\times 0.023$ in the remaining images.

gauge-flow increasingly opposes the motion of the impurity. Further, we shall evaluate the critical velocity by examining the phase slip accumulation at different angles. Notice also the appearance of shock waves in the high v_{imp}, low α images in FIG. 8.4. Here, the impurity deforms the bow waves, leading to a shock front.

To illustrate the influence of the gauge potential, we have the image of a pool of water with a background unidirectional flow. In the absence of a background flow, a rigid bar dragged through the water at sufficiently low velocity creates local deformations in the water level which propagate away from the source of disturbance at a uniform speed. Switching on the gauge potential, these disturbances now propagate on the surface of a medium which is also in motion, where the velocity of the medium is proportional to the density. This may already have been anticipated from our results of the previous chapter, where we discovered that sound waves propagate with an anisotropic velocity, $\mathbf{c} = c^M \hat{\mathbf{a}} + c_\perp \hat{\mathbf{k}}$, where c^M and $c_\perp$ are, respectively, the anisotropic and isotropic contributions, $\hat{\mathbf{a}}$ is a unit vector along $\mathbf{A}$ and $\hat{\mathbf{k}}$ is a unit vector along

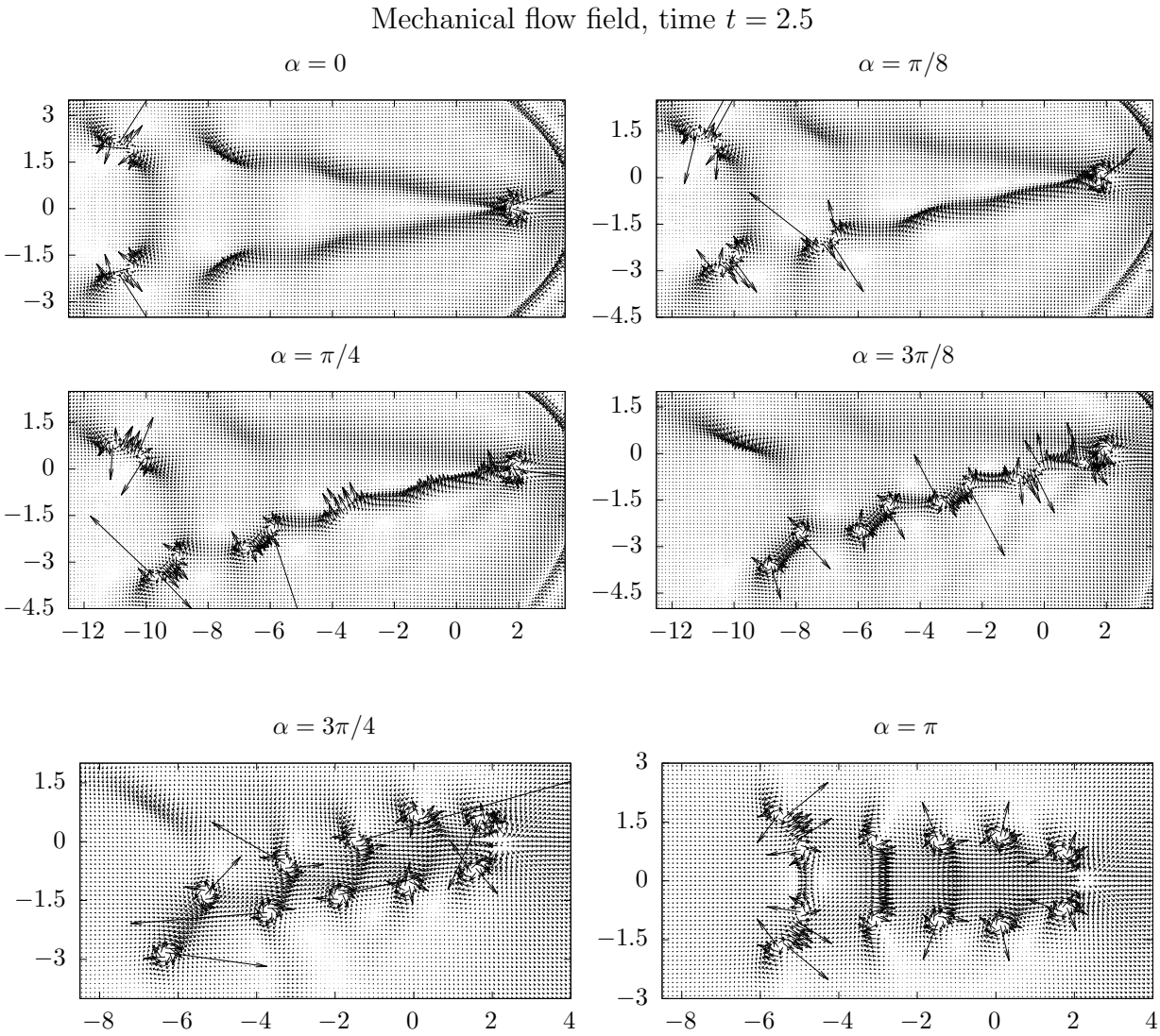

Figure 8.6: Quiver plots showing the mechanical flow field, $\mathbf{v}$, at time $t = 2.5$, for various orientations α of the gauge potential. The impurity velocity, in units $\hbar/(2mL)$, is $v_{imp} = 5.49$. The horizontal and vertical axes label the x and y coordinates, respectively. The top four plots have identical x-range. The magnitude of the field, in units $\hbar/(2mL)$, is given by the arrow length $\times 0.023$.

the direction of propagation of the sound wave. Note that c^M is equivalent to the flow of the medium which carries sound, and, negative in our adopted convention. For orientation α, the speeds of sound along $\pm\mathbf{x}$ and $\pm\mathbf{y}$, are then given by, respectively, $c_{\pm\mathbf{x}}(\alpha) = \pm c_x^M(\alpha) + c_\perp$ and $c_{\pm\mathbf{y}}(\alpha) = \pm c_y^M(\alpha) + c_\perp$, where the x-component of the flow of the medium is $c_x^M(\alpha) = c^M \cos\alpha$ and the y-component is $c_y^M(\alpha) = c^M \sin\alpha$. For the parameter values of our simulations, we have, in units $\hbar/(2mL)$, $c^M \simeq -2.11$ and $c_\perp \simeq 2.94$. Note that $c_x^M(\alpha)$ and $c_{+\mathbf{x}}(\alpha)$ will be particularly relevant here, seeing as the impurity travels along $+\mathbf{x}$. For instance, at angle α, we would expect shock waves to play a significant role for impurity speeds exceeding $c_{+\mathbf{x}}(\alpha)$. We shall return to this point later in our evaluation of the drag force acting on the impurity.

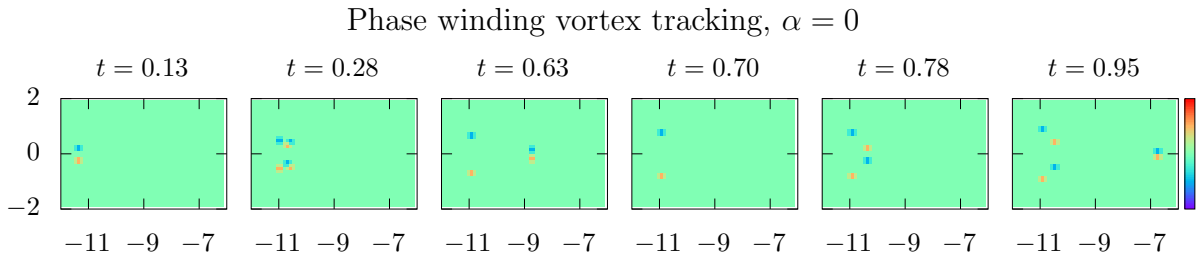

Figure 8.7: Plots showing the phase winding field for $\alpha = 0$, at successive times. By $t = 0.13$, a vortex pair $\left(V_1^r, V_1^b\right)$ is shed close to the center of the impurity. This coincides with the reversal of the on-axis flow in the third image of FIG. 8.5. The pair separates and two additional pairs $\left(V_2^r, V_2^b\right)$ and $\left(V_2^{r'}, V_2^{b'}\right)$ are nucleated close to V_1^r and V_1^b, respectively. As V_2^b and $V_2^{r'}$ recombine, $V_2^{b'}$ and V_2^r close in, and, in turn, recombine by $t = 0.70$. Soon thereafter, a fourth pair $\left(V_3^r, V_3^b\right)$ is created near the recombination region of $\left(V_2^b, V_2^{r'}\right)$, forming a vortex quadrupole. By $t = 0.95$, a fifth pair $\left(V_4^r, V_4^b\right)$ is shed close to the impurity and remains in the wake of the impurity for the duration of the simulation. Subsequently (not shown), the vortex quadrupole separates into two pairs and no further vortices are nucleated.

Before undertaking a thorough examination of the vortex structures which emerge in the fluid, let us briefly highlight a few general observations from the images in FIG. 8.4. Firstly, the wave amplitude is symmetrically distributed about the x-axis, for angles $\alpha = 0$ and $\alpha = \pi$, as one would expect. Furthermore, the vortices seem to be somewhat carried by the gauge-flow. This also appears to be the case for intermediate angles, where vortices appear predominantly in the lower half of the surface plots. Observe further how the vortex structure appears almost segment-like at $\alpha = 0$ and takes on a more point-like form as α is increased from left to right. However, it is unclear from these plots alone why this occurs.

8.3.2.1 Mechanical flow field during vortex formation

In order to gain insight into the process of vortex formation, it is instructive to examine the evolution of the mechanical flow field. In FIG. 8.5, we depict quiver plots of the field for gauge-angle $\alpha = 0$, evaluated using $\mathbf{v} = \hbar/\left(2mL\right)\left[i\left(\psi\boldsymbol{\nabla}\psi^* - \psi^*\boldsymbol{\nabla}\psi\right)/\left(\psi^*\psi\right) - 2\mathbf{A}\right]$. At $t = 0$, the fluid skirts around the impurity due to the non-trivial phase adopted by the ground state wavefunction. When the impurity starts to move, the skirting increases and the fluid fills the void with a forward flow (second image). By $t = 0.12$, the flow near the center of the impurity has reversed, signalling the formation of a vortex pair. In the fourth image, the vortex pair has left the impurity and the flow in the region between the pair and the impurity increases. Note also the on-axis flow reversal close

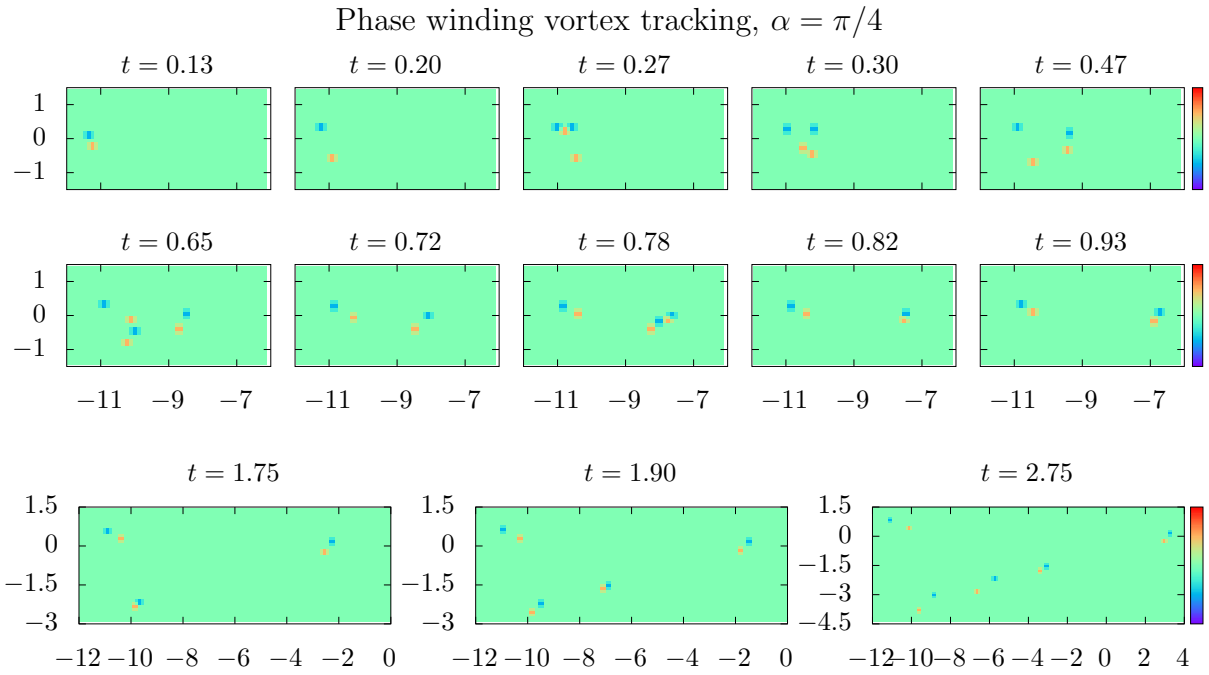

Figure 8.8: Plots showing the phase winding field for $\alpha = \pi/4$, at successive times. As $\left(V_1^r, V_1^b\right)$ separates in the second image, $\left(V_2^r, V_2^b\right)$ is nucleated and propelled to the right of V_1^b. As a result, V_1^r and V_2^r repel, and the pairings $\left(V_1^b, V_2^r\right)$ and $\left(V_1^r, V_2^b\right)$ occur on the left and right, respectively (fifth image). The left pair $\left(V_1^b, V_2^r\right)$ drifts apart and by $t = 0.65$, an additional pair $\left(V_3^r, V_3^b\right)$ is created between the two vortices, forming a vortex quadrupole. Soon thereafter, V_2^r and V_3^b recombine, leaving the pair $\left(V_1^b, V_3^r\right)$, which persists for the duration of the simulation. By $t = 0.78$, a new pair $\left(V_4^r, V_4^b\right)$ is shed near the impurity, leading to a recombination of the pair, $\left(V_1^r, V_2^b\right)$, behind. In the $t = 0.93$ image, we see that this latest pair follows the impurity closely. No further pairs are nucleated close to the impurity. However, three additional pairs are eventually formed far from the impurity, as seen in the last row of images. Although the first two seem to emerge near previous recombination regions, the third does not.

to the impurity, where an additional vortex is formed. By $t = 0.82$, a non-trivial flow reversal occurs in the region close to $(-10.25, 0)$ and an additional vortex pair is formed between the first nucleated pair, forming a vortex quadrupole, which is to say, a vortex cluster of four singly charged vortices with zero total vorticity [190]. Furthermore, the flow field in front of the impurity in the bottom two images, gives us additional insight into the wave amplitude plots in FIG. 8.4. In front of the impurity, the canonical flow points away from the object, until the first bow wave crest is reached, at which point the canonical flow points towards the object. Since the orientation of $\mathbf{A}$ lies along $\alpha = 0$, the canonical flow pressure is negative in between the impurity and the crest and positive on the crest. Hence, the canonical flow pressure favours the possibility for fluid to fall into the region between the impurity and the bow wave crest. Conversely, when $\alpha = \pi$, we have the opposite situation where the canonical flow pressure favours the

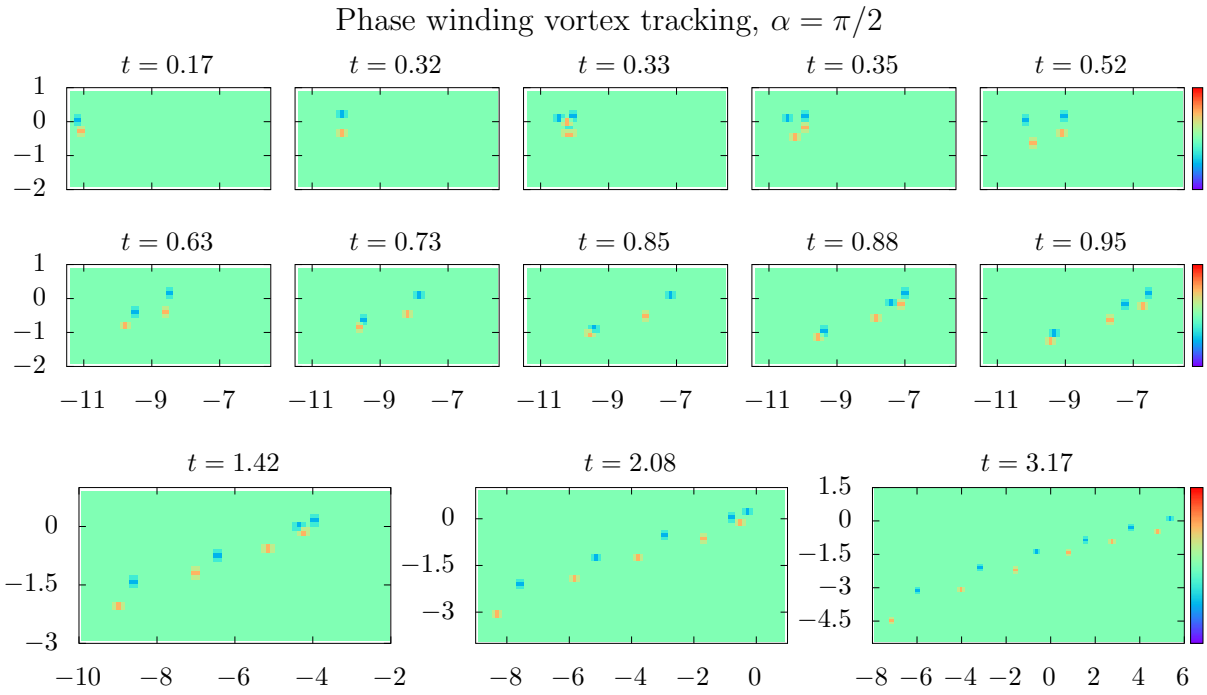

Figure 8.9: Plots showing the phase winding field for $\alpha = \pi/2$, at successive times. After the first pair $\left(V_1^r, V_1^b\right)$ forms, V_1^b arcs around V_1^r. Upon overtaking V_1^r, a new pair $\left(V_2^r, V_2^b\right)$ is formed to the left of V_1^b. As a result, V_1^r and V_2^r repel, V_2^b is stopped in its track for approximately $\Delta t = 0.08$ and the pairings $\left(V_1^r, V_2^b\right)$ and $\left(V_1^b, V_2^r\right)$ occur on the left and right, respectively (fifth image). Subsequently, V_2^b closes in on V_1^r and $\left(V_1^b, V_2^r\right)$ separate, with V_1^b following the impurity closely. As the separation increases, an additional pair $\left(V_3^r, V_3^b\right)$ forms between V_1^b and V_2^r, by $t = 0.88$. The newly created anti-vortex pairs up with the previous vortex, V_2^r, while the newly created vortex, V_3^r, pairs with the anti-vortex flowing in the wake of the impurity, V_1^b. This process is repeated approximately periodically in time, where the anti-vortex V_1^b remains close to the impurity and, in succession, pairs up with the most recently nucleated vortex.

possibility for fluid to be expelled from the region. This gives a qualitative explanation for the difference in the wave amplitude distributions in front of the impurity in the bottom left and bottom right images of FIG. 8.4.

The flow field at a later time, $t = 2.5$, is shown in FIG. 8.6, for a variety of gauge-angles. Here, we notice similar vortex quadrupole structures at low α, but also interestingly, at $\alpha = \pi$, where an on-axis flow reversal occurs between the left-most vortex pair. In the $\alpha = 0$ image, notice the vortical-like structures left in the wake of the impurity at approximately $(-7.5, -1.5)$ and $(-7.5, 1.5)$. However, these do not appear to be singly charged point vortices. When $\alpha = \pi/8$ on the other hand, a vortex pair takes the place of the lower vortical structure of the $\alpha = 0$ image, while the upper vortical structure has considerably diminished. Similar vortical structures are found closer to the impurity in the $\alpha = \pi/8$ and $\alpha = \pi/4$ images, as well the region surrounding $(-9.75, 0.5)$ in the

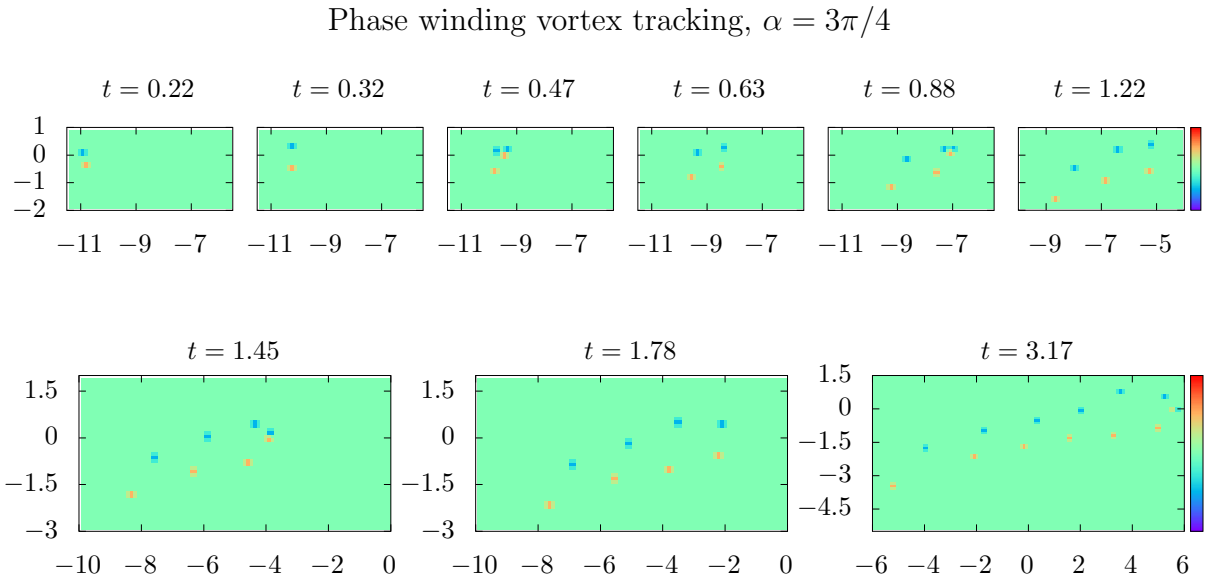

Figure 8.10: Plots showing the phase winding field for $\alpha = 3\pi/4$, at successive times. Similar to the $\alpha = \pi/2$ case, V_1^b arcs around V_1^r and upon overtaking, an additional pair is nucleated. However, this occurs to the right (in front of) V_1^b and the newly created pair is propelled forwards. The process repeats by $t = 0.88$, where a vortex pair is nucleated near V_2^b. However, the next nucleated pair, by $t = 1.45$, occurs close to the impurity and the process repeats approximately periodically in time.

$\alpha = 3\pi/8$ image.

8.3.2.2 Vortex tracking

To understand how the above structures arise, let us visualise and track point vortices using a different method, namely, by computing the phase winding field at each moment in time. At a given point (i, j) on the grid, we define the phase winding, as, $\Omega_{i,j} = \Delta\theta^{(1)}_{i,j} + \Delta\theta^{(2)}_{i,j} + \Delta\theta^{(3)}_{i,j} + \Delta\theta^{(4)}_{i,j}$, where $\Delta\theta^{(1)}_{i,j} = \arg\left[\psi_{i,j+1} - \psi_{i-1,j}\right]$, $\Delta\theta^{(2)}_{i,j} = \arg\left[\psi_{i-1,j} - \psi_{i,j-1}\right]$, $\Delta\theta^{(3)}_{i,j} = \arg\left[\psi_{i,j-1} - \psi_{i+1,j}\right]$ and $\Delta\theta^{(4)}_{i,j} = \arg\left[\psi_{i+1,j} - \psi_{i,j+1}\right]$. In other words, as our loop, we take the infinitesimal square formed by the four nearest neighbours of point (i, j). Note that it is crucial that the condition $-\pi < \Delta\theta^{(n)}_{i,j} \leq \pi$, be enforced on all phase differences computed in $\Omega_{i,j}$.

In figures 8.7-8.11, we depict a time series of the phase winding field due to an impurity travelling at $v_{imp} = 5.49$, in units $\hbar/(2mL)$. Each figure corresponds to a given gauge angle α. In all plots, the time t is given in units $2mL^2/\hbar$ and the horizontal and vertical axes label the x and y coordinates, respectively. The colour boxes to the right of each row of images, all have range $[-2\pi, 2\pi]$. The red (blue) dots represent positively (negatively) charged point vortices, where the phase changes by 2π (-2π) on circulation of a vortex (anti-vortex). In the captions, we label the vortices according

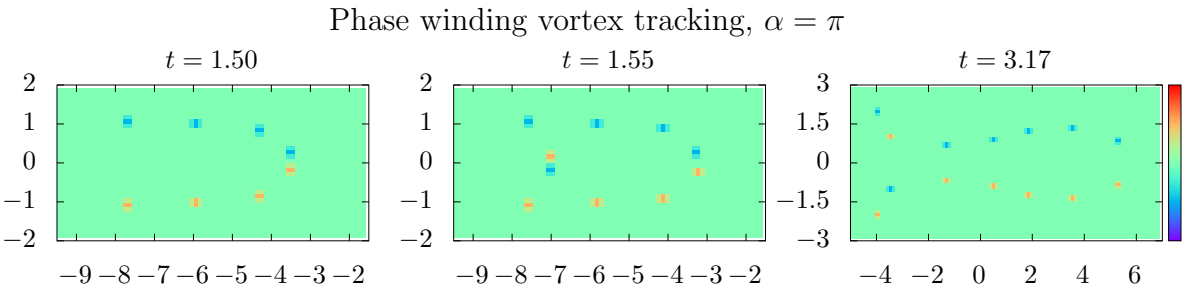

Figure 8.11: Plots showing the phase winding field for $\alpha = \pi$, at successive times. The first, second and third vortex pairs are shed close to the impurity (not shown), by $t = 0.22$, $t = 0.49$ and 0.95, respectively. The right-most pair is located at a distance of approximately $\Delta x = 0.75$ behind the impurity when the next pair is nucleated. Soon after the fourth pair is created, a fifth pair forms far away from the impurity, by $t = 1.55$. This occurs on the axis, close to $\left(V_1^r, V_1^b\right)$. As the pair separates, V_5^r and V_1^b drift upwards and V_1^r and V_5^b drift downwards. In turn, this causes the pairs $\left(V_2^r, V_2^b\right)$ and $\left(V_3^r, V_3^b\right)$ in front, to close in, leading to a "fish-like" vortex configuration..

to their appearance in time and their colour in the image. If two vortex pairs appear simultaneously in an image, a prime is given to the upper vortex pair. For instance, $V_3^{b'}$ denotes the upper anti-vortex nucleated at the third instant of time of vortex creation. A few general features may be abstracted from these time-sequences, which we summarise as follows. The first nucleated vortex pair always occurs close to the center of the impurity, as one would expect. However, interestingly, vortex pairs also later emerge, either, close to a previously nucleated vortex or anti-vortex, in between a previously nucleated pair, or in far away regions devoid of vortices. The latter typically emerge in a region where a pair has previously been annihilated, but not strictly. We interpret the above discussed vortical-like structures in the low α images of FIG. 8.6, as the result of such recombinations. Annihilation proceeds from pair creation close to an existing pair and occurs exclusively for $\alpha \in [0, \pi/2)$, e.g. when the gauge-flow tends to oppose the impurity. With the exception of $\alpha = \pi$, the second instance of vortex formation is marked by off-axis pair creation. This leads to a double recombination in the case $\alpha = 0$, vortex exchange when $\alpha \in [\pi/4, \pi/2]$ and propulsion for $\alpha = 3\pi/4$.

8.3.2.3 The critical velocities

The dependence of the critical velocity for vortex formation on the gauge-angle, α, was noted from the wave amplitude surface plots in FIG. 8.4. Let us now estimate the critical velocity for angles $\alpha = 0$ to $\alpha = \pi$, in steps of $\pi/8$. To do so, we examine the phase slip of the superfluid, which, at the moment of vortex creation, displays a 2π jump. This gives a clear criterion for detecting pair creation. We characterise the

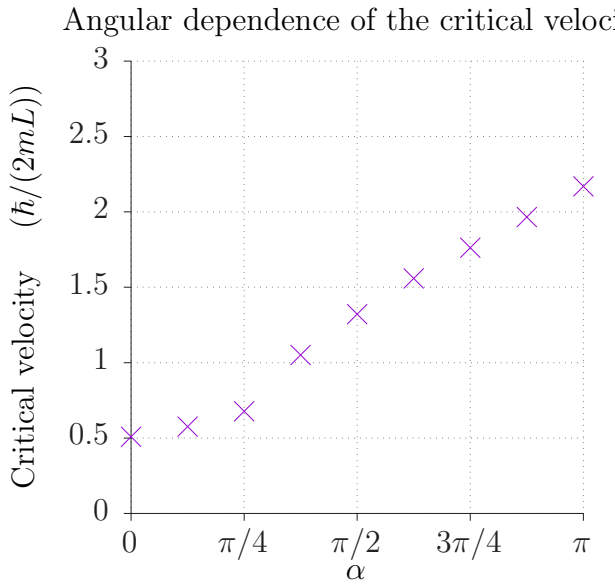

Figure 8.12: Critical velocity for different orientations of the gauge potential relative to the travelling impurity. The critical velocity was estimated as the lowest impurity velocity for which the time-evolution of the maximum phase slip along $y = 0$ displays a single 2π jump. The impurity velocity was resolved with an accuracy of $\Delta v_{imp} = 0.032$.

critical velocity, $v_c(\alpha)$, as the impurity velocity for which the first vortex pair *leaves* the impurity region, and not merely the velocity for which vortex nucleation occurs. We make this distinction because, just below this velocity, successive pair creation and annihilation occurs close to the impurity. In the time-evolution of $\Delta\theta_{max}$, this shows up as a succession of 2π and -2π jumps. Hence, we estimate the critical velocity from the condition that $\Delta\theta_{max}$ display a single 2π transition. In figure 8.12, we show the α-dependence of the critical velocity obtained using this method, for an impurity velocity resolution, $\Delta v_{imp} = 0.032$. Here, we see that the critical velocity increases monotonically with α, as the gauge-flow increasingly flows with the impurity. Note the sharp increase in v_c between $\alpha = \pi/4$ and $\alpha = \pi/2$.

8.3.3 Drag force

We now turn our attention to the numerical evaluation of the drag force acting on the impurity. For a standard superfluid, the reaction of the fluid to a moving impurity occurs in the immediate vicinity of the object potential. In figure 8.13, we show the instantaneous drag force, F_x, below and above the critical velocity, computed using

$$F_x(t) = -\int d^3\mathbf{r}\rho\nabla_x V(\mathbf{r}, t). \tag{8.39}$$

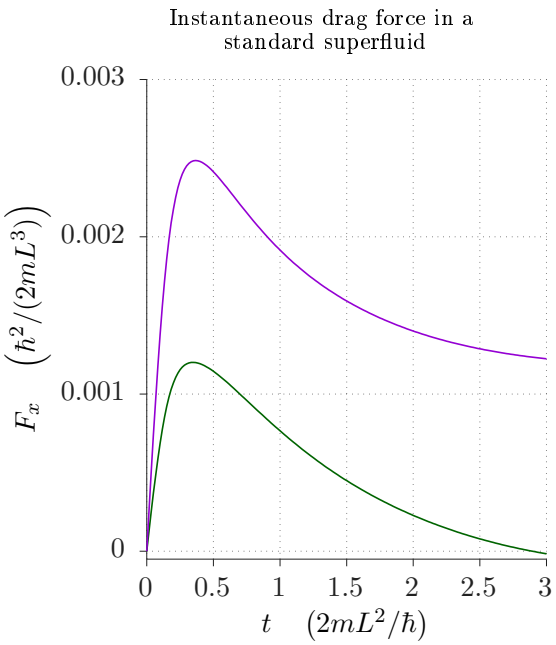

Figure 8.13: Time-evolution of the drag force, F_x, in a standard superfluid. For the lower curve, $v_{imp} = 0.61 < v_c$, and the drag force approaches zero. For the upper curve, $v_{imp} = 1.22 > v_c$ and the drag force approaches a non-vanishing value. The impurity velocity is given in units $\hbar/(2mL)$.

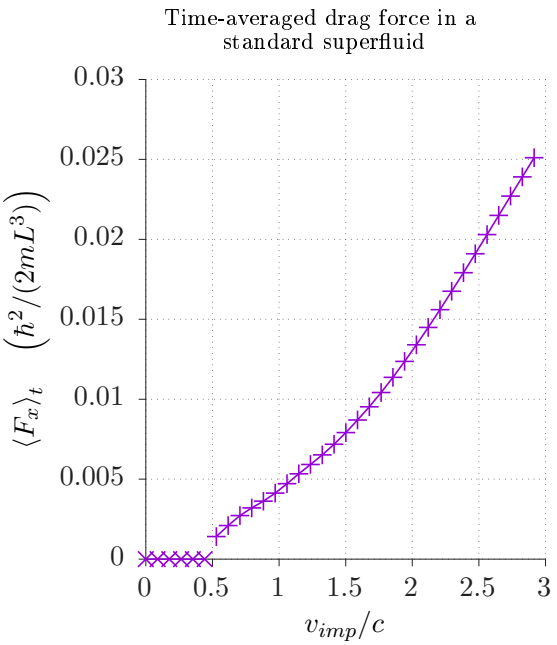

Figure 8.14: Time-averaged drag force in a standard superfluid as a function of the impurity velocity. The drag is zero up to a critical velocity v_c, The bulk speed of sound, in units $(\hbar/(2mL))$, is $c = \sqrt{2g\rho_0} = 2.30$.

At low time, the curves display a peak due to the sudden acceleration of the impurity. After the fluid has accommodated to this abrupt change, the drag force approaches zero when $v_{imp} < v_c$ and a non-vanishing value when $v_{imp} > v_c$. In figure 8.14, we show the time-averaged drag force as a function of the impurity velocity. The time-average was evaluated from curves similar to those of FIG. 8.13, over a time span where the force has already reached a plateau. In previous studies of dilute BEC systems [188, 191], it has been shown that the drag force is zero up to the critical velocity, v_c, approximately linear for $v_c < v_{imp} < c$ and approximately quadratic for $v_{imp} > c$. Our results indicate a similar behaviour. By investigating the phase slip of the fluid, one may verify that the transition to a linear regime occurs when vortices are shed in the wake of the impurity. The subsequent transition to a quadratic regime may be assimilated with shock wave production.

Let us now examine the behaviour of the drag force in a nonlinear gauge-coupled

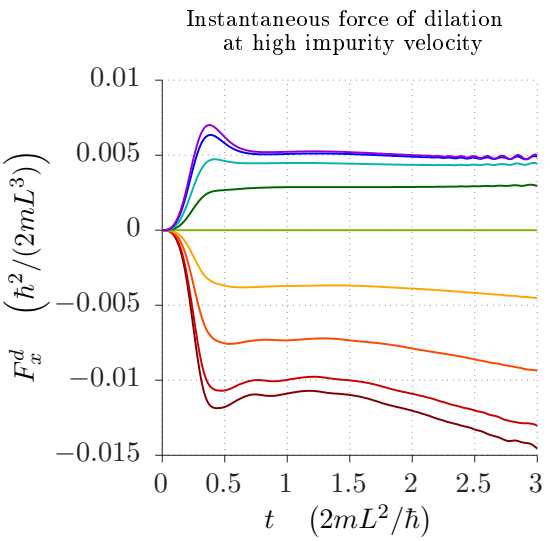

Figure 8.15: Time-evolution of the x-component of the body-force of dilation due to a high velocity impurity ($v_{imp} = 6.10$). Each curve corresponds to a given angle α, from 0 to π in steps of $\pi/8$ (bottom to top).

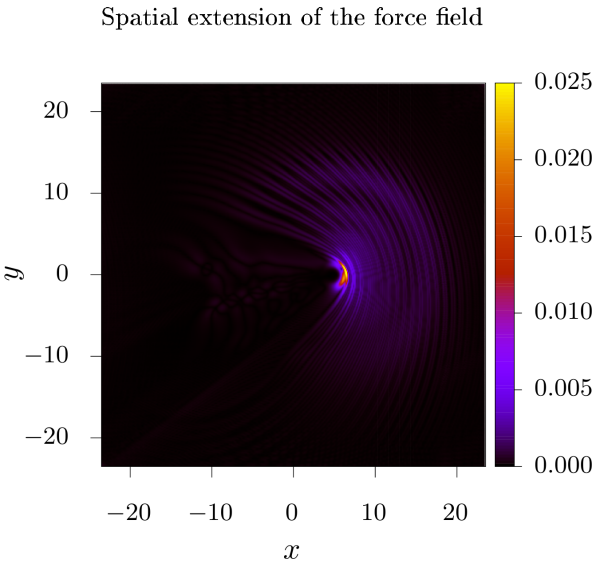

Figure 8.16: Modulus of the force field, $\mathbf{F}$, in units $\hbar^2/(2mL^3)$, at time $t = 3$. The gauge potential is oriented along $\alpha = \pi/4$ and the impurity speed is $v_{imp} = 5.49$, in units $\hbar/(2mL)$.

superfluid. From a numerical point of view, it is appropriate to compute the force, as

$$F_x(t) = -\int d^3\mathbf{r}\left[\rho\nabla_x V + 2a_x\rho\mathbf{v}\cdot\boldsymbol{\nabla}\rho\right]. \tag{8.40}$$

Comparing Eqs. (8.39) and (8.40), one conspicuous difference may be highlighted in particular, namely, that reaction occurs not merely in the vicinity of the impurity, but more generally over regions of non-vanishing overlap between the superfluid flow and density gradients. This is illustrated in FIG. 8.16, where we notice that the force field extends over the whole system. Although, locally, the strongest contribution stems from F_x^{imp}, globally, a non-negligible contribution arises due to F_x^d. Notice the change in the strip profiles across the system, the turbulence in the wake of the object and the wide circular strips emanating from the shock wave.

In figure 8.15, we show the real-time evolution of F_x^d at high impurity velocity, for gauge angles $\alpha = 0$ to $\alpha = \pi$ in steps of $\pi/8$, computed using the second term on the right hand side of Eq. (8.40). Note that the sign of F_x^d follows that of $-\cos\alpha$. The magnitude of F_x^d is greater when the gauge-flow tends to oppose the moving impurity, where the dilation rate of the fluid becomes more prominent. Crucially however, the force does not stabilise generally at long time. This is not too surprising, since the

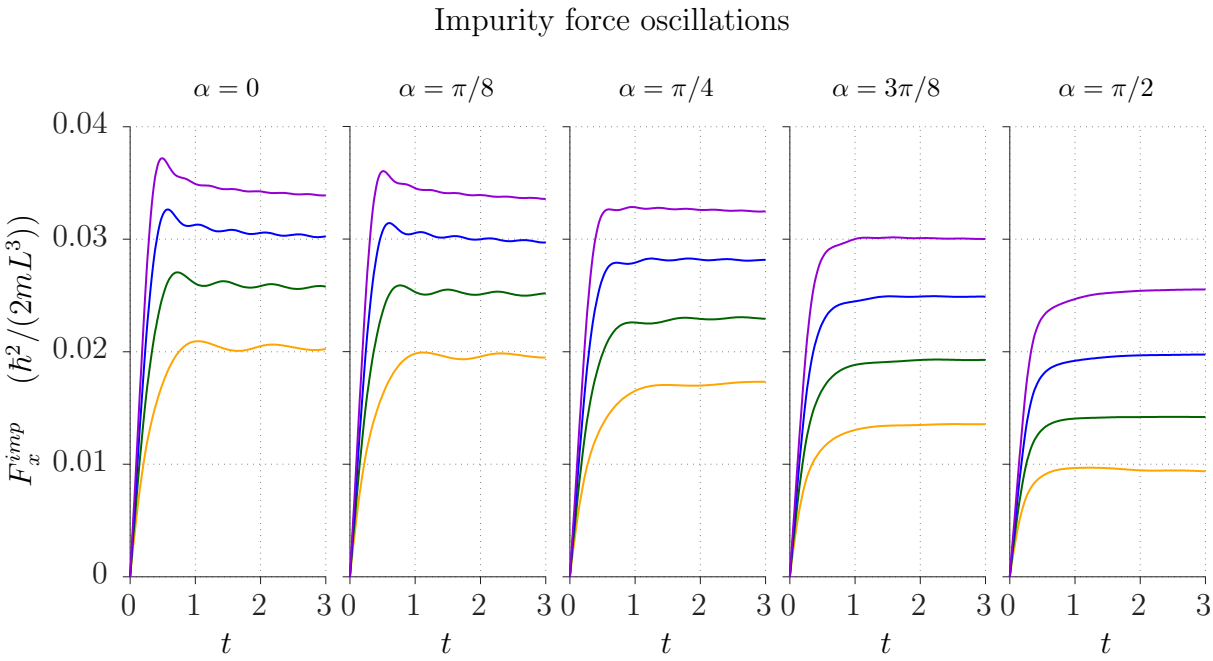

Figure 8.17: Plots showing the angular dependence and impurity velocity dependence of F_x^{imp}. In each plot, the impurity speeds are, in units $\hbar/(2mL)$, $v_{imp} = 3.66$, $v_{imp} = 4.68$, $v_{imp} = 5.69$ and $v_{imp} = 6.71$ from bottom to top (yellow, green, blue, purple), and the time is given in units $2mL^2/\hbar$. The amplitude of the density crest in front of the impurity oscillates in time (see FIG. 8.18), leading to impurity force oscillations.

spatial extension of the force continually increases with time, as the density disturbances propagate out. For the length and time scales of our simulations, the non-stability becomes more important at high impurity velocities and when the gauge-flow tends to opposes the impurity. As a consequence, one may not consider time-averages of the drag force in a meaningful manner.

The impurity force term, F_x^{imp}, on the other hand, is well behaved at long time, over the whole angular range. In FIG. 8.17, we depict the time evolution of F_x^{imp} within the first angular quadrant $\alpha \in [0, \pi/2]$. Here, we retrieve curves similar to those obtained in a standard superfluid. However, notice how the spacing between the curves, changes from one angle to the next. This is in contrast to a standard superfluid, where the spacing increases approximately quadratically with v_{imp}. Observe further how F_x^{imp} oscillates in time when the gauge-flow tends to oppose the impurity, a feature which is absent in a standard superfluid. In particular, note the amplitude and frequency change of the oscillations, as v_{imp} and α are varied. By inspecting the time-evolution of the wave amplitude slice along the x-axis (FIG. 8.18), one may verify that, at low α, the density disturbance undergoes an amplitude modulation during propagation, leading to impurity force oscillations. This could be connected with amplitude changes in the

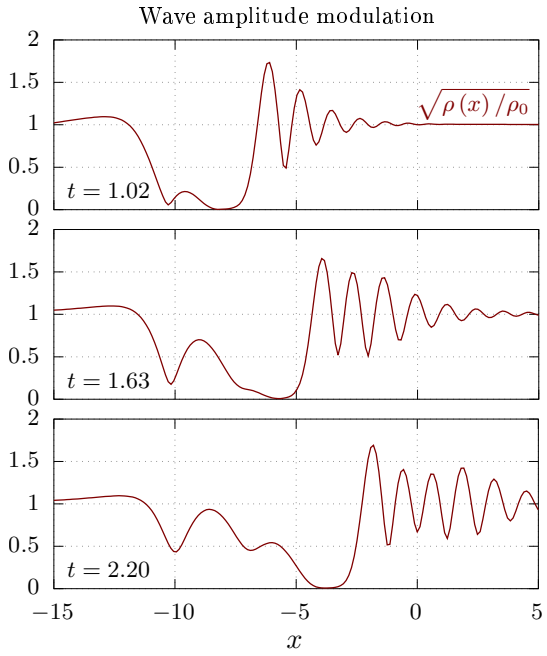

Figure 8.18: Plots showing the wave amplitude slice along $y = 0$ at successive times (with t given in units $2mL^2/\hbar$), for $\alpha = 0$ and $v_{imp} = 3.66$ (the bottom left curve in FIG. 8.17). When the gauge-flow tends to oppose the impurity, the density slice undergoes an amplitude modulation.

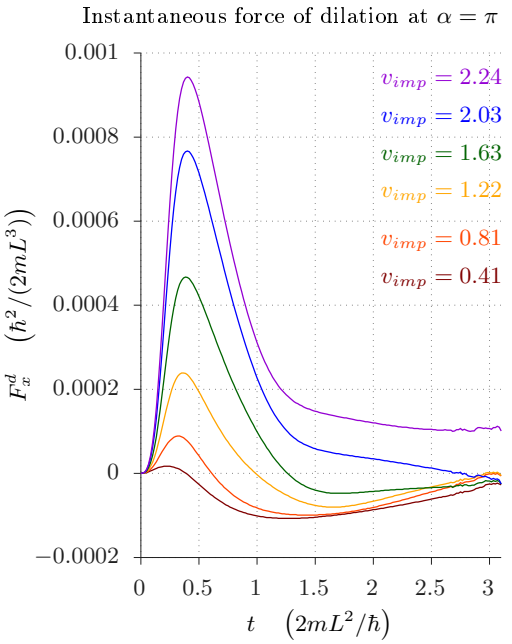

Figure 8.19: Plot showing the instantaneous x-component of the force of dilation at angle $\alpha = \pi$ for different impurity speeds (in units $\hbar/(2mL)$), as indicated. The force approaches zero at low impurity speeds and takes on a positive value only when v_{imp} exceeds $c_x^M(\pi) \simeq 2.11$.

canonical flow waves in front of the impurity (see the fourth and fifth images of FIG. 8.5), which would alter the canonical flow pressure and lead to fluid flow between peaks and troughs.

Before inspecting the time averaged impurity force, let us examine the instantaneous drag force at low impurity velocities. In figure 8.20, we show a series of such curves, for $\pi/2 < \alpha \leq \pi$. The long-time behaviour of several of these curves is unclear and it was not possible to increase the runtime due to boundary effects becoming too prominent. In particular, it is unclear whether F_x approaches a negative value or zero for certain curves. However, a general trend seems apparent, namely, that F_x approaches a non-vanishing, positive value at long time, when $v_{imp} > c_x^M(\alpha)$, where $\mathbf{c}^M(\alpha) = -2\mathbf{a}\rho/m$ is the velocity of the medium for sound. Note that $c_x^M(\alpha)$ is distinct from the critical velocity for vortex formation $v_c(\alpha)$. Hence, in contrast to a standard superfluid, the drag force is not a suitable quantity for estimating the critical velocity.

In order to compare the relative contributions of F_x^{imp} and F_x^d, we show, in FIG. 8.19, the time evolution of F_x^d at $\alpha = \pi$, the angle for which F_x^d contributes most significantly.

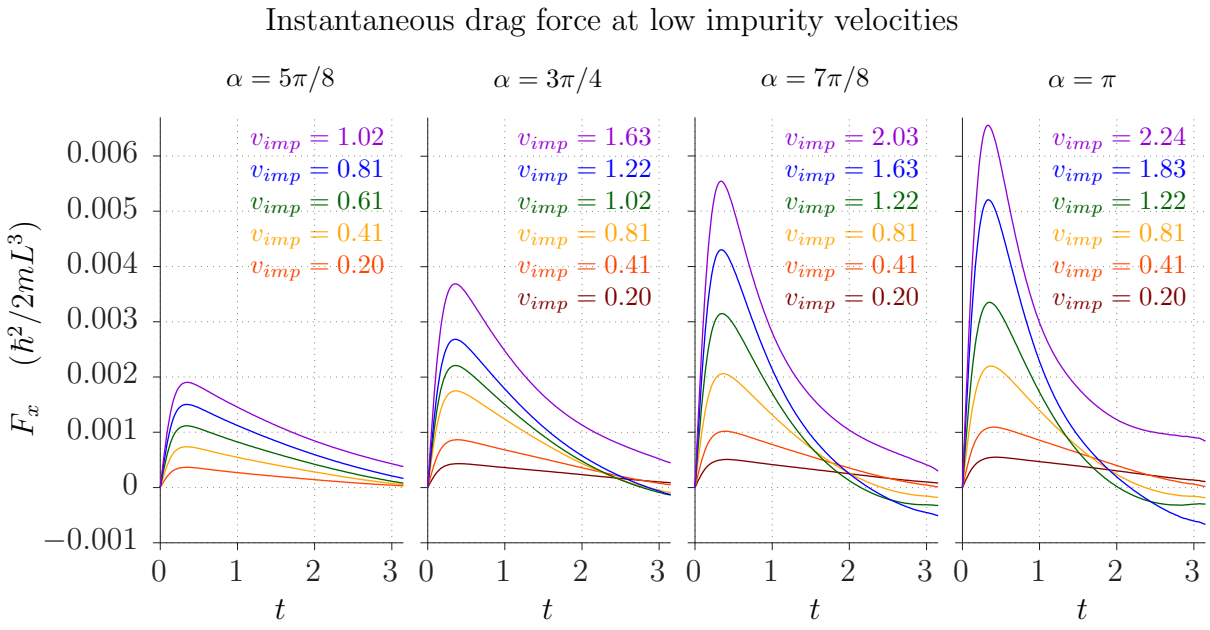

Figure 8.20: Plots showing the instantaneous x-component of the drag force for different impurity speeds v_{imp} (in units $\hbar/(2mL)$) and gauge angles α, as indicated. The time, t, is given in units $2mL^2/\hbar$. When $\alpha \in (\pi/2, \pi]$, the velocity of the medium carrying sound, $\mathbf{c}^M(\alpha)$, has a positive x-component: $c_x^M(5\pi/8) \simeq 0.81$, $c_x^M(3\pi/4) \simeq 1.49$, $c_x^M(7\pi/8) \simeq 1.95$ and $c_x^M(\pi) = 2.11$. At angle α, the drag force approaches a positive value when $v_{imp} > c_x^M(\alpha)$.

This reveals that the trends of the curves in FIG. 8.20 are mostly due to F_x^{imp}. Furthermore, when $v_{imp} < c_x^M(\pi)$, we see that F_x^d approaches zero at long time. A similar behaviour is observed for intermediate angles $\alpha \in (\pi/2, \pi]$, when $v_{imp} < c_x^M(\alpha)$.

For angles $0 \leq \alpha < \pi/2$ (not shown), the velocity of the medium tends to oppose the impurity and F_x takes on a positive long-time value for $v_{imp} > 0$. However, as we have seen, at high impurity velocities, the curves do not approach a constant value at long time, but decrease at an approximately steady rate due to F_x^d. On the other hand, F_x^{imp} does approach a constant value and we may therefore evaluate time-averages and examine its impurity velocity dependence. In figure 8.21, we show $\langle F_x^{imp} \rangle_t$ for the full range of angles, where the time-averages are calculated from curves similar to those of FIG. 8.17, over a time range where the force has already reached a plateau. Since the long-time behaviour of the lower curves in FIG. 8.20 is unclear, we have dismissed these in FIG. 8.21. Here, we clearly notice a general trend in the angular dependence of $\langle F_x^{imp} \rangle_t$, which increases when the gauge-flow increasingly opposes the motion of the impurity. For all the curves, the impurity force is approximately linear at low v_{imp}. However, a transition to a quadratic regime occurs further. We attribute this

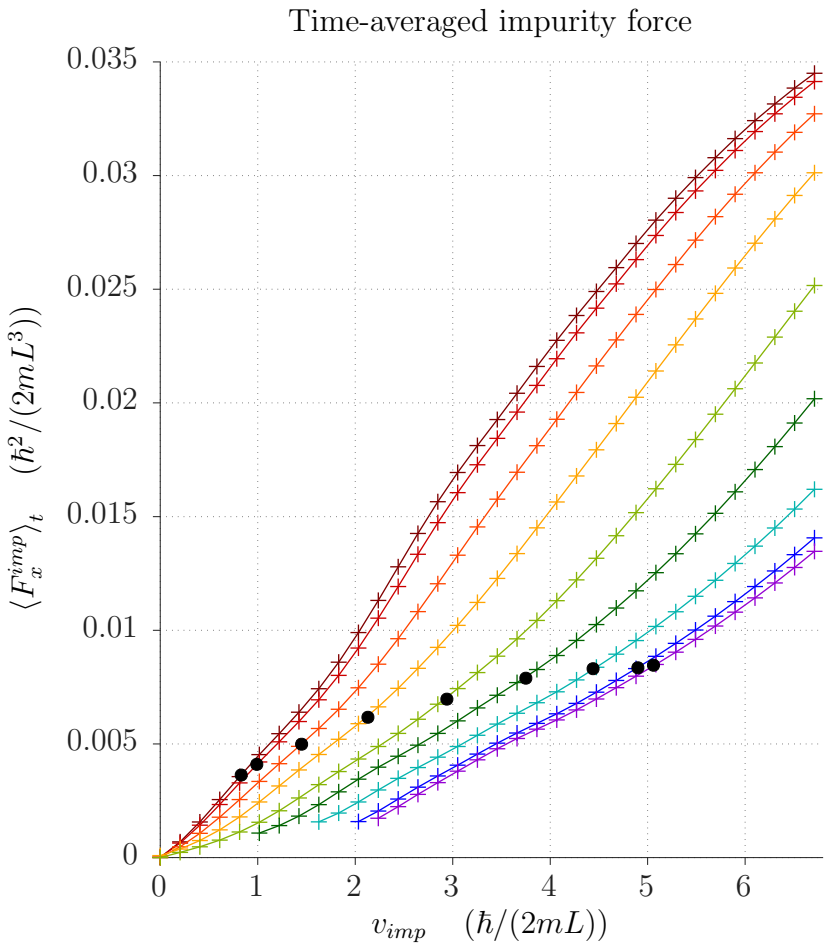

Figure 8.21: Plot showing the time-averaged x-component of the impurity force as a function of the impurity velocity, for angles $\alpha = 0$ to $\alpha = \pi$, in steps of $\pi/8$ from top to bottom. The average was taken for curves similar to those of FIG. 8.17, over a time range where the instantaneous force has already reached a plateau.

transition to shock wave production. Notice how the transition occurs at a higher impurity velocity, as α is increased from 0 to π. In an isotropic superfluid, this happens at approximately the bulk speed of sound. For the anisotropic superfluid considered here, identifying the transition point is not so straight-forward. Nonetheless, we have included in the figure, the speed of sound along the direction of the impurity, $c_{+\mathbf{x}}$, for each angle. These appear as black dots on the curves. Notice how the transition is underestimated by the black dots for the low α curves, overestimated for the high α curves and best at $\alpha = \pi/2$. Note also the high impurity velocity trends of the curves. This is in contrast to a standard superfluid, where the force is approximately quadratic in v_x^{imp} at high velocities (see FIG. 8.14).

8.4 Conclusion

In this final chapter, we investigated the motion of an impurity through a superfluid subject to a uni-directional, density-dependent gauge potential. In particular, we examined the mechanical flow field and phase winding field during vortex formation, for a variety of gauge angles and studied the drag force acting on the impurity. The nonlinear gauge potential presents a number of novel features. Perhaps the most conspicuous example is the nucleation of vortices in regions removed from the impurity. This typically occurs close to, or in between previously nucleated vortices, but also occasionally in far away regions devoid of vortices. The gauge angle strongly influences the properties of the fluid. For instance, the critical velocity for vortex formation, estimated from the phase slip accumulation, decreases as the flow imparted by the gauge potential increasingly opposes the moving impurity. In addition to the standard impurity force contribution, the drag force features a body-force of dilation, which extends throughout the fluid. At long time, the force of dilation approaches zero when the impurity velocity is less than the velocity of the sound medium along the direction of motion of the impurity. This latter velocity is distinct from the critical velocity. Likewise, the drag force approaches zero or a negative value for similar impurity speeds. This is in contrast to a standard superfluid, where the drag force vanishes below the critical velocity. As such, in the case of a nonlinear gauge potential, the drag force is not a suitable quantity for estimating the critical velocity.

Chapter 9

Conclusions and future prospects

The hydrodynamical canonical formalism is an ideal framework for exploring the form of the wave equations of a quantum fluid whose Hamiltonian density features density-dependent effective potentials. This is evidently clear in the case of a nonlinear gauge potential, where the nonlinear character of the kinetic energy density leads to nonlinear flow terms. As another example demonstrating the utility of this formalism, one may envisage a two species condensate. If one could realise a microscopic model such that the effective gauge potential acting on one species depended on the density of the other, it is not difficult to see, within this framework, that one would have two coupled equations where the nonlinear flow term in the wave equation for species 1 (2) depends on the overlap of the gauge potential acting on species 1 (2) and the flow of species 2 (1). This could result in interesting condensate dynamics and phase separation between the species.

We have seen that the nonlinear gauge potential endows a fluid with a number of novel features. For instance, a canonical flow pressure term and a body-force of dilation appear in the momentum transport equation. In turn, these lead to anisotropic sound and critical velocities, intriguing far-away-from-impurity vortex nucleation and a positive drag force for impurity speeds exceeding the component of flow of the medium carrying sound along the direction of the impurity. Another possible prospect for a nonlinear gauge-coupled superfluid, is the time crystal phase of matter, first proposed by Wilczek in 2012 [192, 193]. Such systems would exhibit periodic motion in their ground state. As a model, Wilczek considered particles with attractive interactions, moving on an Aharanov-Bohm ring threaded by a magnetic flux. It was suggested that

the combination of these two interactions would result in a spontaneous breaking of time-translation symmetry, with a soliton rotating around the ring periodically in time. However, subsequently, it was shown that the rotating soliton solution was not the correct ground state of the system and that a static configuration with lower energy could be found [194]. The same author then put forward a no-go theorem excluding the possiblity of time crystals for rotating, external symmetry-breaking scalar potentials [195]. Recall that in the case of a nonlinear gauge potential, the introduction of an immobile impurity into a superfluid in dimension $d = 2$, leads to a canonical flow-dipole about the impurity which is anti-symmetric under a parity transformation, e.g. the gauge potential breaks the rotational symmetry of the ground state. We also learned that the resulting pressure field becomes rotationally symmetric about the impurity, when the impurity flow matches the ground state flow. In fact, by computing the energy functional, one may verify that the energy of the superfluid is lower in this case than when the impurity is immobile. Here one sees that, the energy takes on a minimum value when the relative flow between the impurity and the ground state flow, vanishes. In other words, it is energetically favourable for the impurity to flow with the ground state flow. However, notice that, modelled as an external potential, the impurity is constrained to assume an externally prescribed position and does not move under its own accord. To circumvent this, one may envisage, for instance, a quantum ring setup with two coupled superfluids, where one species represents the nonlinear gauge-coupled superfluid and the other models the impurity. This would endow the impurity with a dynamical degree of freedom. In order to observe a rotating impurity as a ground state solution, one may solve in a rotating frame by modifying the nonlinear potentials accordingly, as discussed in chapter 6. On this note, a rather intriguing imaginary-time propagation may be seen in the 2-dimensional system, for suitable parameter values. We have seen that the pressure field about an impurity placed at the center, is aspherically distributed and the impurity is squeezed as a result. Notice that a similar situation occurs for a travelling impurity in a weakly interacting superfluid, where, at sufficiently high velcities, the pressure gradient across the object leads to a 2π phase-slip jump and associated vortex-pair shedding. It seems natural to ask whether an analogous phenomenon occurs for an immobile impurity in a nonlinear gauge-coupled superfluid, where, above a critical effective interaction strength, $|\mathbf{a}|_c$, the pressure gradient across the object leads to vortex-pair creation. For suitable Gaussian impurity and interaction parameter values, one may verify that, under imaginary-time propagation, a steadily

increasing pressure gradient develops across the object and vortex-pairs are shed along the orthogonal direction to the gauge potential. When the pairs have left the impurity, the pressure gradient vanishes. As the pairs propagate to the edges, a pressure gradient slowly redevelops across the object. Due to the periodic boundary conditions, the pairs recombine at the edges. The process repeats perdiodically in imaginary time. One may then conclude that the system displays a degenerate subspace of lowest energy states. However, the significance of these results and their possible connection with the time-crystal problem, is unclear.

Appendix A

Appendix

A.1 The dimensionless Gross-Pitaevskii-like equation

Our canonical example of nonlinear gauge-coupled quantum fluid is the superfluid fraction of Bose particles governed by the Gross-Pitaevskii-like equation

$$i\hbar\partial_t\psi\left(\mathbf{r},t\right)=\left[\frac{\left(\hat{\mathbf{p}}-\mathbf{A}\right)^2}{2m}-\mathbf{a}\cdot\mathbf{J}+g\left|\psi\right|^2+V\left(\mathbf{r},t\right)\right]\psi\left(\mathbf{r},t\right), \tag{A.1}$$

where $\hat{\mathbf{p}}=-i\hbar\boldsymbol{\nabla}$ is the canonical momentum operator, $\mathbf{J}$ is the gauge-covariant current-density, V is an external scalar potential and the nonlinear gauge potential takes the density-modulated form $\mathbf{A}=\mathbf{a}\left|\psi\right|^2$, where $\mathbf{a}$ determines the orientation and effective strength of the vector potential and given by Eq. (4.38). We consider the case of a monochromatic laser field with constant phase twist, such that $\mathbf{a}$ is uniform over space.

In order to solve the dynamics of the system numerically, it is convenient to render Eq. (A.1) into dimensionless form. This may be achieved by introducing characteristic scales for our units of space and time. If we denote the length of our system by L, we may write a position variable x in terms of this unit, as $x=\tilde{x}L$, where $\tilde{x}$ is a dimensionless quantity. Similarly, let us define a characteristic unit for time, by setting $t=\tilde{t}2mL^2/\hbar$. The reason for adopting this choice of units, is that the energy of the system now scales as $E=\tilde{E}\hbar^2/\left(2mL^2\right)$. These are the natural energy units for rendering Eq. (A.1) dimensionless. Normalising the condensate wavefunction to unity: $\int d^3\mathbf{r}\left|\psi\right|^2=1$, we may express the density in terms of the dimensionless quantity

$\tilde{\rho} = \tilde{\psi}^* \tilde{\psi}$, as $\rho = N\tilde{\rho}/L^3$, where N is the condensate particle number. For instance, the nonlinear interaction term reads $g\rho = gN\tilde{\rho}/L^3$. However, in order for this term to be expressed in natural energy units, we introduce a dimensionless interaction strength $\tilde{g} = g2m/(L\hbar^2)$, such that becomes $g\rho = \tilde{g}N\tilde{\rho}\hbar^2/(2mL^2)$. Similarly, the nonlinear gauge potential $\mathbf{A} = \mathbf{a}\rho = \mathbf{a}N\tilde{\rho}/L^3$, has dimensions $[\mathbf{A}] = \hbar/L$, so that $[\mathbf{a}] = \hbar L^2$. Hence we may introduce a dimensionless effective interaction strength $\tilde{a}\hat{\mathbf{a}}\mathbf{a}/(\hbar L^2)$, such that $\mathbf{A} = \hat{\mathbf{a}}N\tilde{a}\tilde{\rho}\hbar/L$, where $\hat{\mathbf{a}}$ is a unit vector along $\mathbf{A}$. All physical quantities have a dimensionless analogue in these natural units for space, time and energy. For instance, the natural unit scale for a velocity $\mathbf{v}$, where $[\mathbf{v}] = L/T$, is given by $\mathbf{v} = \tilde{\mathbf{v}}\hbar/(2mL)$. Implementing these definitions in Eq. (A.1), we find that the Gross-Pitaevskii-like equation takes on the dimensionless form

$$i\tilde{\partial}_t \tilde{\psi} = \tilde{H}\tilde{\psi}, \tag{A.2}$$

where

$$\tilde{H} = -\tilde{\nabla}^2 + iN\tilde{a}\hat{\mathbf{a}} \cdot \left(\tilde{\boldsymbol{\nabla}}\tilde{\rho} + 2\tilde{\rho}\tilde{\boldsymbol{\nabla}}\right) + N^2\tilde{a}^2\tilde{\rho}^2 + iN\tilde{a}\hat{\mathbf{a}} \cdot \left[\tilde{\psi}^* \left(\tilde{\boldsymbol{\nabla}} - iN\tilde{a}\tilde{\rho}\right)\tilde{\psi} - c.c\right] + N\tilde{g}\tilde{\rho}. \tag{A.3}$$

The terms in the top line account for the kinetic operator in Eq. (A.1), while the two terms in the bottom line result from the current nonlinearity $-\mathbf{a} \cdot \mathbf{J}$ and the GP nonlinearity $g\rho$, respectively. The simulations presented in this thesis were achieved by numerical integration of Eq. (A.2) using the Crank-Nicholson method [196, 197] for a system of dimension $d = 2$ with periodic boundary conditions. The 2-d box has side length $L = 47$ and comprises 416×416 points. We choose the origin of the system to coincide with the center of the box and denote the positions along the horizontal and vertical by x and y respectively. Parameter values $\tilde{a} = 0.73$ and $\tilde{g} = 3.66$ were chosen. Finally, note that the ground state of the system was obtained through the method of imaginary time-evolution.

A.2 Compact form of the nonlinear flow term

The Hamiltonian density in the presence of effective density-dependent scalar and vector potentials $\eta(\rho)$ and $\mathbf{A}(\rho)$, takes the form

$$\mathcal{H} = \rho \left\{ \frac{\left[\boldsymbol{\nabla}\theta - \mathbf{A}\left(\rho\right)\right]^2}{2m} + \eta\left(\rho\right) \right\} + \mathcal{Q}\left(\rho, \boldsymbol{\nabla}\rho\right). \tag{A.4}$$

The quantum Hamilton-Jacobi equation results form the canonical field equation

$$\dot{\theta} + \frac{\delta H}{\delta \rho} = 0. \tag{A.5}$$

Inserting the Hamiltonian density into the above field equation yields

$$\dot{\theta} + \frac{1}{2}mv^2 - \rho\mathbf{v} \cdot \frac{\partial \mathbf{A}}{\partial \rho} + \eta + \rho\frac{\partial \eta}{\partial \rho} + Q = 0 \tag{A.6}$$

where

$$\mathbf{v} = \frac{1}{m}\left(\boldsymbol{\nabla}\theta - \mathbf{A}\right) = \mathbf{u} - \frac{\mathbf{A}}{m} \tag{A.7}$$

Thus, the wave equation of the nonlinear fluid

$$\dot{\theta} + \frac{1}{2}mv^2 + \Phi\left(\rho, \mathbf{u}\right) + Q = 0, \tag{A.8}$$

features a density-dependent and flow-dependent scalar term

$$\Phi\left(\rho, \mathbf{u}\right) = \eta + \rho\frac{\partial \eta}{\partial \rho} - \rho\mathbf{v} \cdot \frac{\partial \mathbf{A}}{\partial \rho}. \tag{A.9}$$

First by defining

$$\lambda = 1 + \frac{\rho}{\eta}\frac{\partial \eta}{\partial \rho}, \tag{A.10}$$

we have

$$\Phi\left(\rho, \mathbf{u}\right) = \lambda\eta - \rho\mathbf{v} \cdot \frac{\partial \mathbf{A}}{\partial \rho}. \tag{A.11}$$

Single component gauge potential For the case in which the gauge potential has a single dynamical component, of the form $\mathbf{A} = \mathbf{a}\alpha\left(\rho\right)$, then simply defining the dimensionless function

$$\gamma = \frac{\rho}{\alpha}\frac{\partial \alpha}{\partial \rho}, \tag{A.12}$$

leads to the following compact form for Φ:

$$\Phi = \lambda\eta - \gamma \mathbf{v} \cdot \mathbf{A}. \tag{A.13}$$

Multi-component gauge potential In the case of a multi-component gauge potential $\mathbf{A} = \mathbf{a}_i \alpha_i(\rho)$, the nonlinear flow term leads to

$$\Phi = \lambda\eta - \rho \mathbf{v} \cdot \mathbf{a}_j \frac{\partial \alpha_j}{\partial \rho}. \tag{A.14}$$

The nonlinear flow term may be written in the form of an overlap between the gauge potential and the flow, by defining

$$\gamma_{ij} = \sum_k a_{ik} \gamma_k a_{kj}, \tag{A.15}$$

with

$$\gamma_k = \frac{\rho}{\alpha_k} \frac{\partial \alpha_k}{\partial \rho}, \tag{A.16}$$

k not summed. Then Φ takes the form

$$\Phi = \lambda\eta - v_i \gamma_{ij} A_j. \tag{A.17}$$

To see why this is the case, we expand

$$v_i \gamma_{ij} A_j = v_i \left(a_{i1}\gamma_1 a_{1j} + a_{i2}\gamma_2 a_{2j} + a_{i3}\gamma_3 a_{3j} \right) A_j. \tag{A.18}$$

The components of the gauge potential are $A_i = a_{ij}\alpha_j$ and may be inverted for α_i, since the basis a_{ij} is assumed to have been rendered into orthonormal form:$a_{ij}a_{jk} = \delta_{ik}$, so that $\alpha_i = a_{ij}A_j$. As a result we see that

$$v_i \gamma_{ij} A_j = v_i \left(a_{i1}\gamma_1\alpha_1 + a_{i2}\gamma_2\alpha_2 + a_{i3}\gamma_3\alpha_3 \right). \tag{A.19}$$

Since $\gamma_1\alpha_1$ say, is

$$\gamma_1\alpha_1 = \rho \frac{\partial \alpha_1}{\partial \rho}, \tag{A.20}$$

we see that the right hand side of expression (A.19), expands out to

$$\begin{aligned}
&+v_1 a_{11}\rho\frac{\partial\alpha_1}{\partial\rho}+v_1 a_{12}\rho\frac{\partial\alpha_2}{\partial\rho}+v_1 a_{13}\rho\frac{\partial\alpha_3}{\partial\rho}\\
&+v_2 a_{21}\rho\frac{\partial\alpha_1}{\partial\rho}+v_2 a_{22}\rho\frac{\partial\alpha_2}{\partial\rho}+v_2 a_{23}\rho\frac{\partial\alpha_3}{\partial\rho}\\
&+v_3 a_{31}\rho\frac{\partial\alpha_1}{\partial\rho}+v_3 a_{32}\rho\frac{\partial\alpha_2}{\partial\rho}+v_3 a_{33}\rho\frac{\partial\alpha_3}{\partial\rho}
\end{aligned} \tag{A.21}$$

which is equivalent to the compact form

$$v_i a_{ij}\rho\frac{\partial\alpha_j}{\partial\rho}. \tag{A.22}$$

Bibliography

[1] Mike H Anderson, Jason R Ensher, Michael R Matthews, Carl E Wieman, and Eric A Cornell. Observation of Bose-Einstein condensation in a dilute atomic vapor. *science*, 269(5221):198–201, 1995.

[2] Kendall B Davis, M-O Mewes, Michael R Andrews, NJ Van Druten, DS Durfee, DM Kurn, and Wolfgang Ketterle. Bose-Einstein condensation in a gas of sodium atoms. *Physical Review Letters*, 75(22):3969, 1995.

[3] Cl C Bradley, CA Sackett, JJ Tollett, and Randall G Hulet. Evidence of Bose-Einstein condensation in an atomic gas with attractive interactions. *Physical Review Letters*, 75(9):1687, 1995.

[4] Curtis Charles Bradley, CA Sackett, and RG Hulet. Bose-Einstein condensation of lithium: Observation of limited condensate number. *Physical Review Letters*, 78(6):985, 1997.

[5] Christopher J Pethick and Henrik Smith. *Bose-Einstein condensation in dilute gases*. Cambridge university press, 2002.

[6] Philippe Nozières. *Theory of quantum liquids: Superfluid Bose liquids*. CRC Press, 2018.

[7] S Inouye, MR Andrews, J Stenger, H-J Miesner, DM Stamper-Kurn, and W Ketterle. Observation of Feshbach resonances in a Bose-Einstein condensate. *Nature*, 392(6672):151, 1998.

[8] MR Andrews, CG Townsend, H-J Miesner, DS Durfee, DM Kurn, and W Ketterle. Observation of interference between two Bose condensates. *Science*, 275(5300):637–641, 1997.

[9] DM Stamper-Kurn, MR Andrews, AP Chikkatur, Stenger Inouye, H-J Miesner, J Stenger, and W Ketterle. Optical confinement of a Bose-Einstein condensate. *Physical Review Letters*, 80(10):2027, 1998.

[10] Matthew PA Fisher, Peter B Weichman, G Grinstein, and Daniel S Fisher. Boson localization and the superfluid-insulator transition. *Physical Review B*, 40(1):546, 1989.

[11] Dieter Jaksch, Christoph Bruder, Juan Ignacio Cirac, Crispin W Gardiner, and Peter Zoller. Cold bosonic atoms in optical lattices. *Physical Review Letters*, 81(15):3108, 1998.

[12] Markus Greiner, Olaf Mandel, Tilman Esslinger, Theodor W Hänsch, and Immanuel Bloch. Quantum phase transition from a superfluid to a Mott insulator in a gas of ultracold atoms. *nature*, 415(6867):39, 2002.

[13] Yu-Ju Lin, Robert L Compton, Karina Jimenez-Garcia, William D Phillips, James V Porto, and Ian B Spielman. A synthetic electric force acting on neutral atoms. *Nature Physics*, 7(7):531–534, 2011.

[14] Y-J Lin, Rob L Compton, K Jimenez-Garcia, James V Porto, and Ian B Spielman. Synthetic magnetic fields for ultracold neutral atoms. *Nature*, 462(7273):628–632, 2009.

[15] Jean Dalibard, Fabrice Gerbier, Gediminas Juzeliūnas, and Patrik Öhberg. Colloquium: Artificial gauge potentials for neutral atoms. *Reviews of Modern Physics*, 83(4):1523, 2011.

[16] N Goldman, G Juzeliūnas, P Öhberg, and IB Spielman. Light-induced gauge fields for ultracold atoms. *Reports on Progress in Physics*, 77(12):126401, 2014.

[17] Michael V Berry. Quantal phase factors accompanying adiabatic changes. *Proceedings of the Royal Society of London A: Mathematical, Physical and Engineering Sciences*, 392(1802):45–57, 1984.

[18] M Peskin and A Tonomura. *The Aharonov-Bohm Eflect*. Springer-Verlag, Berlin, 1989.

[19] Eliot Kapit and Erich Mueller. Optical-lattice Hamiltonians for relativistic quantum electrodynamics. *Physical Review A*, 83(3):033625, 2011.

[20] U-J Wiese. Ultracold quantum gases and lattice systems: quantum simulation of lattice gauge theories. *Annalen der Physik*, 525(10-11):777–796, 2013.

[21] Debasish Banerjee, M Dalmonte, M Müller, E Rico, P Stebler, U-J Wiese, and P Zoller. Atomic quantum simulation of dynamical gauge fields coupled to fermionic matter: From string breaking to evolution after a quench. *Physical Review Letters*, 109(17):175302, 2012.

[22] L Tagliacozzo, A Celi, P Orland, MW Mitchell, and M Lewenstein. Simulation of non-Abelian gauge theories with optical lattices. *Nature communications*, 4:2615, 2013.

[23] Erez Zohar, J Ignacio Cirac, and Benni Reznik. Cold-atom quantum simulator for SU (2) Yang-Mills lattice gauge theory. *Physical Review Letters*, 110(12):125304, 2013.

[24] Luca Tagliacozzo, Alessio Celi, Alejandro Zamora, and Maciej Lewenstein. Optical Abelian lattice gauge theories. *Annals of Physics*, 330:160–191, 2013.

[25] Matthew James Edmonds, Manuel Valiente, G Juzeliūnas, Luis Santos, and P Öhberg. Simulating an interacting gauge theory with ultracold bose gases. *Physical Review Letters*, 110(8):085301, 2013.

[26] MJ Edmonds, Manuel Valiente, and P Öhberg. On the Josephson effect in a Bose-Einstein condensate subject to a density-dependent gauge potential. *Journal of Physics B: Atomic, Molecular and Optical Physics*, 46(13):134013, 2013.

[27] Tassilo Keilmann, Simon Lanzmich, Ian McCulloch, and Marco Roncaglia. Statistically induced phase transitions and anyons in 1D optical lattices. *Nature communications*, 2:361, 2011.

[28] S Greschner, G Sun, D Poletti, and L Santos. Density-dependent synthetic gauge fields using periodically modulated interactions. *Physical Review Letters*, 113(21):215303, 2014.

[29] Lorenzo Cardarelli, Sebastian Greschner, and Luis Santos. Engineering interactions and anyon statistics by multicolor lattice-depth modulations. *Physical Review A*, 94(2):023615, 2016.

[30] Sebastian Greschner and Luis Santos. Anyon Hubbard model in one-dimensional optical lattices. *Phys. Rev. Lett.*, 115:053002, Jul 2015.

[31] Christoph Sträter, Shashi C. L. Srivastava, and André Eckardt. Floquet realization and signatures of one-dimensional anyons in an optical lattice. *Phys. Rev. Lett.*, 117:205303, Nov 2016.

[32] Logan W. Clark, Brandon M. Anderson, Lei Feng, Anita Gaj, K. Levin, and Cheng Chin. Observation of density-dependent gauge fields in a Bose-Einstein condensate based on micromotion control in a shaken two-dimensional lattice. *Phys. Rev. Lett.*, 121:030402, Jul 2018.

[33] U. Aglietti, L. Griguolo, R. Jackiw, S.-Y. Pi, and D. Seminara. Anyons and chiral solitons on a line. *Phys. Rev. Lett.*, 77:4406–4409, Nov 1996.

[34] RJ Dingwall, MJ Edmonds, JL Helm, BA Malomed, and P Öhberg. Non-integrable dynamics of matter-wave solitons in a density-dependent gauge theory. *New Journal of Physics*, 20(4):043004, 2018.

[35] R. J. Dingwall and P. Öhberg. Stability of matter-wave solitons in a density-dependent gauge theory. *Phys. Rev. A*, 99:023609, Feb 2019.

[36] Gleb Leonidovich Kotkin and Valeriĭ Serbo. *Collection of Problems in Classical Mechanics: International Series of Monographs in Natural Philosophy.*

[37] Cornelius Lanczos. *The variational principles of mechanics.* Courier Corporation, 2012.

[38] André Mercier. *Analytical and canonical formalism in physics.* Courier Corporation, 2004.

[39] Richard Talman. *Geometric mechanics.* John Wiley & Sons, 2008.

[40] Jorge José and Eugene Saletan. Classical dynamics: a contemporary approach, 2000.

[41] LD Landau and EM Lifshitz. Mechanics, vol. 1. *Course of theoretical physics*, 3, 1976.

[42] Melvin G Calkin. *Lagrangian and Hamiltonian mechanics.* World Scientific Publishing Company, 1996.

[43] Herbert Charles Corben and Philip Stehle. *Classical mechanics*. Courier Corporation, 2013.

[44] Herbert Goldstein. *Classical mechanics*. Pearson Education India, 2011.

[45] Claude Cohen-Tannoudji, Jacques Dupont-Roc, Gilbert Grynberg, and Patricia Thickstun. *Atom-photon interactions: basic processes and applications*. Wiley Online Library, 1992.

[46] Lev Pitaevskii and Sandro Stringari. *Bose-Einstein condensation and superfluidity*, volume 164. Oxford University Press, 2016.

[47] Massimo Inguscio, Sandro Stringari, and C Wieman. *Bose-Einstein condensation in atomic gases*, volume 140. IOS Press, 1999.

[48] Franco Dalfovo, Stefano Giorgini, Lev P Pitaevskii, and Sandro Stringari. Theory of Bose-Einstein condensation in trapped gases. *Reviews of Modern Physics*, 71(3):463, 1999.

[49] Lev Davidovich Landau and EM Lifshitz. *Course of Theoretical Physics Vol 3 Quantum Mechanics*. Pergamon Press, 1958.

[50] Claude Itzykson and Jean-Bernard Zuber. *Quantum field theory*. Courier Corporation, 2006.

[51] Scottish Universities Summer School in Physics, Roger Cortham Clark, and Graham Holbrook Derrick. *Mathematical methods in solid state and superfluid theory*. Oliver and Boyd, 1967.

[52] Oliver Penrose and Lars Onsager. Bose-Einstein condensation and liquid helium. *Physical Review*, 104(3):576, 1956.

[53] Takehiko Takabayasi. On the formulation of quantum mechanics associated with classical pictures. *Progress of Theoretical Physics*, 8(2):143–182, 1952.

[54] RK Pathria. Statistical mechanics, international series in natural philosophy, 1986.

[55] LP Pitaevskii. Vortex lines in an imperfect bose gas. *Sov. Phys. JETP*, 13(2):451–454, 1961.

[56] LP Pitaevskii. *Zh. Eksp. Teor. Fiz*, 40:646, 1961.

[57] Eugene P Gross. Structure of a quantized vortex in boson systems. *Il Nuovo Cimento (1955-1965)*, 20(3):454–477, 1961.

[58] Eugene P Gross. Hydrodynamics of a superfluid condensate. *Journal of Mathematical Physics*, 4(2):195–207, 1963.

[59] Yakovic Ilich Frenkel. *Wave mechanics: advanced general theory*.

[60] Paul Adrien Maurice Dirac. *The principles of quantum mechanics*. Number 27. Oxford university press, 1981.

[61] Leonard I Schiff. *Quantum Mechanics 3rd*. New York: McGraw-Hill, 1968.

[62] CG Gray, G Karl, and VA Novikov. Progress in classical and quantum variational principles. *Reports on Progress in Physics*, 67(2):159, 2004.

[63] E Deumens, A Diz, R Longo, and Y Öhrn. Time-dependent theoretical treatments of the dynamics of electrons and nuclei in molecular systems. *Reviews of Modern Physics*, 66(3):917, 1994.

[64] László Á Gergely. On Hamiltonian formulations of the Schrödinger system. *Annals of Physics*, 298(2):394–402, 2002.

[65] Marc Henneaux and Claudio Teitelboim. *Quantization of gauge systems*. Princeton university press, 1992.

[66] Kurt Sundermeyer. *Constrained dynamics with applications to Yang-Mills theory, general relativity, classical spin, dual string model*. Springer-Verlag, Berlin, 1982.

[67] J Barcelos-Neto and C Wotzasek. Symplectic quantization of constrained systems. *Modern Physics Letters A*, 7(19):1737–1747, 1992.

[68] Paul AM Dirac. Generalized hamiltonian dynamics. *Proceedings of the Royal Society of London A: Mathematical, Physical and Engineering Sciences*, 246(1246):326–332, 1958.

[69] Paul Adrien Maurice Dirac. *Lectures on quantum mechanics*, volume 2. Courier Corporation, 2001.

[70] Ashok Das. *Lectures on quantum field theory*. World Scientific, 2008.

[71] Dmitri Gitman and Igor V Tyutin. *Quantization of fields with constraints*. Springer Science & Business Media, 2012.

[72] Heinz J Rothe and Klaus Dieter Rothe. *Classical and quantum dynamics of constrained Hamiltonian systems*, volume 81. World Scientific, 2010.

[73] André Burnel. Canonical quantization for constrained systems. In *Noncovariant Gauges in Canonical Formalism*, pages 1–23. Springer, 2009.

[74] Parthasarathi Mitra. *Symmetries and symmetry breaking in field theory*. CRC Press, 2014.

[75] Toshihide Maskawa and Hideo Nakajima. Singular Lagrangian and the Dirac-Faddeev method: Existence theorem of constraints in 'standard form'. *Progress of Theoretical Physics*, 56(4):1295–1309, 1976.

[76] Steven Weinberg. *The quantum theory of fields. Vol. 1: Foundations*. Cambridge University Press, 1995.

[77] L Faddeev and R Jackiw. Hamiltonian reduction of unconstrained and constrained systems. *Physical Review Letters*, 60(17):1692, 1988.

[78] R Jackiw. Quantization without tears, in "constraint theory and quantization methods", 1994.

[79] Peter D Drummond and Mark Hillery. *The quantum theory of nonlinear optics*. Cambridge University Press, 2014.

[80] Harald JW Mãller Kirsten. *Introduction to Quantum Mechanics: Schrödinger Equation and Path Integral*. World Scientific Publishing Company, 2006.

[81] AK Kerman and SE Koonin. Hamiltonian formulation of time-dependent variational principles for the many-body system. *Annals of Physics*, 100(1-2):332–358, 1976.

[82] Ernest-M Henley and Walter Thirring. *Elementary quantum field theory*. McGraw-Hill Book Co., Inc., PWN-Polish Scientific Publishers, 1959.

[83] VL Pokrovskii and M Khalatnikov. Hamiltonian formalism in classical and two-fluid. *JETP Lett*, 23(11), 1976.

[84] VL Pokrovskii and IM Khalatnikov. Transformation of first sound into second in superfluid helium. *Sov. Phys.-JETP (Engl. Transl.);(United States)*, 44(5), 1976.

[85] VV Lebedev and IM Khalatnikov. Lagrange and Hamilton hydrodynamics equations for anisotropic superfluid He 3-A liquid. *Zhurnal Ehksperimental'noj i Teoreticheskoj Fiziki*, 73(4):1537–1548, 1977.

[86] IM Khalatnikov and VV Lebedev. Canonical equations of hydrodynamics of quantum liquids. *Journal of Low Temperature Physics*, 32(5-6):789–801, 1978.

[87] Darryl D Holm and Boris A Kupershmidt. Poisson structures of superfluids. *Physics Letters A*, 91(9):425–430, 1982.

[88] V Zakharov and EA Kuznetsov. Hamiltonian formalism for nonlinear waves. *Physics-Uspekhi*, 40(11):1087–1116, 1997.

[89] Philip J Morrison. Hamiltonian description of the ideal fluid. *Reviews of Modern Physics*, 70(2):467, 1998.

[90] Fritz London. *Superfluids*. Wiley, 1954.

[91] VE Zakharov. Hamiltonian formalism for waves in nonlinear media with dispersion. *Nauchnaia Shkola po Nelineinym Kolebaniiam i Volnam v Raspredelennykh Sistemakh, 2 nd, Gorki, USSR, Mar. 1973.) Radiofizika*, 17(4):431–453, 1974.

[92] David Bohm. A suggested interpretation of the quantum theory in terms of" hidden" variables. i. *Physical Review*, 85(2):166, 1952.

[93] David Bohm. A suggested interpretation of the quantum theory in terms of" hidden" variables. ii. *Physical Review*, 85(2):180, 1952.

[94] David Bohm. *Wholeness and the implicate order*. Routledge, 2005.

[95] David Bohm and Basil J Hiley. *The undivided universe: An ontological interpretation of quantum theory*. Routledge, 2006.

[96] E Madelung. Quantum theory in hydrodynamic form. *Z. Phys.*, 40:322–326, 1926.

[97] Michael JW Hall and Marcel Reginatto. Schrödinger equation from an exact uncertainty principle. *Journal of Physics A: Mathematical and General*, 35(14):3289, 2002.

[98] Michael JW Hall. Superselection from canonical constraints. *Journal of Physics A: Mathematical and General*, 37(31):7799, 2004.

[99] Michael JW Hall and Marcel Reginatto. Ensembles on configuration space. *Fundam. Theor. Phys.*, 184:pp, 2016.

[100] TF Nonnenmacher, G Dukek, and G Baumann. On the nonlinear Schrödinger equation and its fluid-dynamical form. *Lettere al Nuovo Cimento (1971-1985)*, 36(14):453–456, 1983.

[101] TF Nonnenmacher. Functional Poisson brackets for nonlinear fluid mechanics equations. In *Recent Developments in Nonequilibrium Thermodynamics: Fluids and Related Topics*, pages 149–174. Springer, 1986.

[102] Francesco Guerra and Rossana Marra. Origin of the quantum observable operator algebra in the frame of stochastic mechanics. *Physical Review D*, 28(8):1916, 1983.

[103] Yakir Aharonov and David Bohm. Significance of electromagnetic potentials in the quantum theory. *Physical Review*, 115(3):485, 1959.

[104] Yakir Aharonov and David Bohm. Further considerations on electromagnetic potentials in the quantum theory. *Physical Review*, 123(4):1511, 1961.

[105] Y Aharonov and D Bohm. Remarks on the possibility of quantum electrodynamics without potentials. *Physical Review*, 125(6):2192, 1962.

[106] Y Aharonov and David Bohm. Further discussion of the role of electromagnetic potentials in the quantum theory. *Physical Review*, 130(4):1625, 1963.

[107] Richard D Mattuck. *A guide to Feynman diagrams in the many-body problem*. Courier Dover Publications, 2012.

[108] Patrik Fazekas. Electron correlation and magnetism. *Lecture Notes in Physics*, 5:650, 1999.

[109] Edmund C Stoner. The temperature dependence of free electron susceptibility. *Proceedings of the Royal Society of London. Series A-Mathematical and Physical Sciences*, 152(877):672–692, 1935.

[110] K v Klitzing, Gerhard Dorda, and Michael Pepper. New method for high-accuracy determination of the fine-structure constant based on quantized Hall resistance. *Physical Review Letters*, 45(6):494, 1980.

[111] DR Yennie. Integral quantum Hall effect for nonspecialists. *Reviews of Modern Physics*, 59(3):781, 1987.

[112] Richard E Prange and Steven M Girvin. *The quantum Hall effect*, volume 2. Springer-Verlag New York, 1987.

[113] Charles L Kane and Eugene J Mele. Quantum spin Hall effect in graphene. *Physical Review Letters*, 95(22):226801, 2005.

[114] Charles L Kane and Eugene J Mele. Z 2 topological order and the quantum spin Hall effect. *Physical Review Letters*, 95(14):146802, 2005.

[115] Liang Fu, Charles L Kane, and Eugene J Mele. Topological insulators in three dimensions. *Physical Review Letters*, 98(10):106803, 2007.

[116] B Andrei Bernevig, Taylor L Hughes, and Shou-Cheng Zhang. Quantum spin Hall effect and topological phase transition in HgTe quantum wells. *Science*, 314(5806):1757–1761, 2006.

[117] DJ Thouless, Mahito Kohmoto, MP Nightingale, and M Den Nijs. Quantized Hall conductance in a two-dimensional periodic potential. *Physical Review Letters*, 49(6):405, 1982.

[118] Xie Chen, Zheng-Cheng Gu, Zheng-Xin Liu, and Xiao-Gang Wen. Symmetry protected topological orders and the group cohomology of their symmetry group. *Physical Review B*, 87(15):155114, 2013.

[119] Xiao-Liang Qi and Shou-Cheng Zhang. Topological insulators and superconductors. *Reviews of Modern Physics*, 83(4):1057, 2011.

[120] M Zahid Hasan and Charles L Kane. Colloquium: topological insulators. *Reviews of Modern Physics*, 82(4):3045, 2010.

[121] Richard P Feynman. Simulating physics with computers. *International journal of theoretical physics*, 21(6-7):467–488, 1982.

[122] KW Madison, F Chevy, W Wohlleben, and J Dalibard. Vortex formation in a stirred Bose-Einstein condensate. *Physical Review Letters*, 84(5):806, 2000.

[123] JR Abo-Shaeer, C Raman, JM Vogels, and Wolfgang Ketterle. Observation of vortex lattices in Bose-Einstein condensates. *Science*, 292(5516):476–479, 2001.

[124] Yu-Ju Lin and IB Spielman. Synthetic gauge potentials for ultracold neutral atoms. *Journal of Physics B: Atomic, Molecular and Optical Physics*, 49(18):183001, 2016.

[125] Y-J Lin, K Jiménez-García, and IB Spielman. Spin-orbit-coupled Bose-Einstein condensates. *Nature*, 471(7336):83–86, 2011.

[126] MC Beeler, RA Williams, Karina Jimenez-Garcia, LJ LeBlanc, AR Perry, and IB Spielman. The spin Hall effect in a quantum gas. *Nature*, 498(7453):201–204, 2013.

[127] Ross A Williams, Lindsay J LeBlanc, Karina Jimenez-Garcia, Matthew C Beeler, Abigail R Perry, William D Phillips, and Ian B Spielman. Synthetic partial waves in ultracold atomic collisions. *Science*, 335(6066):314–317, 2012.

[128] S Olariu and I Iovitzu Popescu. The quantum effects of electromagnetic fluxes. *Reviews of Modern Physics*, 57(2):339, 1985.

[129] Akira Tonomura, Tsuyoshi Matsuda, Ryo Suzuki, Akira Fukuhara, Nobuyuki Osakabe, Hiroshi Umezaki, Junji Endo, Kohsei Shinagawa, Yutaka Sugita, and Hideo Fujiwara. Observation of Aharonov-Bohm effect by electron holography. *Physical Review Letters*, 48(21):1443, 1982.

[130] Richard A Webb, Simon Washburn, CP Umbach, and RB Laibowitz. Observation of h e Aharonov-Bohm oscillations in normal-metal rings. *Physical Review Letters*, 54(25):2696, 1985.

[131] V Chandrasekhar, MJ Rooks, S Wind, and DE Prober. Observation of Aharonov-Bohm electron interference effects with periods $\frac{h}{e}$ and $\frac{h}{2e}$ in individual micron-size, normal-metal rings. *Physical Review Letters*, 55(15):1610, 1985.

[132] G Timp, AM Chang, JE Cunningham, TY Chang, P Mankiewich, R Behringer, and RE Howard. Observation of the Aharonov-Bohm effect for $\omega_c\tau > 1$. *Physical Review Letters*, 58(26):2814, 1987.

[133] A Levy Yeyati and Markus Büttiker. Aharonov-Bohm oscillations in a mesoscopic ring with a quantum dot. *Physical Review B*, 52(20):R14360, 1995.

[134] Adrian Bachtold, Christoph Strunk, Jean-Paul Salvetat, Jean-Marc Bonard, Laszló Forró, Thomas Nussbaumer, and Christian Schönenberger. Aharonov-Bohm oscillations in carbon nanotubes. *Nature*, 397(6721):673, 1999.

[135] Jeng-Bang Yau, EP De Poortere, and M Shayegan. Aharonov-Bohm oscillations with spin: Evidence for Berry's phase. *Physical Review Letters*, 88(14):146801, 2002.

[136] M Bayer, Marek Korkusinski, Pawel Hawrylak, T Gutbrod, M Michel, and A Forchel. Optical detection of the Aharonov-Bohm effect on a charged particle in a nanoscale quantum ring. *Physical Review Letters*, 90(18):186801, 2003.

[137] Sasa Zaric, Gordana N Ostojic, Junichiro Kono, Jonah Shaver, Valerie C Moore, Michael S Strano, Robert H Hauge, Richard E Smalley, and Xing Wei. Optical signatures of the Aharonov-Bohm phase in single-walled carbon nanotubes. *Science*, 304(5674):1129–1131, 2004.

[138] Saverio Russo, Jeroen B Oostinga, Dominique Wehenkel, Hubert B Heersche, Samira Shams Sobhani, Lieven MK Vandersypen, and Alberto F Morpurgo. Observation of Aharonov-Bohm conductance oscillations in a graphene ring. *Physical Review B*, 77(8):085413, 2008.

[139] Hailin Peng, Keji Lai, Desheng Kong, Stefan Meister, Yulin Chen, Xiao-Liang Qi, Shou-Cheng Zhang, Zhi-Xun Shen, and Yi Cui. Aharonov-Bohm interference in topological insulator nanoribbons. *Nature materials*, 9(3):225, 2010.

[140] Albert Messiah. *Quantum Mechanics [Vol 1-2].* 1964.

[141] G Auletta, M Fortunato, and G Parisi. *Quantum Mechanics*. 2009.

[142] MV Berry. Classical adiabatic angles and quantal adiabatic phase. *Journal of physics A: Mathematical and general*, 18(1):15, 1985.

[143] Frank Wilczek and Alfred Shapere. *Geometric phases in physics*, volume 5. World Scientific, 1989.

[144] Jean Dalibard. Introduction to the physics of artificial gauge fields. *Quantum Matter at Ultralow Temperatures, Proceedings of the International School of Physics "Enrico Fermi*, 191:1–61, 2015.

[145] Christopher Gerry, Peter Knight, and Peter L Knight. *Introductory quantum optics*. Cambridge university press, 2005.

[146] Rodney Loudon. *The quantum theory of light*. OUP Oxford, 2000.

[147] Salvatore Butera, Manuel Valiente, and Patrik Öhberg. Vortex dynamics in superfluids governed by an interacting gauge theory. *New Journal of Physics*, 18(8):085001, aug 2016.

[148] Rutherford Aris. *Vectors, tensors and the basic equations of fluid mechanics*. Courier Corporation, 2012.

[149] Edward Nelson. Derivation of the Schrödinger equation from Nwtonian mechanics. *Physical Review*, 150(4):1079, 1966.

[150] Robert E Wyatt. *Quantum dynamics with trajectories: introduction to quantum hydrodynamics*, volume 28. Springer Science & Business Media, 2006.

[151] William G Faris. *Diffusion, Quantum Theory, and Radically Elementary Mathematics*. Princeton University Press, 2014.

[152] Gerald Rosen. Galilean invariance and the general covariance of nonrelativistic laws. *American Journal of Physics*, 40:683–687, 1972.

[153] Peter R Holland. *The quantum theory of motion: an account of the de Broglie-Bohm causal interpretation of quantum mechanics*. Cambridge university press, 1995.

[154] Vladimir I Arnold, Valery V Kozlov, and Anatoly I Neishtadt. *Mathematical aspects of classical and celestial mechanics*, volume 3. Springer Science & Business Media, 2007.

[155] Harald Iro. *A modern approach to classical mechanics*. World Scientific Publishing Company, 2015.

[156] Harvey R Brown and Peter R Holland. The Galilean covariance of quantum mechanics in the case of external fields. *American Journal of Physics*, 67:204–214, 1999.

[157] Bryce S DeWitt. Dynamical theory in curved spaces. i. a review of the classical and quantum action principles. *Reviews of modern physics*, 29(3):377, 1957.

[158] Shin Takagi. Quantum dynamics and non-inertial frames of reference. i: Generality. *Progress of theoretical physics*, 85(3):463–479, 1991.

[159] Michel Le Bellac and Jean-Marc Lévy-Leblond. Galilean electromagnetism. *Il Nuovo Cimento B (1971-1996)*, 14(2):217–234, 1973.

[160] Germain Rousseaux. Lorenz or Coulomb in Galilean electromagnetism? *EPL (Europhysics Letters)*, 71(1):15, 2005.

[161] Marc De Montigny and Germain Rousseaux. On the electrodynamics of moving bodies at low velocities. *European journal of physics*, 27(4):755, 2006.

[162] Germain Rousseaux. Forty years of Galilean electromagnetism (1973–2013). *The European Physical Journal Plus*, 128(8):81, 2013.

[163] LD Landau. *Fluid mechanics*, volume 6. 1959.

[164] N Bogoliubov. On the theory of superfluidity. *J. Phys*, 11(1):23, 1947.

[165] Tsin D Lee, Kerson Huang, and Chen N Yang. Eigenvalues and eigenfunctions of a Bose system of hard spheres and its low-temperature properties. *Physical Review*, 106(6):1135, 1957.

[166] M. R. Andrews, D. M. Kurn, H.-J. Miesner, D. S. Durfee, C. G. Townsend, S. Inouye, and W. Ketterle. Propagation of sound in a Bose-Einstein condensate. *Phys. Rev. Lett.*, 79:553–556, Jul 1997.

[167] M Gajda, M Lewenstein, K Sengstock, G Birkl, W Ertmer, et al. Optical generation of vortices in trapped Bose-Einstein condensates. *Physical Review A*, 60(5):R3381, 1999.

[168] G Andrelczyk, M Brewczyk, M Gajda, M Lewenstein, et al. Optical generation of vortices in trapped Bose-Einstein condensates. *Physical Review A*, 64(4):043601, 2001.

[169] AE Leanhardt, A Görlitz, AP Chikkatur, D Kielpinski, Y-i Shin, DE Pritchard, and W Ketterle. Imprinting vortices in a Bose-Einstein condensate using topological phases. *Physical Review Letters*, 89(19):190403, 2002.

[170] Stefan Burger, K Bongs, S Dettmer, W Ertmer, K Sengstock, A Sanpera, GV Shlyapnikov, and M Lewenstein. Dark solitons in Bose-Einstein condensates. *Physical Review Letters*, 83(25):5198, 1999.

[171] J Denschlag, Je E Simsarian, Dl L Feder, Charles W Clark, La A Collins, J Cubizolles, Lu Deng, Edward W Hagley, Kristian Helmerson, William P Reinhardt, et al. Generating solitons by phase engineering of a Bose-Einstein condensate. *Science*, 287(5450):97–101, 2000.

[172] Biao Wu, Jie Liu, and Qian Niu. Controlled generation of dark solitons with phase imprinting. *Physical Review Letters*, 88(3):034101, 2002.

[173] A Muryshev, GV Shlyapnikov, W Ertmer, K Sengstock, and M Lewenstein. Dynamics of dark solitons in elongated Bose-Einstein condensates. *Physical Review Letters*, 89(11):110401, 2002.

[174] Christoph Becker, Simon Stellmer, Parvis Soltan-Panahi, Sören Dörscher, Mathis Baumert, Eva-Maria Richter, Jochen Kronjäger, Kai Bongs, and Klaus Sengstock. Oscillations and interactions of dark and dark-bright solitons in Bose-Einstein condensates. *Nature Physics*, 4(6):496, 2008.

[175] S Stellmer, C Becker, P Soltan-Panahi, E-M Richter, S Dörscher, M Baumert, J Kronjäger, K Bongs, and K Sengstock. Collisions of dark solitons in elongated Bose-Einstein condensates. *Physical Review Letters*, 101(12):120406, 2008.

[176] Guoxiang Huang, Manuel G Velarde, and Valeri A Makarov. Dark solitons and their head-on collisions in Bose-Einstein condensates. *Physical Review A*, 64(1):013617, 2001.

[177] David Pines. *Theory of Quantum Liquids: Normal Fermi Liquids*. CRC Press, 2018.

[178] Léon Brillouin. *Wave propagation and group velocity*, volume 8. Academic Press, 2013.

[179] WH Keesom and K Clusius. *Proc. Sect. Sci. K. Ned. Acad. Wet*, 35:307, 1932.

[180] WH Keesom and AP Keesom. New measurements on the specific heat of liquid helium. *Physica*, 2(1):557–572, 1935.

[181] WH Keesom and AP Keesom. On the heat conductivity of liquid helium. *Physica*, 3(5):359–360, 1936.

[182] P Kapitza. Viscosity of liquid helium below the l-point. *Nature*, 141(3558):74, 1938.

[183] JF Allen and AD Misener. Flow of liquid helium ii. *Nature*, 141(3558):75, 1938.

[184] Richard Courant and Kurt Otto Friedrichs. *Supersonic flow and shock waves*, volume 21. Springer Science & Business Media, 1999.

[185] B Jackson, JF McCann, and CS Adams. Vortex formation in dilute inhomogeneous Bose-Einstein condensates. *Physical Review Letters*, 80(18):3903, 1998.

[186] T Winiecki, JF McCann, and CS Adams. Pressure drag in linear and nonlinear quantum fluids. *Physical Review Letters*, 82(26):5186, 1999.

[187] B Jackson, JF McCann, and CS Adams. Dissipation and vortex creation in Bose-Einstein condensed gases. *Physical Review A*, 61(5):051603, 2000.

[188] T Winiecki, B Jackson, JF McCann, and CS Adams. Vortex shedding and drag in dilute Bose-Einstein condensates. *Journal of Physics B: Atomic, Molecular and Optical Physics*, 33(19):4069, 2000.

[189] GE Astrakharchik and LP Pitaevskii. Motion of a heavy impurity through a Bose-Einstein condensate. *Physical Review A*, 70(1):013608, 2004.

[190] Tao Yang, Zhi-Qiang Hu, Shan Zou, and Wu-Ming Liu. Dynamics of vortex quadrupoles in nonrotating trapped Bose-Einstein condensates. *Scientific Reports*, 6:29066, 2016.

[191] F Ancilotto, L Salasnich, and F Toigo. Critical velocity, vortex shedding, and drag in a unitary Fermi superfluid. *Physical Review A*, 87(1):013637, 2013.

[192] Frank Wilczek. Quantum time crystals. *Phys. Rev. Lett.*, 109:160401, Oct 2012.

[193] Alfred Shapere and Frank Wilczek. Classical time crystals. *Phys. Rev. Lett.*, 109:160402, Oct 2012.

[194] Patrick Bruno. Comment on "quantum time crystals". *Physical Review Letters*, 110(11):118901, 2013.

[195] Patrick Bruno. Impossibility of spontaneously rotating time crystals: a no-go theorem. *Physical Review Letters*, 111(7):070402, 2013.

[196] M Delfour, M Fortin, and G Payr. Finite-difference solutions of a non-linear Schrödinger equation. *Journal of computational physics*, 44(2):277–288, 1981.

[197] Moysey Brio, Gary M Webb, and Aramais R Zakharian. *Numerical time-dependent partial differential equations for scientists and engineers*, volume 213. Academic Press, 2010.